

IDENTIFICATION OF PHARMACOLOGICAL VULNERABILITIES IN
DRUG-RESISTANT MELANOMA CELLS

By

Sean Alexander Misek

A DISSERTATION

Submitted to
Michigan State University
in partial fulfillment of the requirements
for the degree of

Physiology—Doctor of Philosophy

2020

ABSTRACT

IDENTIFICATION OF PHARMACOLOGICAL VULNERABILITIES IN DRUG-RESISTANT MELANOMA CELLS

By

Sean Alexander Misek

Most BRAF-mutant melanoma tumors respond to BRAFi/MEKi combination therapy. Despite a strong initial response to these agents, most patients relapse within months or years. The goal of this dissertation is to identify pharmacologically tractable resistance mechanisms, and ultimately to prevent or reverse drug resistance in melanoma.

We found that RhoA is activated in approximately half of BRAFi-resistant melanoma cells/tumors and demonstrated that inhibition of RhoA or disruption of actin polymerization re-sensitizes these cells to vemurafenib. The transcriptional profile of a subset of tumors in the TCGA dataset is similar to that of the BRAFi-resistant cells. Using gene expression-based drug response signatures we predicted that these tumors would be less sensitive to BRAF inhibitors and more sensitive to ROCK inhibitors. This finding is exciting since ROCK is a direct substrate of Rho, and we demonstrated that ROCK inhibition re-sensitizes BRAFi-resistant cells to vemurafenib. Rho-induced F-actin polymerization can modulate the activity of multiple transcriptional coactivators. Two of these transcriptional co-activators, MRTF-A and YAP1, are activated in BRAFi-resistant cells and inhibitors which disrupt these transcriptional processes re-sensitize BRAFi-resistant cells to vemurafenib.

In chapter 3 we applied multiple high throughput approaches to identify pharmacological vulnerabilities of BRAFi-resistant melanoma cells. First, we leveraged the LINCS dataset to identify compounds which reverse a drug resistance gene signature. The most promising

compound that we identified in this analysis was ibrutinib, which is clinically used as a BTK inhibitor. Interestingly, we found that ibrutinib does not reverse BRAFi resistance through BTK inhibition, but rather through the polypharmacology of the compound. The differentially expressed genes in ibrutinib-treated cells are enriched in YAP1 target genes, which suggests that ibrutinib may be modulating vemurafenib resistance by altering YAP1 activation. Consistent with this hypothesis, treatment with ibrutinib prevents the nuclear accumulation of YAP1.

In chapter 4 we sought to identify compounds which selectively killed vemurafenib-resistant melanoma cells. To this end we screened a well-annotated drug repurposing library which contains approximately 2,000 FDA-approved drugs, clinical inhibitors, and tool compounds. We found that BRAFi-resistant cells are more sensitive to inhibitors that disrupt mitosis, such as AURKi, PLKi, Chk1/2i, and compounds which disrupt kinesin and tubulin polymerization. The fate of the resistant cells upon drug treatment was nuclear fragmentation and death. But interestingly, a subset of the parental cells did not die upon drug treatment and instead underwent mitotic slippage and exited from mitosis, likely due to dysregulated Cyclin B1 degradation in the parental cells. This finding likely explains why the resistant cells are more sensitive to this class of inhibitors, and it suggests that disruption of mitosis may be a pharmacological vulnerability for melanoma cells/tumors that have developed resistance to BRAFi/MEKi therapy.

ACKNOWLEDGMENTS

I would first like to thank my labmates, including Andrew, Behirda, Benita, Cassie, Charuta, Cho, Clarissa, Duyen, Erika, Eva, Hoa, Indi, Jade, Jeff, Jian, Kate, Laura, Maja, Melissa, Nils, Tom, Xiaoting, Yajing, and Zhangzhe for the countless hours of discussion in lab and at the lunch table. I would like to thank all of the undergraduate, rotation, and summer students who have worked with me. Thanks to all of my colleagues in BCSN/CRN for your advice, support, and friendship over the years. Completion of this dissertation would not have been possible without the support provided by the department of physiology and the department of pharmacology and toxicology. I would especially like to thank our current program director, Dr. Andrea Doseff, and our past program director, Dr. Susanne Mohr, for their guidance. I would also like to thank the administrative and support staff from both departments, especially Linda, Jasmine, Beverly, and Wendy, for answering all of my naïve questions. Thank you to the BMS program, especially Becky, for all her help in my transition into graduate school.

This work would not be possible without all of our collaborators. In particular I would like to thank Dr. Sue Conrad and Dr. Andrea Doseff for their advice and support over the years. I would like to thank my friends Dan and Jon for all of their friendship and support and for answering an innumerable amount of questions about fellowship writing, bioinformatics, and postdoc positions. A special thank you to my committee members: Dr. Eran Andrechek, Dr. Sophia Lunt, and Dr. Hua Xiao for writing letters of support, providing valuable feedback, and for spending countless hours listening to my presentations.

Thank you to Lauren Aitch and the Aitch foundation for funding my research. I am incredibly honored to work with your foundation and will be forever grateful for the experiences and opportunities you have unlocked for me.

I would like to thank all of my friends that I've made along the way, especially Aaron, Briana, Laura, Scott, and Yajing whose friendship has made grad school much more enjoyable. I'm lucky to have such supportive parents, especially my Dad without whom I probably would not be a scientist.

Finally, I would like to acknowledge my mentors Dr. Kathy Gallo and Dr. Rick Neubig and thank them for all of the time and effort they put into my training. It is invaluable to have such supporting advisors who allowed me to learn by making mistakes and gave me as much autonomy as I wanted while always being there when I need them. Their insistence that I follow the data, wherever it took me, has helped me become the scientist I am today, and has prepared me for wherever my career takes me. I would especially like to thank Kathy for her support when I was an undergraduate student in her laboratory. Without her early guidance I may not have even pursued a Ph. D.

TABLE OF CONTENTS

LIST OF FIGURES	ix
KEY TO ABBREVIATIONS	xiii
CHAPTER 1: Introduction	1
Etiology of Skin Cutaneous Melanoma	2
SKCM cell of origin	4
Genetic drivers of SKCM	5
BRAF	6
NRAS	7
NF1	7
Triple-WT	8
Other mechanisms of ERK/MAPK activation	8
Non-MAPK driver mutations	9
Rho GTPases and RhoA-mediated gene transcription	9
TERT	13
Therapeutic interventions for the treatment of melanoma	14
MAPK inhibitors	14
Immunotherapy	15
Combination of Immunotherapy with MAPK pathway inhibitors	17
Mitogen Activated Protein Kinase inhibitor resistance	17
Models of drug resistance	18
Mechanisms of MAPKi resistance	22
Receptor Tyrosine Kinase	23
NRAS	24
RAF	24
BRAF-independent MEK activation	25
Differentiation	26
Tumor Microenvironment	27
RhoA GTPases and RhoA-mediated gene transcription	28
Contribution of this work	29
CHAPTER 2: Rho-mediated signaling promotes BRAF inhibitor resistance in de-differentiated melanoma cells	31
Abstract	32
Introduction	33
Materials and Methods	36
Cell lines and culture:	36
Cloning:	37

Virus preparation and Infection:.....	37
Compounds and Antibodies:	38
qRT-PCR:	39
RNA-Seq sample preparation and data processing:	39
Immunoblotting:	40
Immunofluorescence staining:.....	40
Cell viability experiments:	42
Bioinformatics:	42
Statistical Analysis:	45
Results	46
RhoA activation in BRAFi-resistant melanoma cells and tumors.....	46
Resistant cell lines with a low level of melanocyte differentiation show high RhoA activity	51
ROCK inhibition sensitizes RhoA ^{High} BRAFi-resistant melanoma cells	54
MRTF and YAP activation in RhoA ^{High} BRAFi-resistant cells	57
Pharmacologically targeting MRTF/YAP-mediated gene transcription	60
Discussion	64

CHAPTER 3: Ibrutinib blocks YAP1 activation and reverses BRAFi resistance in melanoma cells

Abstract	70
Introduction	71
Materials and Methods	73
Cell lines, reagents, and antibodies:	73
Cell culture:	74
Cloning/CRISPR:	74
Virus preparation and infection:	74
Viability experiments:	75
Flow cytometry:.....	76
DEVD Assay:	77
Colony formation:	77
Immunofluorescence staining:.....	78
RNA-Seq sample/data processing:	79
Datasets:	79
LISA:	80
Connectivity map analysis:.....	80
OCTAD Datasets and RNA-Sequence processing:.....	80
Disease signature creation:	81
Drug prediction:.....	81
Results	82
Identification of compounds which reverse a BRAFi resistance signature.....	82
Ibrutinib re-sensitizes BRAFi-resistant cells to vemurafenib	86
BTK deletion or inhibition does not re-sensitize BRAFi-resistant cells to vemurafenib	87

Transcriptional response to ibrutinib treatment.....	88
Ibrutinib reduces the nuclear accumulation of YAP1	92
Discussion	94
CHAPTER 4: BRAFi-resistant melanoma cells are vulnerable to pharmacological disruption of mitosis	96
Abstract	97
Introduction	98
Materials and Methods	100
Cell lines, reagents, and antibodies:	100
Cell culture:	101
Cloning:	101
Virus preparation and infection:	102
Viability experiments:	102
Compound Screen:	103
Cell Cycle Analysis:	103
Assay for Reactive Oxygen Species:.....	104
Immunofluorescence staining:.....	104
Live cell imaging:.....	104
Results	106
BRAFi-resistant melanoma cells are sensitive to inhibitors that disrupt mitosis.....	106
Compound-treated UACC62P, but not UACC62R, cells undergo mitotic slippage.....	110
Differential Cyclin B1 accumulation in UACC62P/R cells	113
Increased sensitivity of BRAFi-resistant M229R cells to Chk1/2 inhibitors	115
Discussion	117
CHAPTER 5: Discussion.....	120
Discussion of results.....	121
Limitations	124
Future directions.....	126
APPENDIX.....	132
REFERENCES.....	172

LIST OF FIGURES

Figure 1.1:	Illustration of the RhoA pathway.....	11
Figure 1.2:	Illustration of RhoA-mediated gene transcription mechanisms.....	13
Figure 1.3:	Illustration of common BRAFi resistance mechanisms.....	18
Figure 2.1:	RhoA is activated in BRAFi-resistant melanoma cells and tumors.....	47
Figure 2.2:	Melanoma differentiation status is inversely correlated with Rho activation.....	50
Figure 2.3:	ROCK inhibition reverses BRAFi resistance in RhoA ^{High} BRAFi-resistant melanoma cells	56
Figure 2.4:	YAP1 and MRTF-A are activated in de-differentiated BRAFi-resistant cells ..	59
Figure 2.5:	De-differentiated BRAFi-resistant cells are more sensitive to dasatinib and CCG-222740	63
Figure 3.1:	Ibrutinib re-sensitizes BRAFi-resistant cells to vemurafenib	85
Figure 3.2:	BTK deletion or inhibition does not alter vemurafenib sensitivity	88
Figure 3.3:	Transcriptional response to ibrutinib treatment	91
Figure 3.4:	Ibrutinib blocks YAP1 nuclear localization	93
Figure 4.1:	Vemurafenib-resistant UACC62R cells are selectively vulnerable to pharmacological disruption of mitosis	109
Figure 4.2:	Compound-treated UACC62P, but not UACC62R, cells undergo mitotic slippage	112
Figure 4.3:	Differential CCNB1 degradation rates in UACC62P/R cells	114
Figure 4.4:	M229R cells are vulnerable to Chk1/2 inhibitors	116
Figure A-2.1:	Vemurafenib resistant cells are more sensitive to RhoA inhibition	133

Figure A-2.2:	Vemurafenib-resistant cells are more sensitive to Cytochalasin D	134
Figure A-2.3:	Genes involved in small GTPase signaling and the actin cytoskeleton are associated with BRAFi resistance.....	135
Figure A-2.4:	Expression of RhoA/C target genes is inversely correlated with PLX4720 sensitivity	136
Figure A-2.5:	A subset of drug-resistant human melanoma tumors have increased expression of RhoA/C target genes	137
Figure A-2.6:	ERK reactivation in BRAFi-resistant cell lines	138
Figure A-2.7:	A RhoA/C signature and a Melanocyte Lineage signature are inversely correlated in BRAFi-treated tumors.....	139
Figure A-2.8:	Sox9 is upregulated and Sox10 is downregulated in RhoA ^{High} BRAFi-resistant cells	140
Figure A-2.9:	EGFR is activated in vemurafenib-resistant cells but erlotinib treatment does not alter stress fiber formation	141
Figure A-2.10:	Correlation between melanocyte identity and tumor purity	142
Figure A-2.11:	ROCK inhibitors prevent stress fiber formation in M229R cells	143
Figure A-2.12:	Single agent response curves for fasudil and Y-27632.....	144
Figure A-2.13:	Expression of MRTF/YAP target genes in vemurafenib-resistant cells.....	145
Figure A-2.14:	Genes associated with MRTF/YAP1-mediated gene transcription are associated with PLX4720 response.....	146
Figure A-2.15:	Increased MRTF/YAP1 signature scores in poorly differentiated human melanoma tumors.....	147
Figure A-2.16:	ROCK inhibitors reduce the nuclear accumulation of YAP1 and MRTF-A....	148
Figure A-2.17:	Single agent response curves for dasatinib and CCG-222740.....	149
Figure A-2.18:	MRTF-A or YAP1 deletion does not alter vemurafenib sensitivity	150

Figure A-2.19: MRTF-B localization is not altered in BRAFi-resistant cells.....	151
Figure A-3.1: Principal Component Analysis of resistant cell line samples and tumor tissue samples.....	152
Figure A-3.2: Drug sensitivity correlates with sRGES drug response predictions	153
Figure A-3.3: Single-agent activity of compounds identified in the computational screen	154
Figure A-3.4: A BRAFi resistance signature is inversely correlated with melanoma overall survival.....	155
Figure A-3.5: Identification of compounds that reverse a BRAFi resistance gene expression signature.....	156
Figure A-3.6: Identification of compounds which re-sensitize BRAFi-resistant cells to vemurafenib	157
Figure A-3.7: The combination of vemurafenib and ibrutinib increases the number of Annexin V-positive cells but does not alter caspase3/7 activity	158
Figure A-3.8: BTK is weakly expressed in M229P/R cells.....	159
Figure A-3.9: Quantification of BTK knockout efficiency	160
Figure A-3.10: Differential gene expression networks are associated with developmental gene signatures	161
Figure A-3.11: Expression of ibrutinib targets in M229P/R cells	162
Figure A-3.12: Aromatase inhibitors do not alter BRAFi sensitivity.....	163
Figure A-3.13: Ibrutinib does not alter TAZ localization in BRAFi-resistant cells.....	164
Figure A-3.14: Skin cancer cell lines are not sensitive to single agent ibrutinib treatment	165
Figure A-4.1: AURK, PLK, and Tubulin inhibitors do not synergize with vemurafenib in UACC62P/R cells	166
Figure A-4.2: Identification of compound classes which are selective for BRAFi-resistant cells	167

Figure A-4.3:	ROS production is not altered in BRAFi-resistant cells	168
Figure A-4.4:	p- γ H2AX staining is not altered in compound-treated UACC62P/R cells.....	169
Figure A-4.5:	TNF α does not alter AURK, PLK, Tubulin, or Chk1/2 inhibitor sensitivity ...	170
Figure A-4.6:	Chk1/2 inhibitors do not synergize with vemurafenib in M229P/R cells.....	171

KEY TO ABBREVIATIONS

ABL	ABL Proto-Oncogene 1, Non-Receptor Tyrosine Kinase
Akt	AKT Serine/Threonine Kinase
AM	Acral Melanoma
AP-1	Activator Protein 1
APC	Anaphase Promoting Complex
ARHGEF12	Rho Guanine Nucleotide Exchange Factor 12
ARID2	AT-Rich Interaction Domain 2
AURKi	Aurora Kinase Inhibitor
AXL	AXL Receptor Tyrosine Kinase
B7	CD80 Molecule
BCL-xL	BCL2 Like 1
BCR	CR Activator Of RhoGEF And GTPase
BIM	Bcl-2-like protein 11
BRAF	Proto-Oncogene B-Raf
BRAF _i	Proto-Oncogene B-Raf Inhibitor
BRCA	Breast Cancer Type 1 Susceptibility Protein
BTK	Burton Tyrosine Kinase

CCLC	Cancer Cell Line Encyclopedia
CCNB1	Cyclin B1
CD40	CD40 Molecule
CD8	CD8 Molecule
CDKN2A	Cyclin Dependent Kinase Inhibitor 2A
Chk1/2i	Checkpoint Kinase 1/2 Inhibitor
CM	Cutaneous Melanoma
CMap	Connectivity Map
c-Met	MET Proto-Oncogene, Receptor Tyrosine Kinase
CML	Chronic myeloid leukemia
CNS	Central Nervous System
COT	Mitogen-Activated Protein Kinase Kinase Kinase 8
CRAF	proto-oncogene c-RAF
CRISPR	Clustered Regularly Interspaced Short Palindromic Repeats
CTD2	Cancer Target Discovery and Development
CTLA-4	Cytotoxic T-Lymphocyte Associated Protein 4
CTRPv2	Cancer Therapeutics Response Portal version 2
CytoD	Cytochalasin D

DAPI	4',6-diamidino-2-phenylindole
DCT	Dophachrome Tautomerase
DEVD-AFC	N-acetyl-L- α -aspartyl-L- α -glutamyl-L-valyl-N-[2-oxo-4-(trifluoromethyl)-2H-1-benzopyran-7-yl]-L- α -asparagine
DFG	BRAF DFG Motif
Dia2	Diaphanous Related Formin 2
DUSP	Dual Specificity Phosphatase
EGFP	Enhanced Green Fluorescent Protein
EGFR	Epidermal Growth Factor Receptor
ERBB2	Erb-B2 Receptor Tyrosine Kinase 2
ERK1/2	Mitogen-Activated Protein Kinase 1/2
ETS	ETS Proto-Oncogene 1, Transcription Factor
FGFR	Fibroblast Growth Factor Receptor
GAP	GTPase-accelerating protein
GAPDH	Glyceraldehyde-3-Phosphate Dehydrogenase
GDSC	Genomics of Drug Sensitivity in Cancer
GEF	Guanine nucleotide exchange factor
GEMM	Genetically Engineered Mouse Model
GNA11	G Protein Subunit Alpha 11

GNA11	G Protein Subunit Alpha 11
GNAQ	G Protein Subunit Alpha Q
GPCR	G Protein Coupled Receptor
GSEA	Gene Set Enrichment Analysis
GWAS	Genome-Wide Association Study
H2A	Histone 2A
H2AX	H2A.X Variant Histone
HGF	Hepatocyte Growth Factor
HLA	Human Leukocyte Antigen
HRP	Horseradish peroxidase
IDH1	Icocitrate Dehydrogenase 1
IDO	Indoleamine 2,3-Dioxygenase 1
IGF-1R	Insulin Like Growth Factor 1 Receptor
IL-2	Interleukin 2
INF γ	Interferon Gamma
KIT	KIT Proto-Oncogene, Receptor Tyrosine Kinase
LAG-3	Lymphocyte Activating 3
LATS1	Large Tumor Suppressor Kinase 1

LATS2	Large Tumor Suppressor Kinase 2
LCK	LCK Proto-Oncogene, Src Family Tyrosine Kinase
LINCS	The Library of Integrated Network-Based Cellular Signatures
L-NMMA	N5-[imino(methylamino)methyl]-L-ornithine, citrate
MAGIC	Markov Affinity-based Graph Imputation of Cells
MAP3K	Mitogen Activated Protein Kinase Kinase Kinase
MAPK	Mitogen Activated Protein Kinase
MAPKi	Mitogen Activated Protein Kinase Inhibitor
MBS	Moebius Syndrome
MC1R	Melanocortin 1 Receptor
MDSC	Myeloid-derived suppressor cell
MEK1/2	Mitogen-Activated Protein Kinase Kinase 1/2
MIPE	Mechanism Interrogation Plate
MITF	Melanocyte Inducing Transcription Factor
MLANA	Melanoma Antigen Recognized By T-Cells 1
MLC	Myosin Light Chain
MLK	Mixed Lineage Kinase
MM	Mucosal Melanoma

MRTF-A	Myocardin-related transcription factor A
MYC	MYC Proto-Oncogene, BHLH Transcription Factor
NF1	Neurofibromin 1
NF κ B	Nuclear Factor kappa-light-chain-enhancer of activated B cells
NGFR	Nerve Growth Factor Receptor
NOTCH	Notch Receptor 1
NRAS	Neuroblastoma RAS Viral Oncogene Homolog
NRF2	Nuclear Factor, Erythroid 2 Like 2
ORF	Open Reading Frame
p27	Cyclin Dependent Kinase Inhibitor 1B
PARP	Poly(ADP-Ribose) Polymerase
PCR	Polymerase Chain Reaction
PD-1	Programmed Cell Death 1
PDGFR β	Platelet Derived Growth Factor Receptor Beta
PD-L2	Programmed Cell Death 1 Ligand 2
PDX	Patient Derived Xenograft
PI3K	Phosphatidylinositol-4,5-Bisphosphate 3-Kinase
PLKi	Polo Like Kinase inhibitor

PRISM	Profiling Relative Inhibition Simultaneously in Mixtures
PTEN	Phosphatase And Tensin Homolog
PTPN11	Protein Tyrosine Phosphatase Non-Receptor Type 11
Rac1	Rac Family Small GTPase 1
RASA1	RAS P21 Protein Activator 1
RasGAP	Ras GTPase-activating Protein
RB1	RB Transcriptional Corepressor 1
RhoA	Ras Homolog Family Member A
RhoB	Ras Homolog Family Member B
RhoC	Ras Homolog Family Member C
RND3	Rho Family GTPase 3
ROCK	Rho-Associated Protein Kinase 1
ROS	Reactive Oxygen Species
RTK	Receptor Tyrosine Kinase
SFK	SRC Family Kinase
SKCM	Skin Cutaneous Melanoma
SNP	Single Nucleotide Polymorphism
SOS1	SOS Ras/Rac Guanine Nucleotide Exchange Factor

SOX10	SRY-Box Transcription Factor 10
SOX9	SRY-Box Transcription Factor 9
Src	SRC Proto-Oncogene, Non-Receptor Tyrosine Kinase
SRF	Serum Response Factor
STR	Short Tandem Repeat
TAZ	WW Domain Containing Transcription Regulator 1
TCGA	The Cancer genome Atlas
TEAD	TEA Domain Transcription Factor
TERT	Telomerase Reverse Transcriptase
TGF β	Transforming growth factor beta
TGF β 1	Transforming Growth Factor Beta 1
TIDE	Tracking of Indels by Decomposition
TLR	Toll-like Receptor
TP53	Tumor Protein P53
TPM	Transcripts Per Million
TUBA1B	Tubulin Alpha 1b
TWT	Triple-Wildtype
TYR	Tyrosinase

TYRP1	Tyrosinase Related Protein 1
UM	Uveal Melanoma
UV	Ultraviolet
VEGFR-1	Vascular Endothelial Growth Factor Receptor 1
WNT	WNT Family Member 1
YAP1	Yes-associated Protein 1
YES1	YES Proto-Oncogene 1, Src Family Tyrosine Kinase

CHAPTER 1:
Introduction

Despite the progress made in the development of new therapeutic approaches for treating cancer, it remains the second leading cause of death in the United States. One obstacle virtually all targeted cancer therapies face is that tumors evolve to develop drug resistance. This can occur through alterations to the tumor genome or epigenome or adaptive responses in gene transcription, protein translation, or protein activation states. Cancer cell non-autonomous interaction/crosstalk with the tumor microenvironment also plays a role in the development of drug resistance. Inter- and intra-tumor heterogeneity further exacerbates resistance since not all tumors, or cells within an individual tumor, will respond uniformly to a drug. This may result in selection for and expansion of pre-resistant cellular clones within a tumor. In this dissertation, I discuss the molecular mechanisms of melanoma drug resistance and identify pharmacological vulnerabilities of drug-resistant melanoma cells. The goal of this research is to reveal new potential therapeutic approaches to treat drug-resistant tumors or prevent the development of drug resistance outright.

Etiology of Skin Cutaneous Melanoma

Skin cutaneous melanoma (SKCM) is the 5th most common cancer type in the United States and resulted in over 7,000 deaths in 2019. The primary environmental risk factor for the development of SKCM is ultraviolet (UV) light exposure, which results in C-to-T transitions in DNA. Indeed, C-to-T mutations represent over 80% of the total somatic mutation burden in most SKCM tumors¹. This results in SKCM having the highest somatic mutation rate among most major cancer types¹⁻³. Mutations in *BRAF*, *NRAS*, or *NFI* form the basis for classification of SKCM tumors into 4 different subtypes, although differences in these subtypes are not reflected in the gene expression profiles of SKCM tumors¹.

Approximately a quarter of all melanoma tumors arise from pre-existing nevi and the remainder of melanomas arise from areas of otherwise normal skin⁴. Most nevi remain benign and will never develop into malignant SKCM even though many of these nevi harbor the most common SKCM driver mutation, *BRAF*^{V600E}⁵. Benign nevi, however, may gradually accumulate point mutations, which generally harbor a UV-induced mutational signature⁵. Eventually the lesion may develop additional genomic alterations, most commonly including alterations in the *TERT* promoter, *CDKN2A*, or *SWI/SNF* subunits, which promote development into invasive SKCM⁵. After invasive SKCM develops, tumors typically acquire additional copy number alterations, including whole genome doubling in approximately 40% of cases often followed by distant organ metastasis^{5,6}. Since most mutations in metastatic SKCM tumors are shared between the primary and metastatic tumors, it further supports the idea that metastatic divergence is a late event during disease progression⁶.

The 5-year survival rates for localized melanomas are approximately 99% and are typically resolved surgically; this survival rate drops to 25% in patients with distant metastases. The most common metastatic sites for SKCM include lung, brain, liver, and bone⁷. Breslow skin thickness⁸ is the most important factor in differentiating between tumors which metastasize and those that do not since thicker tumors are likely further along in disease progression⁹⁻¹¹. In SKCM, much like in many other cancer types, most deaths are caused by metastatic disease rather than by the primary tumor. Consistent with this, the goal of targeted therapies such as inhibitors of the MAPK pathway or immunotherapy is to treat metastatic tumors, rather than primary tumors.

While this dissertation focuses cutaneous melanoma, there are other subtypes of melanoma which emerge from different tissues. Acral melanoma arises from skin on the palms, soles of the feet, and nail beds; mucosal melanoma arises from the mucosal lining of internal tissues including the mouth and nose; and uveal melanoma develops from cells in the uveal tract of the eye¹². While all forms of melanoma arise from melanocytes, the genetics of each melanoma subtype differs. The subtype with the most divergent genetic underpinning is uveal melanoma since virtually all uveal melanoma tumors lack *BRAF*, *NRAS*, and *NFI* mutations^{13,14}. Instead, nearly 100% of uveal melanoma tumors have recurrent point mutations in the G_{alpha} subunits *GNAQ* and *GNA11*, and the majority of metastatic uveal melanoma tumors have *BAP1* loss^{13,14}. These mutations render the G proteins encoded by *GNAQ* and *GNA11* constitutively active and promote tumor growth by activating YAP1-mediated gene transcription^{15,16}. The genetics of acral melanoma and mucosal melanoma tumors are more similar to cutaneous melanoma tumors, since a subset of acral melanoma and mucosal melanoma tumors harbor activating mutations in *BRAF*, *NRAS*, and *NFI*¹⁷. Another hallmark of acral melanoma and mucosal melanoma tumors is an increased prevalence of mutations or copy number gains in *KIT*, which encodes a receptor tyrosine kinase^{17,18}.

SKCM cell of origin

The cell of origin for all melanomas is the melanocyte, which is a neural crest-derived melanin-producing cell. Like melanocytes, most SKCM tumors retain the ability to synthesize melanin and are pigmented¹⁹. These well-differentiated tumors express a suite of lineage-defining genes including *DCT*, *TYR*, *TYRP1*, *MC1R*, *SOX10*, and *MITF*; all of these genes are critical in melanin biosynthesis^{1,20}. *SOX10* and *MITF* are two central melanocyte lineage transcription factors that coordinate melanin production and both genes are critical for the growth and survival

of melanoma cells. When SKCM tumors are clustered by gene expression, a subset of tumors is characterized by high expression of MITF target genes¹. Consistent with the role of MITF in melanocyte biology, tumors with high expression of MITF target genes are more pigmented. Interestingly, there is a cluster of tumors which is characterized by low expression of MITF target genes. These tumors have low levels of pigmentation and have elevated expression of genes which are associated with neuronal development or are nerve-specific. Since melanocytes are derived from neuronal precursor cells, these data suggest that a subset of poorly pigmented SKCM tumors are de-differentiated. A genome-wide association study (GWAS) meta-analysis of risk factors for the development of melanoma identified single nucleotide polymorphisms (SNPs) in multiple melanocyte lineage genes, including *TYR* and *MC1R*²¹. These data suggest that both germline and tumor-specific alterations in the melanin biosynthetic pathway contribute to melanoma biology.

Genetic drivers of SKCM

As discussed earlier, over 90% of SKCM tumors harbor mutations in *BRAF*, *NRAS*, or *NF1*. These mutations are almost always mutually exclusive of one another¹. The presence of these mutations does not have an influence on how SKCM tumors cluster in gene expression space, and this is likely because mutations any of these genes results in hyperactivation of the ERK/MAPK pathway. Hyperactivation of the ERK/MAPK pathway is not unique to melanoma and is found in other tumor types at a high frequency²²⁻²⁵. The ERK/MAPK pathway is classically thought of as a linear pathway wherein an extracellular signal is relayed in a stepwise signaling cascade of RAS → RAF → MEK → ERK to modulate expression or post-translational modification of nuclear substrates like Cyclin D1 and p27^{kip1} ultimately promoting entry into the cell cycle. While this model provides a reasonable overview of the function of the MAPK pathway,

it fails to capture many of the intricacies involved in this signaling mechanism. The MAPK pathway does not function merely as a relay race of proteins; rather it functions akin to a complex 3-dimensional machine that includes auxiliary proteins that positively and negatively influence ERK/MAPK pathway activation (reviewed in²⁶). Under physiological conditions this affords the cell precise temporal control over ERK/MAPK pathway activation and ultimately entry into the cell cycle. Certain point mutations in *BRAF* and *NRAS* render these proteins constitutively active and unresponsive to negative feedback mechanisms. One such negative feedback mechanism is provided through the Ras GTPase Activating Protein (GAP) NF1, which itself is inactivated in a subset of SKCM tumors¹. Through its function as a RasGAP, NF1 accelerates NRAS GTP hydrolysis, thus preventing activation of the ERK/MAPK pathway²⁷. This section will discuss the genetic drivers of SKCM, with a focus on the MAPK pathway.

BRAF

The most frequent point mutation in SKCM tumors is in the codon encoding V600 of BRAF and is found in approximately 60% of SKCM tumors. The BRAF^{V600E} variant is approximately 700-fold more active than BRAF^{WT}²⁸. BRAF V600 is located within the activation loop which forms a strong hydrophobic intramolecular interaction with the P-loop, holding the kinase in an inactive conformation²⁹. Phosphorylation of the P-loop induces a structural rearrangement in BRAF which causes the conserved DFG motif to move out of the ATP binding site allowing ATP to bind and BRAF to phosphorylate its substrate, MEK. The BRAF^{V600E} mutation mimics the effect of phosphorylation since it introduces a charge into the P-loop, rendering BRAF constitutively active. Some BRAF inhibitors, such as vemurafenib, preferentially bind to

BRAF^{V600E} since these inhibitors selectively bind to the ATP binding site when BRAF is in an activated conformation²⁹⁻³¹.

NRAS

Approximately 25% of SKCM tumors have *NRAS* mutations¹. *NRAS*-mutant tumors generally have a worse prognosis than *BRAF*-mutant tumors, even before the wide-spread clinical adoption of BRAF inhibitors³². *NRAS*-mutant tumors generally have a higher mutational burden compared to *BRAF*-mutant tumors, which may explain the poorer overall survival in these tumors^{1,32}. The most common *NRAS* variant found in melanoma tumors is in *NRAS*^{Q61}. These variants undergo rapid nucleotide exchange and have impaired GTP hydrolysis, which renders the protein constitutively active³³. *NRAS*, like most GTPases, is difficult to target pharmacologically and there are no FDA-approved *NRAS* inhibitors.

NF1

Approximately 10% of SKCM tumors harbor mutations in the *NF1* gene. Unlike *BRAF* and *NRAS*, pathological *NF1* mutations are inactivating and there is a high frequency of frameshift mutations. Mutations in *NF1* are spread throughout the gene instead of at point mutation hotspots¹. *NF1* is a Ras GAP, which accelerates *NRAS* GTP hydrolysis^{27,34}. Loss of *NF1*, either through mutation or chromosomal deletion, increases *NRAS* activation. Among all SKCM subtypes, *NF1* mutant tumors have the highest mutation burden and patients diagnosed with these tumors are generally older. *NF1* mutations also significantly co-occur with additional RASopathy genes including *RASA1*, *RASA1*, *PTPN11*, and *SOS1*^{3,35}.

Triple-WT

The remaining subset of tumors which lack *BRAF*, *NRAS*, and *NFI* mutations fall into the final subclass of Triple-WT (TWT) tumors. These tumors are atypical when compared to the other three subclasses since on average the mutation burden in these tumors is much lower and only ~30% of these tumors display a UV mutation signature^{1,36}. Since most TWT tumors lack a UV-induced mutation signature it suggests that the initiating events for this class of tumors may be different from the other three subclasses of SKCM tumors. The genetic drivers in this class of tumors are unclear, although a subset of these tumors harbor *KIT* mutations and have more complex DNA structural rearrangements and copy number alterations^{1,37}.

Other mechanisms of ERK/MAPK activation

It is clear from the genetic evidence that MAPK pathway activation is a common driving feature of SKCM. In addition to alterations in *BRAF*, *NRAS*, and *NFI* there are other mechanisms by which the MAPK pathway can be aberrantly activated in SKCM. These auxiliary means of MAPK pathway activation were often first identified in drug-resistant melanoma cells. This is likely because *BRAF* and *NRAS* are such powerful activators of the MAPK pathway that these more subtle mechanisms only become readily apparent in the absence of these driver oncogenes, or in response to these driver oncogenes becoming inactivated. Activation of cell surface receptors including *AXL*, *ERBB2*, *PDGFR β* , and *IGF-1R* stimulates the ERK/MAPK pathway in melanoma cells either through upregulation of the receptor or through increased levels of the secreted ligand for the receptor³⁸⁻⁴⁰. Other signaling inputs such as activating *Rac1* mutations⁴¹, *MLK* activation⁴², or *COT* overexpression⁴³ can activate the ERK/MAPK pathway, especially in the presence of *BRAF* inhibitors. Downregulation or inactivation of proteins that negatively regulate ERK/MAPK

pathway activation, including dual specific phosphatases (DUSPs), also promotes MAPK pathway activation⁴⁴.

Non-MAPK driver mutations

Owing to the high mutational burden in most SKCM tumors, there is a diversity of functional mutations and genomic alterations in most SKCM tumors. These mutations are not mutually exclusive with *BRAF*, *NRAS*, and *NFI* mutations. Some of these mutations, for example in TP53, occur later in tumor development and likely contribute to genomic instability in advanced tumors^{1,5,6}. Several recurrently mutated genes in melanoma, including *CDKN2A*, *PTEN*, and *RBI*, are involved in G1 cell cycle progression¹. Since ERK/MAPK pathway activation promotes G1 progression, these mutations may mimic the transcriptional effect of MAPK pathway activation, especially in cells treated with ERK/MAPK pathway inhibitors. Another cluster of mutated genes is the epigenetic modulators, such as *IDH1* and *ARID2*. Other potentially pathogenic mutations have been identified⁴⁵, but more work will be needed in order to fully understand the true mutational landscape of SKCM tumors.

Rho GTPases and RhoA-mediated gene transcription

Various oncogenic signaling pathways are activated in SKCM cells and tumors through non-mutational mechanisms. These pathways, such as WNT⁴⁶, MYC⁴⁷, TGF β ⁴⁸, NRF2⁴⁹, PI3K⁵⁰, NOTCH⁵¹, and the Rho GTPases, are generally important in cancer cells⁵². and SKCM cells are no exception. The signaling mechanisms of Rho GTPases, particularly the RhoA subfamily, and their effector pathways, are examined in detail in this dissertation (Figure 1.1). The RhoA subfamily of GTPases consists of RhoA, RhoB, and RhoC⁵³; herein this subfamily will be referred

to as RhoA. These three GTPases have a high degree of homology and signal similarly in many contexts⁵³. Upstream activators, such as GPCR-mediated G_{12/13} activation, promote nucleotide exchange and allow cycling from a GDP-bound (inactive) state to a GTP-bound (active state)^{54,55}. Nucleotide exchange is facilitated by various guanine nucleotide exchange factors (GEFs) and because the cytosolic GTP/GDP ratio is approximately 10:1⁵⁵, GEFs generally activate RhoA. The intrinsic GTPase activity of RhoA can be accelerated by various GTPase-activating proteins (GAPs), resulting in inactivation of RhoA⁵⁵. Mutations in RhoA, RhoA GEFs, or RhoA GAPs are uncommon in SKCM tumors, indicating that aberrant RhoA activity is controlled by less direct mechanisms. Most studies on RhoA in melanoma cells have characterized its role in cell migration and metastasis⁵⁶⁻⁶³. However, elevated protein expression of the RhoA isoform is associated with better overall survival in SKCM patients, which conflicts with the experimental role of RhoA in SKCM cells⁶⁴. Interestingly, in our own studies we found that high RhoC mRNA levels portend poor survival in SKCM patients⁶⁵, however it's unclear whether this finding also extends to protein levels.

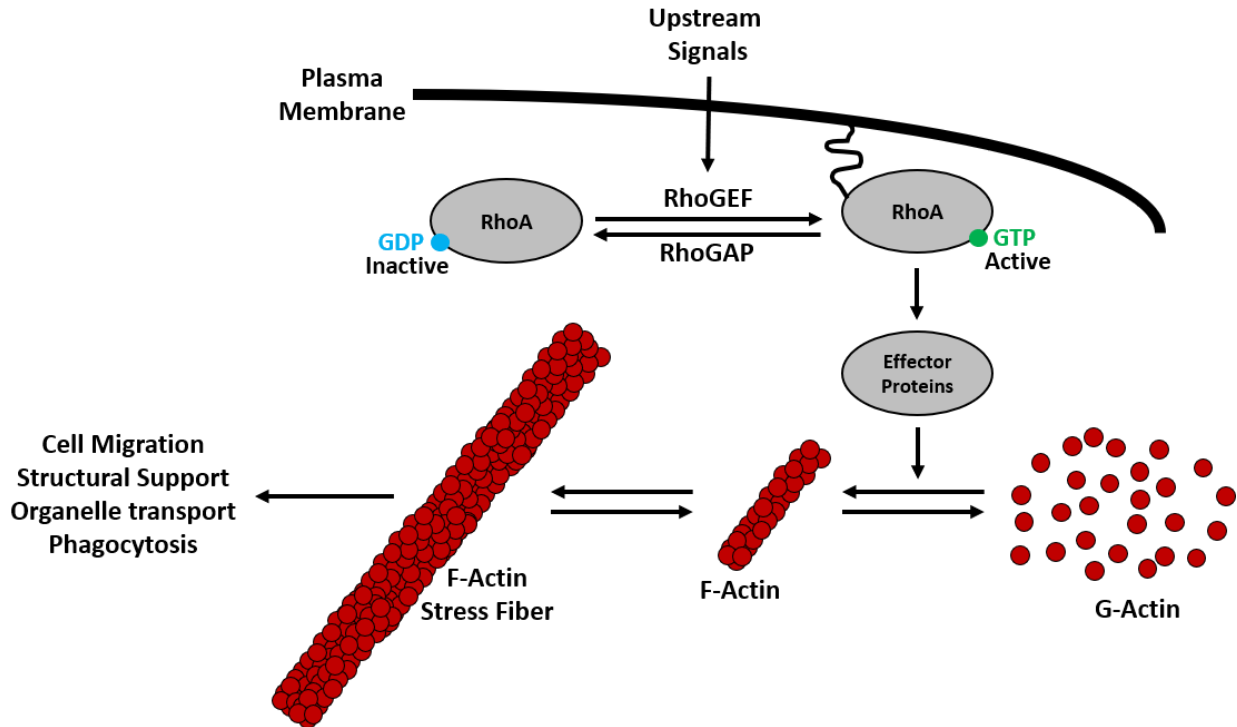


Figure 1.1: Illustration of the RhoA pathway.

Activation of RhoA catalyzes the polymerization of monomeric G-actin into F-actin polymers through various effector proteins including Diaphanous Related Formin 2 (Dia2), Moebius Syndrome 1 (MBS), and Rho Associated Coiled-Coil Containing Protein Kinase (ROCK). F-actin fibers are bundled into larger actin stress fibers which form a complex with focal adhesions⁶⁶. By modulating F-actin polymerization, RhoA also controls gene expression by regulating the activity of multiple transcriptional co-activators and transcription factors (Figure 1.2). Two of these transcriptional co-activators are Myocardin-Related Transcription Factor (MRTF) and YES Associated Protein 1 (YAP1). Binding of MRTF through its N-terminal RPEL domains, which are conserved RPxxxEL motifs, to G-actin monomers obscures the nuclear localization sequence, preventing MRTF nuclear translocation^{67,68}. Upon RhoA activation,

cytosolic G-actin pools are depleted, allowing for release of MRTF and translocation into the nucleus, where it can bind to transcription factors such as SRF to regulate gene transcription and histone positioning^{68,69}. In addition to this predominant mechanism of MRTF regulation, other mechanisms such as phosphorylation can also modulate MRTF activity. Like MRTF, YAP1 is also regulated by the actin cytoskeleton, but through a different mechanism. LATS1/2 phosphorylates YAP1 on S127 to promote nuclear exclusion and proteasomal degradation⁷⁰. Upon RhoA-mediated F-actin polymerization, LATS1/2 becomes inactivated. Unphosphorylated YAP1 can subsequently translocate into the nucleus, bind to TEAD-family transcription factors, and regulate gene transcription. Like RhoA, many studies on MRTF and YAP1 in melanoma have focused on characterizing their role in migration and metastasis^{63,65,71-75}. However, there are also several studies which characterized MRTF and YAP1 in BRAFi-resistant melanoma cells which will be discussed in a later section.

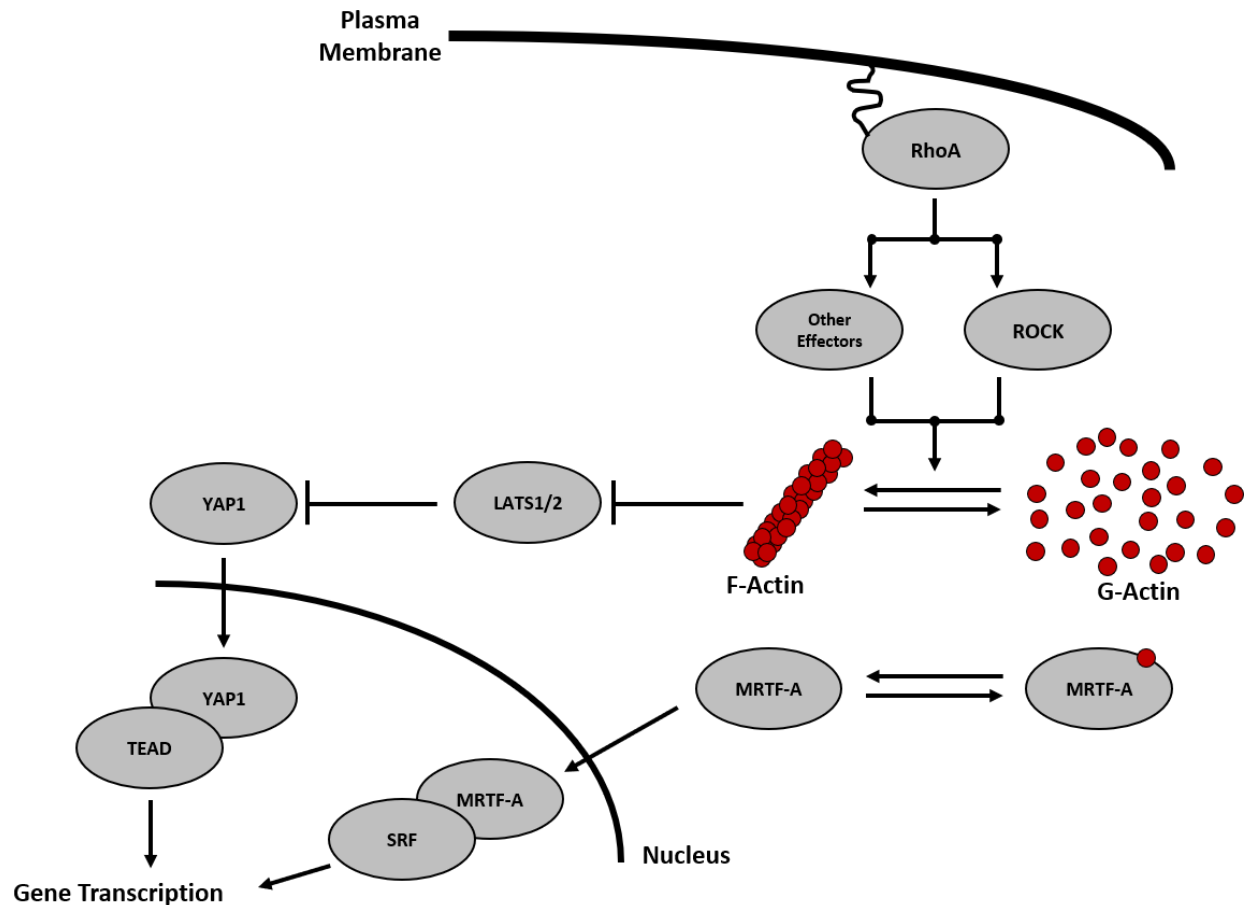


Figure 1.2: Illustration of RhoA-mediated gene transcription mechanisms

TERT

TERT is the catalytic subunit of telomerase, an RNA-dependent polymerase which controls telomere length. *TERT* promoter mutations were first identified in familial melanoma tumors and were subsequently identified at a high frequency in sporadic SKCM tumors^{76,77}. These promoter mutations create a new binding site for ETS and TCF transcription factors and which results in upregulated *TERT* expression. It was originally thought that these mutations promoted melanoma survival by increasing telomere length, however more recently a new two-stage model has been proposed to explain the function of these mutations⁷⁸. In the first stage of this model *TERT*

promoter mutations extend the lifespan of cells by repairing the shortest telomeres, and in the second stage genomic instability further upregulates TERT to sustain cellular proliferation. The presence of *TERT* promoter mutations portends a worse prognosis in SKCM patients, highlighting the clinical relevance of these mutations⁷⁹.

Therapeutic interventions for the treatment of melanoma

Most SKCM tumors that have not metastasized can be treated surgically with little risk of recurrence. Treatment with BRAF/MEK inhibitors or immunotherapy is typically only used in tumors that have metastasized. The two pillars of modern anti-melanoma therapy are small molecule targeted therapy with BRAF and MEK inhibitors, or immunotherapy with immune checkpoint inhibitors. This section will discuss the risks, benefits, and rationale behind both approaches.

MAPK inhibitors

The first FDA-approved BRAF inhibitor for the treatment of melanoma was vemurafenib (PLX4032). Vemurafenib binds to the ATP binding site of active BRAF³⁰, which forms the structural basis for its selectivity for BRAF^{V600E} mutant over BRAF^{WT} cells and tumors⁸⁰⁻⁸³. Single agent treatment with vemurafenib or the related compound dabrafenib (another mutant BRAF inhibitor) extends overall survival and progression-free survival in patients with BRAF^{V600E} metastatic SKCM^{84,85} compared to the classically used chemotherapeutic agent dacarbazine. However, resistance to single agent BRAF inhibitor therapy rapidly develops. The precise resistance mechanisms will be discussed in a later section; resistance to single agent BRAFi therapy generally occurs through secondary alterations which re-activate the ERK/MAPK

pathway. Owing to this, the paradoxical drug combination of BRAF inhibitors and low dose MEK inhibitors delays the development of drug resistance³⁹ and provides a survival benefit over single agent BRAF inhibitors^{86,87}. One additional BRAF + MEK inhibitor combination (encorafenib + binimetinib) was more recently FDA approved and has a lower toxicity profile compared to vemurafenib + cobimetinib or dabrafenib + trametinib⁸⁸. While immunotherapy (discussed later) is now the standard of care for most SKCM patients, BRAF/MEK inhibitors still retain clinical utility. In patients with severe disease burden, particularly with central nervous system metastasis, BRAFi/MEKi may be a preferred treatment strategy since it provides a more rapid and reliable response in *BRAF*-mutant tumors. Retrospective analyses of clinical data also suggests that BRAFi/MEKi retains efficacy in patients who had previously progressed on immunotherapy, so it is the preferred treatment option in this setting⁸⁹.

Immunotherapy

Administration of high dose Interleukin 2 (IL-2), which was approved by the FDA in 1998, was an early initial attempt at using immunotherapy to treat SKCM tumors. This therapeutic approach had a minor benefit but did not improve overall survival in SKCM patients⁹⁰. Later, low dose interferon treatment provided a minor benefit in extending overall survival in SKCM patients⁹¹, with the greatest benefit seen in patients with sentinel node involvement and ulcerated tumors⁹². The modern era of immunotherapy began with the approval of the Cytotoxic T-lymphocyte Associated Protein 4 (CTLA-4) neutralizing antibody, ipilimumab, in 2011. Ipilimumab extended overall survival from 6.4 months to 10 months, but approximately 20% of patients had durable responses with no disease recurrence for up to 10 years⁹³. CTLA-4 is an inhibitory receptor on T-cells which binds to B7-family proteins expressed on the surface of

antigen presenting cells. In the context of cancer this prevents immune engagement of cancer cells, and ultimately prevents immune-mediated tumor destruction⁹⁴. PD-1 is another T-cell inhibitory receptor, and treatment with PD-1 neutralizing antibodies, nivolumab or pembrolizumab, was superior to single agent therapy with ipilimumab^{95,96}. The current frontline standard of care for metastatic melanoma combines anti-CTLA-4 and anti-PD-1 neutralizing antibodies. The five-year survival data from the Checkmate 067 trial which tested the combination of nivolumab and ipilimumab was recently published and demonstrated that the combination improves overall survival to 52%, up from 26% or 44% with single agent ipilimumab or nivolumab, respectively⁹⁷. However, serious toxicity resulting in discontinuation of treatment is more common with the combination than with single agent therapy^{98,99}. Predicting which patients will respond to immune checkpoint inhibitors is difficult, and only a few biomarkers have been identified (reviewed in detail here¹⁰⁰). These biomarkers include tumor mutational burden, alterations in the HLA pathway, alterations in the IFN γ pathway, expression of ligands for T-cell inhibitory receptors, and immune cell infiltration. Yet it remains challenging to extend these correlations into the clinic.

Owing to the demonstrated vulnerability of SKCM tumors to immune-modulating therapeutics, additional immunotherapy approaches are currently under development. These approaches include neutralizing antibodies against other T-cell inhibitory receptors like LAG-3¹⁰¹, or therapies against other targets such as IDO¹⁰², CD40¹⁰³, or TLRs¹⁰⁴. Other approaches, like adoptive cell transfer are also under clinical investigation and have overall response rates comparable to immune checkpoint inhibitors¹⁰⁵.

Combination of Immunotherapy with MAPK pathway inhibitors

There are pros and cons associated with both BRAF/MEK inhibitors and immunotherapy in treating SKCM. BRAF/MEK inhibitors induce a rapid and consistent response in most *BRAF*-mutant tumors, but most patients eventually relapse. In contrast, many patients are initially resistant to immunotherapies and the effects of treatment are not as rapid, yet a fraction of patients, perhaps 15-35%, experience durable long-term responses. Combination of these treatment modalities improves efficacy in *in vivo* mouse models¹⁰⁶⁻¹⁰⁸ which provided the rationale for testing these drug combinations in patients. The combination of the BRAF inhibitor dabrafenib, the MEK inhibitor trametinib, and the anti-PD1 immunotherapeutic pembrolizumab (NCT02130466) elicited a response in 73% of patients, but the fraction of patients experiencing adverse effects during treatment was high¹⁰⁹. Other clinical trials testing these drug combinations (NCT03149029, NCT0265337, NCT02858921, NCT02130466, NCT02902042, and NCT02908672) are currently underway.

Mitogen Activated Protein Kinase inhibitor resistance

The purpose of my dissertation is to characterize mechanisms by which SKCM cells develop resistance to BRAF inhibitors and to identify new pharmacological vulnerabilities in these cells. Most commonly, SKCM drug resistance occurs due to re-activation of the MAPK pathway (Figure 1.3). However, advances in sequencing and imaging technology have enabled the discovery of a new class of differentiation-associated resistance mechanisms. In this section, I will discuss mechanisms of BRAFi/MEKi resistance and the experimental models used to study drug resistance.

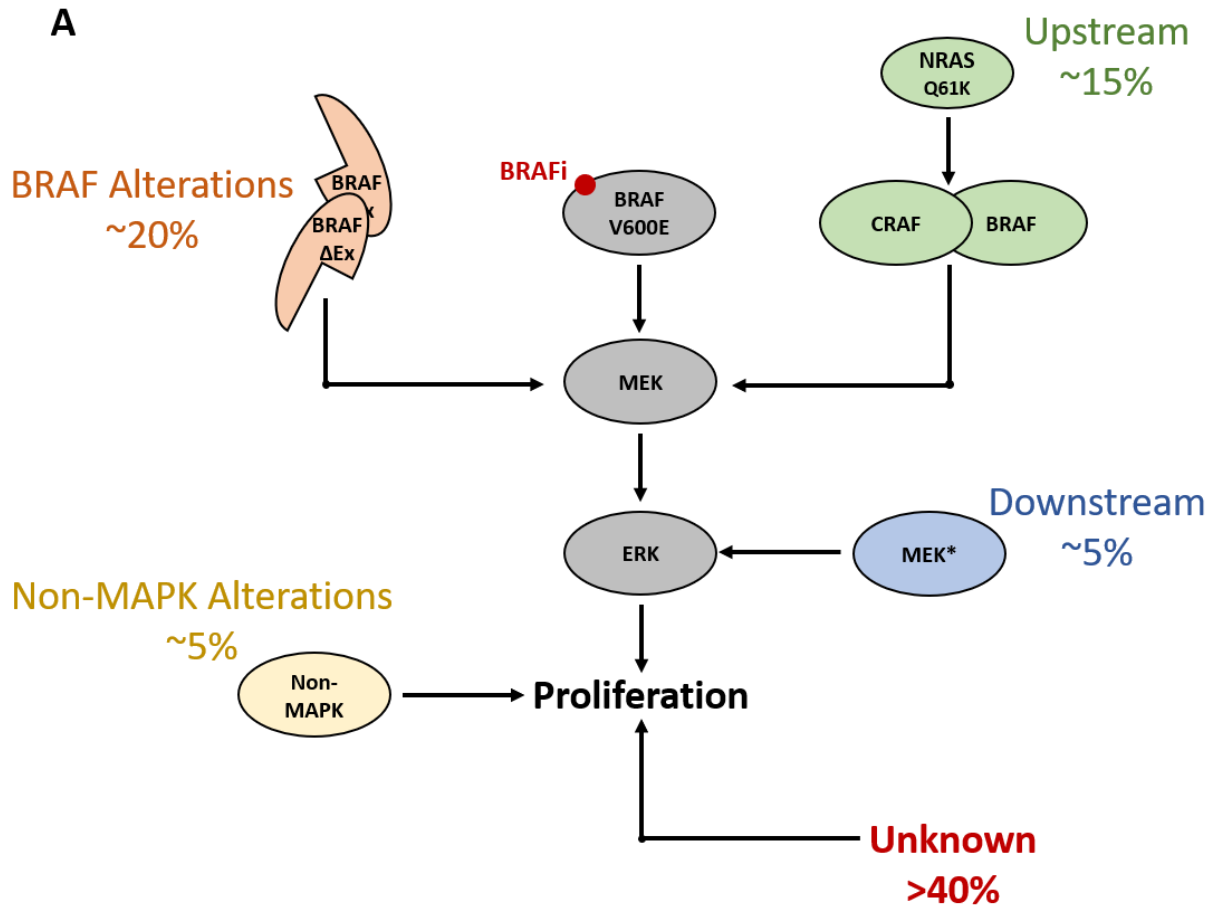


Figure 1.3: Illustration of common BRAFi resistance mechanisms.

Models of drug resistance

Drug resistance mechanisms can be characterized through a top-down approach or a bottom-up approach. In the top-down approach mechanisms of resistance are first identified in patient samples, and then further characterized *in vitro* and *in vivo*. In a bottom-up approach, drug resistance mechanisms are first characterized in experimental model systems, and then patient tumors are analyzed to determine the clinical relevance of those mechanisms. Ultimately, both methods should be used in combination. Without *in vitro* and *in vivo* experimental models,

resistance-associated mutations identified in patients can only be correlated with resistance, never causally linked. If resistance mechanisms which were initially identified experimentally cannot be identified in patient tumors, it suggests that the experimental models are inadequate, or the identified resistance mechanism may be an experimental artifact.

Most studies on MAPKi resistance utilize cell lines which are intrinsically resistant to BRAF inhibitors or MAPKi-resistant cell lines which were generated *in vitro*. Several large-scale databases including GDSC¹¹⁰, CTD^{2 111}, and PRISM^{112,113} enable the analysis of genomic correlates with BRAFi/MEKi response and resistance. All of these databases profiled hundreds or thousands of drugs and chemical compounds against hundreds of cancer cell lines. These databases can be used as discovery tools and have been useful in characterizing some drug resistance mechanisms^{50,114}. The more widely adopted method is to generate MAPKi-resistant cell lines *in vitro* and systematically profile the cell lines to determine how they developed resistance. Methods for generating BRAFi-resistant cell include gradually increasing the BRAFi in culture until resistant cells emerge or continuously culturing or pulsing cells with a high concentration of a BRAFi until resistance develops. In some cases, resistant cell lines have been established by isolating specific clones which developed drug resistance. It is unclear which of these methods is superior since there have been no large-scale comparative studies, nor has there been a study which characterizes how well each method mimics the clinical spectrum of resistance mechanisms. What we can say is that there is a high degree of inter-laboratory inconsistency in the development of BRAFi-resistant cells. The most frequently utilized melanoma cell line to study BRAFi resistance is A375, and at least 18 laboratories have independently developed BRAFi-resistant variants of this human cell line¹¹⁵. While these studies have generally found that the MAPK pathway is re-

activated, the mechanism was different in almost all of the studies. Different culture conditions in each laboratory or divergent evolution of cancer cell lines¹¹⁶ would likely lead to the selection of different subclones during drug selection. This serves as an illustrative example of some of the challenges faced with reproducibility when studying drug resistance.

High throughput screens can be performed on drug resistant cell lines to identify the landscape of genes and mutations which cause MAPKi resistance. In some cases, libraries of open reading frames are expressed in melanoma cells to identify genes that *can* promote resistance to BRAF inhibitors⁴³. Other screens have used CRISPR deletion to systematically profile the landscape of genes that are essential for BRAFi resistance. This latter approach was initially used to find genes which can sensitize cells to BRAF inhibitors¹¹⁷ and was more recently applied to identify genes which are essential for resistance in experimental models of acquired BRAFi resistance¹¹⁸. Similar screens have been used to characterize non-coding genomic regions which can modulate BRAFi resistance¹¹⁹. Finally, saturation mutagenesis screens in known resistance genes¹²⁰⁻¹²² have been used to define the landscape of mutations which can confer resistance. This mutation scanning approach is exciting since it can serve as reference map for mutations identified in human tumors.

Genetically engineered mouse models (GEMMs) and patient-derived xenograft (PDX) models have also been utilized to generate a wealth of information on MAPKi resistance. Multiple SKCM GEMM strains have been used to study MAPKi resistance¹²³⁻¹²⁵. Most commonly, these strains are driven by melanocyte-specific inducible BRAF^{V600E} expression in combination with deletion of SKCM tumor suppressors like *PTEN* and *CDKN2A*. One benefit to using GEMMs to

study melanoma is that the inducing agent can be applied topically to a specific region allowing for tighter control of orthotopic tumor formation. GEMMs also allow for the preclinical studies of immunotherapy and MAPKi combination therapies or for deciphering the interplay between tumor-infiltrating lymphocytes (TILs) and MAPKi response. One downside to this approach is that these models typically lack the high mutational burden that is found in most human SKCM tumors, which may limit the types of resistance mechanisms that can be identified. To circumvent this problem hundreds of PDX models have been established from human SKCM tumors¹²⁶. A subset of these PDX lines were established from tumors which developed clinical resistance to MAPKi therapy and a fraction of these MAPKi-resistant PDX lines have a matched pre-treatment PDX line. These models capture the complexity of human SKCM tumors on the genomic level and provide reproducible models for evaluating clinically relevant MAPKi resistance mechanisms. Ideally, new experimental drug combinations should be tested against a panel of these PDX models to partially mimic the inter-tumor heterogeneity of human SKCM tumors. Other elegant studies have used PDX models to study how tumors evolve when treated with MAPKi¹²⁷. The drawback of using PDX models is that it is throughput limited and they require the use of immunocompromised mice or very expensive humanized mice.

Putative resistance drivers have been successfully identified with next generation sequencing of pre- and post-resistance tumor tissue¹²⁸⁻¹³⁰. This approach was successful in identifying resistance-associated genomic alterations, although without rigorous validation studies these results are difficult to interpret. For each tumor pair, numerous resistance-associated mutations were identified. However, some mutations are likely due to differences in sampling location. In addition, most identified mutations are silent passenger mutations which were enriched

for during drug treatment. Another limitation of these studies is that they were all performed on relatively low numbers of tumor samples, far below the number necessary to identify most recurrent mutations. Thus, while the sequencing is unbiased, identification of resistance mutations requires prior knowledge of the molecular mechanisms of drug resistance. Whole exome sequencing is limited to identifying mutations, copy number alterations, and structural rearrangements so this approach invariably results in an under-representation of the spectrum of resistance-associated alterations in human SKCM tumors. To circumvent this problem there have been several studies which have characterized BRAFi-resistant tumors on the transcriptional and epigenetic levels. One of these studies profiled the genome, transcriptome, and methylome of matched pre- and post-resistance tumors¹³¹ and identified several novel transcription-associated resistance mechanisms in addition to re-identifying many resistance mechanisms which were previously characterized in human SKCM tumors. Recent advances in single cell sequencing now enable us to characterize the spectrum of resistance mechanisms in human tumors on a single cell level¹³²⁻¹³⁴.

Mechanisms of MAPKi resistance

The most common class of BRAFi resistance mechanisms involve re-activation the ERK/MAPK pathway¹³⁵. Owing to this discovery, the paradoxical combination of BRAFi/MEKi is now clinically preferred over single agent BRAFi therapy since the addition of low dose MEKi delays the development of drug resistance. However, dose limiting toxicity prevents dosing at levels necessary to block all MAPK-reactivating resistance mechanisms. Also, re-activation of the MAPK pathway has been demonstrated to occur at multiple levels which may or may not be sensitive to MEKi.

Receptor Tyrosine Kinase

In response to MAPK inhibitors, cells can re-activate the MAPK pathway by elevating receptor tyrosine kinase (RTK) activity. Secretion of RTK ligands, such as HGF, renders SKCM cells resistant to BRAF inhibitors⁴⁰. This finding demonstrates that BRAFi resistance can emerge through cancer cell non-autonomous mechanisms (discussed later) as well as through cancer cell autonomous autocrine and paracrine signaling. Upregulation of c-Met, the receptor for HGF, was found at both the mRNA and the protein levels in approximately 40% of patients with acquired MAPKi resistance¹³¹. In addition, this study demonstrated that upregulation of c-Met drives acquired MAPKi resistance. Resistance can also arise through activation of other RTKs including IGF-1R³⁹, FGFR^{136,137}, PDGFR β ³⁸, ERBB2⁴³, VEGFR-1¹³⁸, EGFR^{136,139,140}, and AXL. EGFR and AXL are especially interesting since a subpopulation of intrinsically BRAFi-resistant cells (discussed later) is partially defined by high expression of these proteins^{114,132,141,142}. One general observation from these data is that SKCM cells do not rely on activation of a single RTK in the development of resistance. This is in contrast to what is found in lung cancer cells which develop secondary and tertiary mutations in EGFR in response to treatment with EGFR inhibitors¹⁴³⁻¹⁴⁵. Instead, melanoma cells appear to utilize a variety of methods to reactivate the MAPK pathway. Feedback activation of RTKs also activates other oncogenic pathways like PI3K/Akt in addition to the MAPK pathway. To date there have been a multitude of clinical trials which combine BRAF inhibitors with various RTK inhibitors (reviewed in¹⁴⁶), though none have yielded promising results.

NRAS

During BRAFi administration in BRAF-mutant cell lines and tumors, rare cellular clones with activating NRAS mutations are selected which eventually can become the dominant clone that permits BRAFi-resistant tumor growth. In an initial study, NRAS mutations were identified a limited number of patient samples as well as in a SKCM cell line with *in vitro*-derived BRAFi resistance³⁸. This finding was subsequently validated in larger cohorts of patients with BRAFi-resistant tumors^{128,147}. One confusing observation is that cells which developed NRAS mutations were insensitive to a BRAF inhibitor, even though NRAS signals upstream of BRAF. This is because NRAS-mutant BRAFi-resistant cells depend on CRAF, rather than BRAF, for MAPK pathway re-activation^{148,149}. In this context, BRAF inhibition will lead to CRAF-BRAF heterodimers. This results in a partially active heterodimer wherein BRAF is inactivated and CRAF is activated resulting in downstream MEK activation.

RAF

Alterations in RAF isoforms other than BRAF can be sufficient to drive BRAFi resistance and alterations in the BRAF^{V600E} allele itself have the potential to confer BRAFi resistance. For instance, amplification of the BRAF^{V600E} allele was detected in patients who developed BRAFi resistance¹³⁰. Cells with BRAF^{V600E} amplification are still responsive to vemurafenib but compared to cells without BRAF^{V600E} amplification at least 10 times higher concentrations of vemurafenib are required to fully inhibit ERK phosphorylation¹³⁰. While in lung cancer resistance to EGFR inhibitors frequently develops through acquisition of gatekeeper mutations which prevent drug binding, analogous gatekeeper mutations are not found in BRAF-mutant melanoma resistance. However, additional structural changes in BRAF can lead to aberrant dimerization and activation.

In a subset of SKCM patients, exons 4-8 are spliced out of BRAF^{V600E} resulting in a truncated 61-kDa splice variant¹⁵⁰. The exon 4-8 fragment contains the RAS binding domain and its deletion results in a truncated variant of BRAF^{V600E} which can dimerize and become activated independent of RAS binding.

BRAF-independent MEK activation

Activation of the MAPK pathway downstream of BRAF has also been implicated in BRAFi resistance. The most common of these mechanisms is acquisition of MEK1/2 mutations. Several large-scale studies of patient tumors have identified activating MEK mutations in BRAFi-resistant tumors^{38,122,128}. These MEK mutations confer resistance to both BRAF and MEK inhibitors. While these mutations are distributed along the linear sequence of the protein, they are all clustered near the ATP-binding site in the 3-dimensional structure. Independent of an activating MEK mutation, expression or mutation of other genes can drive aberrant MEK activation in the absence of active BRAF signaling. Recurrent *RAC1*^{P29S/L} mutations were identified in 4-9% of SKCM tumors in several large sequencing cohorts^{2,3,128}, although it is still unclear whether these mutations are selected for during BRAFi therapy in patients. An initial study found that cells with *RAC*^{P29S} mutations are resistant to both BRAF and MEK inhibitors and partially prevent dabrafenib-induced MEK inhibition⁴¹. These initial findings were subsequently expanded an elegant study which characterized a Rac1^{P29S}-induced mesenchymal phenotypic switch which is partially dependent on MRTF/SRF-mediated gene transcription¹⁵¹. Another study found that mixed lineage kinases (MLKs) mediate resistance to BRAF inhibitors by directly phosphorylating MEK⁴². Other mitogen activated protein kinase kinase kinases (MAP3Ks) including COT, which was identified in an ORF screen⁴³ are capable of directly activating MEK. In total, these findings

suggest that a major mechanism of BRAFi resistance is the re-activation of MEK independent of upstream BRAF signaling.

Differentiation

Around the time that vemurafenib was first approved, multiple genomic alterations, predominantly in the MAPK pathway, were identified which conferred resistance to BRAF inhibitors in SKCM. However, a subset of cell lines and patients which fail to respond to these inhibitors lack previously identified resistance-conferring genomic alterations. An initial study leveraged a large panel of transcriptomically profiled SKCM cell lines to identify genes whose expression correlated with vemurafenib response¹¹⁴. Two populations of cells emerged from this analysis; AXL^{Low}/MITF^{High} cells which were sensitive to vemurafenib, and AXL^{High}/MITF^{Low} cells which were resistant. This spectrum was also observed in human SKCM tumors, suggesting that tumors which have low MITF expression may be intrinsically resistant to MAPKi therapy. It was subsequently demonstrated that melanoma cell lines with acquired MAPKi resistance downregulate MITF and upregulate AXL, suggesting that the balance of expression between these two genes is important in both innate and acquired MAPKi resistance¹⁵². Using RNA-seq data derived from bulk tumor tissue, SKCMs can be binned into groups based upon their AXL/MITF expression ratio. In contrast, based on single cell sequencing all SKCM tumors had a population of cells which were in an AXL^{High}/MITF^{Low} state and another population in an AXL^{Low}/MITF^{High} state¹³². In a small cohort of these patient tumors, the AXL/MITF ratio shifted to an AXL^{High}/MITF^{Low} state after MAPKi treatment. Two models can be built to explain these observations. In the first model, drug treatment selects for a stable subpopulation of MITF^{Low} cells that expands to become the dominant clone over time. In the second model, drug treatment induces

transcriptional re-programming to shift the cells from an $AXL^{Low}/MITF^{High}$ state to an $AXL^{High}/MITF^{Low}$ state. Early evidence suggested that the second model is likely correct since, during the acquisition of drug resistance, melanoma cells can enter into a poorly differentiated state which is reversible upon drug withdrawal^{142,153}. However, it is still possible that a subpopulation of well-differentiated cells may withstand drug treatment, and progressively out-compete the poorly-differentiated cells upon drug withdrawal. Analysis of SKCM cells on a single cell level has provided strong evidence that individual melanoma cells progressively de-differentiate. In the first study, multiplexed FISH was used to demonstrate that melanoma cells can stochastically switch into a pre-resistant state and upon drug treatment undergo epigenetic “burn-in” to a stably resistant state¹⁴¹. Any melanoma cell within the culture is, in principle, capable of undergoing this cell state transition, which is counter to the stable subpopulation model. A second elegant study used single cell RNA-seq to track the differentiation trajectory of SKCM PDX lines during MAPKi therapy¹²⁷. In this model, melanoma cells progressively de-differentiate into a “pre-resistant” state where they then make a cell fate decision to enter into one of two resistant states. The first resistant state is neural crest stem cell-like characterized by high expression levels of NGFR and the second state is well differentiated with high expression of melanocyte lineage genes. Collectively these data suggest a model wherein MAPKi drug treatment results in progressive de-differentiation of SKCM cells during the acquisition of drug resistance.

Tumor Microenvironment

Pressing questions in the field include how to effectively combine MAPK inhibitors and immunotherapy in the clinic and understanding the role of the immune compartment in the response to MAPK inhibitors. Tumors which develop MAPKi resistance show reduced expression

of multiple immune marker genes, including CD8⁺ T-cell marker genes¹³¹. Protein expression of CD8 was also decreased in tumor sections from these same tumors, suggesting that tumors which are refractory to MAPKi lose CD8⁺ T-cells. A follow-up study from the same group found that overexpression of PD-L2 accelerates the development of BRAFi resistance in an isogenic mouse model and conversely blocking PD-L2 delays the development of resistance. Since PD-L2 is a ligand for the T-cell inhibitory receptor PD-1, these data suggest that the T-cell compartment is also functionally important in BRAFi resistance. Other immune cell types implicated in MAPKi resistance include B-cells¹⁵⁴, macrophages¹⁵⁵, myeloid-derived suppressor cells (MDSCs)¹⁵⁶, and others¹⁵⁷. Some immune cells mediate direct killing of the cancer cells and other immune cells facilitate cancer cell proliferation. Non-immune cells can also facilitate the proliferation of cancer cells. Melanoma-associated fibroblasts secrete extracellular matrix components which signal to the melanoma cells and promote BRAFi resistance¹⁵⁸. In total, these data suggest that MAPKi resistance develops in part through cancer cell non-autonomous mechanisms.

RhoA GTPases and RhoA-mediated gene transcription

The first evidence for the involvement of RhoA GTPases in BRAFi resistance identified a switch in RND3-RhoA signaling during BRAF inhibition⁵⁹. In melanoma cell lines, acute BRAFi treatment induces myosin light chain (MLC) phosphorylation and induces the formation of actin stress fibers, two readouts of RhoA activation. However, it was still unclear from these data whether activation of RhoA was important in acquired BRAFi resistance. Another study found that expression of RhoB is upregulated by vemurafenib and promotes vemurafenib resistance¹⁵⁹, which was the first evidence directly implicating RhoA GTPases in BRAFi resistance. RhoA effector pathways are also important in drug resistance. Inhibition of ROCK1, a direct RhoA target,

sensitizes BRAF-mutant melanoma cells to BRAF inhibitors¹⁶⁰. A parallel study from the same group demonstrated a similar observation with MEK inhibitors in NRAS-mutant melanoma cells¹⁶¹. More recent studies have identified a role for other RhoA effector pathways in BRAFi resistance¹⁶². While RhoA activation has been linked to BRAFi sensitivity, it is unclear whether RhoA is activated in cells that acquire BRAFi resistance and how RhoA may promote BRAFi resistance. This question was partially answered when it was discovered that actin stress fibers are elevated in melanoma cell lines with acquired BRAFi resistance¹⁶³. Interestingly, this study also demonstrated that RhoA-induced BRAFi resistance is partially mediated by the transcriptional co-activator YAP1. This study builds upon evidence in the literature which suggests that YAP1 promotes BRAFi resistance by extending those findings to show that YAP1 activation is dependent on cytoskeletal re-arrangement^{131,164,165}. MRTF, another transcriptional co-activator that signals downstream of RhoA, is critical for Rac1^{P29S}-induced BRAFi resistance. A recent study found that both MRTF-A and YAP1 are activated in cellular models of acquired BRAFi resistance¹⁶⁶. In total, these data demonstrate that RhoA-mediated gene transcription is an emerging BRAFi resistance mechanism, although it remains unclear how this pathway becomes activated in BRAFi-resistant cells.

Contribution of this work

While considerable research has been undertaken to define how SKCM tumors develop resistance to BRAFi/MEKi therapy, a gap remains in leveraging this information for clinical benefit. One solution to this problem is to re-purpose FDA approved drugs to treat BRAFi melanoma. The goal of this dissertation is to identify pharmacological vulnerabilities in BRAFi-resistant melanoma cells. A disadvantage to this approach is that we are limited to searching “under

the lamppost” of targets which are currently clinically actionable. However, a distinct advantage is that this approach eliminates the extensive pre-clinical optimization of the molecule and clinical safety testing which are major impediments to bringing new therapies into clinical use. In my studies, I take two approaches to address this problem. In the first approach, I use bioinformatic and experimental approaches to identify resistance mechanisms, and then pharmacologically target those resistance mechanisms. In the second approach, I identify pharmacological vulnerabilities which are specific to BRAFi-resistant cells regardless of whether they re-sensitize the cells. The long-term goal of this work is to identify therapeutic approaches to prevent or reverse BRAFi resistance in melanoma.

CHAPTER 2:
**Rho-mediated signaling promotes BRAF inhibitor resistance in
de-differentiated melanoma cells**

Oncogene 2020, 39, 1466-1483

Sean A Misek, Kate M Appleton, Tom S Dexheimer, Erika M Lisabeth, Roger S Lo, Scott D
Larsen, Kathleen A Gallo, Richard R Neubig

SAM performed all experiments

Abstract

Over half of cutaneous melanoma tumors have $BRAF^{V600E/K}$ mutations. Acquired resistance to BRAF inhibitors (BRAFi) remains a major hurdle in attaining durable therapeutic responses. In this study we demonstrate that approximately 50-60% of melanoma cell lines with vemurafenib resistance acquired *in vitro* show activation of RhoA family GTPases. In BRAFi-resistant melanoma cell lines and tumors, activation of RhoA is correlated with decreased expression of melanocyte lineage genes. Using a machine learning approach, we built gene expression-based models to predict drug sensitivity for 265 common anti-cancer compounds. We then projected these signatures onto the collection of TCGA cutaneous melanoma and found that poorly differentiated tumors were predicted to have increased sensitivity to multiple Rho kinase (ROCK) inhibitors. Two transcriptional effectors downstream of Rho, MRTF and YAP1, are activated in the Rho^{High} BRAFi-resistant cell lines, and resistant cells are more sensitive to inhibition of these transcriptional mechanisms. Taken together, these results support the concept of targeting Rho-regulated gene transcription pathways as a promising therapeutic approach to restore sensitivity to BRAFi-resistant tumors or as a combination therapy to prevent the onset of drug resistance.

Introduction

Most cutaneous melanomas have point mutations in V-Raf Murine Sarcoma Viral Oncogene Homolog B (BRAF), a serine/threonine kinase with the V600E/K point mutations being the most common². These mutations result in constitutive BRAF activity and downstream Mitogen Activated Protein Kinase (MAPK) pathway activation, independent of upstream stimuli. Given the prevalence of these mutations in human melanoma tumors, several drugs have been developed which target mutant BRAF, including vemurafenib and dabrafenib. The most common class of BRAFi resistance mechanisms result in MAPK-reactivation^{128,131,135}. This includes alterations in the BRAF gene itself such as BRAF amplification^{130,167}, or aberrant splice variants¹⁵⁰, which can drive resistance to BRAFi therapy. Alterations in other genes in the MAPK pathway such as Mitogen-Activated Protein Kinase Kinase (*MEK*)¹⁶⁸, Neuroblastoma RAS Viral Oncogene Homolog (*NRAS*)³⁸, Neurofibromin 1 (*NFI*)¹⁶⁹, and others^{43,170,171} also promote resistance to BRAF inhibitors. Receptor Tyrosine Kinase (RTK) activation is another mechanism by which cells can generate BRAFi resistance, at least partially through re-activation of the MAPK pathway, through either upregulation of the receptor itself^{38,142,172}, or through increased expression of the RTK ligand¹³⁶.

The combination of BRAF inhibitors with Mitogen-Activated Protein Kinase Kinase 1/2 (MEK1/2) inhibitors was proposed as an approach to overcome BRAF inhibitor resistance³⁸ and it is clinically superior to BRAF inhibitor monotherapy against BRAF^{V600}-mutant tumors^{84,87,173}. However, acquired resistance to the BRAF and MEK inhibitor combination is still common¹³⁵, consistent with non-MAPK pathway resistance mechanisms being important clinically^{131,174}. Some MAPK-independent resistance mechanisms result from cancer cell intrinsic, epigenomically driven, adaptive responses to drug pressure early during therapy¹⁷⁴. These may result in wide-

ranging phenotypic switches resulting in MAPK inhibitor resistance in patients and ultimately relapse during therapy¹³¹. Melanoma cells grown without drug pressure stochastically switch between a rapid-cycling cell state and a rare slow-cycling cell state¹⁴¹. These cells are selected for during treatment with a BRAFi, ultimately giving rise to a stable population of resistant cells^{167,174}. These data are further supported by the observation that BRAFi/MEKi-resistant cells and tumors can be re-sensitized to treatment with BRAF or MEK inhibitors after a “drug holiday”¹⁷⁵⁻¹⁷⁷.

Among the non-MAPK resistance mechanisms, compensatory activation of other GTPases may be important during the development of drug resistance. The RhoA subfamily (RhoA, RhoB, and RhoC) of GTPases act as molecular switches which regulate actin dynamics. The RhoA and RhoC isoforms are highly similar and often function redundantly in the cell, but in some contexts these two isoforms signal differently¹⁷⁸. In melanoma the RhoA subfamily, especially RhoC, promotes invasion and metastasis^{59,179,180}, and inhibition of the RhoA isoform suppresses tumor growth⁵⁷. Canonically, the RhoA GTPases (encompassing RhoA, B, and C) promote the formation of actin stress fibers by stimulating G-actin polymerization and inhibiting F-actin depolymerization¹⁸¹⁻¹⁸³. Actin stress fibers have been shown to be increased in melanoma cells with acquired BRAFi resistance¹⁶³ and we confirm and extend that finding here.

In addition to regulating actin dynamics, RhoA GTPases also regulate gene transcription. This occurs, in part, through actin polymerization-dependent activation of Myocardin-Related Transcription Factor (MRTF) and YES Proto-Oncogene 1 (YAP1). MRTF and YAP1 are transcriptional co-activators which, upon activation, translocate into the nucleus and regulate gene transcription. Silencing of MRTF or Serum Response Factor (SRF), a transcription factor by which MRTF modulates gene expression, prevents melanoma metastasis⁶³. Previously, we have developed a series of MRTF-pathway inhibitors including CCG-203971 and CCG-222740¹⁸⁴⁻¹⁸⁶

and demonstrated that CCG-203971 prevents melanoma metastasis, induces G1 cell cycle arrest, and reduces growth of melanoma cells¹⁸⁵. YAP1 promotes BRAFi/MEKi resistance in melanoma through suppression of apoptosis via BCL-xL and BIM dysregulation^{131,163-165}. Accumulation of YAP1 protein and enrichment of a YAP1 gene signature has been documented in about 40% of clinical melanoma samples from patients who relapsed on MAPK inhibitor therapies¹³¹.

Previous studies have demonstrated that non-mutational, acquired resistance mechanisms represent a major hurdle in maintaining a durable response to MAPK-directed therapeutics¹³¹. We hypothesize that activation of the RhoA pathway is one such acquired resistance mechanism. In this study, we build upon existing literature to demonstrate that actin stress fiber accumulation and RhoA signaling are elevated in approximately half of the vemurafenib-resistant melanoma cell lines tested and that this mechanism is also active in a significant fraction of clinical tumors. RhoA^{High} but not RhoA^{Low}-resistant lines are partially re-sensitized to vemurafenib by two structurally distinct ROCK inhibitors. We also demonstrate that RhoA activation is linked to loss of melanocyte lineage genes, a pattern also observed in human tumors. Finally, de-differentiated BRAFi-resistant cells have increased MRTF and YAP1 activation and these cells are more sensitive to pharmacological inhibition of these transcriptional mechanisms. De-differentiation of melanoma cells is a major mechanism of acquired BRAFi-resistance^{141,142,153,187,188} and we have identified signaling alterations commonly associated with de-differentiation. This information is critical for developing therapeutic strategies to target this class of drug-resistant tumors.

Materials and Methods

Cell lines and culture:

To select for Vemurafenib-resistant cells UACC62 and SK-Mel-19 cells were seeded into 10-cm tissue culture plates at ~30% confluence and grown in DMEM as described below. After the cells had adhered to the plate (~16 h), culture medium was supplemented with 2 μ M vemurafenib. Medium was exchanged every 2-3 days for 10 mL of fresh media supplemented with 2 μ M vemurafenib. Cells were split at a 1:3 ratio into a new 10-cm tissue culture plate when they reached ~75% confluence (approximately 3-4 weeks) and approximately weekly for each subsequent passage. After two months of selection, cell populations were expanded in vemurafenib-containing media and frozen.

Three additional pairs of parental (P) and vemurafenib-resistant (R) melanoma lines, M229P/R, M238P/R, and M249P/R cells, were generously provided by Dr. Roger Lo at UCLA³⁸. SK-Mel-19 and UACC62 cells were obtained from Dr. Maria Soengas at The University of Michigan and were made resistant as described above.

Cells were cultured in DMEM (Gibco #11995-065) supplemented with 10% FBS (Gibco #10437-028) and 1% Antibiotic-Antimycotic reagent (ThermoFisher, Waltham, MA, USA #15240062). Vemurafenib-resistant cells were continuously cultured in the presence of 2 μ M vemurafenib. Cells were split at ~75% confluence. Vemurafenib was removed from the culture medium when cells were seeded for experiments (e.g. immunofluorescence staining or qRT-PCR), except where otherwise indicated. Cells were routinely tested for mycoplasma contamination by DAPI staining. STR profiling on all cell lines was performed at the MSU genomics core. In all cases, isogenic pairs of cell lines had the same STR profile.

Cloning:

CIRSPR sgRNA guide sequences were cloned into the pLentiCRISPRv2 vector (from Feng Zhang, Addgene plasmid #52961). All guide RNA sequences were confirmed by Sanger sequencing.

Human RhoA^{G12V} was amplified and N-terminal HA-tagged. This PCR product was used as a template for a second round of PCR amplification to add the Gateway adapter sequences. Human MRTFA was amplified out of the p3xFLAG-MRTFA vector (Addgene plasmid#11978) and tagged with gateway adapters which preserve the N-terminal 3x FLAG tag from the vector. The RhoA and MRTFA PCR products were first cloned into pDONR221 using the Gateway BP Clonase II Enzyme Mix from ThermoFisher (#11789020) using the manufacturer's protocol. RhoA, MRTFA, and Gus (which is included in the BP reaction kit) were subcloned into the pLX301 lentiviral expression vector (from David Root, Addgene plasmid #25895) using the Gateway LR Clonase II Enzyme mix from ThermoFisher (#11791020). The presence of the correct insert in the final plasmid was confirmed by Sanger sequencing.

Virus Preparation and Infection:

HEK-293T cells were seeded into 10-cm plates and were allowed to attach overnight. The next day at approximately 60-70% confluence, the cells were transfected with a plasmid cocktail containing 5000 ng of the pLentiCRISPRv2 or pLX301 plasmid, 3750 ng of psPAX2 (Addgene plasmid #12260), 1250 ng of pMD2.G (Addgene plasmid #12259), and 20 μ L of Lipofectamine 2000 in 400 μ L of OptiMEM. The next morning the medium was changed to 10 mL of fresh culture medium, and the next day each plate was supplemented with an additional 5 mL of culture medium. After 24 h, the culture medium was harvested and filtered through a 0.45-micron syringe filter. Virus was stored at 4 C and was used within 2 weeks.

Target melanoma cells (e.g. UACC62P/R) were seeded into 10-cm plates and were allowed to attach overnight. The next afternoon at approximately 30% confluence the medium was changed to 10-mL of complete medium and was supplemented with 1 mL of viral supernatant. The next morning, the medium was changed and the cells were incubated an additional 24 h. The cells were then treated with 10 µg/mL puromycin until all the untransformed cells died (approximately 72 h). For all virus experiments, the cells were used within 1-2 passages and each biological replicate for each experiment used a different batch of cells. We did not pick individual clones for the CRISPR cell lines, but instead used a pooled infection approach. Validation of CRISPR knockout efficiency was done by immunoblotting for the target protein.

Compounds and Antibodies:

Vemurafenib (#S1267), Y-27632 (#S1049), fasudil (#S1573), and dasatinib (#S1021) were purchased from Sellekchem, Houston, TX, USA. Latrunculin B (#10010631), cytochalasin D (#11330), and erlotinib (#10483) were purchased from Cayman Chemical, Ann Arbor, MI, USA. Rho Inhibitor I (#CT04-A) was purchased from Cyoskeleton Inc, Denver, CO, USA. CCG-222740¹⁸⁶ was synthesized in the lab of Dr. Scott Larsen at the University of Michigan. All compounds were diluted in DMSO to a stock concentration of 10 mM. Compound stock solutions were frozen at -20 °C. Antibodies against YAP1 (#14074), MLC2 (#3672), pMLC2 (#3674), Sox10 (#89356), and pEGFR (#3777) were purchased from Cell Signaling, Danvers, MA, USA. Antibodies against MRTF-A (#sc21558), MRTF-B (#sc98989), and Actin (#sc1616) were purchased from Santa Cruz, Dallas, TX, USA. Donkey anti-Mouse800 (#926-32212), Donkey anti-Goat680 (#926-68074), and Donkey anti-Rabbit680 (#926-68073) immunoblotting secondary antibodies were purchased from LI-COR, Lincoln, NE, USA. Alexa Fluor goat anti-rabbit488 (#A11034) and

donkey anti-goat488 (#A11055) were purchased from Invitrogen. Alexa Fluor546 Phalloidin (#A22263) was purchased from ThermoFisher.

qRT-PCR:

Cells were cultured and treated as indicated, rinsed once in PBS, and total cellular RNA was harvested with the RNeasy kit purchased from the Qiagen, Hilden, Germany (#74104). RNA was eluted in nuclease-free H₂O. cDNA was synthesized using the High-Capacity cDNA RT kit from ThermoFisher (#4368814) from 1000 ng of total RNA, according to the manufacturer's protocol. qPCR was performed using the SYBR Green PCR Master Mix (#4309155) from ThermoFisher according to the manufacturer's protocol using an Agilent Mx3000P qPCR instrument. Primers were purchased from Integrated DNA Technologies, San Jose, CA, USA. Primers were designed using the Harvard Primer Bank tool (<https://pga.mgh.harvard.edu/primerbank/>). Fold-change analysis was performed using the $\Delta\Delta CT$ method.

RNA-Seq sample preparation and data processing:

Total cellular RNA was extracted from UACC62P and UACC62R cells (two biological replicates per cell line) using the same method which was used for qPCR experiments. RNA concentration was measured by Qubit and quality control was performed on an Agilent 2100 Bioanalyzer in the MSU Genomics Core. All RNA samples had a RIN score > 8. Barcoded libraries were prepared using the Illumina TruSeq Stranded mRNA Library Preparation Kit on a Perkin Elmer Sciclone G3 robot following manufacturer's recommendations. Completed libraries were QC'd and quantified using a combination of Qubit dsDNA HS and Caliper LabChipGX HS DNA assays. Libraries were pooled and run on two lanes, and sequencing was performed in a 1x50 bp single-

end read format using HiSeq 4000 SBS reagents. Base calling was done by Illumina Real Time Analysis, RTA_ v2.7.7 and output of RTA was demultiplexed and converted to FastQ format with Illumina Bcl2fastq v2.19.0. Sequencing was performed at a depth of >30M reads/sample. Quality control was performed on the FastQ files using FastQC v0.11.5, and reads were trimmed using Trimmomatic v0.33. Reads were mapped using HISAT2 v2.1.0 and analyzed using HTSeq v0.6.1. Differential gene expression was calculated using edgeR. Raw RNA-Seq reads and processed HTSeq read counts are available on GEO under GSE115938.

Immunoblotting:

Cells were cultured and treated as indicated, placed on ice, and rinsed once in cold PBS. Cells were lysed in 2x Laemmli Sample Buffer (Biorad, #1610737). Samples were sonicated with a probe sonicator for approximately 5 sec, then boiled at 100 °C for 10 min. Samples were loaded onto a 12% polyacrylamide gel and transferred to Immobilon-FL PVDF Membrane (Millipore Sigma, Burlington, MA, USA, #IPFL00010). Membranes were blocked in 5% BSA + TBS-Tween (1:1000) for 1 h, then incubated in primary antibody overnight at 4 °C. Membranes were washed 3x in TBS-Tween and were then incubated in the appropriate secondary antibody at a 1:20000 dilution for 1 h at room temperature. All antibodies were diluted in blocking buffer. Membranes were washed 3x in TBS-Tween then dried and imaged on a LI-COR Odyssey FC imaging system.

Immunofluorescence staining:

Cells were seeded into 8-well chamber slides and were treated as indicated in the figure legends. Cells were fixed with 3.7% formaldehyde for 15 min then blocked in 2% BSA PBS-Triton (0.1%) for 1 h at room temperature. Cells were incubated overnight at 4 °C in primary antibody at a 1:100

(MRTF-A or MRTF-B) or 1:500 (YAP1) dilution in blocking buffer. Cells were washed 3x in PBS then were incubated in the appropriate secondary antibody at a 1:1000 dilution for 1 h at room temperature. Cells were washed 3x in PBS then were mounted in ProLong Gold Antifade + DAPI (ThermoFisher, #P36935). Slides were cured overnight at room temperature and were then imaged on a Nikon TE2000-U Fluorescence Microscope at 20x magnification.

Cells were stained with Alexa Fluor546 Phalloidin (#A22263) to visualize F-Actin. For these experiments, cells were fixed and blocked as described above. Cells were then incubated in Phalloidin diluted 1:100 in blocking buffer for 1 h at room temperature before being washed and mounted. For all immunofluorescence experiments, images were blinded by an independent party or an automated R script before quantification. For a cell to be considered as stress fiber-positive, the cell was required to contain at least one stress fiber which spanned >90% the length of the cell. We repeated all staining experiments at least 3 times and typically analyzed at least 10 fields per biological replicate. In total we analyzed at least 400 cells per experimental group, but in most cases over 1000 cells per experimental group. For subcellular localization experiments, data are represented as a stacked bar graph wherein the fraction of cells that have predominantly nuclear, pan-cellular, or cytosolic localization is plotted as a fraction of the total cells. A cell was considered to have “cytosolic” localization if there was clear nuclear exclusion. Inversely a cell was described as having “nuclear” localization if the staining intensity was appreciably higher than in the cytosol. If there was no apparent difference between the nuclear and cytosolic staining, then the cell was described as having “pan-cellular” distribution of the protein being assessed.

Cell viability experiments:

Cells were seeded into 384-well tissue culture plates (PerkinElmer, Waltham, MA, USA, #6007689) at a density of 1000 cells/well in 20 μ L of media and were allowed to attach overnight. The next day, drugs were pre-diluted at 4x final concentration in culture medium then added to the 384-well plates so that the final volume was 40 μ L/well. For the single compound dose response experiments, the compound was pre-diluted at 2x the final concentration and 20 μ L was added to each well. A PBS or growth medium barrier was added to the outer wells of the plate to limit evaporation. Cells were cultured under these conditions for 72 h. To assess viability, 10 μ L of CellTiter-Glo (Promega, Madison, WI, USA, #G7573) was added to each well. Plates were incubated for 5 min at room temperature then briefly centrifuged (4000 rpm, 60 seconds) before being read on a Bio-Tek Synergy Neo plate reader. Viability signal is plotted versus log(Vemurafenib concentration) for each treatment condition. The Area Under the Curve (AUC) was calculated for each curve using GraphPad Prism for the range log concentration from -9 to -5.

Bioinformatics:

Dataset Processing

Cancer Cell Line Encyclopedia (CCLE) gene expression Affymetrix CEL files (Version 19-Mar-2013) were downloaded from the Broad Institute CCLE data portal. CEL files were processed using Affymetrix Expression Console (Build 1.4.0.38). Probe IDs were collapsed to gene names using the CollapseDataset function on GenePattern. The TCGA RNA-Seq dataset for Skin Cutaneous Melanoma (SKCM) was downloaded from the UCSC Cancer Genome Browser portal. No further data processing was performed prior to analysis.

RNA-Seq data for 62 human tumors paired for pre- and post- MAPK inhibitor resistance was downloaded from GSE65185¹³¹. Analysis of these data was performed on the pre-processed CuffnormFPKM dataset included in this series. RNA-Seq data for *in vitro* generated vemurafenib-resistant M229P/R and M238P/R cells was downloaded from GSE75313¹⁷⁴. These data were processed using the above described RNA-Seq data processing pipeline.

Melanoma scRNA-Seq data was downloaded from GSE72056 and filtered to include only melanoma cells. Missing values were imputed with the MAGIC algorithm¹⁸⁹.

Data for the M229 cells treated with vemurafenib for different times was downloaded from GSE110054. No further processing was performed on this dataset prior to ssGSEA analysis.

Gene Ontology/KEGG pathway analysis

Using the CCLE dataset, 38 adherent cell lines with BRAF^{V600} mutations were identified. For all cell lines, PLX4720 (activity area) was correlated with gene expression. A definition of Activity Area can be found in this study¹⁹⁰. Genes highly expressed in resistant cells (genes with a Pearson correlation coefficient < -0.5 when correlated with PLX4720 sensitivity) and genes weakly expressed in resistant cells (Pearson correlation coefficient > 0.5) were identified. Gene ontology and KEGG pathway analysis was performed on the gene sets using GATHER (<http://changlab.uth.tmc.edu/gather/gather.py>) with network inference.

GSEA/ssGSEA

GSEA (v19.0.24) was performed using GenePattern (<http://software.broadinstitute.org/cancer/software/genepattern/>) with ‘number of permutations’ = 1000, and ‘permutation type’ = phenotype. All other parameters were left as default. ssGSEA

(9.0.9) was performed on GenePattern with all parameters left as default. The ssGSEA output values were z-score normalized.

A RhoA/C gene signature was generated by using all genes which are upregulated > 2-fold by overexpression of either RhoA or RhoC from the GSE5913 dataset in NIH-3T3 cells. These two lists were merged and duplicates were removed. This resulted in a list of 79 genes.

The melanocyte lineage signature included all genes in the GO_MELANIN_METABOLIC_PROCESS (GO: 0006582) and GO_MELANOCYTE_DIFFERENTIATION (GO: 0030318) MSigDB signatures. The combined list was filtered to remove duplicate genes.

The YAP1 signature used was the CORDENONSI_YAP_CONSERVED_SIGNATURE in the C6 collection on MSigDB. The MRTF signature is comprised of all genes downregulated > 2-fold upon MRTF knockdown in B16F2 melanoma cells⁶³.

Drug Response Signatures

The correlated gene expression profiling and drug IC50 values were downloaded from the GDSC data portal (<https://www.cancerrxgene.org/downloads>). Gene expression data was median centered so that the median expression of each gene across the cell lines was equal to 0. Data was randomly divided into a training (80%) and test (20%) set. A predictive model was built on the training set for each compound (n = 265 compounds) using a random forest algorithm (randomForest package in R) with ntrees = 500 and mtry = sqrt(#genes). Each model was validated on the test dataset by calculating the Pearson correlation coefficient between the predicted and actual IC50s. Models with a Pearson correlation coefficient > 0.3 were considered predictive. To

use gene expression data to predict drug response on clinical tumors, the TCGA SKCM data were median-centered using the same method used on the GDSC training data. Since the TCGA and GDSC datasets were collected on different gene expression analysis platforms, the two datasets were filtered to include only overlapping genes. Models from GDSC which were deemed predictive for a drug response were then projected onto the TCGA dataset. Melanocyte Lineage signature scores of TCGA samples were negatively skewed from a normal distribution (corrected $z^3 = -1.94$). Of the 473 tumors, 70 were > 2 SD below the mean and none > 2 SD above the mean. Consequently, samples at least 2 SD below the mean are considered “lineage low” and all other tumor samples are considered “lineage high”. The average predicted IC_{50} for the Lineage low and Lineage high tumors was calculated by averaging the predicted $\log(IC_{50})$ for each sample class.

Statistical Analysis:

Most bioinformatics analysis was performed using R v3.3.0. Data analysis and statistics were performed using GraphPad Prism v6 or v7. Dose response curves were fit using nonlinear least square regression [$\log(\text{agonist})$ vs. response – Variable slope (four parameters)]. The AUC was calculated for each dose response curve in GraphPad Prism over a vemurafenib concentration range of 10^{-9} to 10^{-5} . Datasets with two groups were analyzed by unpaired two-tailed t-tests. Pearson correlation coefficients were calculated in R (for drug response signatures) or GraphPad Prism (for all other analysis). Data are presented as mean \pm S.E.M, and a p-value < 0.05 was considered statistically significant.

Results

RhoA activation in BRAFi-resistant melanoma cells and tumors

We analyzed a panel of matched parental (denoted by a P at the end of the cell line name) and BRAFi-resistant (denoted by an R at the end of the cell line name) melanoma cell lines and found that three of the resistant cell lines (UACC62R, M229R, and M238R) assumed a fibroblast-like morphology, while there was no overt change in the other two resistant cell lines (SK-Mel-19R and M249R). Since cell shape is controlled through modulation of the actin cytoskeleton, we examined F-actin structure by staining the cells with fluorescently labeled phalloidin. There was an increase in the number of actin stress fiber-positive UACC62R, M229R, and M238R cells compared to matched parental control cell lines; there was no overt change in stress fiber levels in the SK-Mel-19R and M249R cells (Figure 2.1A and 2.1B). Since an increase in stress fibers would suggest that Rho activation is altered, we also analyzed Myosin Light Chain 2 (MLC2) phosphorylation in the matched parental and resistant cell lines. MLC2 is a RhoA effector so MLC2 phosphorylation is a readout for increased RhoA activation. MLC2 phosphorylation is increased in the stress fiber-positive UACC62R and M238R cell lines, but not in stress fiber-negative SK-Mel-19R or M249R cells (Figure 2.1C). Interestingly, there was no change in MLC2 phosphorylation in the M229R cells despite the fact that they are stress fiber positive, which may suggest that these cells utilize an alternative signaling mechanism to activate RhoA and increase stress fibers or that RhoA may utilize different effector pathways in different cells.

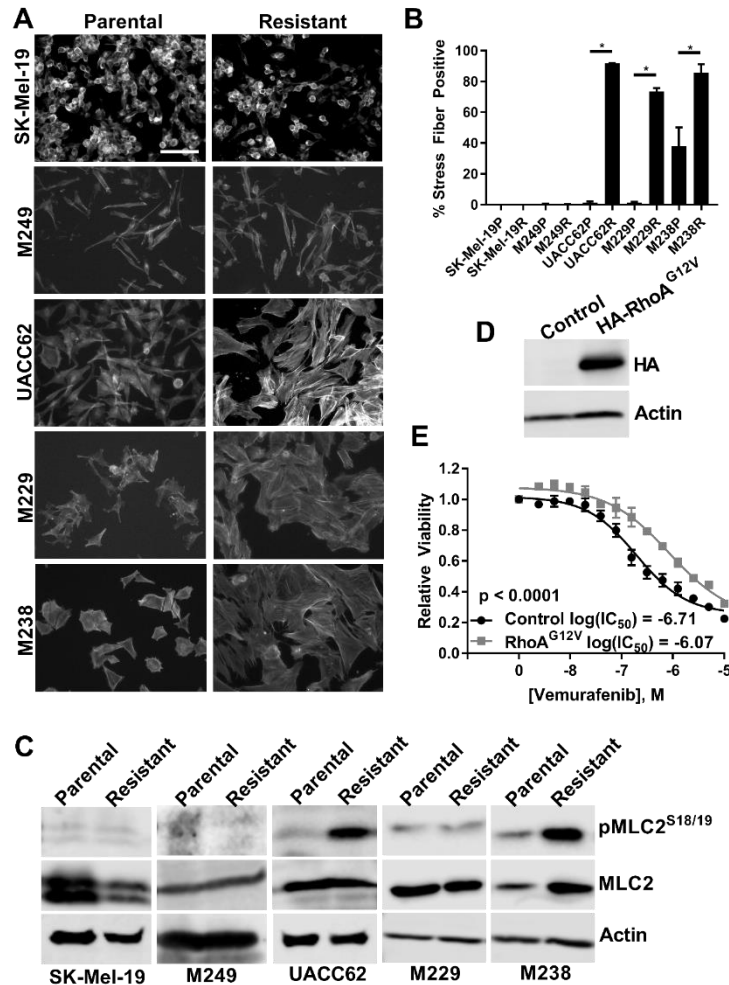


Figure 2.1: RhoA is activated in BRAFi-resistant melanoma cells and tumors **A.** Cells were seeded into 8-well chamber slides and were allowed to attach overnight. The next day cells were fixed and stained with fluorescently labeled phalloidin. Representative images from $n = 3$ biological replicates and $n = 1$ technical replicate. Scale bar is $10 \mu\text{m}$. **B.** Actin stress fiber positive cells were quantified using ImageJ. Statistical analysis was performed using unpaired t-tests to compare matched parental (denoted by a P at the end of the cell line name) and resistant (denoted by an R at the end of the cell line name) lines. * indicates that $p < 0.05$. **C.** MLC2^{S18/19} phosphorylation in the parental and resistant cells was assessed by immunoblotting. Total MLC2 and Actin were used as loading controls. Representative blots from $n = 3$ biological replicates and $n = 1$ technical replicate. **D.** UACC62P cells stably expressing HA-RhoA^{G12V} were lysed and immunoblotted with anti-HA and anti-Actin antibodies. Representative images from $n = 3$ biological replicates and $n = 1$ technical replicate. **E.** UACC62P cells stably expressing Gus (control) or HA-RhoA^{G12V} were seeded into 384-well plates and treated with a 14-point vemurafenib concentration gradient with a top dose of $10 \mu\text{M}$ as described in the materials and methods. Data is average from $n = 3$ biological replicates with $n = 3$ technical replicates.

These data suggested that RhoA was activated in the resistant cell lines, but it was not clear whether RhoA itself was functionally important in BRAFi resistance. To address this question, we generated UACC62P cells which stably express RhoA^{G12V} (Figure 2.1D). This specific mutation is not found in any Skin Cutaneous Melanoma (SKCM) tumors in the TCGA dataset, however, the constitutively active RhoA^{G12V} model is a useful tool for studying mechanisms of Rho signaling since it is independent of upstream stimuli. Consistent with our observations suggesting that RhoA is activated in a subset of the resistant cell lines, overexpression of RhoA^{G12V} reduced vemurafenib sensitivity by approximately 6-fold (Figure 2.1E). To further confirm the role of RhoA in vemurafenib resistance, we pharmacologically inhibited the function of RhoA using the cell permeable Botulinum Exotoxin C3 (Rho Inhibitor I) to test whether RhoA inhibition reverses vemurafenib resistance (Figure A-2.1). M238R and UACC62R cells were more sensitive to single agent treatment with Rho Inhibitor I, suggesting that these cells are re-wired to depend on RhoA signaling for their survival. M229R cells did not have increased sensitivity to single agent treatment with Rho Inhibitor I, rather Rho Inhibitor I treatment increases vemurafenib sensitivity. As expected, Rho Inhibitor I was not selective for M249R cells over M249P cells, which is consistent with the idea that these cells do not develop resistance through RhoA activation. Since RhoA activation should result in an increase in actin polymerization, we next tested whether actin polymerization is functionally important for vemurafenib resistance. Similar to the findings with Rho Inhibitor I, cytochalasin D was more active against all three of the RhoA^{High} cell lines as a single agent treatment and it partially re-sensitized M229R cells to vemurafenib (Figure A-2.2).

To more broadly confirm this finding, we correlated cell sensitivity to PLX4720 (a BRAF inhibitor which is structurally similar to vemurafenib) with the gene expression results for 38 BRAF^{V600-}

mutant cell lines from the Cancer Cell Line Encyclopedia (CCLE). Genes which are highly expressed in PLX4720-resistant cells (genes with a Pearson correlation of gene expression values vs drug activity area < -0.5) were analyzed by Gene Ontology and KEGG pathway analysis. One of the most statistically significant GO terms was “small GTPase mediated signal transduction” (Figure A-2.3A) and the most statistically significant KEGG pathway was “Regulation of actin cytoskeleton” (Figure A-2.3B). A RhoA/C gene signature was also inversely correlated ($R = -0.42$) with PLX4720 sensitivity (Figure A-2.4). Collectively, these data support the idea that RhoA activation is positively correlated with BRAFi resistance across a wide array of melanoma cell lines. To determine whether these cell line observations are applicable in the clinical context, we analyzed RNA-seq data from 41 tumors before and after development of resistance to BRAFi/MEKi¹³¹. More than half of the resistant tumors ($n = 24$) had an increased RhoA/C signature score over the baseline tumor (Figure A-2.5). Taken together, these data suggest that RhoA is activated in approximately half of BRAFi-resistant cells and tumors and that RhoA activation is inversely correlated with BRAFi sensitivity.

Since the most common class of BRAFi resistance mechanisms is through MAPK re-activation we then wondered whether RhoA activation was mutually exclusive with MAPK reactivation-mediated resistance. If resistance is developed through MAPK re-activation then the resistant cells should retain ERK phosphorylation when treated with vemurafenib. As expected, vemurafenib inhibits ERK phosphorylation in all 5 parental cell lines. Vemurafenib fails to inhibit ERK phosphorylation in the two RhoA^{Low} resistant lines (SK-Mel-19R and M249R), which in the case of M249R is expected since these cells developed resistance by acquiring an NRAS^{Q61K} mutation. In the three RhoA^{High} resistant cell lines, vemurafenib partially inhibited ERK phosphorylation in two (M229R and UACC62R) but failed to suppress ERK phosphorylation in the other (M238R)

(Figure A-2.6). This finding is important since it suggests that Rho may be important even in cells which harbor MAPK-reactivating resistance mechanisms.

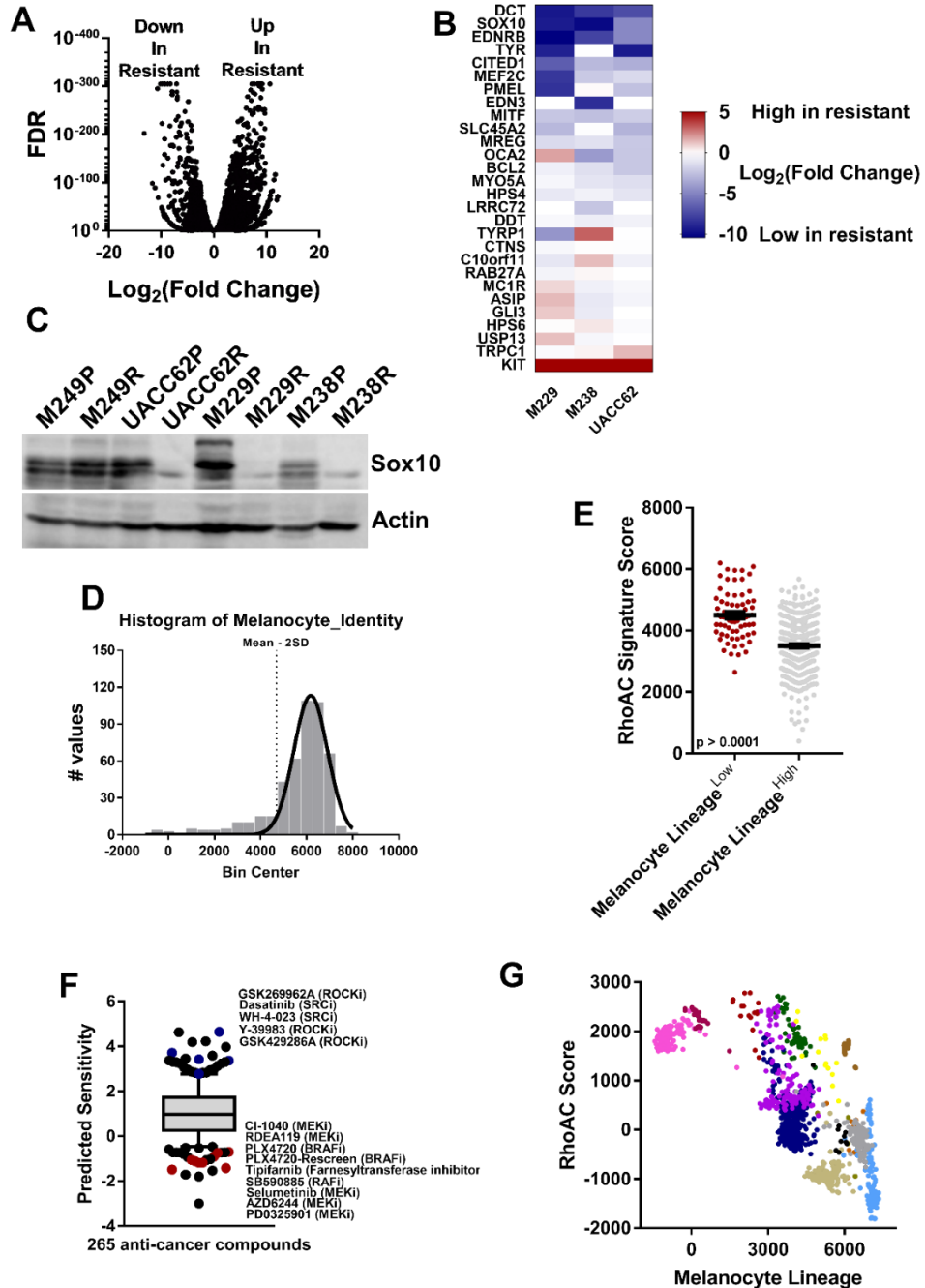


Figure 2.2: Melanoma differentiation status is inversely correlated with Rho activation A. RNA-Seq was performed on parental (UACC62P) and Vemurafenib-resistant (UACC62R) cells. Differential gene expression was visualized on a volcano plot. n = 2 biological replicates and n =

Figure 2.2 (cont'd) 1 technical replicate per treatment condition. **B.** Heatmap of differential expression of Melanocyte Lineage signature genes in M229P/R, M238P/R, and UACC62P/R cells. Blue indicates that the gene is downregulated in the resistant cell line, and red indicates that the gene is upregulated in the resistant cell line. **C.** Sox10 protein expression was assessed across a panel of 4 parental and resistant melanoma cell lines. Actin was used as a loading control. Representative image from $n = 3$ biological replicates and $n = 1$ technical replicate. **D.** Histogram of Melanocyte Lineage signature scores for samples in the SKCM TCGA dataset ($n = 473$). Dotted line represents 2 SD below the mean of the Gaussian fit. Samples were stratified into Melanocyte Lineage high and Melanocyte lineage low samples as described in the Materials and Methods section. **E.** ssGSEA was used to calculate the RhoA/C signature score for each TCGA SKCM tumor sample. ssGSEA was performed as described in the Materials and Methods section. The output signature score from this analysis was not subjected to further processing. The tumors were stratified based on their Melanocyte Lineage signature score as described in panel D of this figure and in Materials and Methods. The average RhoA/C signature score for each class of tumor samples is plotted where tumor samples with a high Melanocyte Lineage score are in grey and tumor samples with a low Melanocyte Lineage score are in red. **F.** Predictive signatures were generated for 265 common anti-cancer compounds using a random forest algorithm. The models were made such that gene expression data was used to predict drug response. The drug response data was derived from the GDSC dataset¹¹⁰ and the numerical values for drug sensitivity are the IC_{50} values from this dataset. The samples were stratified into Melanocyte Lineage Low and Melanocyte Lineage High and the average predicted IC_{50} for each drug for each class of samples was calculated. The differential predicted IC_{50} was subsequently determined by calculating the differential in the average IC_{50} between the two classes of tumor samples. The values on the Y-axis of this plot are the fold change in predicted IC_{50} between the Melanocyte Lineage Low and Melanocyte Lineage High samples. A positive value means that the compound was predicted to be more effective against Melanocyte Lineage Low tumor samples, while a negative value means that the compound was predicted to be more effective against Melanocyte Lineage High tumor samples. **G.** Previously published single cell RNA-Seq data was used for this experiment¹³². These data were downloaded and processed as described in Materials and Methods. The RhoA/C signature and the Melanocyte Lineage signatures were calculated using ssGSEA. Since this dataset is comprised of tumor cells derived from multiple different tumors the cells group together based upon tumor of origin. The cells are color coded based on the tumor from which they were derived from and the colors were chosen arbitrarily.

Resistant cell lines with a low level of melanocyte differentiation show high RhoA activity

We next wanted to understand mechanistically why the RhoA pathway is only activated in a subset of vemurafenib-resistant cells. We performed RNA-Seq on the UACC62P/R cell line pair (Figure 2.2A), and also analyzed published RNA-Seq data for the M229P/R and M238P/R cells. The most striking finding was that a number of genes linked to the melanocyte lineage and pigment production were downregulated in all three of the RhoA^{High} resistant cell lines. To more

quantitatively analyze this phenotype we generated a “Melanocyte Lineage” gene signature which is comprised of genes involved in pigment production and the melanocyte lineage. A majority of the signature genes are downregulated in all three of the Rho^{High} resistant cell lines (Figure 2.2B) which suggests that loss of melanocyte identity is associated with Rho activation in BRAFi-resistant cells. There is also a temporal association between expression of the melanocyte lineage genes and RhoA/C signature genes (Figure A-2.7). One of the most strongly downregulated genes, at the mRNA level, is the transcription factor Sox10 which is one of the “master regulators” of the melanocyte lineage; we confirmed that Sox10 is also downregulated at the protein level (Figure 2.2C). Interestingly, there was no change in Sox10 protein expression in the M249P/R cells which did not have increased stress fibers (Figure 2.2C). We also found that Sox9 is upregulated at the mRNA level in all three of the RhoA^{High} resistant cell lines but not in the RhoA^{Low} resistant lines (Figure A-2.8). These results are consistent with previous findings which suggest that Sox10 suppresses Sox9 expression¹⁹¹, and suggest that this switch in transcription factor expression may be reflective of the differentiation status of the resistant cells.

Since Sox10 silencing results in activation of multiple RTKs, including EGFR, we sought to determine whether EGFR is activated in Sox10^{Low} BRAFi-resistant cells. EGFR mRNA is upregulated approximately 8-40-fold in Sox10^{Low} BRAFi-resistant cells (Figure A-2.9A) and this mRNA upregulation is accompanied by an increase in EGFR phosphorylation (Figure A-2.9B). We next tested whether EGFR was required for actin remodeling, however, treatment with the EGFR inhibitor erlotinib did not alter the assembly of actin stress fibers (Figure A-2.9C).

To determine whether this de-differentiation phenotype was also important in human SKCM tumors we projected the “Melanocyte Lineage” signature onto the SKCM TCGA dataset

and then fit a Gaussian distribution to the signature scores. The distribution was skewed towards lower signature scores (corrected $z^3 = -1.94$). While most of the tumors fell within 2 standard deviations of the mean, there was a subset of tumors ($n = 70$) which had low expression of melanocyte lineage genes (low was defined as being $> 2SD$ below the mean) (Figure 2.2D). There were no tumors which had a signature score $> 2 SD$ above the mean. As expected, tumor purity was correlated with the expression of melanocyte lineage genes (Figure A-2.10), but this does not fully explain why these tumors have lower expression of these genes given the magnitude of the downregulation of the melanocyte lineage signature. Consistent with the finding that RhoA is activated in de-differentiated BRAFi-resistant cell lines, we also found that tumors with decreased expression of melanocyte lineage genes have increased expression of RhoA/C target genes (Figure 2.2E).

The small fraction of tumors ($n = 70$ out of 473 total tumors) which have decreased expression of melanocyte lineage genes may be due to the fact that all of the tumors in this dataset were treatment-naïve with respect to BRAF inhibitors. Since the transcriptional profile of these lineage-low tumors is similar to that of the BRAFi-resistant cell lines, it is possible that these tumors may have intrinsic resistance to BRAF inhibitors. To test this hypothesis, we generated gene expression signatures from GDSC data to predict drug response for 265 common anti-cancer compounds using a random forest machine learning algorithm (see materials and methods). These signatures were then projected onto the TCGA dataset to predict drugs to which the de-differentiated tumors should be differentially sensitive to (Figure 2.2F). As expected, the de-differentiated tumors are predicted to be less sensitive to multiple BRAF and MEK inhibitors, including PLX4720 (a structurally similar vemurafenib analog). These predictions support the idea

that the ~15% of treatment-naive melanoma tumors with a de-differentiated transcriptional signature are less sensitive to BRAF inhibition even before selection by BRAFi treatment. This supports what we observed in experimentally derived resistant cell line models. Also, de-differentiated tumors are predicted to have increased sensitivity to multiple ROCK inhibitors which is interesting since ROCK is one of the canonical RhoA effector proteins^{192,193}.

The observation that RhoA activation is inversely correlated with differentiation status in human tumors could be marred by the contribution of non-malignant cells to the overall bulk gene expression profile of the tumor. For example, it is expected that in some cases cancer-associated fibroblasts or endothelial cells might have high RhoA activity^{194,195}. To more directly address the hypothesis that differentiation status is inversely correlated with Rho activation in *melanoma cells* we used publicly available single cell RNA-Seq data¹³² to correlate a RhoA/C signature and the Melanocyte Lineage signature. As expected, cells clustered together based on their tumor of origin which is due to the strong inter-tumor transcriptomic heterogeneity¹³². Even within a single tumor, poorly differentiated cells have elevated RhoA activation (Figure 2.2G). In total, these data suggest that tumors which acquire a de-differentiated phenotype have elevated RhoA activation and are predicted to be more sensitive to inhibition of RhoA signaling.

ROCK inhibition sensitizes RhoA^{High} BRAFi-resistant melanoma cells

It is difficult to therapeutically target RhoA directly, so an alternative approach is to target downstream effector pathways. Since we predicted that poorly differentiated human melanoma tumors are more sensitive to ROCK inhibitors, it is possible that de-differentiated BRAFi-resistant cells are more sensitive to ROCK inhibitors. It is also possible that ROCK inhibition might re-

sensitize the resistant cells to Vemurafenib. To test this hypothesis we used two ROCK inhibitors, Y-27623 and Fasudil, which have structurally distinct chemical scaffolds. We also confirmed that both Y-27632 and fasudil reduce actin stress fiber formation in M229R cells (Figure A-2.11). RhoA^{High} BRAFi-resistant cells (but not RhoA^{Low} resistant cells) are more sensitive to either of the ROCK inhibitors as a single agent (Figure A-2.12). ROCK inhibition also re-sensitizes RhoA^{High} (but not RhoA^{Low}) BRAFi-resistant cells to vemurafenib (Figure 2.3A-H). Re-sensitization to vemurafenib was most pronounced in M229R cells (Figure 2.3I-K) which is interesting since these cells do not have increased MLC2 phosphorylation. Since increased sensitivity to ROCK inhibitors alone, or the effect of ROCK inhibitors on re-sensitizing cells to vemurafenib, is only observed in cells which have increased stress fibers it suggests that this combination treatment may be specific for cells/tumors which activate this signaling mechanism.

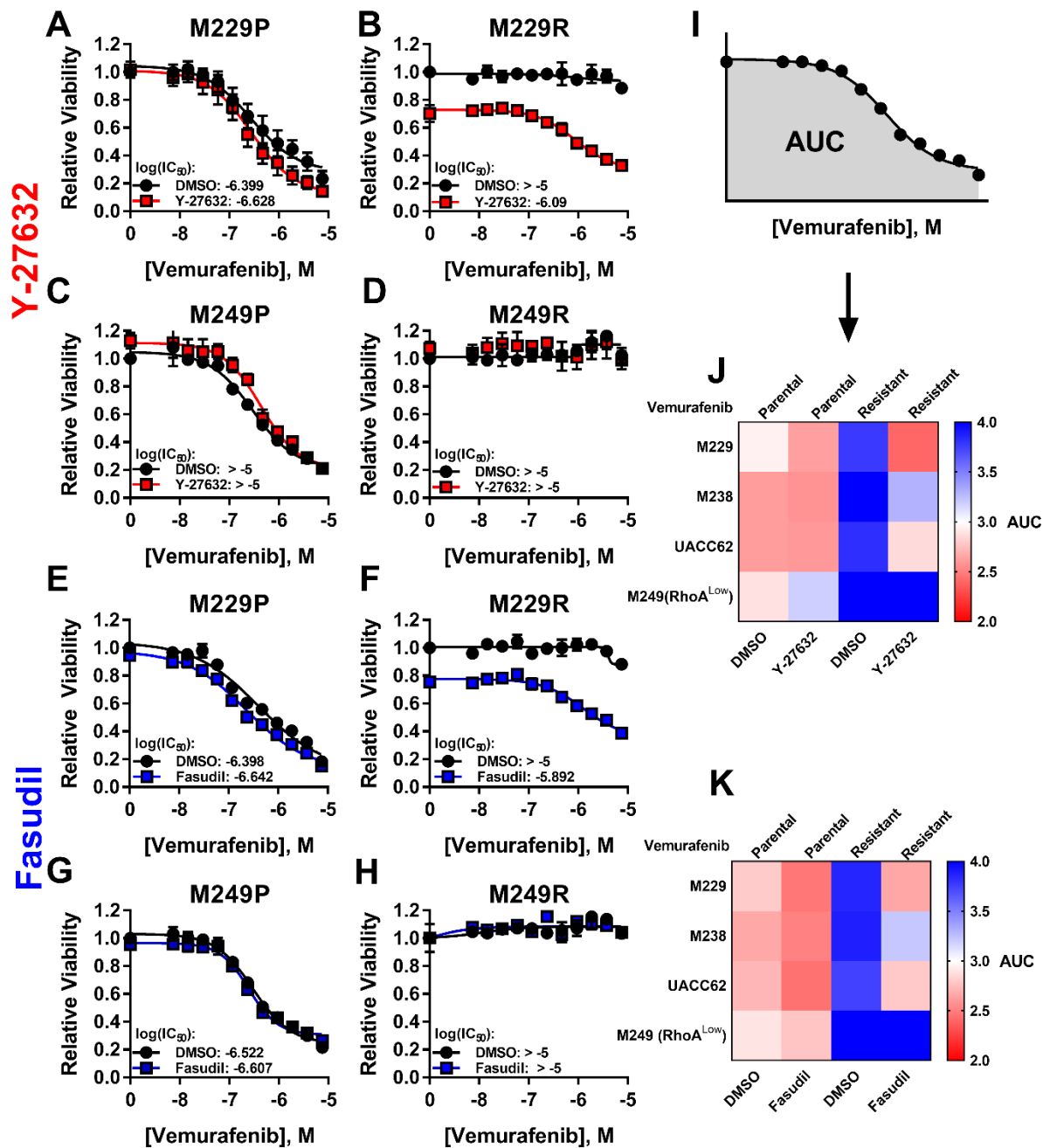


Figure 2.3: ROCK inhibition reverses BRAFi resistance in RhoA^{High} BRAFi-resistant melanoma cells Parental and Vemurafenib-resistant cell lines were seeded into 384-well plates at a density of 1,000 cells/well and cells were allowed to attach overnight. The next day, cells were treated with Vemurafenib at the indicated concentrations with or without the ROCK inhibitors Y-27632 (red) or Fasudil (blue) at 10 μ M. Cells were grown for 72 h then viability was measured with CellTiter-Glo. Pooled viability data from n = 3 biological replicates and n = 1 technical replicate. **A-H.** Cell lines were treated as labeled with ROCK inhibitors (Y-27632 or Fasudil) along with Vemurafenib. **I.** Schematic of Area Under Curve (AUC) calculation. Larger AUC indicates lower sensitivity to the drug combination and smaller AUC indicates greater sensitivity to the drug

Figure 2.3 (cont'd) combination. J. Heatmap of AUC values for the Vemurafenib/Y-27632 drug combination for four parental and resistant cell line pairs. **K.** Heatmap of AUC values for the Vemurafenib/Fasudil drug combination for four parental and resistant cell line pairs. Blue values indicate a high AUC and red values indicate a low AUC.

MRTF and YAP activation in RhoA^{High} BRAFi-resistant cells

In addition to modulating cytoskeletal re-arrangement, RhoA also regulates gene expression. Two transcriptional co-activators downstream of RhoA are YAP1 and MRTF. MRTF and YAP1 have similar transcriptional outputs and can perform redundant functions in several contexts^{196,197}. To determine whether YAP1 and MRTF are activated in RhoA^{High} BRAFi-resistant cells, we measured the subcellular localization of YAP1 and MRTF-A (Figure 2.4A and 2.4B). YAP1 nuclear localization is elevated in M229R and M238R cells compared to matched parental cell lines and is elevated to a lesser extent in UACC62R cells. The converse is true with respect to MRTF-A localization since nuclear MRTF-A is increased in UACC62R cells but not M229R or M238R cells (Figure 2.4A and 2.4B). Expression of several MRTF/YAP1 target genes is also elevated in the cells which have increased nuclear MRTF/YAP1 localization (Figure A-2.13A). Several YAP1- and MRTF-related genes are highly expressed in BRAF-mutant cell lines with intrinsic BRAFi resistance (Figure A-2.14). These include the YAP1/MRTF target gene CYR61 and genes encoding proteins which activate RhoA (ARHGEF12, GNA11, GNA12, TGF β 1) as well as YAP1 and YES1.

YAP1 and MRTF gene signature activation is increased in the paired pre- and post-resistance human melanoma tumors which had an increase in RhoA/C signature gene expression (Figure 2.4C). Out of this subset of tumors, only 3/24 failed to upregulate either YAP1 or MRTF target genes. Half (12/24) of the tumors had upregulation of both YAP1 and MRTF gene

signatures, which could possibly result from the high degree of redundancy in the transcriptional output from YAP1 and MRTF. Another explanation is that this could result from the tumors consisting of a mixed population of YAP1^{High} and MRTF^{High} cells. Some tumors appeared to have selective activation of YAP or MRTF, which is interesting considering the apparent mutual exclusivity of MRTF-A/YAP1 activation in the experimentally derived cell line models. This is again consistent with the transcriptional alterations in the RhoA^{High} BRAFi-resistant cell lines since MRTFA and YAP1 gene signatures are both increased in the poorly differentiated tumors (Figure A-2.15). Taken together, these data demonstrate that YAP1 and/or MRTF are activated in nearly all of the poorly differentiated BRAFi-resistant cells/tumors.

We hypothesized that since increased MRTF-A/YAP1 nuclear localization is only in RhoA^{High} resistant cells that RhoA may be regulating their nuclear accumulation. To test this, we treated parental and resistant cells with Y-27632 and Fasudil and measured the subcellular localization of MRTF-A and YAP1 with immunofluorescent staining. Treatment with either ROCK inhibitor reduced YAP1 nuclear accumulation in M229R cells and reduced MRTF-A nuclear accumulation in UACC62R cells (Figure A-2.16).

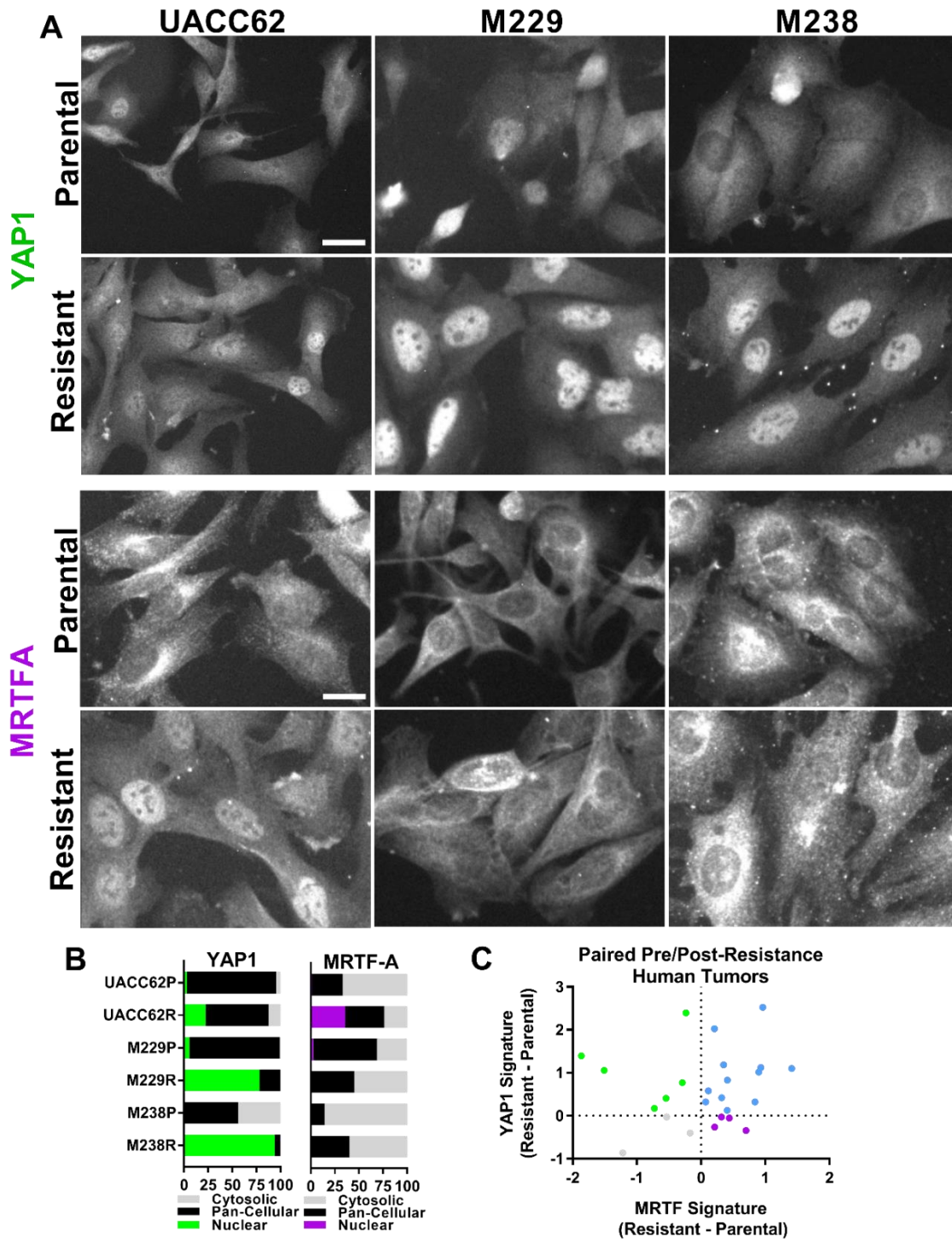


Figure 2.4: YAP1 and MRTF-A are activated in de-differentiated BRAFi-resistant cells A. M229P/R, M238P/R, and UACC62P/R cells were seeded into 8-well chamber slides and were allowed to attach overnight. The next day, cells were fixed and stained with an anti-YAP1 or anti-

Figure 2.4 (cont'd) MRTF-A antibodies. Representative images from n = 3 biological replicates and n = 1 technical replicate. Scale bar is 5 μ m. **B.** Quantification of staining from panel 'A'. Data are represented as a stacked bar graph wherein the fraction of cells that have predominantly nuclear, pan-cellular, or cytosolic localization is plotted as a fraction of the total cells. **C.** MRTF and YAP1 signatures were predicted for human melanoma tumor pairs which had an increase in RhoA/C signature score from (Figure 2.1G). Change in MRTF and YAP1 signature score between baseline and resistant tumors is plotted.

Pharmacologically targeting MRTF/YAP-mediated gene transcription

Since our results indicated that YAP1 and MRTF are activated in de-differentiated BRAFi-resistant cells, we reasoned that pharmacologically targeting these transcriptional mechanisms would be sufficient to re-sensitize cells to vemurafenib. YAP1 is activated by YES1, a Src family kinase. Previous studies have used the Src family kinase inhibitor dasatinib to inhibit YES1, resulting in a downregulation of YAP1 activity¹⁹⁸. There is also evidence which suggests that other Src family kinases activate YAP1¹⁹⁹. Using Src inhibition as an approach to block YAP1 activity is also interesting since our bioinformatics analysis predicted that poorly differentiated human tumors are more sensitive to Src inhibitors, including dasatinib (Figure 2.2F). To confirm this in the context of vemurafenib-resistant cells, we treated M229R and M238R cells with dasatinib and measured YAP1 nuclear localization. YAP1's nuclear localization is decreased in both cell lines upon dasatinib treatment (Figure 2.5A and 2.5B). While dasatinib reduces nuclear accumulation of YAP1, which theoretically should reduce YAP1-mediated gene transcription, expression of several YAP1 target genes is not altered by dasatinib treatment (Figure A-2.13B-D).

We next wanted to determine whether dasatinib re-sensitizes de-differentiated BRAFi-resistant cells to vemurafenib. Dasatinib treatment has only a minor effect on potentiating the vemurafenib response in the parental UACC62P and M229P cells, however, the vemurafenib response is greatly potentiated in the resistant UACC62R and M229R cells (Figure 2.5C-F). While

UACC62R does not have as robust YAP1 activation as M229R and M238R, the minor increase in YAP1 nuclear localization could explain why these cells also respond to dasatinib. This effect is consistent across all three de-differentiated BRAFi-resistant cell lines (Figure 2.5G). All three of the de-differentiated BRAFi-resistant cell lines also have increased sensitivity to dasatinib as a single agent (Figure A-2.17). Interestingly, in contrast with other similar experiments, we did not observe any change in vemurafenib sensitivity upon deletion of YAP1 with CRISPR (Figure A-2.18C and A-2.18D).

Our lab has developed a series of MRTF pathway inhibitors, including CCG-222740^{184-186,200}. We sought to determine whether this inhibitor can re-sensitize de-differentiated BRAFi-resistant cells to Vemurafenib. CCG-22740 has only a modest effect on re-sensitizing M229R or M238R cells, which have strong YAP1 but low MRTF-A activation and has the stronger re-sensitization effect in UACC62R cells (Figure 2.5H-L) which was the only BRAFi-resistant cell line with strong nuclear localization of MRTF-A. Also, UACC62R cells are more sensitive to CCG-222740 as a single agent (Figure A-2.17). Interestingly, despite the effect of CCG-222740 on viability and vemurafenib re-sensitization, CCG-222740 (10 μ M, 24 h) does not alter expression of several MRTF target genes at the mRNA level (Figure A-13B-D). To more directly determine the effect of MRTF-A on BRAFi resistance, we generated cells which stably express wildtype MRTF-A (Figure 2.5M). Cells expressing MRTF-A are approximately 10-fold less sensitive to vemurafenib (Figure 2.5N). Interestingly when we performed the inverse experiment, deletion of MRTF-A with CRISPR in resistant cells did not alter vemurafenib sensitivity (Figure A-2.18A and A-2.18B). Although we did not observe any overt change in MRTF-B localization when parental and resistant cell lines were compared under basal conditions (Figure A-2.19), it is

possible that MRTF-A depletion may induce MRTF-B activation. Taken together these data demonstrate that inhibition of RhoA-mediated gene transcription in de-differentiated melanoma cells, which can be mediated either by YAP1 or MRTF, re-sensitizes the melanoma cells to vemurafenib.

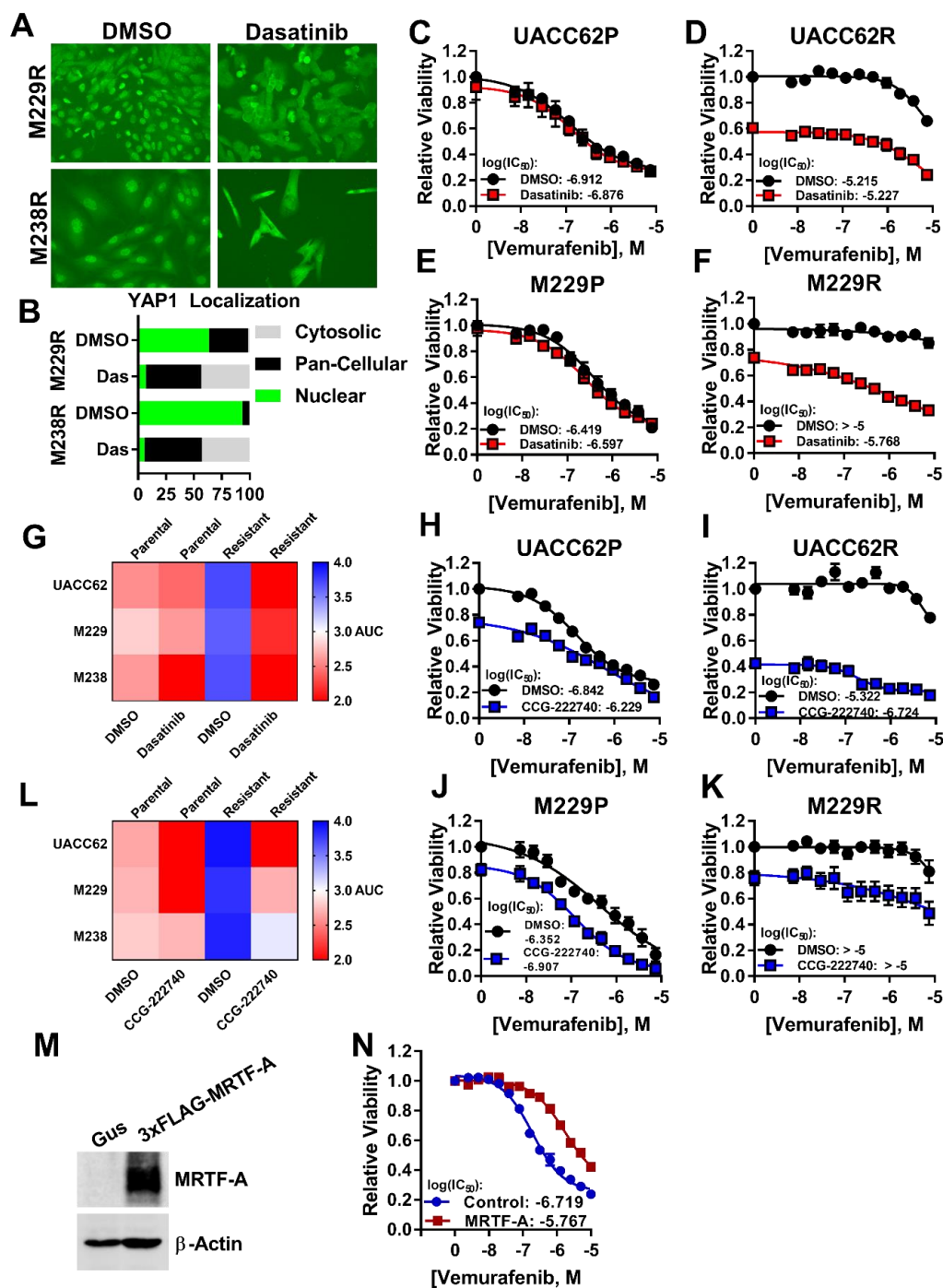


Figure 2.5: De-differentiated BRAFi-resistant cells are more sensitive to dasatinib and CCG-222740 **A.** Cells were seeded into 8-well chamber slides and were allowed to attach overnight. The next day, cells were treated with dasatinib (500 nM) for 16 h, then cells were fixed and stained with an anti-YAP1 antibody. Representative images from $n = 3$ biological replicates and $n = 1$ technical replicate. **B.** Quantification of YAP1 localization from panel “A”. Data are represented

Figure 2.5 (cont'd) as a stacked bar graph wherein the fraction of cells that have predominantly nuclear, pan-cellular, or cytosolic localization is plotted as a fraction of the total cells. **C-F.** Parental and Resistant cell lines were seeded into 384-well plates at a density of 1,000 cells/well and cells were allowed to attach overnight. The next day, cells were treated in dose response with Vemurafenib at the indicated concentrations +/- 100 nM dasatinib (red). After 72 h viability was measured with CellTiter-Glo. Dose response curves are viability data are from n = 3 biological replicates and n = 1 technical replicate. **G.** Heatmap of AUC values for the vemurafenib/dasatinib drug combination for four parental and resistant cell line pairs. **H-K.** Parental and Resistant cell lines were seeded into 384-well plates at a density of 1,000 cells/well and cells were allowed to attach overnight. The next day, cells were treated in dose response with Vemurafenib at the indicated concentrations +/- 10 μ M CCG-222740 (blue). After 72 h viability was measured with CellTiter-Glo. Dose response curves are viability data are from n = 3 biological replicates and n = 1 technical replicate. **L.** Heatmap of AUC values for the Vemurafenib/CCG-222740 drug combination for four parental and resistant cell line pairs. Blue values indicate a high AUC and red values indicate a low AUC. **M.** UACC62P cells were engineered to stably express Gus (Control) or MRTF-A as described in Materials and Methods. Immunoblots to measure MRTF-A levels were performed as described in Materials and Methods with β -Actin serving as a loading control. **N.** UACC62P cells stably expressing Gus (control) or MRTFA were seeded into 384-well plates and treated with a 14-point vemurafenib concentration gradient with a top dose of 10 μ M as described in the materials and methods. Data is average from n = 3 biological replicates with n = 3 technical replicates.

Discussion

In this study we sought to identify a pharmacological “Achilles heel” for BRAFi-resistant melanoma cells/tumors. In theory, if pathway-centric dependences can be identified for cells with acquired resistance, then co-targeting these resistance pathways concurrently with MAPK pathway inhibitors may delay, prevent, or reverse resistance. We found evidence for RhoA pathway activation in approximately half of BRAFi/MEKi-resistant human melanoma cells and tumors. In isogenic BRAFi-resistant cell lines, Rho pathway activation was accompanied by both an increase in actin stress fibers and usually MLC2 phosphorylation. These findings are consistent with previous reports which demonstrate that actin stress fibers are increased in cell line models of acquired BRAFi resistance¹⁶³. Building off these findings, we demonstrated that ROCK inhibition re-sensitizes Rho^{High} BRAFi-resistant cells to vemurafenib, highlighting the importance of this signaling pathway in adaptive BRAFi resistance. This finding also supports our bioinformatics

predictions, since multiple ROCK inhibitors were among the drugs predicted to be selective for poorly differentiated melanoma tumors.

We next wanted to identify signaling mechanisms which are associated with RhoA pathway activation. These signaling mechanisms could serve as biomarkers for RhoA activation or these pathways could directly promote RhoA activation. Upon acquisition of drug resistance all of the RhoA^{High} cell lines downregulate an array of melanocyte lineage genes such as TYR, MLANA, and SOX10. This is accompanied by upregulation of multiple cancer invasion-associated genes including AXL and SOX9 as well as several collagen and integrin isoforms. De-differentiation of melanoma cells has previously been linked to drug resistance. For instance, a decrease in MITF/AXL gene expression ratio marks BRAFi resistance^{114,132,174}. In another study silencing of SOX10, which was one of the most downregulated genes in our analysis, promotes BRAFi resistance¹⁴². But whether de-differentiation is directly inducing RhoA activation, or if RhoA activation is simply associated with de-differentiation is a question that still needs to be addressed.

As a result of modulating the actin cytoskeleton, Rho regulates gene transcription. Rho-induced F-actin polymerization allows for MRTF and YAP1 to translocate into the nucleus where they subsequently regulate gene transcription^{67-69,201-203}. Interestingly, some reports suggest that MRTF and YAP1 physically interact and are present in close proximity on similar gene promoters¹⁹⁶, while others suggest more indirect mechanisms of shared gene expression control¹⁹⁷. While YAP1 has been previously demonstrated to promote BRAFi resistance in melanoma^{131,163-165}, the role of MRTF in BRAFi resistance is unknown. In this study we demonstrate that nuclear accumulation of either MRTF-A or YAP1 is increased in RhoA^{High} BRAFi-resistant cells. We also demonstrate that overexpression of MRTF-A induces vemurafenib resistance. Conversely, our

data demonstrates that an MRTF pathway inhibitor increases vemurafenib sensitivity. Further work is required to determine how MRTF promotes BRAFi resistance and whether those signaling mechanisms are similar to the mechanisms by which YAP1 promotes BRAFi resistance. Interestingly, we observed YAP1 activation in 2 of 3 RhoA^{High} resistant cell lines, and MRTF-A activation in the 3rd cell line. This may suggest that MRTF-A and YAP1 are acting redundantly in this context and that activation of either MRTF-A or YAP1 is sufficient to promote drug resistance.

Our data demonstrate that MRTF-A and YAP1 are activated in vemurafenib-resistant cells our data are conflicting on whether MRTF-A and YAP1 are required for the development of drug resistance. In this study deletion of YAP1 in M229R cells did not alter vemurafenib response, where other studies found that YAP1 silencing either partially reverses vemurafenib resistance or increases vemurafenib sensitivity^{131,163,165}. One of these studies utilized M229, a cell line which we also used. In our study, cells were used within 14 days of viral CRISPR transduction. We hypothesize that YAP1 is promoting drug resistance by binding to transcription factors such as TEADs and regulating gene transcription. However, it is also possible that YAP1 may promote drug resistance via altering chromatin remodeling, in which case short-term deletion of YAP1 may not provide sufficient time for this process to take place.

Similarly, MRTF-A overexpression promotes vemurafenib resistance but we did not see reversal of resistance when MRTF-A was deleted. This could be because MRTF-A may promote drug resistance via altering chromatin remodeling, or it could be because MRTF-A deletion induces compensatory activation of other transcriptional mechanisms. We recently identified Pirin as a target for the CCG-222740 series of compounds²⁰⁰. Given the role of Pirin in melanoma²⁰⁴⁻

²⁰⁶, it is possible that compound effects on vemurafenib sensitivity may also involve Pirin actions that may or may not be directly related to MRTF-A.

This study focuses on MRTF/YAP1-mediated gene transcription downstream of RhoA, however there are other signaling mechanisms which may be important in RhoA-mediated drug resistance. Several studies have highlighted various signaling interactions between ERK and RhoA. For example RhoA increases ERK nuclear localization²⁰⁷ and RhoA silencing reduces ERK phosphorylation²⁰⁸. Other studies in different model systems observe the opposite effect since treatment with the ROCKi Y-27632 increases ERK phosphorylation and expression of constitutively active RhoA decreases ERK phosphorylation²⁰⁹. While these data are conflicting, these studies do raise the possibility that RhoA activation may modulate ERK activity in drug-resistant cells. RhoA activation could also promote BRAFi resistance through other transcriptional mechanisms such as AP-1²¹⁰ or NFκB²¹¹. Both AP-1²¹² and NFκB²¹³ promote BRAFi resistance, so transcriptional mechanisms other than MRTF/YAP1 may play a role in RhoA-mediated drug resistance. But the potential interaction between these transcription factors is especially interesting since AP-1 cooperates with TEAD^{214,215} and NFκB²¹⁶ to regulate gene transcription, suggesting that multiple RhoA effectors may work together to promote drug resistance.

This study demonstrates that Rho^{High} BRAFi-resistant cells are re-sensitized to vemurafenib by ROCK inhibitors and that this Rho^{High} phenotype is linked to de-differentiation. The direct signaling mechanisms which lead to Rho activation in melanoma cells are still unclear, but it is enticing to suggest that induction of TGFβ upon Sox10 loss¹⁴² may lead to RhoA activation. However, it is possible that TGFβ may be inducing de-differentiation^{217,218} and RhoA activation simultaneously through different signaling mechanisms. Future studies will be

necessary to elucidate details of these signaling networks. While it is already known that YAP1 promotes BRAFi resistance, these studies build upon that knowledge to demonstrate that dasatinib blocks the nuclear accumulation of YAP1 and enhanced drug sensitivity in BRAFi-resistant cells. Since dasatinib and other SRC kinase inhibitors are already FDA-approved for other indications, it highlights the potential of a re-purposing approach for treatment of BRAFi/MEKi-resistant melanomas. In this context, dasatinib may be most effective in combination with vemurafenib; in at least one resistant cell line vemurafenib potency was restored to that of parental cells. These studies also link MRTF-A activation to BRAFi resistance for the first time, highlighting the potential of targeting MRTF-mediated transcription to prevent or treat drug resistant melanoma. In total, these studies provide robust predictions of precision therapy approaches to prevent or treat clinical BRAFi resistance based on pharmacological inhibition of RhoA-mediated gene transcription.

CHAPTER 3:
Ibrutinib blocks YAP1 activation and reverses BRAFi resistance in melanoma cells

Sean Misek performed all wet lab experiments. Patrick Newbury, Evgenii Chekalin, Shreya Paithankar, and Bin Chen performed computational compound prediction analysis.

Abstract

Most BRAF-mutant melanoma tumors respond initially to BRAFi/MEKi therapy, although few patients have durable long-term responses to these agents. The goal of this study was to utilize an unbiased computational approach to identify inhibitors which reverse an experimentally derived BRAFi resistance gene expression signature. Using this approach, we found that ibrutinib effectively reverses this signature and we demonstrate experimentally that ibrutinib re-sensitizes a subset of BRAFi-resistant melanoma cells to vemurafenib. Ibrutinib is used clinically as a BTK inhibitor; however, neither BTK deletion nor treatment with acalabrutinib, another BTK inhibitor with reduced off-target activity, re-sensitized cells to vemurafenib. These data suggest that ibrutinib acts through a BTK-independent mechanism in vemurafenib re-sensitization. To better understand this mechanism, we analyzed the transcriptional profile of ibrutinib-treated BRAFi-resistant melanoma cells and found that the transcriptional profile of ibrutinib was highly similar to that of multiple SRC kinase inhibitors. Since ibrutinib, but not acalabrutinib, has significant off-target activity against multiple SRC family kinases, it suggests that ibrutinib may be acting through this mechanism. Furthermore, genes either upregulated or downregulated by ibrutinib treatment are enriched in YAP1 target genes and we showed that ibrutinib, but not acalabrutinib, reduces YAP1 activity in BRAFi-resistant melanoma cells. Taken together, these data suggest that ibrutinib, or other SRC family kinase inhibitors, may be useful for treating some BRAFi/MEKi-refractory melanoma tumors.

Introduction

Approximately 90% of melanoma tumors harbor activating mutations in the MAPK pathway and most of these tumors have BRAF^{V600} mutations². Most BRAF-mutant melanoma tumors initially respond to BRAF inhibitors (BRAFi), however, this response is often short-lived and most tumors develop resistance^{87,173}. Mechanisms of resistance to BRAFi/MEKi therapy most commonly occur through re-activation of the mitogen activated protein kinase (MAPK) pathway^{38,43,128,130,131,135,141,150,167-171,174-177}. However, there are few if any effective clinical interventions that overcome BRAFi resistance after it develops. In this study, we sought to identify compounds which reverse a BRAFi resistance gene signature. This systems-based approach has been widely explored in cancer drug discovery²¹⁹⁻²²³, yet few studies have investigated resistance in melanoma. Ultimately, the goal is to identify drugs which could be combined with BRAFi/MEKi therapy to prevent or reverse drug resistance.

One advantage to using this approach is that it allows for the identification of compounds whose effects may result from complex polypharmacology. There are several examples of the clinical utility of drugs that exhibit polypharmacology, including crizotinib, afatinib, ceritinib, dasatinib, erlotinib, nilotinib, ponatinib, and imatinib²²⁴. In the case of imatinib, it was first developed to inhibit a BCR-ABL fusion protein in CML²²⁵⁻²²⁷. But later imatinib was used to target dermatofibrosarcoma protuberans tumors harboring gene fusions which result in aberrant PDGFR activation or gastrointestinal stromal tumors which have activating PDGFRA or KIT mutations since imatinib has off-target activity against PDGFR and KIT²²⁸⁻²³³. Several molecules, many of which are not kinase inhibitors, are currently under clinical investigation and have a mechanism of action linked to previously unappreciated off-target effects²³⁴. These examples

likely represent only a fraction of circumstances in which kinase inhibitor polypharmacology is clinically relevant. Because of this, there have been recent large-scale efforts to profile kinase inhibitor polypharmacology²³⁵. Defining the entire polypharmacology network will result in a sizeable increase in the number of clinically actionable applications.

In this study we identify a new role for ibrutinib, an FDA-approved BTK inhibitor, in reversing BRAFi resistance in melanoma *in silico* and *in vitro*. Our studies suggest that ibrutinib may modulate YAP1 activation in BRAFi resistant melanoma cells. YAP1 is a transcriptional co-activator whose activity is regulated by the actin cytoskeleton, as well as through changes in the phosphorylation state of YAP1²³⁶⁻²³⁹. Some phosphorylation events on YAP1 by LATS1/2 lead to inactivation and subsequent proteasomal degradation²⁴⁰ whereas phosphorylation at other sites, targeted by YES1 and other kinases, is critical for YAP1 nuclear translocation and activation¹⁹⁸. YAP1 is activated in BRAFi-resistant melanoma cells and silencing or deletion of YAP1 reverses BRAFi resistance^{131,163-165,241}. In addition to melanoma, YAP1 has been implicated in many other cancer types including breast cancer²⁴², glioblastoma²⁴³, pancreatic cancer²⁴⁴, hepatocellular carcinoma²⁴⁵, and non-small-cell lung cancer²⁴⁶. Despite the importance of YAP1 in cancer, it is still difficult to pharmacologically target YAP1. Verteporfin, a drug used to treat macular degeneration, blocks YAP1-TEAD activity *in vitro*, but in some models has limited efficacy *in vivo*²⁴⁷. Since YAP1 activity is regulated by its phosphorylation state, it may be possible to utilize the polypharmacology of FDA-approved kinase inhibitors to indirectly block YAP1 activation. In this study we found that ibrutinib blocks the nuclear accumulation of YAP1, suggesting that it may be possible to re-purpose ibrutinib or related SRC-family kinase inhibitors to treat YAP1-driven cancers.

Materials and Methods

Cell lines, reagents, and antibodies:

Parental (denoted by a *P* suffix in the cell line name) and matched isogenic BRAFi-resistant cells (denoted by an *R* suffix in the cell line name) were either a gift (M229P/R, M238P/R) from Dr. Roger Lo (UCLA) or generated in our laboratory (UACC62P/R). These cells were generated and cultured as described below ²⁴¹.

Luteolin (#10004161), BVT-948 (#16615), ketoprofen (#10006661), lestaurtinib (#12094), L-NMMA (#10005031), ibrutinib (#16274), acalabrutinib (#19899), fadrozole (#24272), letrozole (#11568), exemestane (#15008), and vemurafenib (#10618) were purchased from Cayman Chemical (Ann Arbor, USA). Pyrvinium pamoate (#HY-A0293) was purchased from MedChemExpress (Monmouth Junction, USA). Clofilium tosylate (#C2365) was purchased from Sigma Aldrich (St. Louis, USA). All compounds (except L-NMMA) were diluted in DMSO to a stock concentration of 10 mM. L-NMMA was diluted in H₂O to a stock concentration of 0.5 mM. All compounds were aliquoted and stored at -20°C.

Antibodies against YAP1 (#14074) and TAZ (#83669) were purchased from Cell Signaling (Danvers, USA). An antibody against Actin (#sc1616) was purchased from Santa Cruz Biotechnology (Dallas, USA). Donkey anti-Mouse800 (#926-32212), Donkey anti-Goat680 (#926-68074), and Donkey anti-Rabbit680 (#926-68073) immunoblotting secondary antibodies were purchased from LI-COR (Lincoln, USA). Anti-rabbit-HRP (#7074) immunoblotting secondary was purchased from Cell Signaling Technology. Alexa Fluor goat anti-rabbit488 (#A11034) and donkey anti-goat488 (A11055) were purchased from Invitrogen (Carlsbad, USA).

Cell culture:

Cells were cultured in DMEM (ThermoFisher, Waltham, USA #11995-065) supplemented with 10% FBS (ThermoFisher, #10437-028) and 1% Antibiotic-Antimycotic (ThermoFisher, #15240062) and were passaged at approximately 75% confluence. The BRAFi-resistant cell line variants were maintained in culture medium supplemented with 2 μ M vemurafenib. Vemurafenib was removed from the culture medium when cells were seeded for experiments, except where otherwise indicated. Cells were routinely tested for mycoplasma contamination by DAPI staining. Short Tandem Repeat (STR) profiling on all cell lines was performed at the MSU genomics core. In all cases, isogenic pairs of cell lines had identical STR profiles. After thawing cells were used for either 2 months or 20 passages, whichever came first.

Cloning/CRISPR:

For CRISPR experiments the sgRNA were: sgControl (5'-TCCCCGAGACCATCTTAGGG-3'), sgBTK#1 (5'-ATGAGTATGACTTTGAACGT-3'), and sgBTK#2 (5'-CCCTTCATCATATACAACCT-3'). These guide sequences were cloned into pLentiCRISPRv2-Puro (from Feng Zhang, Addgene plasmid #52961). Successful cloning was confirmed by Sanger sequencing. To measure knockout efficiency, amplicons containing the CRISPR cut sites were amplified from the genomic DNA with PCR and the ratio of frameshifted/functional DNA species was measured with Sanger sequencing using the TIDE algorithm²⁴⁸.

Virus preparation and infection:

HEK-293T cells were seeded into 10-cm plates at a density of 4×10^6 cells/plate and the cells were allowed to attach overnight. The next day the cells were transfected with a plasmid cocktail containing 5000 ng of the pLentiCRISPRv2 plasmid, 5000 ng of psPAX2 (Addgene plasmid #12260), 500 ng of pMD2.G (Addgene plasmid #12259), and 20 μ L of Lipofectamine 2000 (ThermoFisher, #11668019) in 400 μ L of OptiMEM (ThermoFisher, #31985070). The next morning the medium was changed to 10 mL of fresh complete culture medium, and the following day each plate was supplemented with an additional 5 mL of culture medium. After 24 h, the culture medium was harvested and filtered through a 0.45- μ m syringe filter. Virus was stored at 4°C and was used within 2 weeks.

Melanoma cells were seeded into 10-cm plates at a density of 5×10^5 cells/plate in 10 mL of complete culture medium. While the cells were still in suspension, 3 mL of viral supernatant was added to each plate. The cells were incubated with virus overnight, then the medium was changed to 10 mL of fresh medium. After 24 h, the medium was changed to 10 mL of fresh medium supplemented with puromycin (2 μ M). The cells were cultured in the presence of selection antibiotic until all the cells on the kill control plate died (approximately 3 days). Individual clones for the CRISPR cell lines were not selected, but instead we used a pooled infection approach. Validation of CRISPR knockout efficiency was performed by Sanger sequencing as described above.

Viability experiments:

Cells were seeded into 384-well tissue culture plates (PerkinElmer, Waltham, USA, #6007689) at a density of 1000 cells/well in 20 μ L of growth medium. The next day, compounds were pre-diluted in growth medium then added to the 384-well plates so that the final volume of each well was 40 μ L. A PBS or growth medium barrier was added to the outer wells of the plate to limit evaporation. Cells were cultured under these conditions for 72 h. To assess viability, 8 μ L of CellTiter-Glo (Promega, Madison, USA, #G7573) was added to each well. Plates were incubated on orbital shaker for 5 min at room temperature, then briefly centrifuged (4000 rpm, 60 s) before being read on a Bio-Tek Synergy Neo plate reader with the #11 and #41 Ex/Em filter cubes. Viability signal is plotted versus log (Vemurafenib concentration) for each treatment condition.

Flow cytometry:

Cell cycle: Cells were rinsed once in PBS before being trypsinized, washed once in PBS and immediately fixed in 70% ethanol for 20 min at room temperature. The cells were washed once and were re-suspended in PBS supplemented with 20 μ g/mL propidium iodide (#P1304MP, ThermoFisher) and 200 μ g/mL RNaseA. The cells were briefly mixed and were incubated on ice for 20 min. Following incubation, the cells were filtered through a 70 μ M filter and were run on an Accuri C6 flow cytometer (BD Biosciences, Franklin Lakes, USA). Data were analyzed with the FCS Express flow cytometry analysis software package.

Annexin V/Propidium Iodide: Both floating and adherent cells were collected by trypsinization. The cells were pelleted, washed once in PBS, and then re-suspended in 200 μ L of Annexin V binding buffer (10 mM HEPES pH 7.4, 140 mM NaCl, 2.5 mM CaCl₂) and 1 μ L of APC-

conjugated Annexin V (ThermoFisher, #A35110) on ice in the dark for 20 min. The cells were pelleted and re-suspended in 500 μ L Annexin V binding buffer with 2 μ g/mL propidium iodide. After 20 min the cells were filtered through a 70 μ M filter and were run on an Accuri C6 flow cytometer. Data were analyzed with the FCS Express flow cytometry analysis software package.

DEVD Assay:

Both the floating and attached cells were collected, rinsed as described above and then lysed in 200 μ L of Triton-X100 lysis buffer (25 mM HEPES, 100 mM NaCl, 1 mM EDTA, 10% glycerol, 1% Triton X-100) supplemented with protease/phosphatase inhibitors. The lysates were centrifuged at 20,000g for 15 min. In a 384-well plate 10 μ L of 2x Cytobuffer (100 mM PIPES pH 7.4, 20% glycerol, 2 mM EDTA, 1 mM DTT, 40 μ M DEVD-AFC²⁴⁹ (Enzo Biochem, Farmingdale, USA, #ALX260032M005), 5 μ L of lysis buffer, and 5 μ L of cellular lysate was added to each well. In control wells an extra 5 μ L of lysis buffer was added in place of the cellular lysate. The plates were prepared on ice to limit enzymatic activity. The plates were read on a Bio-Tek Synergy Neo plate reader at an excitation wavelength of 400 nm and an emission wavelength of 500 nm. Reads were taken every 60 sec for 1 h and caspase3/7 activity is expressed as fold change in nM/AFC/mg/min.

Colony formation:

Cells were seeded into 6-well plates at a density of 1000 cells/well and were allowed to attach overnight. The next day the medium was changed, and the cells were treated as described in the figure legends. The growth medium was changed every 3 days. After 14 days the cells were fixed

in 3.7% formaldehyde and the cells were stained with crystal violet. Images of the plates were acquired on a flat-bed scanner.

Immunofluorescence staining:

Cells were seeded into 8-well chamber slides and were treated as indicated in the figure legends. Cells were fixed with 3.7% formaldehyde for 15 min, and then blocked in 2% BSA PBS-Triton X-100 (0.1%) for 1 h at room temperature. Cells were incubated overnight at 4°C in primary antibody at a (1:1,000) dilution in blocking buffer. Cells were washed 3x in PBS then were incubated in the appropriate secondary antibody at a (1:1,000) dilution for 1 h at room temperature. Cells were washed 3x in PBS then were mounted in ProLong Gold Antifade + DAPI (ThermoFisher, #P36935). Slides were cured overnight at room temperature, and then transferred to 4°C. Slides were imaged on a Nikon TE2000-U fluorescence microscope at 20x magnification.

For all immunofluorescence experiments, images were blinded with an R script before quantification. We repeated all immunofluorescence experiments at least three times and typically analyzed 5-10 fields per biological replicate. In total we analyzed at least 200 cells per experimental group, but in most cases over 1000 cells per experimental group. For subcellular localization experiments, data are represented as a stacked bar graph wherein the fraction of cells that have predominantly nuclear, pan-cellular, or cytosolic localization is plotted as a fraction of the total cells. A cell was considered to have “cytosolic” localization if there was a clear nuclear exclusion. Inversely a cell was described as having “nuclear” localization if the staining intensity was appreciably higher than in the cytosol. If there was no apparent difference between the nuclear and cytosolic staining, then the cell was described as having “pan-cellular” distribution.

RNA-Seq sample/data processing:

Total cellular RNA was extracted from drug-treated M229R cells using the Qiagen (Hilden, Germany) RNeasy kit (#74104) with three biological replicates per cell line. All RNA samples had a RIN score > 8. Libraries were prepared using the Illumina TruSeq Stranded mRNA Library Preparation Kit, prepared libraries were quality controlled and quantified using a Qubit and Labchip Bioanalyzer. Libraries were pooled and run on a NovaSeq6000 instrument. Sequencing was performed by 2 x 150 bp paired-end read format. Base calling was done by Illumina RTA and converted to FASTQ using bcl2fastq software. Sequencing was performed at a depth of approximately 30 M reads/sample. Quality control was performed on the FASTQ files using FastQC v0.11.5, and reads were trimmed using Trimmomatic v0.33. Reads were mapped using HISAT2 v2.1.0 and analyzed using HTSeq v0.6.1. Differential gene expression was calculated using edgeR. Raw RNA-Seq reads and processed HTSeq read counts are available on GEO under GSE145990. When appropriate RNA-Seq data was upper quintile normalized prior to analysis.

Datasets:

Sources for the previously published RNA-Seq data used in this study are as follows. M229P/R and M238P/R RNA-Seq data was downloaded from GSE75313¹⁷⁴. UACC62P/R RNA-Seq data was previously generated by our group and was deposited under GSE115938²⁴¹. The PRISM drug response dataset was downloaded from the DepMap data download portal (depmap.org/portal/download).

LISA:

Epigenetic landscape in silico subtraction analysis (LISA) was run on lisa.cistrome.org ²⁵⁰. Gene lists were filtered to include only significantly differentially expressed genes (FDR < 0.01). Gene set 1 was filtered to include only upregulated genes, and gene set 2 was filtered to include only downregulated genes. Only the top 500 genes were used in each list. In cases where there were fewer than 500 differentially expressed genes, only the genes which had an FDR < 0.01 were included in the analysis. The ChIP-Seq output data was plotted as a scatter plot of enrichments in the upregulated vs downregulated gene sets.

Connectivity map analysis:

The top 200 upregulated/downregulated genes (FDR < 0.01) were analyzed to identify CMap Classes which have similar gene expression perturbation signatures on the online clue.io portal. In cases where there were fewer than 200 upregulated or downregulated genes with an FDR < 0.01, only genes which passed the FDR cutoff were included in the analysis.

OCTAD Datasets and RNA-Sequence processing:

We used the same pipeline to process RNA-Seq samples from public databases such as TCGA, TARGET, GTEx, and SRA and compiled them into one single dataset called OCTAD ²⁵¹. Whenever possible, RNA-Seq samples used in this study were processed using the same pipeline to mitigate batch effects. In addition, RUVg ²⁵² was used to remove unwanted variation, and weakly expressed genes were removed while computing differentially expressed genes. Normalized raw counts were used for DE analysis and TPM was used for other analyses. The clustering of these samples with melanoma samples compared to non-melanoma primary tumor

samples demonstrates the feasibility of performing differential expression analysis between cell lines and tissue samples (Figure A-3.1).

Disease signature creation:

Gene expression data from BRAFi-resistant melanoma cell lines was compared with either 50 healthy normal skin samples from the GTEx database, or to BRAF^{V600E}-mutant melanoma tumor samples to generate BRAFi-resistance gene expression signatures. We used edgeR to perform DE analysis (\log_2 fold change > 1, adjusted p-value < 0.001) ²⁵³. The detailed data processing and parameter selection were detailed in the OCTAD study ²⁵¹. The enrichment of the genes in the BRAFi-resistance gene signatures was computed with ssGSEA ²⁵⁴. The association of enrichment scores for both of the signatures with patient survival was computed and visualized using the survminer package. Patient mutation status and survival data were retrieved from cBioPortal ²⁵⁵. EnrichR was used for pathway enrichment analysis ²⁵⁶.

Drug prediction:

The LINCS database containing gene expression profiles for compound-treated cells has been widely used for candidate drug prediction in our previous studies ^{221,257}. The LINCS library is comprised of 476,251 signatures and 22,268 genes including 978 landmark genes. The 1,974 mapped drugs listed in the Repurposing Hub were considered in this study ²⁵⁸. To compute RGEN scores, we first ranked genes based on their expression values in each drug signature. An enrichment score for each set of up- and down-regulated disease genes was computed separately using a Kolmogorov–Smirnov-like statistic, followed by the combination of scores from both

sides. The score is based on the number of the genes (up or down-regulated) at either the top or bottom of a drug-gene list ranked by expression change after drug treatment. One compound might have multiple available expression profiles because they were tested in various cell lines, drug concentrations, treatment durations, or even different replicates, resulting in multiple RGENs for one drug-disease prediction. We termed this score summarized RGEN (sRGEN). The computation of RGEN and the summarization RGEN were detailed elsewhere and recently implemented as a standalone R package²⁵¹. Compounds were filtered to include only compounds that had a sample size greater than 1 in the LINCS L1000 dataset and were filtered to exclude compounds that were anti-neoplastic or were previously studied in melanoma. A sRGEN threshold of -0.3 was the cutoff for compounds which effectively reversed the BRAFi resistance signature.

Results

Identification of compounds which reverse a BRAFi resistance signature

We employed a systems-based approach to identify compounds that reverse an experimentally derived BRAFi resistance signature (Figure 3.1A). This approach was originally proposed in the Connectivity Map project²¹⁹, and was extended in other studies^{222,259}, including a recent study from the Chen lab²²¹ which used sRGEN to quantify the reversal potency and demonstrated its positive correlation with drug efficacy. Sample collection, signature creation, sRGEN computation, and *in silico* validation were streamlined in the OCTAD pipeline which was described in the Materials and Methods section. This approach has been applied to identify potential therapeutic compounds for primary cancers, but this study is our first attempt to apply this method to study drug resistance.

We collected three datasets that include RNA-Seq profiles of parental and BRAFi-resistant melanoma cell lines (M229P/R, M238P/R, and UACC62P/R) with 2 biological replicates for each cell line. Initially we compared the profiles of parental and resistant cell lines for each dataset, but the gene signature did not effectively predict compound response using the CTRPv2 data; therefore, we decided to compare the resistant samples to healthy skin samples (n = 558) in the OCTAD database. We then used the most variable genes to select the 50 samples with the best correlation between healthy skin samples and BRAFi resistant samples. The comparison between these samples resulted in 191 DE genes that were included in the LINCS 978 landmark genes (\log_2 fold-change >1 and adjusted p-value < 0.001). The prediction identified 245 compounds with sRGES lower than -0.3. To computationally validate the predictions and tune parameters, we correlated the sRGES and compound sensitivity data for UACC62P cells in the CTRPv2 dataset (Figure A-3.2). The significant correlation (Spearman: 0.47, p-value: 1.6e-9) suggests that sRGES predictions are effective in predicting compound sensitivity in melanoma. Since one compound may be profiled against multiple cell lines in the LINCS L1000 dataset, we filtered RGES values by the mean score, standard deviation, and number of occurrences, and then performed enrichment analysis to confirm consistency across multiple cell lineages.

Nine compounds that reversed the BRAFi resistance gene expression signature *in silico* (Figure 3.1B) were selected and were examined for their ability to inhibit growth of matched parental and BRAFi-resistant melanoma cell lines. We identified 4 compounds that reduce cell viability in both M229P and M229R cells, with no apparent selectivity for one over the other (Figure A-3.3). This lack of selectivity is likely because both the parental and resistant cells were compared to normal tissue, instead of being directly compared against each other. Next, we created

a gene expression resistance signature consisting of 87 genes by comparing the gene expression data from the resistant cell lines with BRAF^{V600E}-mutant primary melanoma tumor samples in the OCTAD database. The expression signature is significantly associated with poor overall survival in melanoma patients with BRAF^{V600E} mutations (p = 0.006, Cox model), but not with BRAF^{WT} melanoma patients (p = 0.028), suggesting that this gene expression signature may be clinically relevant (Figure A-3.4). With this new signature 3/9 of the compounds (ibrutinib, pyrvinium, and lestaurtinib) were among the top 5% of compounds identified, with ibrutinib being the most effective in reversing the BRAFⁱ resistance signature (Figure A-3.5).

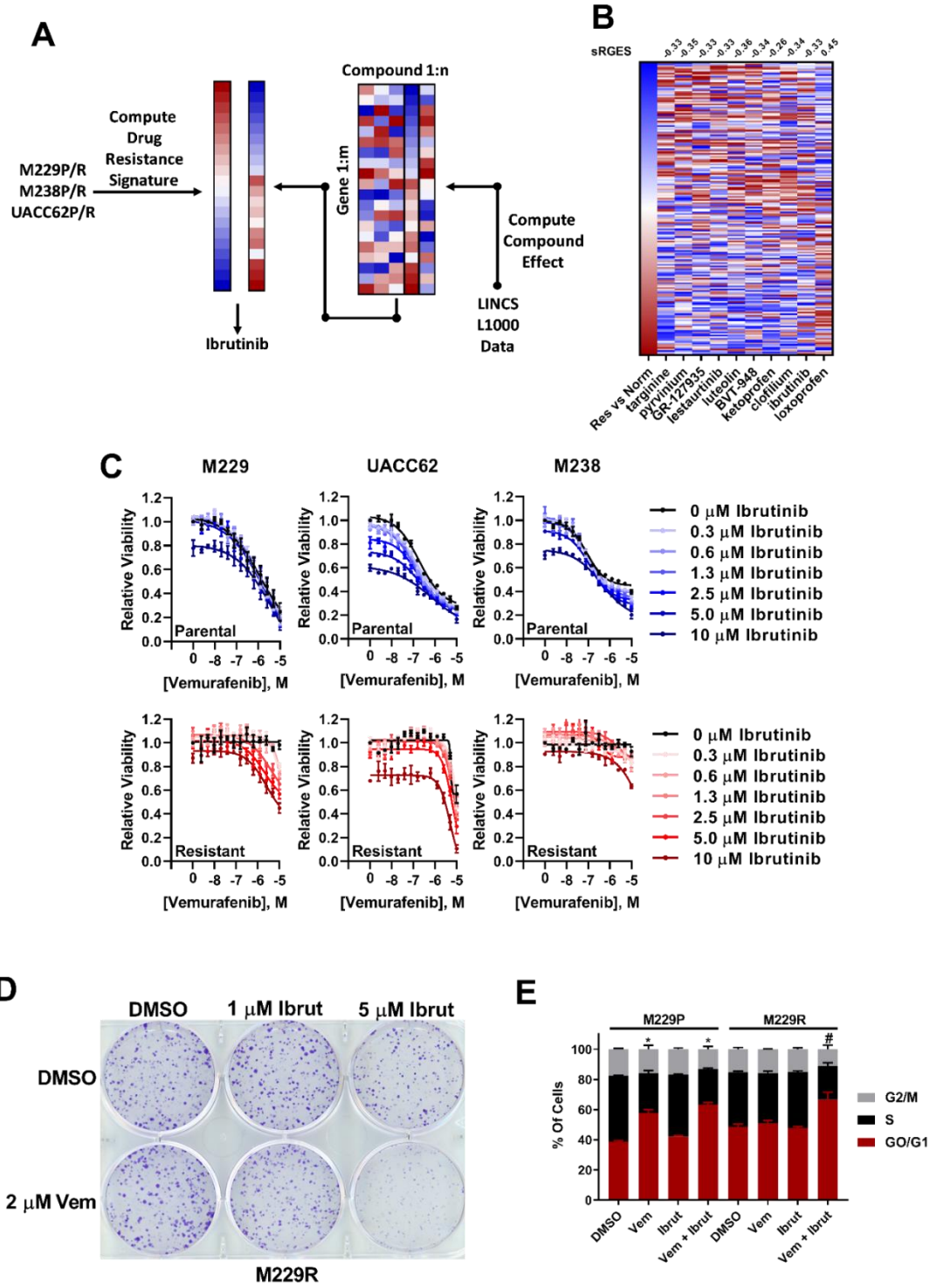


Figure 3.1: Ibrutinib re-sensitizes BRAFi-resistant cells to vemurafenib **A.** Diagram of drug resistance and reversal signatures. **B.** The BRAFi-resistance signature was computed by comparing BRAFi-resistant cell lines and normal tissue samples. Red boxes indicate upregulated genes, and blue boxes indicate

Figure 3.1 (cont'd) downregulated genes. Loxoprofen was included as a control, since this compound was not predicted to reverse the BRAFi-resistance signature. For compounds with multiple gene expression profiles, the profile with the median RGES was chosen for visualization. The sRGES values for the BRAFi-resistance signature and the compound-treated signatures are listed above the heatmap. **C.** M229P/R, UACC62P/R, and M238P/R cells were treated in a dose response matrix of ibrutinib (top concentration 10 μ M, 1/2 dilution series) and vemurafenib (top concentration 10 μ M, 1/2 dilution series). After 72 h, viability was measured with CellTiter-Glo. (n = 3 biological replicates) **D.** M229R cells were seeded into a 6-well plate at a density of 5,000 cells/well. The next day the cells were treated with the indicated concentrations of vemurafenib and ibrutinib. The colony formation assay was performed and analyzed as described in materials and methods. (n = 3 biological replicates) **E.** M229P/R cells were treated with -/+ 2 μ M vemurafenib, -/+ 1 or 5 μ M ibrutinib for 72 h. The cells were stained and analyzed by flow cytometry as described in materials and methods (n = 3 biological replicates). Significant differences of G0/G1 for compound treated samples vs the relevant DMSO control are indicated (One-way ANOVA, * p < 0.01 vs M229P-DMSO, # p < 0.01 vs M229R-DMSO).

Ibrutinib re-sensitizes BRAFi-resistant cells to vemurafenib

We reasoned that compounds which significantly reverse a BRAFi resistance gene expression signature should also reverse BRAFi resistance in melanoma cells in an experimental setting. To test this hypothesis, we profiled the synergy between vemurafenib and the top 9 hits from the computational screen in a 14x7 concentration response matrix with vemurafenib to identify compounds that can potentiate vemurafenib response. Out of the top 9 compounds identified in our screen, only ibrutinib reversed BRAFi resistance (Figure 3.1C, red curves and Figure A-3.6). One interesting observation is that while the computational screen was performed using RNA-Seq data from all three isogenic parental and resistant cell line pairs, only M229R was re-sensitized to vemurafenib by ibrutinib. Synergistic growth inhibition was also observed in a long-term colony formation assay, which was more apparent with higher concentrations of ibrutinib (Figure 3.1D). Since BRAF inhibitors arrest melanoma cells at the G1 checkpoint, if ibrutinib is truly re-sensitizing the resistant cells to vemurafenib it should also re-sensitize the cells to vemurafenib-induced G1 arrest. M229P cells accumulate in G0/G1 state during vemurafenib treatment but M229R cells do not. Consistent with re-sensitization we found that accumulation of M229R cells in G0/G1 is restored upon treatment with the combination of vemurafenib and

ibrutinib (Figure 3.1E). There was also an increased level of Annexin V-positive cells in the combination-treated group, although there was no change in Caspase 3/7 activity (Figure A-3.7). Taken together, these data suggest that ibrutinib re-sensitizes a subset of BRAFi-resistant cell lines to vemurafenib.

BTK deletion or inhibition does not re-sensitize BRAFi-resistant cells to vemurafenib

Since ibrutinib is known to have targets other than BTK^{235,260,261} we wanted to know whether BTK was responsible for BRAFi resistance. To test this hypothesis experimentally, we generated BTK knock out cell pools using CRISPR. BTK mRNA expression is nearly absent in both M229P and M229R (Figure A-3.8) cells making it technically ineffective to assay knockout efficiency by qPCR or immunoblotting, so we measured knockout efficiency by Sanger sequencing of gDNA amplicons which contain the region of the CRISPR cut site. The Sanger sequencing traces were subsequently de-convoluted with the TIDE algorithm²⁴⁸ to identify the fraction of cells that had functional knockout (Figure 3.2A and A-3.9). Using this approach, we found that the functional knockout efficiency was approximately 70%. Even though ibrutinib is used clinically as a BTK inhibitor, deletion of BTK did not alter the vemurafenib response in either the parental or resistant cells (Figure 3.2B). This suggested to us that ibrutinib may be re-sensitizing the cells through off-target inhibition of other kinases instead of by on-target inhibition of BTK. Since acalabrutinib is a BTK inhibitor analog of ibrutinib with significantly reduced off-target activity^{260,261}, we asked whether acalabrutinib^{260,261} reverses BRAFi resistance. Consistent with our hypothesis, acalabrutinib failed to re-sensitize BRAFi-resistant cells to vemurafenib (Figure 3.2C). Taken together, these data show that the effect of ibrutinib to re-sensitize BRAFi-resistant cells to vemurafenib is independent of on-target BTK inhibition.

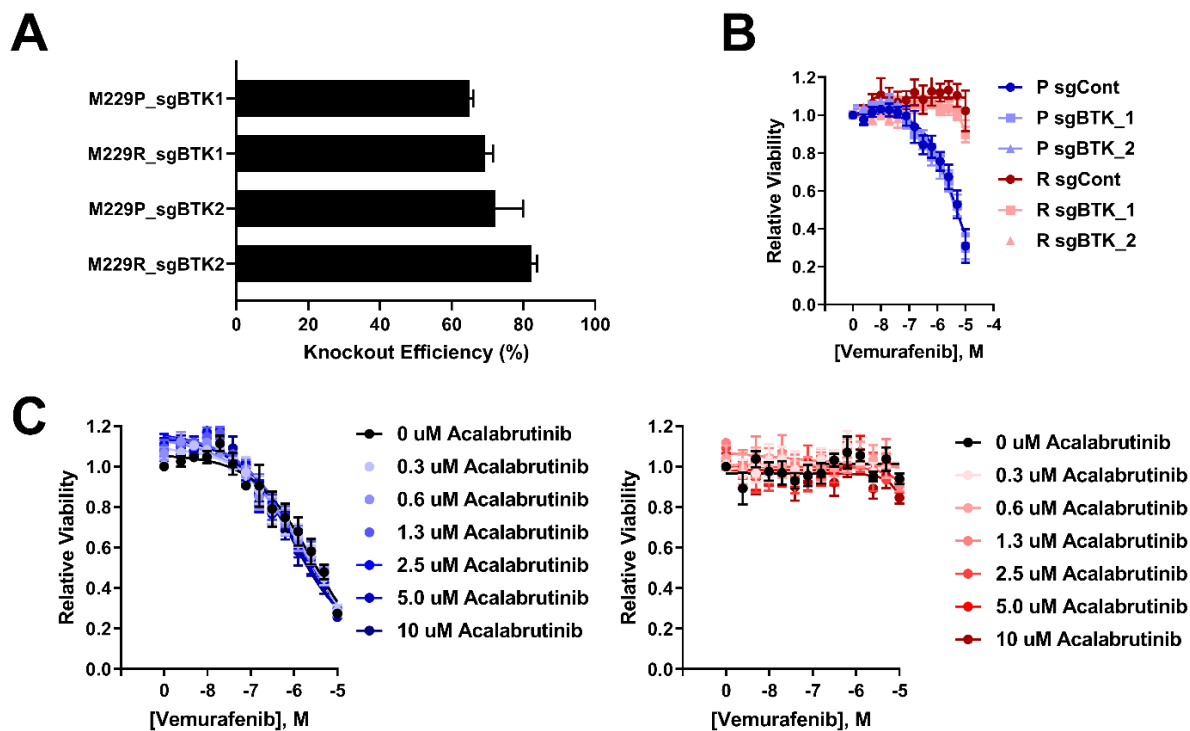


Figure 3.2: BTK deletion or inhibition does not alter vemurafenib sensitivity **A.** M229P/R BTK^{KO} cells were generated as described in Materials and Methods. Sanger sequencing was performed to measure the extent of BTK deletion in M229P/R cell pools. The fraction of cells with functional BTK deletion was quantified with TIDE (n = 3 biological replicates)/ **B.** M229P/R sgControl and sgBTK cells were treated with 14 concentrations of vemurafenib (10 μ M top concentration, $\frac{1}{2}$ dilution series) and, after 72 h, viability was measured with CellTiter-Glo as described in Materials and Methods. (n = 3 biological replicates) **C.** M229P/R cells were treated with 7 different concentrations of acalabrutinib (10 μ M top concentration, $\frac{1}{2}$ dilution series) and 14 different concentrations of vemurafenib (10 μ M top concentration, $\frac{1}{2}$ dilution series). After 72 h, viability was measured with CellTiter-Glo (n = 3 biological replicates).

Transcriptional response to ibrutinib treatment

To better understand how ibrutinib re-sensitizes BRAFi-resistant cells to vemurafenib we performed RNA-seq on M229R cells after treatment with vemurafenib, ibrutinib, acalabrutinib, or combinations. Consistent with the observation that ibrutinib, but not acalabrutinib, re-sensitizes BRAFi-resistant cells to vemurafenib we found that there were 101 differentially expressed genes (FDR < 0.01) with ibrutinib treatment while there were no differentially expressed genes with acalabrutinib treatment (Figure 3.3A). Compared to single agent treatment, there was a synergistic

induction of differential gene expression with the combination of vemurafenib and ibrutinib (V+I) and V+I significantly reversed the BRAFi resistance signature used in the compound sensitivity predictions (Spearman correlation = -0.25, p-value = 0.0007) (Figure 3.3B). We then identified networks of differentially expressed genes in cells cultured in the presence of ibrutinib or V+I. With either single agent ibrutinib or the combination of ibrutinib and vemurafenib, the gene networks were primarily associated with development of various organs (Figure A-3.10). To understand the effect of ibrutinib on melanoma cells in greater detail, we profiled transcriptional regulators that are predicted to be altered in cells cultured with ibrutinib or the combination of ibrutinib and vemurafenib using LISA²⁵⁰ to identify transcription factors which may contribute to the differential gene expression in compound-treated cells. Among the top transcription regulators identified were YAP1 and two transcription factors, TEAD1 and TEAD4, which are bound by YAP1 (Figure 3.3C). Interestingly, this enrichment was observed in genes that are both downregulated by ibrutinib treatment and genes that are upregulated by ibrutinib treatment. It is possible that this could be because YAP1 can function as a transcriptional repressor in addition to its canonical role as a transcriptional co-activator²⁶².

We reasoned that inhibitors with the same functional target as ibrutinib should have a similar transcriptional signature to ibrutinib. To address this, we compared the gene expression signatures of ibrutinib- and vemurafenib-treated cells to the signatures of other compounds in the Connectivity Map (Cmap) dataset. SRC inhibitors had a highly similar transcriptional signature to that of ibrutinib (Figure 3.3D). This observation is interesting since ibrutinib, but not acalabrutinib, has significant off-target activity against multiple SRC family kinases (SFKs) (Figure A-3.11)^{260,261}. Another interesting observation was that the transcriptional signature of aromatase

inhibitors was similar to that of ibrutinib, especially since expression of androgen receptor target genes was significantly enriched (Figure 3.3C). However, treatment with several aromatase inhibitors did not alter BRAFi response in M229R cells (Figure A-3.12) suggesting that ibrutinib does not affect BRAFi sensitivity by modulating aromatase activity. As a further support that the method that we employed here works, we also performed the same comparison with vemurafenib-treated cells and found high similarity with BRAF and MEK inhibitors in the Cmap dataset, which is consistent with the pharmacology of vemurafenib. Together, these results suggest that ibrutinib alters YAP1 activity and the effects of ibrutinib on melanoma cells may be due to off-target anti-SFK activity.

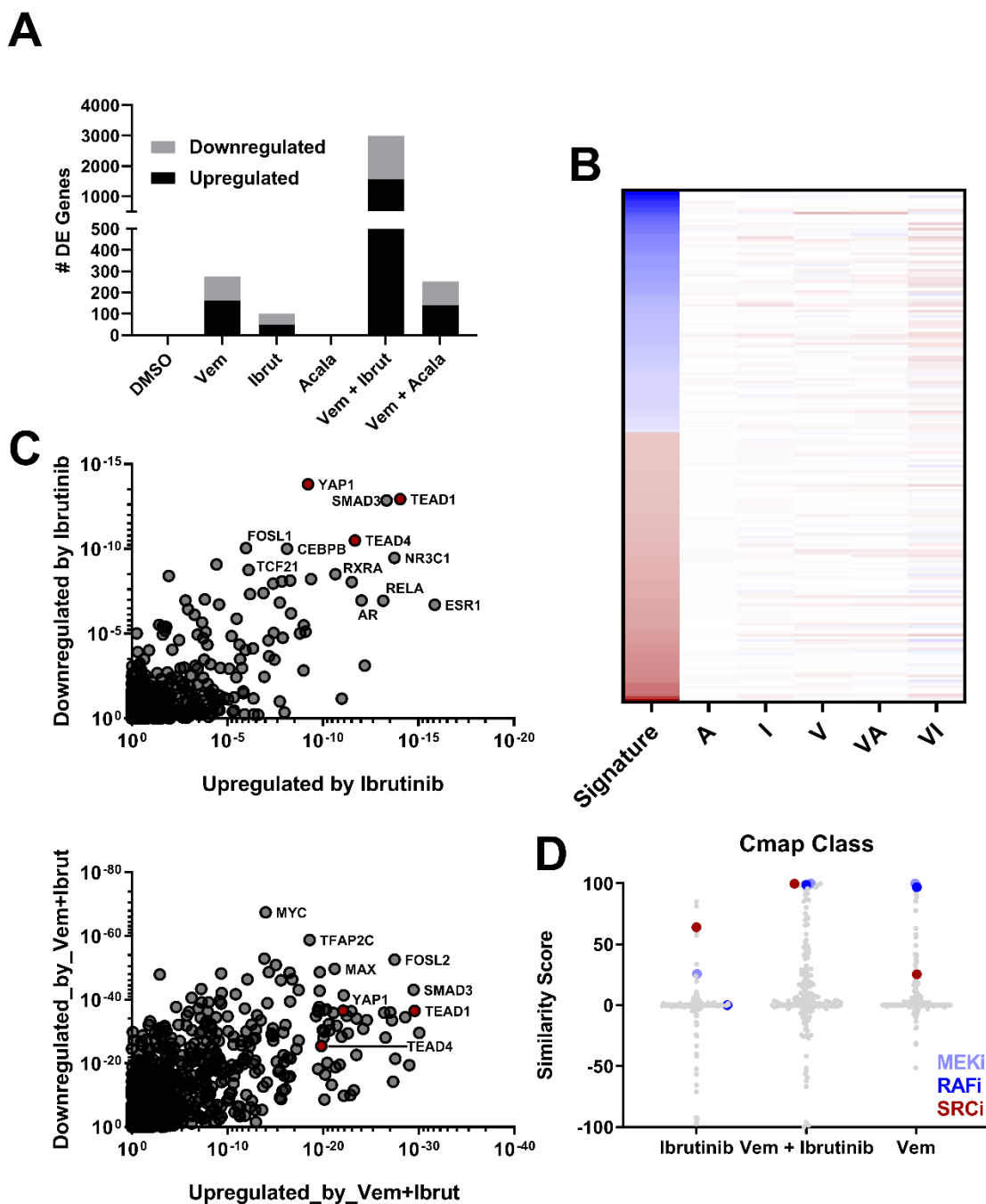


Figure 3.3: Transcriptional response to ibrutinib treatment **A.** M229R cells were treated with DMSO, vemurafenib (2 μ M), ibrutinib (5 μ M), acalabrutinib (5 μ M), or the combination of ibrutinib/acalabrutinib and vemurafenib. After 24 h RNA was extracted and RNA-Seq was performed as described in the materials and methods. **B.** Expression of genes in the BRAFi resistance signature which was used in the initial screen where ibrutinib was identified. For each compound the profiles of the three replicates were merged by taking the median expression value. For each treatment group the fold change in gene expression was compared to the DMSO control. Red boxes indicate that the gene is upregulated, and blue boxes indicate

Figure 3.3 (cont'd) that the gene is downregulated. Only treatment with vemurafenib + ibrutinib significantly reversed the BRAFi resistance signature (Spearman correlation = -0.25, p-value = 0.0007). **C.** LISA analysis of differentially expressed genes in the ibrutinib and vemurafenib + ibrutinib treatment groups. Data analysis was performed as described in Materials and Methods. X- and Y-axis values are enrichment p-values. **D.** CMap class analysis was performed as described in Materials and Methods. Transcriptional signatures of ibrutinib, vemurafenib, or vemurafenib + ibrutinib were compared to transcriptional signatures in the Cmap dataset.

Ibrutinib reduces the nuclear accumulation of YAP1

YAP1 has been previously implicated in BRAFi resistance^{131,163-165,241}, so it is critical to understand whether ibrutinib is altering YAP1 activity. Transcriptionally inactive YAP1 is sequestered in the cytosol and upon various stimuli YAP1 can translocate into the nucleus where it modulates gene transcription. As we previously demonstrated²⁴¹, M229R cells have an increased nuclear/cytosolic ratio of YAP1 localization. Consistent with our computational predictions, ibrutinib reduced the proportion of cells with nuclear YAP1 localization; acalabrutinib did not have any effect on YAP1 localization (Figure 3.4A and 3.4B). Interestingly, ibrutinib did not have any effect on YAP1 localization in M238R or UACC62R cells despite the fact that both resistant lines had elevated levels of nuclear YAP1 (Figure 3.4C and 3.4D). It is possible that YAP1 could be regulated through other mechanisms in these cells, perhaps by control of serine phosphorylation by MST1/LATS²³⁷. These data are consistent with our observation that ibrutinib re-sensitizes M229R cells to vemurafenib but only has a minor effect on M238R and UACC62R cells. We also observed an increase in the fraction of cells with predominantly nuclear TAZ localization in all three cell lines but neither ibrutinib nor acalabrutinib altered TAZ localization (Figure A-3.13). Taken together, these data suggest that in a subset of BRAFi-resistant melanoma ibrutinib can alter YAP1 activity, which may contribute to re-sensitization to BRAFi treatment.

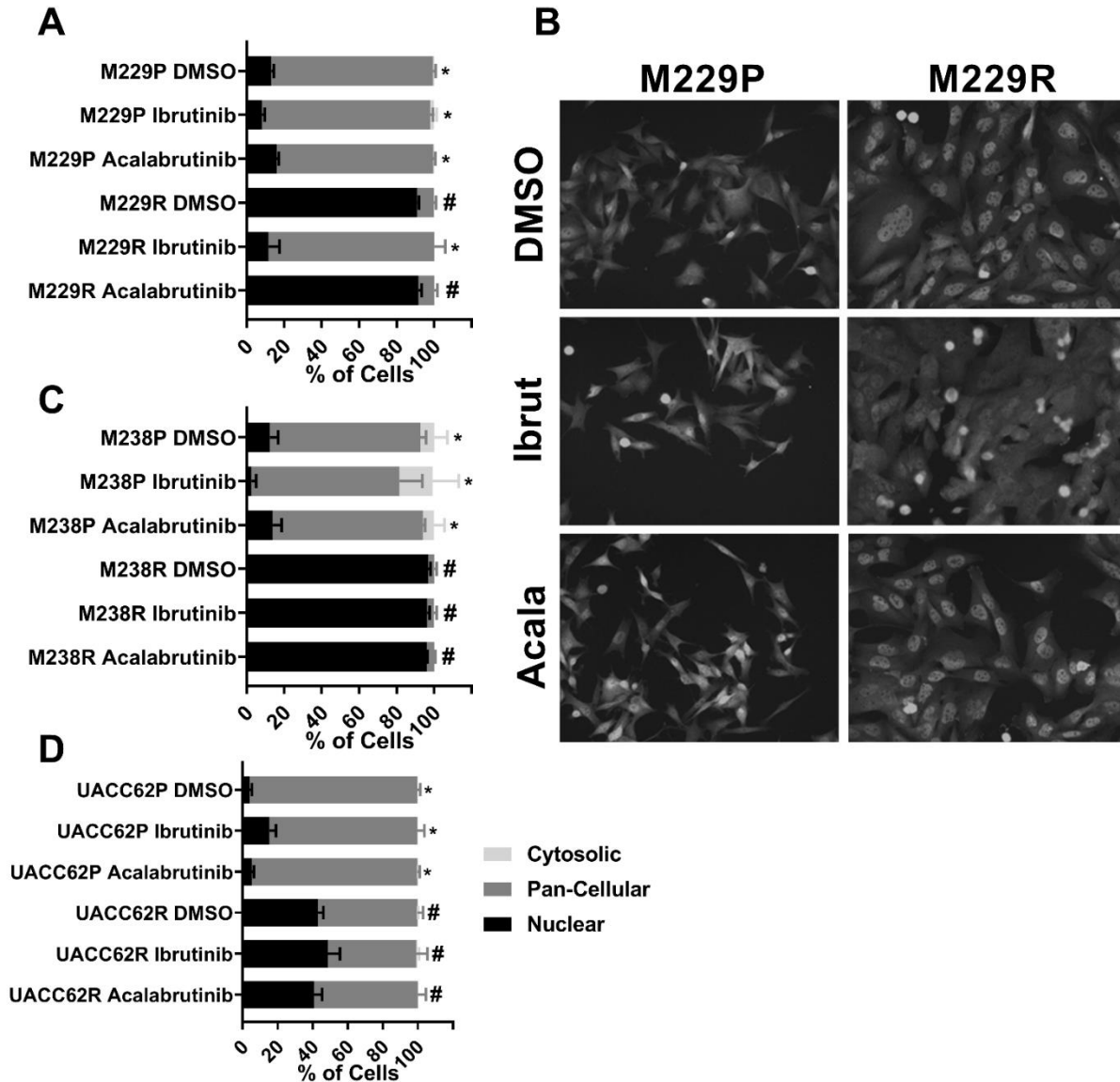


Figure 3.4: Ibrutinib blocks YAP1 nuclear localization **A.** M229P/R cells were stained with an anti-YAP1 antibody as described in the materials and methods section. The percentage of cells with nuclear, cytosolic, or pan-cellular YAP1 localization was quantified as described in the materials and methods section. **B.** Representative images from the experiment in Fig 4A. **C.** M238P/R or **D.** UACC62P/R cells were stained with an anti-YAP1 antibody as described in the materials and methods section. The percentage of cells with nuclear, cytosolic, or pan-cellular YAP1 localization was quantified as described in the materials and methods section. Statistical analysis (one-way ANOVA) was performed on % of cells with nuclear YAP1 localization where $p < 0.01$ was considered statistically significant. Bars marked with # indicate a statistically significant difference when compared with DMSO-treated parental cells and bars marked with * indicate a statistically significant difference when compared with DMSO-treated resistant cells ($n = 3$ biological replicates for all imaging experiments).

Discussion

In this study we used an unbiased computational approach to identify compounds that reverse a gene expression signature for BRAFi resistance. This identified a role for ibrutinib in re-sensitizing a subset of melanoma cells with acquired BRAFi resistance to vemurafenib. Our data show that this is not due to on-target BTK inhibition, but is due to off-target inhibition, presumably of at least one SFK. Other studies have also identified a role for SFKs in BRAFi resistance^{153,263,264}, further supporting the idea that off-target anti-SFK activity of potential melanoma therapeutics may be mechanistically important. One study in particular characterized a novel dual RAF/SRC inhibitor which retains activity against melanoma tumors which had previously developed resistance to dabrafenib/trametinib therapy²⁶⁵.

Additionally, we found that ibrutinib, but not acalabrutinib, prevents the nuclear accumulation of YAP1, which would render YAP1 transcriptionally inactive²⁶⁶. There is evidence in the literature that SFKs may be critical in modulation of YAP1 activation. For example, YES1, a SFK that is bound by ibrutinib²³⁵, phosphorylates and activates YAP1¹⁹⁸. Other SFKs including LCK, as well as SRC itself, have also been demonstrated to modulate YAP1 activation^{199,267}, suggesting that modulation of YAP1 activity could be a general feature of SFKs.

Understanding the polypharmacology of ibrutinib will be critical for effectively repurposing ibrutinib, an FDA approved drug, or related SFK inhibitors for the treatment of BRAFi-resistant melanoma. There is currently an ongoing clinical trial testing ibrutinib as a single agent therapy in patients with treatment-refractory metastatic melanoma (NCT02581930). Based on our findings that ibrutinib treatment alone is ineffective in BRAFi resistant or BRAFi-naïve (Figure

A-3.14) melanoma cell lines, we would not expect a significant efficacy of ibrutinib as a single agent in the clinic. However, our data do suggest ibrutinib may re-sensitize a subset of resistant melanoma to BRAF inhibitors. Beyond melanoma, ibrutinib is used clinically to treat mantle cell lymphoma and chronic lymphocytic leukemia, and YAP1 has been implicated in both diseases^{268,269}. So the findings from this study may also be important in understanding differences in treatment response in these patients as well. It would be important to identify biomarkers, perhaps related to YAP1 activity or nuclear localization that would predict activity of SFK inhibition in BRAFi-resistant melanomas.

In this study we demonstrate that ibrutinib re-sensitizes a subset of BRAFi-resistant melanoma cells to vemurafenib. Mechanistically, we propose a model in which off-target SFK inhibition results in decreased YAP1 activity. The translational potential of this research is increased by the fact that ibrutinib is already FDA-approved, and thus can be used off-label for other indications. These data would suggest that ibrutinib or other SFK inhibitors, many of which are already FDA-approved, could have utility in BRAFi/MEKi-resistant melanoma tumors, as well as other YAP1-driven cancers.

CHAPTER 4:
**BRAFi-resistant melanoma cells are vulnerable to pharmacological
disruption of mitosis**

Sean Misek performed all experiments. Tom Dexheimer assisted in performing the compound screens. Maisah Akram assisted with data analysis.

Abstract

Combination therapy with BRAF and MEK inhibitors (BRAFi/MEKi) has remarkable efficacy against melanoma tumors, but in most cases resistance eventually develops. The purpose of this study was to identify pharmacological vulnerabilities in BRAFi-resistant melanoma cells, with the goal of identifying new therapeutic options for patients whose tumors have developed resistance to BRAFi/MEKi therapy. We screened a well-annotated compound library against a panel of isogenic pairs of parental and BRAFi-resistant melanoma cell lines to identify classes of compounds that selectively target the BRAFi-resistant cells. Two different classes of inhibitors emerged. One group of compounds shared the property of cell cycle arrest at M-phase, and included inhibitors of aurora kinase (AURK), polo-like kinase (PLK), tubulin, and kinesin. To understand why BRAFi-resistant cells were more sensitive to pharmacological inhibition of mitosis, we used live cell microscopy to track mitosis in real time. Parental, but not BRAFi-resistant, melanoma cells underwent mitotic slippage to evade compound-induced arrest, likely due to differences in Cyclin B1 degradation between the parental and resistant cells. Second, another BRAFi-resistant cell line had increased sensitivity to Chk1/2 inhibitors, possibly due to an accumulation of DNA damage resulting in mitotic failure. This study shows that BRAFi-resistant melanoma cells are vulnerable to pharmacological disruption of mitosis and suggests a targeted synthetic lethal approach to treat BRAF-mutant melanomas that have become resistant to BRAF/MEK-directed therapies.

Introduction

Many mechanisms of BRAFi/MEKi resistance in melanoma are well understood^{38,43,128,130,131,135,141,150,167,169,176,177}, yet systematic approaches to identifying effective second-line therapeutic approaches are still largely lacking. One appealing strategy is to re-purpose existing drugs to treat drug-resistant melanoma since FDA-approved therapies can be quickly translated for other indications. Large-scale efforts have sought to systematically profile compounds against annotated panels of cancer cell lines, initially with datasets like Genomics of Drug Sensitivity in Cancer (GDSC)¹¹⁰ or Cancer Target Discovery and Development (CTD²)¹¹¹, and more recently with Profiling Relative Inhibition Simultaneously in Mixtures (PRISM)^{112,113}. The ultimate goal is to correlate genomic features with drug responses and map those associations back to patient tumors. More targeted screens have also been used to identify compounds with activity against drug-resistant cancer models²⁷⁰⁻²⁷³.

The strategy we took in this study was to screen a library of FDA-approved compounds against pairs of isogenic parental and BRAFi-resistant melanoma cell lines. Chemical compound screens compare well with functional genomics-based CRISPR screens, but also present several distinct advantages. Most standard CRISPR screens are based upon perturbation of individual genes often leading to compensation by redundant isoforms, whereas compound screens typically contain inhibitors that can target multiple members of the same protein family. Furthermore, CRISPR screens typically rely on measurement of responses that require long-term deletion of a target gene. Thus, if a gene is essential for survival of all cells, it is impossible to assess the differential dependence of various cell populations on that gene. For example, in the Project Achilles dataset, AURK and PLK were identified as essential genes, which is particularly relevant here since both

AURK and PLK inhibitors were identified in this study. Finally, a drug repurposing approach immediately highlights promising drug candidates that have activity against the target cells.

A major observation in this study is that treating melanoma cells with mitotic inhibitors will result in the cells undergoing mitotic slippage. Gradual degradation of Cyclin B1 during prolonged cell cycle arrest results in premature chromosome decondensation²⁷⁴. The cells subsequently exit from the cell cycle without dividing into a 4n state. These cells are senescent, but under certain conditions such as loss of p53 the cells can re-enter into the cell cycle²⁷⁵. Since mitotic slippage initially gives rise to tetraploid cells, subsequent rounds of mitosis in cells which underwent mitotic slippage will give rise to polyploid cells.

In this investigation we found that BRAFi-resistant melanoma cells are particularly vulnerable to disruption of mitosis through multiple and distinct mechanisms. Pharmacological inhibition of AURK, PLK, or tubulin polymerization can arrest cells in mitosis and prevent chromosome alignment during metaphase. These classes of compounds selectively induce prolonged cell cycle arrest and apoptosis in BRAFi-resistant cells. We elucidated the mechanistic basis for this selectivity by demonstrating that parental melanoma cells retain the ability to degrade Cyclin B1 and evade death by undergoing mitotic slippage, whereas their BRAFi resistant counterparts fail to downregulate Cyclin B1 and undergo apoptosis. We also found that a BRAFi-resistant melanoma cell line is more sensitive to pharmacological inhibition of Chk1/2 than the isogenic parental cell line. We hypothesize this is due to accumulation of DNA damage which results in mitotic failure, and ultimately cell death. In summary our work has identified two distinct mechanisms through which BRAFi-resistant melanoma cells are vulnerable to pharmacological

disruption of mitosis. These studies open up the exciting possibility that mitotic inhibitors may serve as potential new treatment strategies for BRAFi-resistant melanoma tumors. In addition, exploiting these vulnerabilities may be valuable in preventing the development of BRAFi resistance outright.

Materials and Methods

Cell lines, reagents, and antibodies:

Parental (denoted by a P suffix in the cell line name) and matched isogenic BRAFi-resistant cells (denoted by an R suffix in the cell line name) were either a gift from Dr. Roger Lo (UCLA) (M229P/R, M238P/R, or M249P/R)³⁸ or generated in our laboratory (UACC62P/R), as previously described²⁴¹.

BI-2536 (#17385), Volasertib (#18193), GSK461364 (#18099), Danusertib (#18387), AMG900 (#19176), MLN8237 (#13602), Docetaxel (#11637), Ispinesib (#18014), Mebendazole (#18872), AZD7762 (#11491), LY2603618 (#20351), SCH900776 (#18131), and Vemurafenib (#10618) were purchased from Cayman Chemical (Ann Arbor, USA). All compounds were diluted in DMSO to a stock concentration of 10 mM and aliquots were stored at -20°C. An antibody against γ H2AX (#9718) was purchased from Cell Signaling Technology (Danvers, USA). Alexa Fluor goat anti-rabbit488 (#A11034) was purchased from Invitrogen (Carlsbad, USA). Recombinant human TNF α protein (#210-TA-005) was purchased from R&D Systems (Minneapolis, USA).

Cell culture:

Cells were cultured in DMEM (ThermoFisher, Waltham, USA #11995-065) supplemented with 10% FBS (ThermoFisher, #10437-028) and 1% Antibiotic-Antimycotic (ThermoFisher, #15240062) and were passaged at approximately 75% confluence. The BRAFi-resistant cell line variants were maintained in culture medium supplemented with 2 μ M vemurafenib. Vemurafenib was removed from the culture medium when cells were seeded for experiments, except where otherwise indicated. Cells were routinely tested for mycoplasma contamination by DAPI staining. Short Tandem Repeat profiling of all cell lines was performed at the MSU genomics core. In all cases, isogenic pairs of cell lines had identical STR profiles.

Cloning:

Scarlet-H2A was amplified using PCR (donor plasmid: Addgene #85051, from Dorus Gadella) and subcloned into pDONR221 using the Gateway BP Clonase II enzyme mix (#11789020) from ThermoFisher. It was subsequently subcloned into the pLX301 lentiviral expression vector (from David Root, Addgene plasmid #25895) using the Gateway LR Clonase II enzyme mix (#11791020) from ThermoFisher. TUBA1B was amplified using PCR (donor plasmid: Addgene #57159, from Michael Davidson) and an EGFP-TUBA1B fusion protein was generated with two-stage overhang extension PCR using the TUBA1B and EGFP cDNA fragments. The EGFP-TUBA1B fusion protein was subcloned into pDONR221 and was subsequently cloned into pLX303 (from David Root, Addgene #25897). CyclinB1-GFP was amplified using PCR (donor plasmid: Addgene #26061, from Jonathon Pines) and was subcloned into pDONR221 and subsequently subcloned into pLX303. Successful cloning was confirmed by Sanger sequencing.

Virus preparation and infection:

HEK-293T cells were seeded onto 10-cm plates at a density of 4×10^6 cells/plate and the cells were allowed to attach overnight. The next day the cells were transfected with a plasmid cocktail containing 5000 ng of the pLentiCRISPRv2 plasmid, 5000 ng of psPAX2 (Addgene plasmid #12260), 500 ng of pMD2.G (Addgene plasmid #12259), and 20 μ L of Lipofectamine 2000 (ThermoFisher, #11668019) in 400 μ L of OptiMEM (ThermoFisher, #31985070). The next morning the medium was changed to 10 mL of fresh complete culture medium, and the following day each plate was supplemented with an additional 5 mL of culture medium. After 24 h, the culture medium was harvested and filtered through a 0.45- μ m syringe filter. Virus was stored at 4°C and used within 2 weeks.

Melanoma cells were seeded onto 10-cm plates at a density of 5×10^5 cells/plate in 10 mL of complete culture medium. Prior to adherence of cells, 3 mL of viral supernatant was added to each plate. The cells were incubated with virus for 24 h, then the medium was changed to 10 mL of fresh medium. After at least 7 days the cells were used in live cell imaging experiments.

Viability experiments:

Cells were seeded into white 384-well tissue culture plates (PerkinElmer, Waltham, USA, #6007689) at a density of 1000 cells/well in 20 μ L of growth medium. The next day, compounds were pre-diluted in growth medium and then added to the 384-well plates so that the final volume of each well was 40 μ L. A PBS or growth medium barrier was added to the outer wells of the plate to limit evaporation. Cells were cultured under these conditions for 72 h. To assess viability, 8 μ L of CellTiter-Glo (Promega, Madison, USA, #G7573) was added to each well. Plates were

incubated on an orbital shaker for 5 min at room temperature, then briefly centrifuged (4000 rpm, 60 s) before being read on a Bio-Tek Synergy Neo plate reader with the #11 and #41 Ex/Em filter cubes. Viability signal was plotted versus log (Vemurafenib concentration) for each treatment condition.

Compound Screen:

Cells were seeded into white 384-well plates at a density of 1,000 cells/well. The next day the NCATS MIPE chemical library²⁷⁶ was pinned into the plates at a final concentration of 200 nM. After 72 h, 8 μ L of CellTiter-Glo was added to each well. The plates were incubated on an orbital shaker for 5 min, briefly spun down, and cell viability was measured as described above. In some cases, noise in the assay produced viability measurements that were greater than 100%. In these situations, the viability measurement was set to 100%.

Cell Cycle Analysis:

Cells were rinsed once in PBS, incubated with trypsin, washed once in PBS and immediately fixed in 70% ethanol for 20 min at room temperature. The cells were washed once and were re-suspended in PBS supplemented with 20 μ g/mL propidium iodide (#P1304MP, ThermoFisher) and 200 μ g/mL RNaseA. The cells were briefly mixed and were incubated on ice for 20 min. Following incubation, the cells were filtered through a 70 μ M filter and were run on an Accuri C6 flow cytometer (BD Biosciences, Franklin Lakes, USA). Data were analyzed with the FCS Express flow cytometry analysis software package.

Assay for Reactive Oxygen Species:

Cells were seeded at a density of 10,000 cells/well in a 96-well plate and allowed to attach overnight. The next day ROS levels were measured. Cells were also treated with 1 mM H₂O₂ for 15 min as a positive control. The ROS assay (#MAK145, Sigma-Aldrich, St. Louis, USA) was performed as described in the manufacturer's protocol for adherent cells.

Immunofluorescence staining:

Cells were seeded into 8-well chamber slides and were treated as indicated in the figure legends. Cells were fixed with 3.7% formaldehyde for 15 min then blocked in 2% BSA PBS-Triton X-100 (0.1%) for 1 h at room temperature. Cells were incubated overnight at 4°C in phospho- γ H2AX antibody at a dilution of 1:1,000 in blocking buffer. Cells were washed thrice in PBS then were incubated in the appropriate secondary antibody at a 1:1,000 dilution for 1 h at room temperature. Cells were washed 3 times in PBS and slides were then mounted in ProLong Gold Antifade + DAPI (ThermoFisher, #P36935). Slides were cured overnight at room temperature, then transferred to 4°C. Slides were imaged on a Nikon TE2000-U fluorescence microscope at 20x magnification. All images were automatically quantified using an ImageJ pipeline. Briefly, nuclear masks were created from the DAPI channel and the γ H2AX staining intensity was measured within each mask. Data is reported as relative γ H2AX fluorescence intensity. At least 500 cells were quantified per treatment condition.

Live cell imaging:

To quantify the rate and outcome of mitosis in melanoma cells, UACC62P/R and M229P/R cells were engineered to express Scarlet-H2A and EGFP-TUBA1B. Cells were seeded at a density of

5,000 per well in a glass-bottom 96-well plate. The next day the cells were treated as described in the figure legends and were imaged at 3-min intervals on a BioTek Cytation 3. Over 40 cells per treatment condition were analyzed to measure mitotic rate and outcome. The T_0 for mitotic entry was defined as nuclear envelope breakdown and the final time was defined as either completion of mitosis (chromosome segregation and complete de-condensation), mitotic slippage (complete de-condensation of chromosomes), or prolonged arrest at the end of imaging.

To generate high resolution images, cells were seeded at a density of 10,000 per well in 8-well glass-bottom chamber slides. The next day the growth medium was changed to CO₂-independent growth medium (Gibco, #18045088) and the cells were treated as described in the figure legends. Cells were imaged with a 20x air objective on a DeltaVision microscope equipped with an sCMOS camera, environmental chamber, and ultimate focus drift correction system. Five z-sections were imaged in 2 μ m steps at 3-min time intervals. Equivalent exposure conditions were used for all images.

The described DeltaVision setup and imaging parameters were used to generate quantitative Cyclin B1 protein expression data. At least 10 cells were analyzed per treatment condition. Cyclin B1 expression was quantified at each time interval in with FIJI v1.52p. Cyclin B1 expression was normalized to the expression value at the first analyzed timepoint.

Results

BRAFi-resistant melanoma cells are sensitive to inhibitors that disrupt mitosis

In this study, we sought to identify compounds that selectively target BRAFi-resistant melanoma cells as potential therapeutic strategies and as a window to understanding mechanisms through which resistance arises. In our initial screen we profiled the NCATS Mechanism Interrogation PlateE (MIPE) library of 1910 compounds²⁷⁶ against a pair of matched isogenic parental and BRAFi-resistant melanoma cells, UACC62P and UACC62R which were developed by *in vitro* selection with vemurafenib²⁴¹. The NCATS MIPE library contains a mechanistically and structurally diverse set of compounds, the majority of which are FDA-approved or investigational new drugs and are directed at over 900 unique protein targets. The library is also redundant, containing multiple inhibitors against many of the protein targets. Using this approach allows us to not only identify efficacious compounds, but also to gain new mechanistic insights into the molecular mechanisms of BRAFi resistance. Figure 4.1A shows a graphical representation of sensitivity of each compound against the UACC62P (x-axis) and UACC62 (y-axis). As expected, RAF and MEK inhibitors in this library selectively targeted the parental UACC62P cells which carry the BRAF^{V600E} mutation, demonstrating that our assay is able to identify compounds that differ in their selectivity towards the parental and BRAFi-resistant melanoma cells. In this inverse? analysis (Figure 4.1A), compounds that target PLK, AURK, tubulin, and kinesin selectively reduced viability of the UACC62R cells. Since the screen was performed at a single concentration of each compound, fresh powder for 9 of the identified compounds, including 3 PLK inhibitors (BI2536, Volasertib, and GSK461364), 3 AURK inhibitors (Danusertib, AMG900, and MLN8237), 2 tubulin inhibitors (Docetaxel and Mebendazole), and the kinesin inhibitor Ispinesib was used to validate the screen hits in concentration response studies. While all of the top hits were

validated, interestingly, the differential compound sensitivity was found to be due to a change in the maximum percent inhibition (E_{\max}), rather than due to a difference in the IC_{50} (Figure 4.1B). Our results suggest that mitotic blockade selectively reduces viability of BRAFi resistant melanoma cells. There was no obvious synergy between vemurafenib and any of the identified compounds (Figure A-4.1). This would suggest that alterations in the UACC62R cells render them more vulnerable to disruption of mitosis.

We then expanded the screen to include three additional cell line pairs, M238P/R, M229P/R, and M249P/R³⁸. Two of these, M229R and M238R, share some features with the UACC62R cells in that, compared with their Vem-sensitive parental counterparts, the resistant cells lack expression of differentiation-associated melanocyte lineage genes²⁴¹. M238R cells showed a compound sensitivity pattern similar to UACC62R, with top hits including AURK inhibitors (Figure A-4.2). Interestingly, the AURK inhibitors that selectively target UACC62R over UACC62P cells were different from those that target M238R over M238P cells (Table. S2). One possible explanation could be that the various cell lines express drug efflux pumps or drug metabolizing enzymes with different activities towards the AURK inhibitors. While M229R cells have a similar transcriptional profile to UACC62R and M238R cells, these cells also had increased sensitivity to Chk1/2 inhibitors over its parental counterpart (Figure A-4.2). As a control experiment, we also screened the M249P and M249R melanoma pair, which does not share transcriptional profiles with the other Vem-resistant melanoma cells. In M249R cells, vemurafenib resistance has been shown to be due to acquisition of the activating NRAS^{Q61} mutation³⁸ which leads to reactivation of the ERK/MAPK pathway. We were unable to identify enrichment of mitotic inhibitors in compounds

with selectivity towards M249R cells, consistent with resistance developing through MAPK reactivation (Figure A-4.2).

PLK, AURK, tubulin, and kinesin are critical for the execution of mitosis, so we reasoned that altered regulation of mitosis might provide the mechanistic basis for the differences in selectivity between the UACC62P and UACC62R cells. Consistent with this idea we found that treatment with mitotic inhibitors results in the accumulation of cells with 4n DNA content, suggesting that the cells are arresting the cells in mitosis (Figure 4.1C).

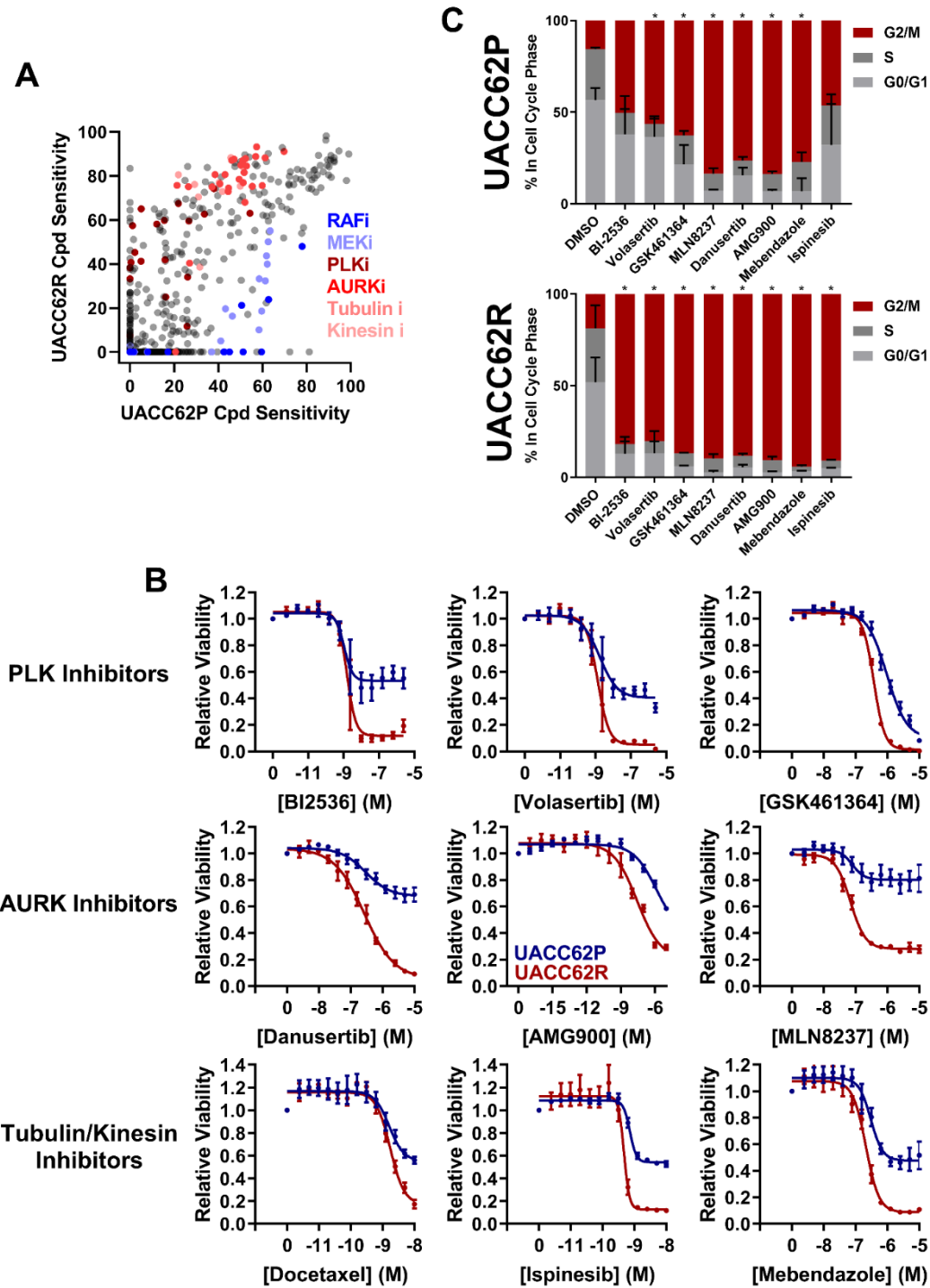


Figure 4.1: Vemurafenib-resistant UACC62R cells are selectively vulnerable to pharmacological disruption of mitosis. A. The NCATS MIPE chemical library was screened against parental and resistant UACC62P/R cells at 200 nM as described in the Materials and Methods section. Compound sensitivity data are plotted as % reduction in viability of UACC62P cells vs UACC62R cells for each of compound in the screen. The larger the sensitivity value, the greater was the measured reduction in cell viability. The screen was performed with $n = 1$ biological/technical replicates for each cell line. **B.** Fresh powder for 9 of the

Figure 4.1 (cont'd) compounds identified in the initial screen was ordered and the effect of these compounds on cell viability was analyzed at the indicated concentrations. Blue lines represent data for the UACC62P cells, and red lines indicate data for UACC62R cells. Data are represented as mean \pm SE of the technical replicate averages for each of the biological replicates (n = 3). **C.** Cell cycle analyses of vehicle and drug-treated UACC62P/R cells were performed as described in the Materials and Methods section. All compounds were used at concentrations of 1 μ M except for Ispinesib which was analyzed at 1 nM. Statistical analyses were performed on the proportion of cells in G2/M for the drug-treated samples vs the DMSO control using One-way ANOVA analysis, * indicates $p < 0.01$. Data are represented as mean \pm SE for n = 3 biological replicates.

Compound-treated UACC62P, but not UACC62R, cells undergo mitotic slippage

Our data demonstrate that BRAFi-resistant cells are more sensitive than their parental counterparts to inhibitors which disrupt mitosis. However, the mechanism behind this increased sensitivity was unclear. We initially hypothesized that increased levels of DNA damage in BRAFi-resistant cells would increase sensitivity to pharmacological disruption of mitosis. However, we found that neither ROS, which could in principle induce DNA damage, nor γ H2AX staining, a marker of DNA damage, were elevated in UACC62R cells over levels in UACC62P cells (Figure A-4.3 and A-4.4). We previously described that compared with their parental counterparts UACC62R melanoma cells express genes associated with de-differentiation. To investigate whether the increased sensitivity of parental UACC62P cells to mitotic inhibitors might be attributed to their more differentiated state compared with UACC62R cells, we treated both UACC62 P and UACC62R cell with TNF α which has been shown to cause de-differentiation of melanoma cells^{277,278}, and assessed the impact on sensitivity to a panel of mitotic inhibitors (Figure A-4.5). The lack of effect of TNF α on sensitivity to mitotic inhibitors suggests that the de-differentiated attributes of UACC62R cells do not explain their vulnerability to mitotic inhibitors (Figure A-4.5).

We then sought out to determine how mitosis is affected in BRAFi-resistant and isogenic parental cells treated with or without mitotic inhibitors. Fusion proteins of enhanced green fluorescent protein with the α -tubulin B chain (EGFP-TUBA1B) and of the red fluorescent protein, mScarlet with histone H2A (mScarlet-H2A) were used to label the mitotic spindle and chromosomes, respectively. We initially hypothesized that the mitotic integrity in treatment-naïve UACC62R cells might already be impaired, rendering them more vulnerable to pharmacological disruption of mitosis than the non-resistant parental cells. However, DMSO-treated UACC62P and UACC62R cells had similar mitotic timing duration and success rates (Figure 4.2A). In contrast to the effects of compound-treatment on cell viability (Figure 4.1B), treatment with GSK461364 (PLKi), MLN8237 (AURKi), or Mebendazole (Tubulin inhibitor), almost completely prevented both UACC62P and UACC62R cells from successfully completing mitosis. Interestingly, a significant fraction of the compound-treated UACC62P cells initially arrested in mitosis, but after several hours underwent mitotic slippage (Figure 4.2B and 4.2C). In contrast only very few of the compound-treated UACC62R cells did the same. The proportion of cells that undergo mitotic slippage is inversely correlated with the measured decrease viability in response to mitotic drug treatment in (Figure 4.1B) and may explain why mitotic disrupters selectively targets UACC62R cells.

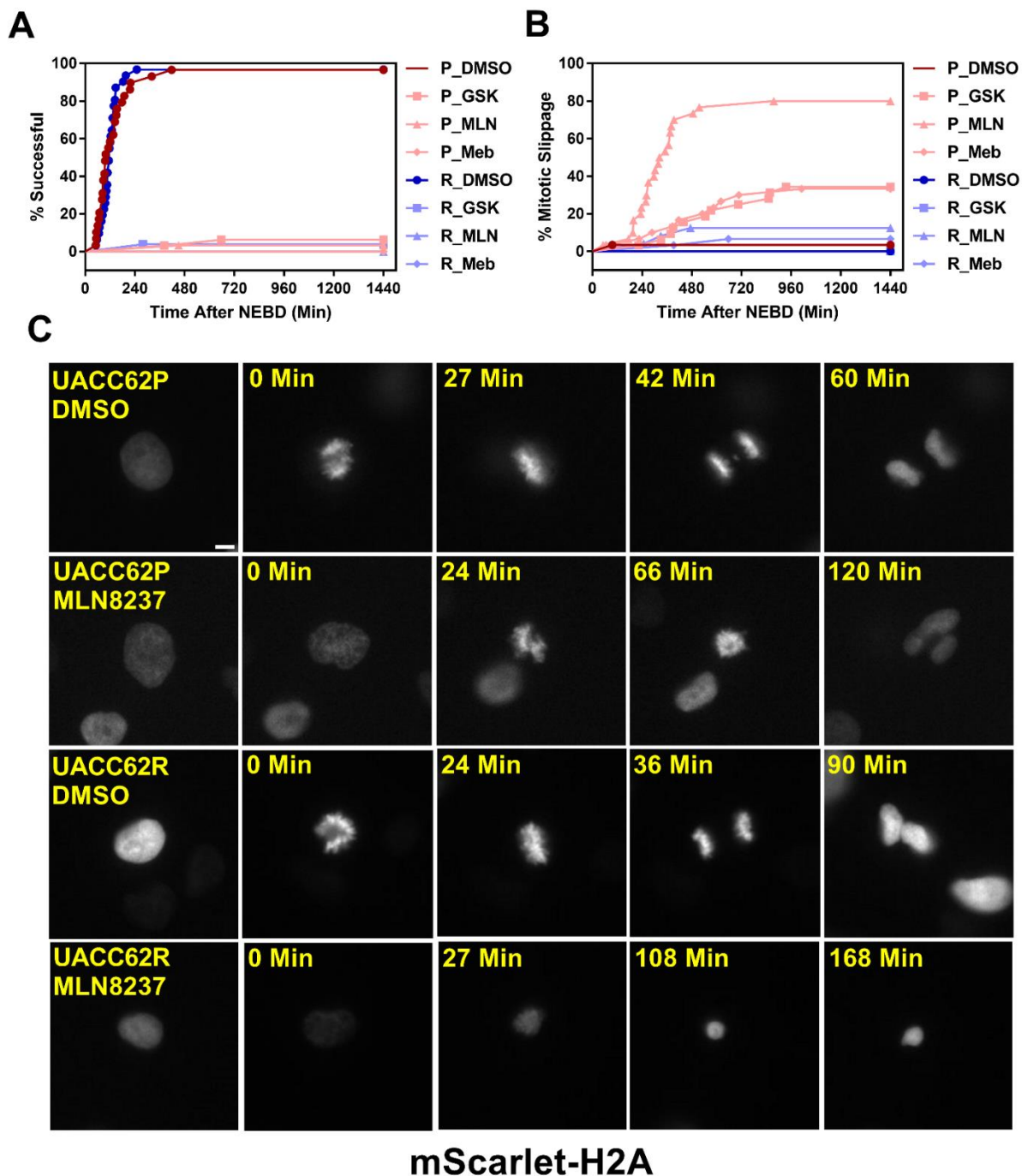


Figure 4.2: Compound-treated UACC62P, but not UACC62R, cells undergo mitotic slippage. UACC62P/R cells were engineered to stably express GFP-TUBA1B and mScarlet-H2A. The cells were seeded into glass-bottom 96-well plates and the next day the cells were treated with 1 μ M GSK461364, MLN8237, or Mebendazole. Mitotic timing and outcomes were analyzed as described in Materials and Methods. The fraction of cells which **A**, successfully completed mitosis or **B**, underwent mitotic slippage are plotted as a function of time. At least 40 cells were analyzed per treatment condition. **C**. Representative images of DMSO or MLN8237-treated UACC62P/R cells. Images were captured using the DeltaVision microscopy setup as described in the Materials and Methods section. Scale bar = 10 μ M.

Differential Cyclin B1 accumulation in UACC62P/R cells

Under physiological conditions, degradation of Cyclin B1 drives the exit of cells from mitosis. In arrested cells, however, a failure to reduce Cyclin B1 levels below a critical threshold can result in cells undergoing mitotic slippage leading to greater than 2n DNA content and polyploid nuclei²⁷⁴. We therefore hypothesized that our finding that UACC62P cells, but not UACC62R cells, undergo mitotic slippage upon treatment with might be due to differences in degradation of Cyclin B1 at the mitotic spindle checkpoint. To explore this idea, we used a similar approach where we engineered UACC62P/R cells to stably express EGFP-CCNB1 (Cyclin B1) along with mScarlet-H2A so to monitor in real time mitotic progression and Cyclin B1 levels by live cell imaging. EGFP-Cyclin B1 expression mirrors that of endogenous Cyclin B1 and expression of EGFP-Cyclin B1 does not have a significant effect on perturbing cell cycle progression or altering expression of cell cycle-related genes²⁷⁹. Prior to the initiation of mitosis, EGFP-Cyclin B is sequestered in the cytosol in DMSO-treated UACC62P cells and then rapidly co-localizes with mScarlet-H2A upon chromosome condensation and nuclear envelope breakdown (Figure 4.3A). Most DMSO-treated UACC62R cell displayed kinetics of EGFP-Cyclin B1 expression levels, similar to that of DMSO-treated UACC62P cells (Figure 4.3B). In response to treatment with the Aurora A kinase inhibitor, MLN8237, the levels of Cyclin B1 in UACC62R cells gradually reduced to approximately 50% of their original levels. In contrast, in the UACC62P cells treated with MLN8237, the levels of EGFP-Cyclin B1 reduced to a much greater extent, which could allow these cells to undergo mitotic slippage. In total, these data suggest that differential levels of Cyclin B1 dictate whether MLN8237-treated melanoma cells undergo prolonged cell cycle arrest or mitotic slippage.

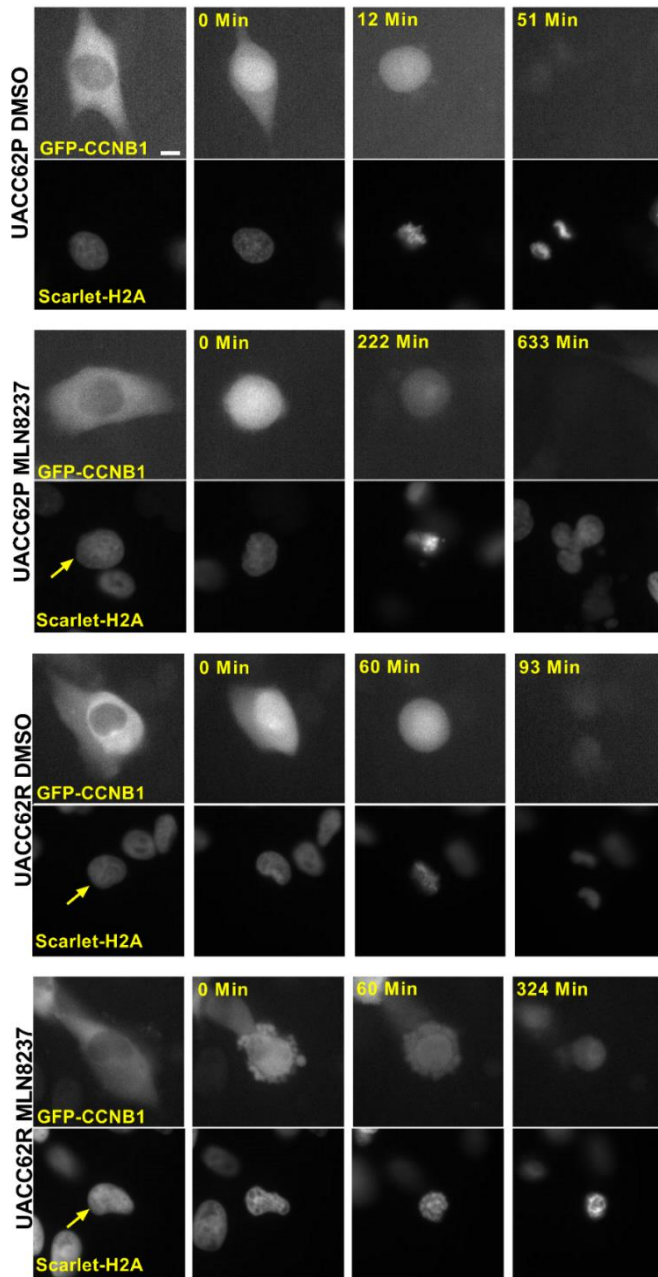
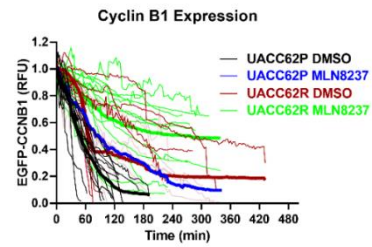
A**B**

Figure 4.3: Differential CCNB1 degradation rates in UACC62P/R cells. **A.** Representative images of EGFP-CCNB1 and mScarlet-H2A in DMSO or MLN8237-treated UACC62P/R cells. Scale bar = 10 μ M. **B.** Quantification of CCNB1 expression levels in DMSO or MLN8237-treated UACC62P/R cells was performed as described in Materials and Methods. At least 10 cells were analyzed per treatment condition.

Increased sensitivity of BRAFi-resistant M229R cells to Chk1/2 inhibitors

Our initial compound screen showed that while vemurafenib resistance led to increased sensitivity to AURK, PLK, tubulin, and kinesin inhibitors in UACC62 and M238 melanoma cells, M229R cells also had increased sensitivity to Chk1/2 inhibitors (Figure A-4.2). In a follow-up concentration response assay, we confirmed that three Chk1/2 inhibitors selectively target M229R cells over the vemurafenib sensitive parental cell line (Figure 4.4A). Similar to our findings with the AURK/PLK/Tubulin/Kinesin inhibitors, these inhibitors show no synergy with vemurafenib (Figure A-4.6). While the mitotic success rate was reduced in Chk1/2i-treated M229R cells compared with M229P cells, the fraction of cells undergoing mitotic slippage was identical in M229P and M229R cells (Figure 4.4B). After 240 min approximately 70% of compound-treated M229P cells had completed mitosis whereas only 30 or 60% of M229R cells had successfully completed mitosis. These data suggest that while M229R cells are also differentially sensitive to disruption of mitosis, in this case Chk1/2 inhibitors. However, the increased vulnerability of M229R cells over M229P cells to Chk1/2 inhibitors appears to due to a mechanism other than the differences in mitotic slippage. Under physiological conditions Chk1/2 activation monitors/safeguards DNA fidelity during replication and prevents premature entry into mitosis²⁸⁰. Conditions of Chk1/2 inhibition would be expected to result in the accumulation of DNA damage, ultimately leading to failure in mitosis. The basal levels of γ H2AX staining were similar in vehicle treated M229P and M229R cells. However, treatment with any of three structurally distinct Chk1/2 inhibitors resulted in increased γ H2AX staining in M229R cells over M229P cells (Figure 4.4C and 4.4D). The increased DNA damage is unlikely due to elevated ROS levels, since ROS was not elevated in M229R cells. (Figure A-4.3). Overall, these data suggest that Chk1/2 inhibitors

selectively induce the accumulation of DNA damage in M229R cells, ultimately leading to a high rate of mitotic failure.

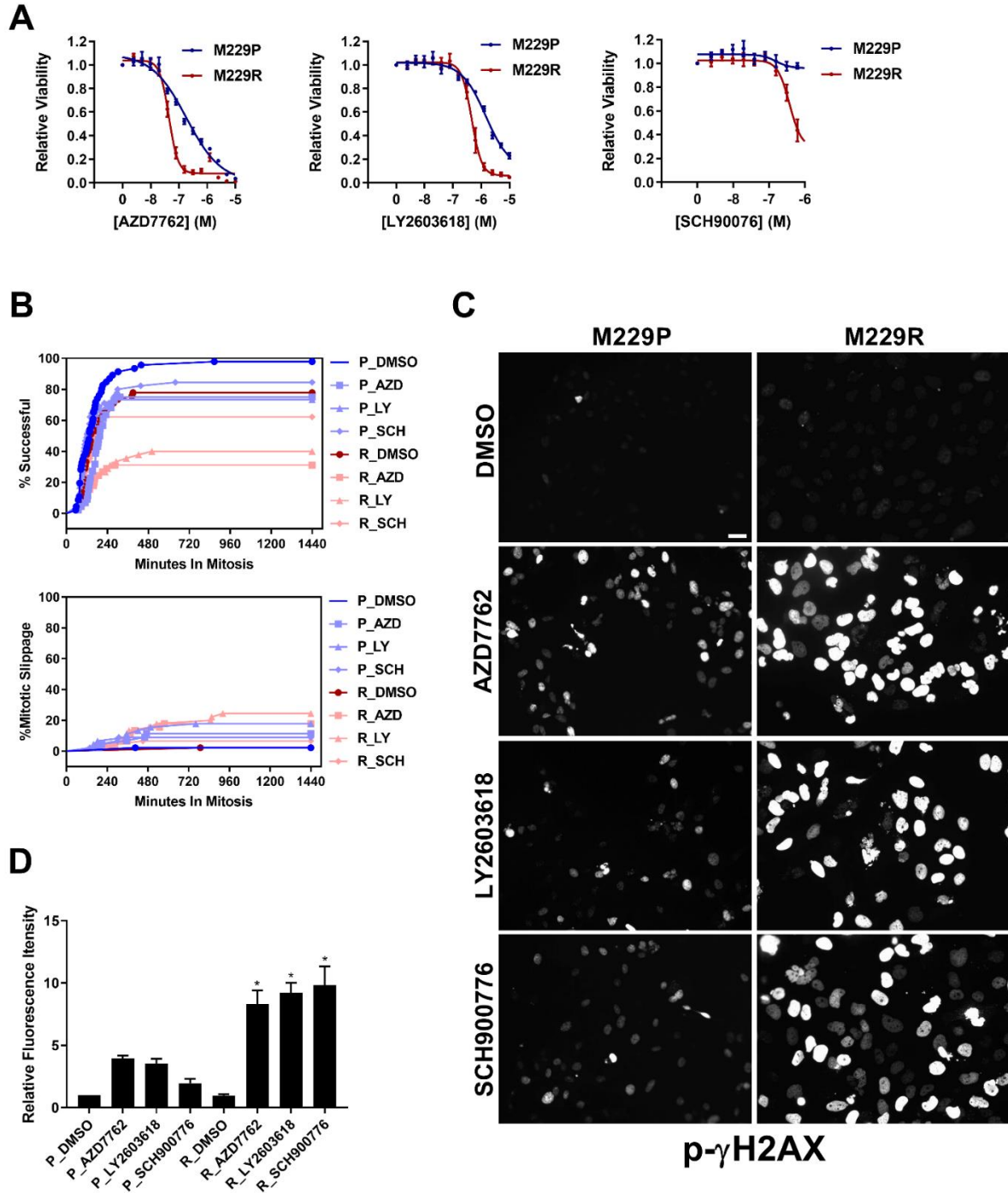


Figure 4.4: M229R cells are vulnerable to Chk1/2 inhibitors. A. M229P/R cells were seeded into 384-well plates and treated with AZD7762, LY2603618, and SCH900776 as indicated. After 72 h, viability was measured as described in Materials and Methods. Data are represented as mean \pm SE of the technical

Figure 4.4 (cont'd) replicate averages for each of the biological replicates ($n = 3$). **B.** M229P/R cells were engineered to express mScarlet-H2A and EGFP-TUBA1B as described in the Materials and Methods. Cells were seeded into glass-bottom 96-well plates and the next day the cells were treated with 100 nM AZD7762, 1 μ M LY2603618, or 1 μ M SCH900776. Mitotic rate/outcome was measured on the Cytation 3 microscope setup as described in Materials and Methods. At least 40 cells were analyzed per treatment condition. **C.** M229P/R cells were treated with 100 nM AZD7762, 1 μ M LY2603618, or 1 μ M SCH900776 for 24 h. The cells were subsequently fixed and stained with an antibody raised against p- γ H2AX. Scale bar = 10 μ M. **D.** Quantification of γ H2AX from the experiment in Figure. 4C was as described in Materials and Methods. Statistical analysis was performed with one-way ANOVA analysis, * indicates $p < 0.01$ vs the M229R DMSO group. None of the compound-treated M229P groups were statistically significant in comparison to M229P DMSO. Data are represented as mean \pm SE for $n = 3$ biological replicates.

Discussion

In this study we found that a subset of BRAFi-resistant melanoma cells are more sensitive to AURK, PLK, tubulin, and kinesin inhibitors and/or Chk1/2 inhibitors. For the first group of compounds, our data suggest that the mechanistic basis of this selectivity is an inability of these cells to undergo mitotic slippage. Mitotic slippage is a well characterized resistance mechanism for multiple classes of inhibitors, including those which disrupt tubulin polymerization/depolymerization²⁸¹⁻²⁸³. Our data suggest that the inability of UACC62R cells to undergo mitotic slippage could result from differential Cyclin B1 degradation, since Cyclin B1 degradation is an initiating event during mitotic slippage. Under physiological conditions, Cyclin B1 is targeted for degradation by the anaphase-promoting complex (APC) during metaphase²⁸⁴. MLN8237-treated UACC62P/R cells appeared to arrest in prophase or prometaphase since while the chromosomes were condensed there was no alignment of the chromosomes along the metaphase plate. These data would suggest that the APC is still inactivated in these cells, which should prevent the degradation of Cyclin B1. It is possible that there is a low level of APC activation in UACC62P, but not UACC62R, cells which would result in the gradual degradation of Cyclin B1 and eventually mitotic slippage. Another possibility is that the APC may be fully

inactivated in both UACC62P and UACC62R cells, but APC-independent Cyclin B1 degradation mechanisms could have higher activity levels UACC62P cells. Further clarification of these mechanisms will be important since they could serve as biomarkers for identifying tumors which are more responsive to disruption of mitosis.

Another BRAFi-resistant cellular model, M229R, was more sensitive to Chk1/2 inhibitors. While the molecular mechanism governing this selectivity is different from that of UACC62P/R cells, the commonality is that both cellular models are vulnerable to inhibitors which disrupt mitosis. Chk1/2 inhibitors induced a more severe accumulation of γ H2AX levels in M229R cells than in M229P cells. This could suggest that an excessive amount of DNA damage is causing the M229R cells to arrest and ultimately die during mitosis. One possible explanation for the differential response to Chk1/2 inhibitors is functional redundancy between Chk1/2 and other DNA repair pathways. In this hypothetical model, M229R cells are defective in other DNA repair mechanisms, which would increase their dependence on Chk1/2 for DNA repair, ultimately resulting in an elevated accumulation of DNA damage in Chk1/2i-treated M229R cells. This model would also explain why there is no difference in γ H2AX staining in DMSO-treated M229R cells since in the absence of Chk1/2 inhibitors M229R cells would still retain the ability to perform DNA repair, albeit at a slower rate. An analogous model explains why BRCA-mutant tumors have elevated sensitivity to PARP inhibitors.

We identified pharmacological vulnerabilities in three different poorly differentiated BRAFi resistant melanoma cell lines. For the cell line that developed BRAFi resistance by acquiring an NRAS mutation no compound class showed selective toxicity. This observation might suggest that

cells/tumors whose resistance is associated with a dedifferentiation phenotype are generally more vulnerable to compounds which disrupt mitosis. If biomarkers for response to these anti-mitotic agents can be established, it may be possible to identify a subset of tumors which are vulnerable to second-line therapy with these classes of approved drugs. While we did not observe synergy between BRAF inhibitors and mitotic inhibitors in BRAFi-resistant cells, the combination of these agents still warrants further investigation. One question is how to best sequence treatment with these agents. We found that BRAFi-resistant cells are more sensitive to mitotic inhibitors, which would suggest that in some cases tumors may be more sensitive to these agents after they develop resistance to MAPKi therapy in the clinic. However, another possibility is that these agents could be combined at the onset of treatment to prevent or forestall the development of drug resistance. This is especially true if mechanisms of resistance to BRAF/MEK inhibitors are mutually exclusive to mechanisms of resistance for mitosis inhibitors.

CHAPTER 5:
Discussion

Discussion of results

The thought process that guided my early dissertation studies was to identify resistance mechanisms which arose in BRAFi resistant cells, and then use those mechanisms to find compounds which reverse BRAFi resistance. If we extend this thought process to clinical application, it would require the re-biopsy of tumors after resistance develops. Resistance driver mechanisms would then need to be identified in each tumor before the appropriate second-line therapy could be administered. This approach is also made more complicated because different tumor foci in one patient may develop resistance through different mechanisms. An alternative approach would be to initially treat patients with two (or more) drugs that have strong anti-tumor effects as monotherapies, and which retain their efficacy when used in combination. These two drugs should have mutually exclusive resistance mechanisms so that a single alteration in a tumor cell is unable to generate resistance to both compounds. This approach has been used to design a combination of two BCR-ABL inhibitors which prevents the development of resistance²⁸⁵, whereas using the two compounds sequentially results in rapid development of resistance. This approach is similar to how HIV triple therapy prevents the development of resistance. One reason why resistance invariably arises in treatment with the combination of BRAF and MEK inhibitors is because a single genetic alteration can emerge which confers resistance to both drugs. How this approach can be best implemented in the setting of melanoma resistance is still unclear. Should pre-treatment biomarkers be used to select two or more different targeted therapies? Or should targeted therapies be combined with drugs that are generally effective against tumors regardless of biomarkers? For this approach to work it will be critical to understand the landscape of potential resistance mechanisms for each drug. A preliminary draft of this map could be generated by systematically overexpressing all protein-coding genes to identify those that promote resistance to

each drug. Drug combinations with non-overlapping resistance mechanisms could subsequently be identified.

We and others have found that a subset of MAPKi-resistant melanoma cells de-differentiate as a mechanism of resistance. De-differentiated SKCM cells should be unable to synthesize melanin, resulting in amelanotic tumors. However, human MAPKi-resistant SKCM tumors are still pigmented, suggesting that these tumors retain an intact melanin biosynthetic pathway. One possibility is that temporal control of de-differentiation is important for the development of drug resistance. Even though de-differentiated melanoma cells proliferate at a much slower rate, these cells may have a selective growth advantage under drug pressure. These cells would continue to acquire genomic alterations resulting in the eventual emergence of cellular clones that have resistance driver mutations. The mutations might result in MAPK-reactivation, which would allow the resistant cells to proliferate more quickly and eventually out-compete the de-differentiated cells. This model agrees with the observation that SKCM cells can shift into a pre-resistant state, and the pre-resistant cells can convert into de-differentiated drug-resistant cells upon application of drug pressure ¹⁴¹. One anecdotal example which supports this hypothesis is my observation that during drug selection of SK-Mel-19R cells, the cells initially enter a slow-dividing state for the first 2-3 weeks of selection. Eventually fast-growing drug-resistant cells emerge and become the dominant clone in the culture in the span of one week. Although while the exact mechanism of how SK-Mel-19R cells develop resistance is unknown, we know that vemurafenib is unable to block ERK activation in these cells, which would suggest that a secondary alteration in the MAPK pathway is driving resistance. If this model is true, then it may be preferential to use a combination of drugs that effectively target both the well-differentiated and

the de-differentiated melanoma cells. Such an approach may prevent the emergence of clones that develop resistance through genomic alterations.

In these studies, I identified several mechanisms of MAPKi resistance; however, the best approach for translating these findings into the clinic is still unclear. One problem is that there is a high degree of inter-patient, inter-tumor, and intra-tumor heterogeneity in MAPKi resistance mechanisms. To address the challenge of inter-patient heterogeneity, it will be necessary to develop biomarkers for MAPKi resistance mechanisms. If resistance has developed through selection for a mutation, then the mutated DNA itself can serve as a biomarker. As sequencing technology develops it may be possible to detect these low frequency mutations in treatment-naïve tumors. However, it is still challenging to develop biomarkers for tumors that have developed resistance through non-mutational mechanisms. This is especially true for the RhoA-associated resistance mechanisms that were identified in this dissertation. In a clinical setting it may be possible to use indirect readouts of RhoA activation, such as phosphorylation of downstream substrates, as biomarkers for pathway activation. Another option is to measure MRTF/YAP1 activation, perhaps by quantifying protein localization or by measuring expression of target genes. Another major hurdle is inter- and intra-tumor heterogeneity since multiple drug resistance mechanisms could simultaneously develop within one patient. In these cases, identifying and subsequently targeting an individual resistance mechanism may not be sufficient since invariably individual cells could be selected which may have developed resistance through an alternative mechanism. This would suggest that a superior approach may be to focus on preventing the development of resistance instead of applying new drug combinations after resistance develops.

Limitations

This research described in this dissertation has yielded important insights into MAPKi resistance in melanoma; these studies are not without limitations. A major drawback of these studies is their over-reliance on a limited number of conventional melanoma cell lines. All of the resistant cell lines used in this study were derived *in vitro* in growth medium containing 10% FBS, which has high levels of the potent RhoA activator lysophosphatidic acid (LPA). This could in principle have biased the cells towards developing resistance by activating RhoA, which may be less likely to occur in tumors exposed to physiological LPA concentrations. A majority of human SKCM tumors had elevated expression of a RhoA/C gene signature, however many tumors also downregulated the RhoA/C gene signature. Thus, it remains unclear whether RhoA/C is aberrantly activated in these, or whether this is simply due to stochastic changes in gene expression. An alternative interpretation could be that changes in the RhoA/C signature are due to infiltration of non-malignant cells, such as fibroblasts or macrophages, into the tumor. Since the gene expression analyses were performed using RNA-seq data from bulk tumors, if these non-tumor cells in the tumor microenvironment have higher expression of RhoA/C target genes then it would be reflected in a higher RhoA/C signature. It is also important to note that in an ideal scenario RhoA/C activation in human tumors would be measured with a Rhotekin-RBD pulldown assay, or indirectly by measuring activation-specific phosphorylation of MLC2 and other RhoA/C effectors, but this has not yet been done.

In many cases a BRAFi-resistance mechanism or pharmacological vulnerability was unique to a single cell line, which calls into question the extent to which these findings are generalizable. Ideally these studies should have been performed with a larger panel of cell lines,

perhaps greater than 10, which would allow for the identification of recurrent events. Another problem with these cell lines is that we lack a clear picture of how much heterogeneity exists within the original cell line as well as the drug resistant counterpart. Early during drug selection, the cell lines gave rise to hundreds of resistant clones. However, it is unclear whether this diversity is still present in the resistant cultures or whether one or a small number of fast-growing clone(s) eventually overtook the resistant population. Single cell sequencing or barcoding approaches during the process of the development of resistance would shed light on the process of how resistance develops.

A major limitation of these studies is a lack of *in vivo* validation. It is unclear whether the observations made in cell lines are relevant in human SKCM tumors. Expanding these studies using PDX models were from tumors that developed clinical MAPKi resistance would be extremely informative. These MAPKi resistance models likely capture much of the true heterogeneity of human SKCM tumors and clinically relevant resistance mechanisms. Another approach to clinically validating the findings presented in this dissertation would be to provide evidence for these resistance mechanisms and pharmacological vulnerabilities in MAPKi-resistant human tumors. While I performed some validation studies, they were all based upon gene expression and lacked functional validation or protein/activity-level validation. For example, a central finding in this dissertation is that pharmacologically inhibiting YAP1-mediated gene transcription re-sensitizes cells with acquired BRAFi resistance to BRAF inhibitors. However, no evidence that YAP1 nuclear localization is elevated in human tumors has been published in the scientific literature and this was not explicitly examined in my thesis research. There is, however,

indirect evidence that YAP1 target genes are upregulated in BRAFi resistant human SKCM^{131,241}. The same limitation is true regarding MRTF and RhoA activation.

The findings in this dissertation rely heavily upon pharmacological inhibition of signaling pathways, however validation of these findings in gene knockout studies is lacking. In cases where these validation experiments were performed, they were negative control experiments (e.g. *BTK* knockout in Chapter 3). A glaring issue is that in some cases there is an inexplicable difference between experiments performed with inhibitors and experiments performed with CRISPR. For example, dasatinib and ibrutinib block YAP1 nuclear accumulation and re-sensitize cells to vemurafenib, however in my hands, deletion of YAP1 did not alter vemurafenib sensitivity. In another example, while I found that CCG-222740, an “MRTF pathway inhibitor” re-sensitizes BRAFi-resistant cells to vemurafenib and that overexpression of MRTF-A promotes vemurafenib resistance, MRTF-A knockout did not. One consideration is when ablating genes from cancer cells using CRISPR, the clones that survive knockout may have in place an alternative pathway which obviates the need for the deleted gene. Finally, we still do not have a good understanding of how CCG-222740 regulates MRTF-A activity, which makes interpretation of these data even more challenging.

Future directions

The most critical next step for this research will be functionally validating these findings in patient samples. Testing whether MRTF-A and YAP1 are activated in human BRAFi-resistant tumors could be performed by IHC on archived tumor blocks, and analogous validation studies for

other proteins could be performed using similar methods. However, I believe that the most critical experiment will be to run (what some people rather comically call) a “pre-clinical trial” with PDX models. In this experiment a panel of PDX models, which developed MAPKi resistance in the patient, would be used to test the efficacy of the drug combinations which were characterized in this dissertation. For example, ibrutinib, dasatinib, or CCG-222740 could be combined with clinical BRAFi and MEKi combinations (e.g. vemurafenib + cobimetinib; dabrafenib + trametinib; or encorafenib + binimetinib). In analogous experiments, the compounds identified in chapter 4 could be screened against a panel of matched pre- and post-resistance PDX lines to determine if there is a difference in vulnerability to these compounds. An inferior approach could be to inoculate immunocompromised mice with isogenic parental and BRAFi-resistant cell lines to test drug efficacy *in vivo*. However, I do not believe this experiment would yield much new information. Performing this type of experiment would be useful for confirming target engagement *in vivo*, but it fails to answer the central question of whether these drug combinations are effective in human tumors.

In Chapter 2, I describe my finding that RhoA is activated in BRAFi-resistant melanoma cells. However, the mechanism of how RhoA is activated in these cells is still unclear. The RNA-seq study presented in this chapter was initially performed to identify this mechanism, however the unanticipated large extent of differential gene expression in the resistant cells made deduction of this mechanism difficult. A better method for answering this question would be to perform a functional screen to test the essentiality of individual genes/proteins in RhoA activation. The simplest approach would be to screen the parental and BRAFi-resistant cells with the NCATS MIPE library to identify compounds which prevent actin stress fiber formation in the resistant

cells. The readout for this screen would be imaging based, either with live-cell reporters or with fixed phalloidin-stained cells since stress fiber formation is a biomarker for RhoA activation. High throughput data analysis for this type of screen would be simple to perform by building an image-based classifier with a convolutional neural network or other similar algorithm, allowing for thousands of compounds to be profiled simultaneously. This method could also be extended to identify compounds which modulate YAP1 or MRTF-A nuclear localization in these cells, perhaps even in parallel with measuring RhoA activation. An example of how this could be done is by engineering the cells to express fluorescently tagged wild type YAP1 or MRTF-A and then use an image-based classifier to identify the fraction of cells with nuclear localization. A more direct approach to measuring the essentiality of individual genes would be by using CRISPR-based screens to perturb individual genes and measure the effect on RhoA activation. New image-based CRISPR screens which allow for the multiplexing of gene perturbation and microscopy on a single cell level ²⁸⁶ would be the most ideal approach for this. The advantage to using this approach is that it would allow for the definitive identification of genes which modulate RhoA activity. One benefit of identifying how RhoA is activated in the resistant cells is that it may serve as a biomarker for stratifying patients based on predicted response to RhoA pathway inhibitors. In the situation wherein RhoA activation is driven by a GPCR or other cell surface receptor, it would be much more straightforward to develop small molecule or antibody-based therapeutics against that target.

Chapter 3 describes my research revealing a role for ibrutinib in re-sensitizing BRAFi-resistant cells to vemurafenib. Interestingly, my data suggests that ibrutinib is likely acting through an off-target mechanism rather than on-target BTK inhibition. I performed initial experiments with CRISPR knockout cell lines to try to identify which ibrutinib targets are important for vemurafenib

re-sensitization, but unfortunately these experiments were inconclusive. It is possible that ibrutinib modulates of multiple kinases, rather than just one, in mediating vemurafenib re-sensitization. In this case, systematically deleting all ibrutinib targets one by one would likely not yield a positive result. A better approach for target identification would be to perform a combinatorial CRISPR screen which covers all possible pairwise combinations of ibrutinib targets. Multi-guide CRISPR vectors would allow for more complex combinations with three or more gRNA sequences. These findings do speak to the potential of polypharmacology of kinase inhibitors in cancer treatment. Using ibrutinib to treat melanoma is not particularly exciting, however identifying the functional target(s) is since it may highlight more efficacious compounds or a novel drug target.

Chapter 4 presents the discovery that cell cycle arrested UACC62P cells continue to degrade Cyclin B1, whereas arrested UACC62R cells do not. As discussed in Chapter 4, I believe there are two possible explanations for this phenomenon. One possible explanation is that there may be a low level of APC activity in the UACC62P cells that is not present in UACC62R. Alternatively, there may be other E3 ubiquitin ligases with higher activity in UACC62P than in UACC62R cells. The simplest experiment to test the first hypothesis is to determine whether blocking APC activity, perhaps with a small molecule inhibitor²⁸⁷, prevents aberrant Cyclin B1 degradation in the UACC62P cells. It is likely that aberrant Cyclin B1 degradation in UACC62P cells leads to mitotic slippage, meaning that after 24-48 h of compound treatment nearly all of the living cells would have undergone mitotic slippage. Since compound-treated cells which fail to degrade Cyclin B1 should die, a CRISPR library containing all genes or just E3-ubiquitin ligases could be screened against AURKi or PLKi-treated UACC62P cells to find guides which drop out. The selected guides which would reveal genes that are critical for Cyclin B1 degradation. In an

analogous approach, open reading frames for all E3 ubiquitin ligases could be systematically expressed in UACC62R cells to identify the ones that prevent cell death, which would be enriched in surviving clones.

Among the generated resistant cell lines, it is interesting that M229R cells are particularly sensitive to Chk1/2 inhibitors, whereas M238R and UACC62R cells are more sensitive to AURK, PLK, and tubulin inhibitors. It is also interesting that M238 and UACC62 cells have WT TP53 whereas M229 has mutant TP53²⁸⁸. Since TP53 loss is synthetic lethal with Chk1 inhibition ²⁸⁹ it raises the question of whether TP53 status biases cells towards vulnerability to Chk1/2 inhibitors. Simple experiments could be performed to re-express WT TP53 in these cells to test whether Chk1/2i vulnerability is reduced. Additionally, the compound screen could be extended to include more cell lines to see if TP53-mutant lines trend towards being more sensitive to Chk1/2 inhibitors.

UACC62P cells treated with AURKi, PLKi, and tubulin inhibitors undergo mitotic slippage, but the fate of these cells is unclear. In many cases cells which undergo mitotic slippage enter into a senescent state and exit from the cell cycle. Long-term imaging experiments, perhaps for 3-4 days, will be needed to determine whether these cells re-enter into the cell cycle after compound treatment. It is also known that certain perturbations, such as loss of TP53, can drive cells to re-enter into the cell cycle after mitotic slippage. Since TP53 is frequently mutated in SKCM tumors it will be important to determine whether loss of TP53 facilitates cell cycle re-entry after melanoma cells undergo mitotic slippage.

The experiments described in this dissertation demonstrate that pharmacological inhibition of RhoA-mediated YAP1 and MRTF-A activation may be an effective strategy to reverse drug resistance in SKCM. Furthermore, several pharmacological vulnerabilities were identified in BRAFi-resistant SKCM cells. In order to effectively treat SKCM tumors new drug treatments which prevent or reverse drug resistance will need to be developed, and the findings presented in this thesis can be leveraged to accomplish that goal.

APPENDIX

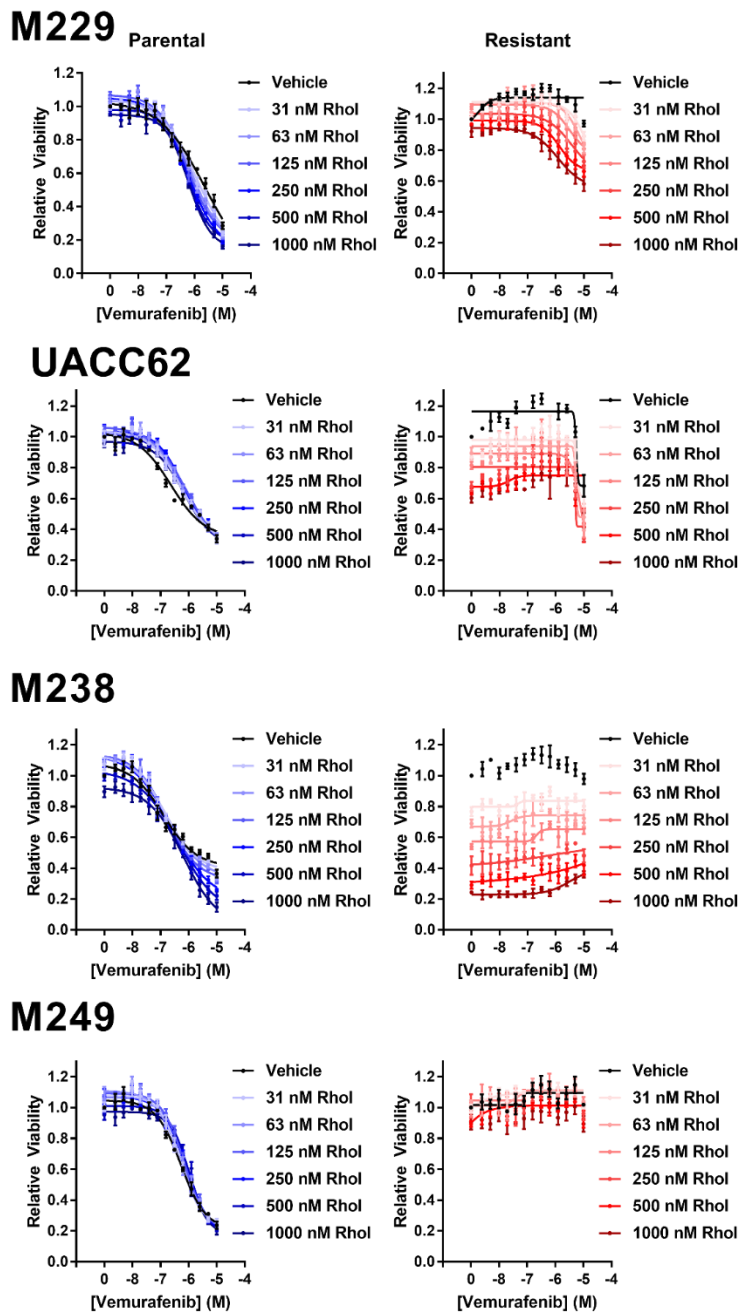


Figure A-2.1: Vemurafenib resistant cells are more sensitive to RhoA inhibition M229P/R, UACC62P/R, M238P/R, and M249P/R cells were seeded into 384-wel plates at a density of 1000 cells/well and were allowed to attach overnight. The next day the cells were treated in a 7x14 concentration matrix wherein the cells were treated with the 7 indicated concentrations of Rho Inhibitor I (RhoI) and the 14 indicated concentrations of vemurafenib. After 72 h the samples were processed as described in materials and methods.

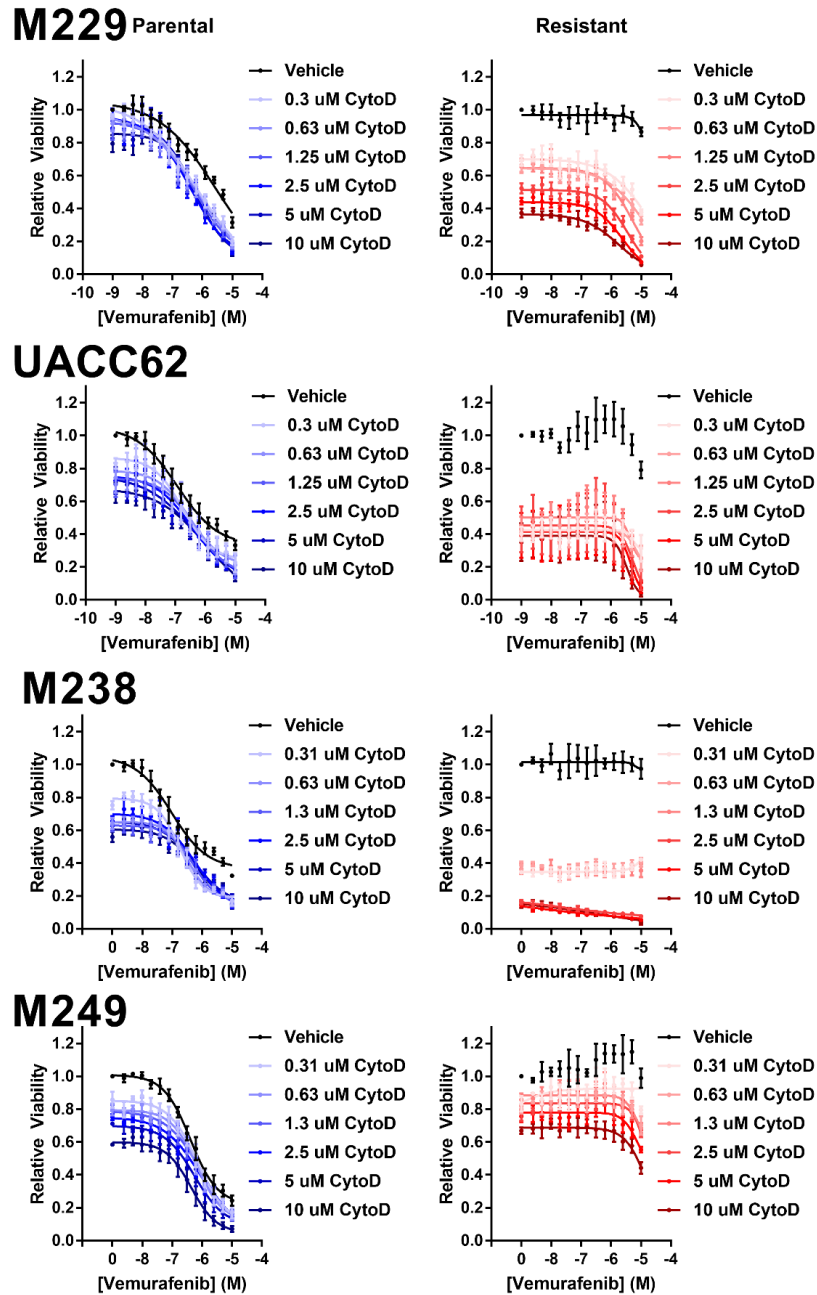


Figure A-2.2: Vemurafenib-resistant cells are more sensitive to Cytochalasin D M229P/R, UACC62P/R, M238P/R, and M249P/R cells were seeded into 384-wel plates at a density of 1000 cells/well and were allowed to attach overnight. The next day the cells were treated in a 7x14 concentration matrix wherein the cells were treated with the 7 indicated concentrations of Cytochalasin D (CytoD) and the 14 indicated concentrations of vemurafenib. After 72 h the samples were processed as described in materials and methods.

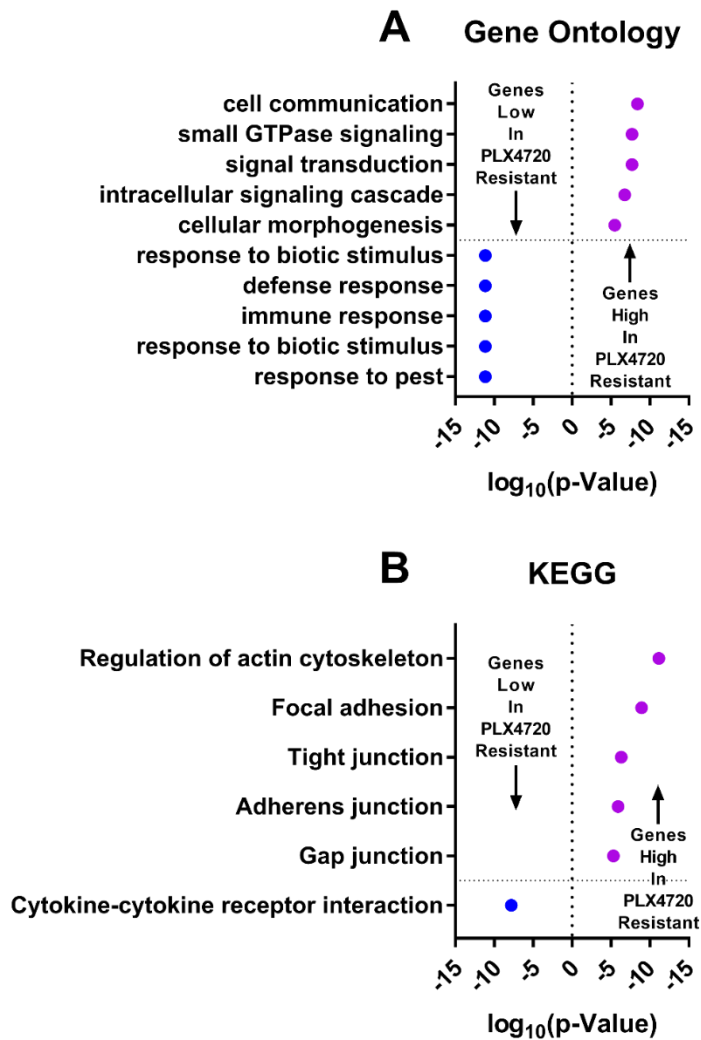


Figure A-2.3: Genes involved in small GTPase signaling and the actin cytoskeleton are associated with BRAFi resistance The CCLE dataset was filtered to include the 38 adherent cell lines with BRAF^{V600} mutations. PLX4720 sensitivity (activity area) was correlated with gene expression values in these 38 cell lines. Genes which were inversely correlated with PLX4720 response (Pearson correlation coefficient < -0.5) or positively correlated with PLX4720 response (Pearson correlation coefficient > 0.5) were analyzed by **A. Gene Ontology** and **B. KEGG** pathway analysis as described in Materials and Methods. The X-axis on each plot is the enrichment score for each GO or KEGG term.

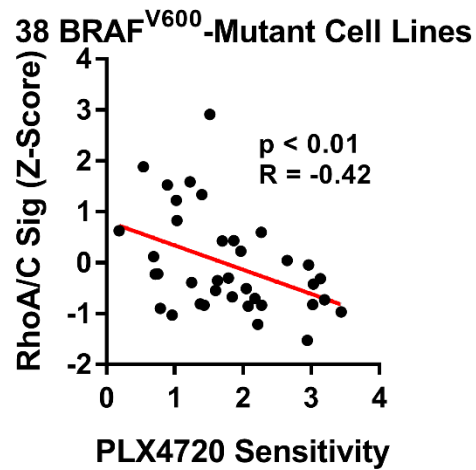


Figure A-2.4: Expression of RhoA/C target genes is inversely correlated with PLX4720 sensitivity ssGSEA was used to calculate a RhoA/C pathway signature score as described in Materials and Methods. The RhoA/C signature scores were Z-score normalized and then correlated with PLX4720 sensitivity. The sensitivity data is the Activity Area data from the CCLE dataset. High activity areas indicate that the compound had a larger effect on reducing cell viability than a small activity area. A description of how activity area is calculated can be found in Materials and Methods.

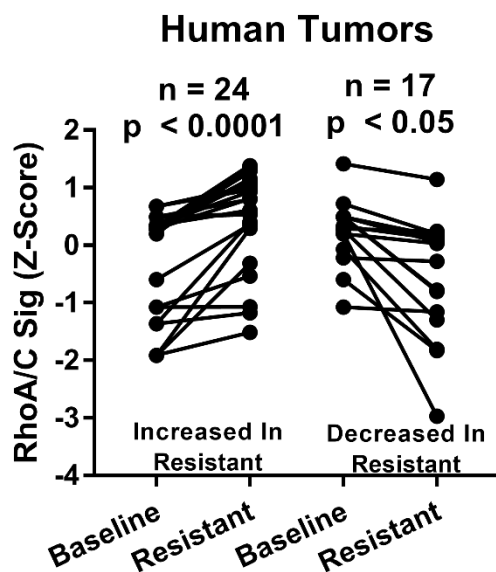


Figure A-2.5: A subset of drug-resistant human melanoma tumors have increased expression of RhoA/C target genes RNA-seq data for 62 human tumors pre- and post- MAPK inhibitor resistance was downloaded from GSE65185. Analysis was performed on the CuffnormFPKM dataset included in this series. The RhoA/C activation signature score was calculated for each sample using ssGSEA and were subsequently Z-score normalized. The RhoA/C signature score was compared between the matched pre- and post-resistance samples and the samples were stratified into samples where the RhoA/C signature score was increased in the resistant tumor and samples where the RhoA/C signature was decreased in the resistant tumor.

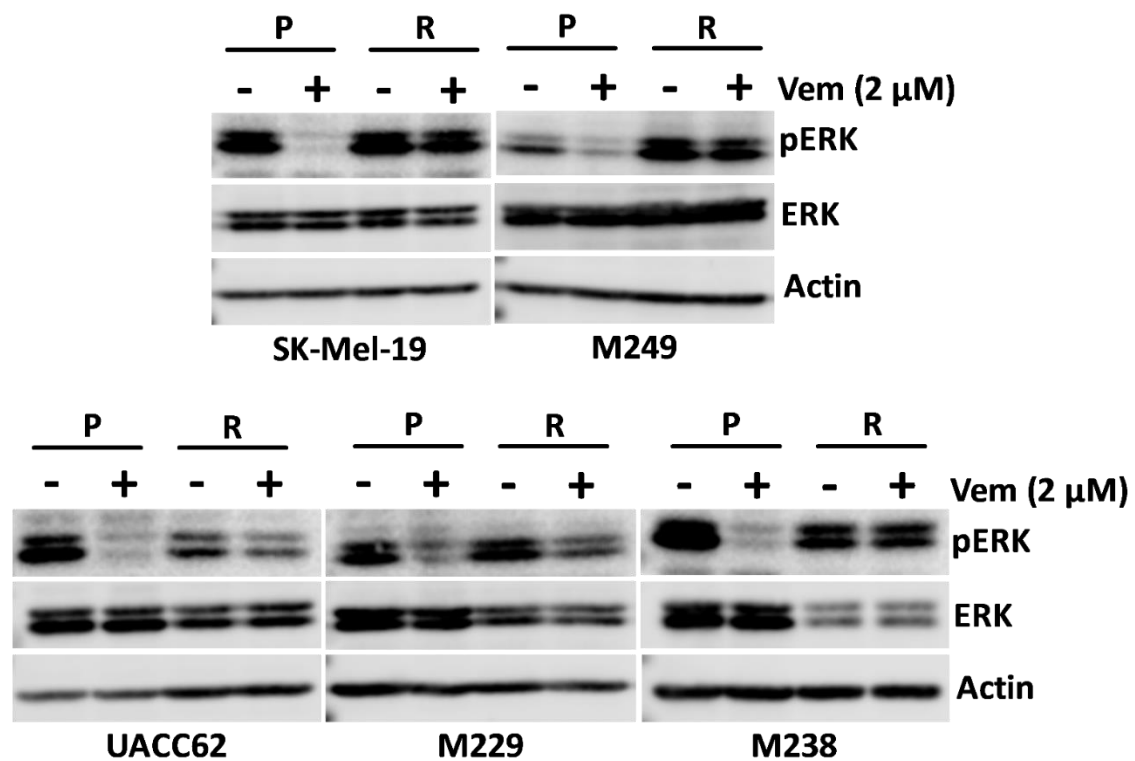


Figure A-2.6: ERK reactivation in BRAFi-resistant cell lines The 5 matched parental and resistant cell lines were seeded into 6-well plates and were allowed to attach overnight in the absence of vemurafenib. The next day the medium was changed to fresh growth medium \pm 2 μ M vemurafenib. After 6 hours total cellular lysates were harvested and processed as described in Materials and Methods and immunoblots were performed with the indicated antibodies.

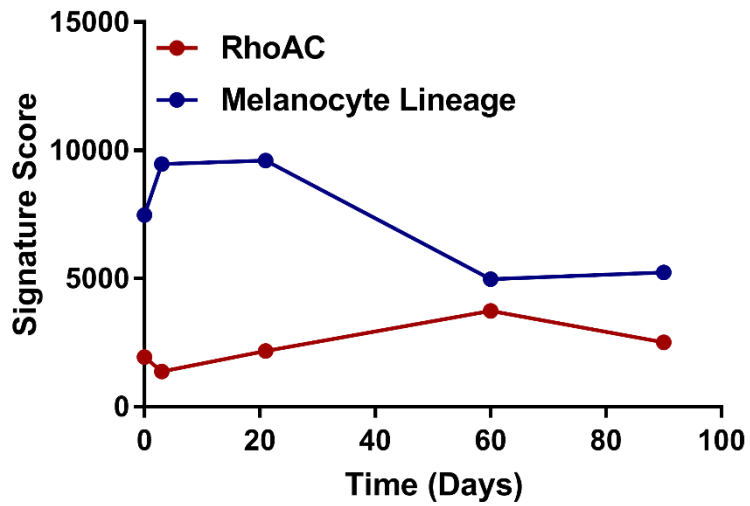


Figure A-2.7: A RhoA/C signature and a Melanocyte Lineage signature are inversely correlated in BRAFi-treated tumors The RhoA/C and Melanocyte Lineage signature scores were calculated using ssGSEA and the raw signature scores for each sample were plotted as a function of vemurafenib treatment duration.

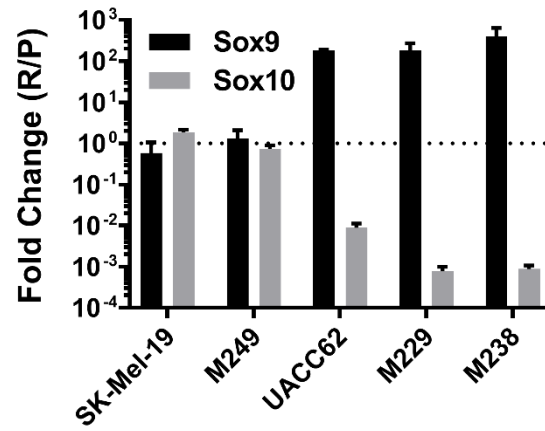


Figure A-2.8: Sox9 is upregulated and Sox10 is downregulated in Rho^{High} BRAFi-resistant cells The cell lines were seeded into 6-well plates and were allowed to attach overnight. The next day total cellular RNA was harvested and cDNA was synthesized as described in Materials and Methods. qPCR was performed for Sox9, Sox10, and GAPDH as described in Materials and Methods.

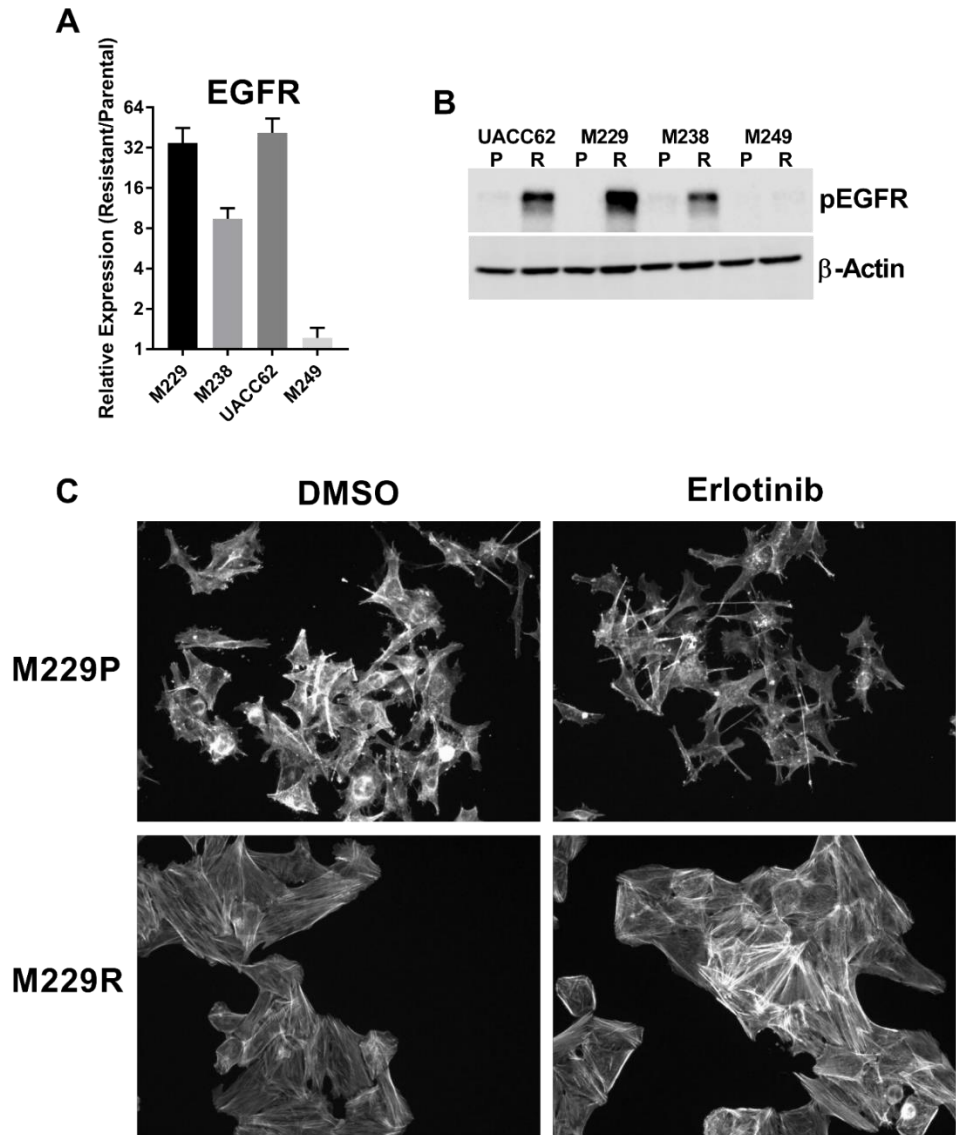


Figure A-2.9: EGFR is activated in vemurafenib-resistant cells but erlotinib treatment does not alter stress fiber formation **A.** Total mRNA was harvested from the indicated cell lines and cDNA was transcribed as described in materials and methods. qPCR was performed for the indicated genes as described in materials and methods. **B.** Protein lysates were extracted from the indicated cell lines and immunoblots for pEGFR and β -actin were performed as described in materials and methods. **C.** M229P/R cells were seeded into 8-well chamber slides and were allowed to attach overnight. The next day the cells were treated $-/+$ 10 μ M erlotinib. After 24 h the cells were fixed and stained with fluorescently labeled phalloidin as described in materials and methods.

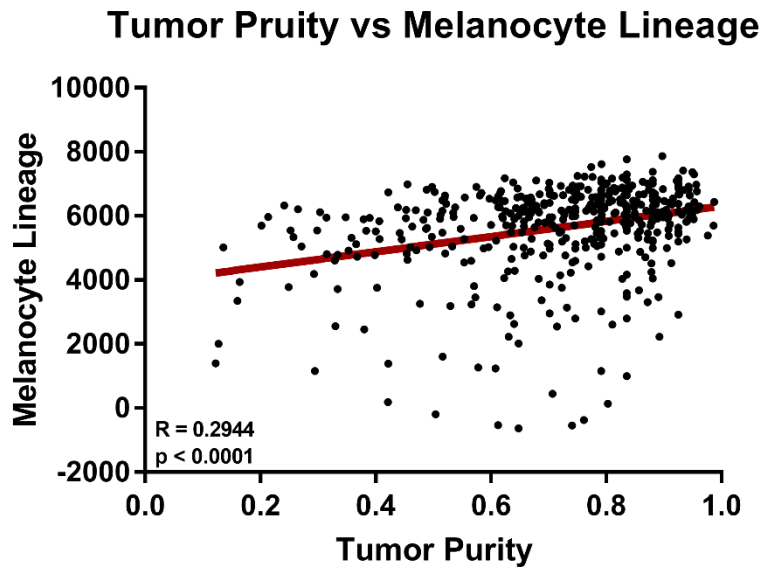


Figure A-2.10: Correlation between melanocyte identity and tumor purity The TCGA Skin Cutaneous Melanoma (SKCM) dataset was downloaded and processed as described in Materials and Methods. The Melanocyte Lineage signature score for each sample was calculated using ssGSEA and was correlated with the predicted tumor purity. The values for the predicted tumor purity were previously derived in another study.

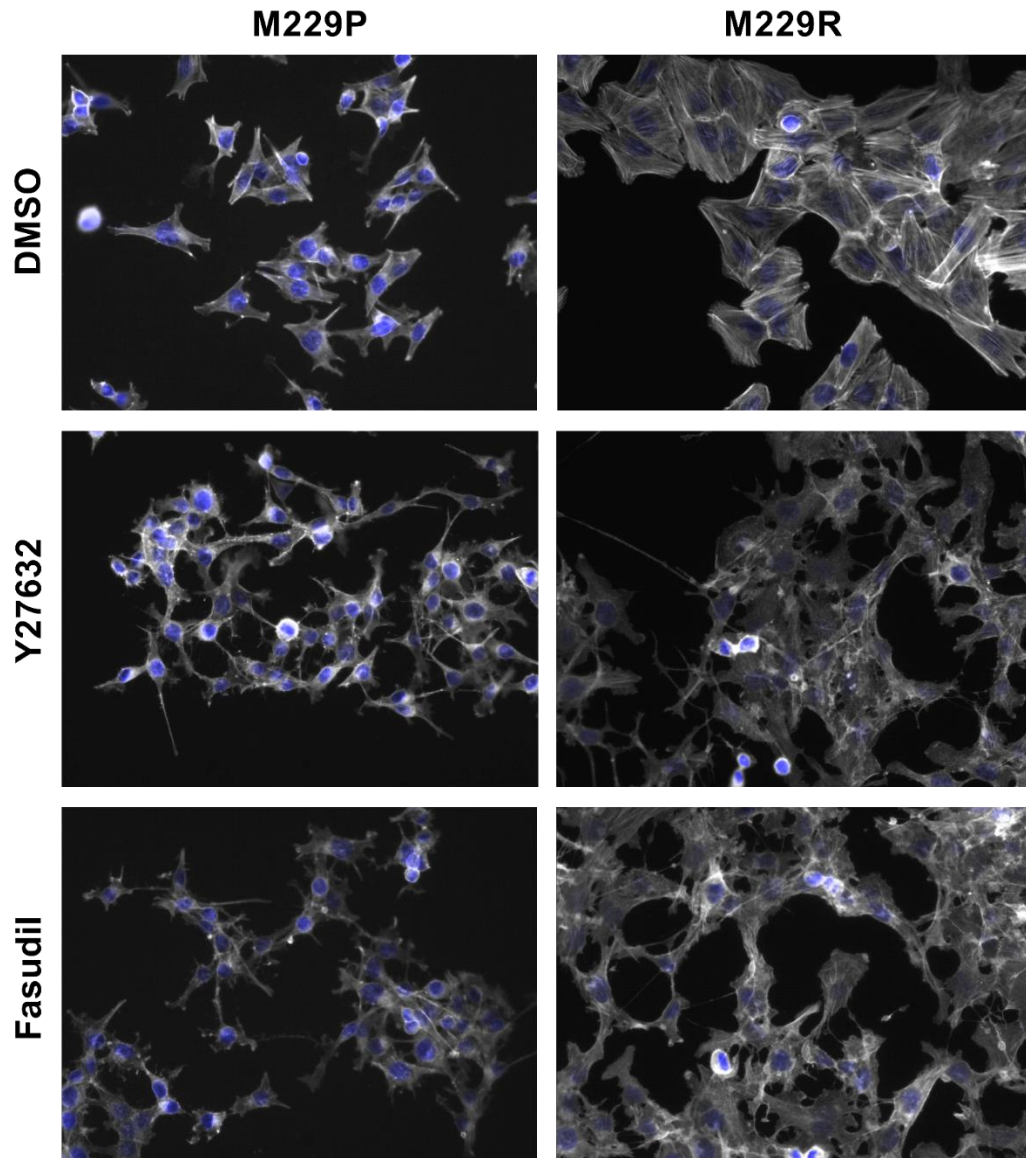


Figure A-2.11: ROCK inhibitors prevent stress fiber formation in M229R cells M229P/R cells were seeded at a density of 5000 cells/well in 8-well chamber slides and were allowed to attach overnight. The next day the cells were treated +/- 10 μ M Y-27632 or Fasudil. After 24 h the cells were fixed and stained with fluorescently labeled phalloidin (white) and DAPI (blue) as described in Materials and Methods.

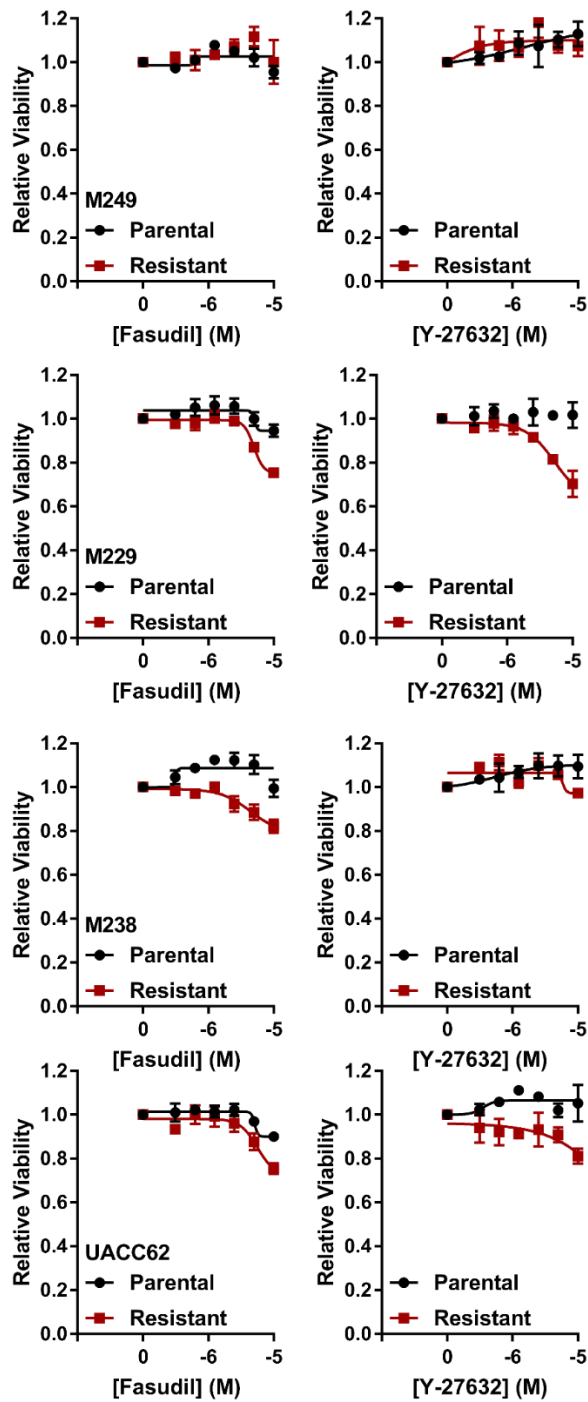


Figure A-2.12: Single agent response curves for fasudil and Y-27632 Four matched parental and resistant cell lines were treated with 7 concentrations of fasudil or Y-27632 for 72 h and viability was measured with Cell Titer Glo as described in Materials and Methods. Data was plotted and analyzed as described in Materials and Methods.

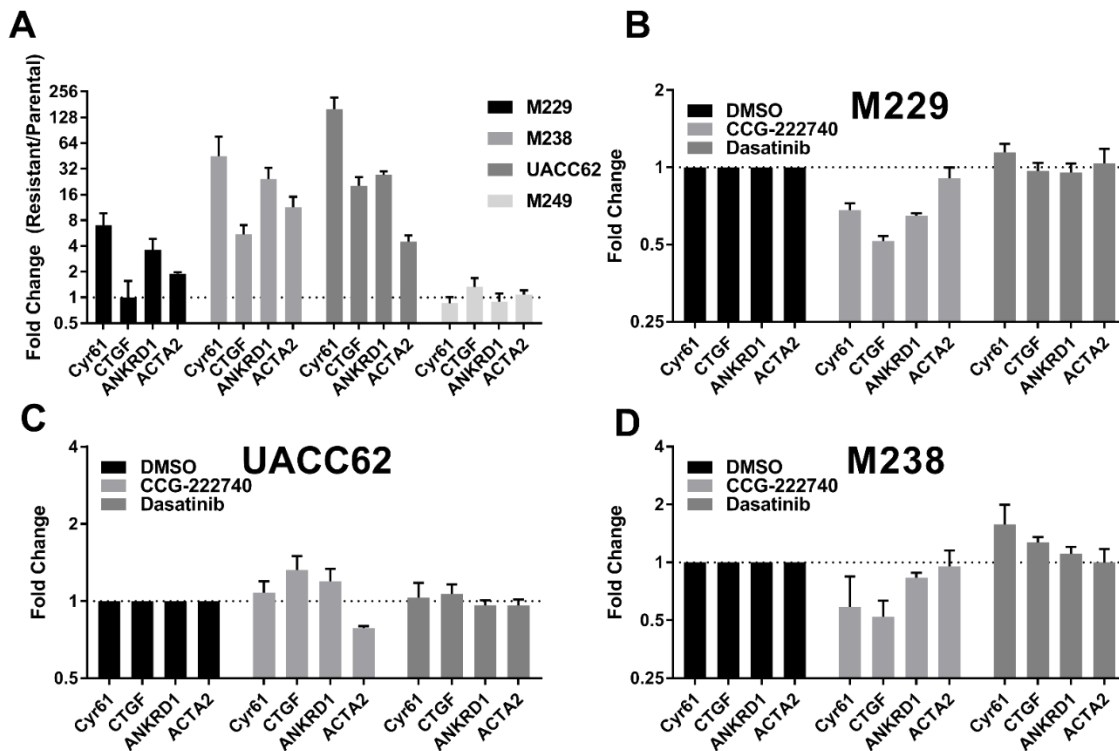


Figure A-2.13: Expression of MRTF/YAP target genes in vemurafenib-resistant cells **A.** Total mRNA was extracted from the indicated cell lines and cDNA was transcribed as described in materials and methods. qPCR was performed for the indicated genes as described in materials and methods. Data is presented as the fold change in expression between resistant and parental cells wherein larger values indicate that gene expression is elevated in the resistant cells. **B.** M229R, **C.** UACC62R, **D.** M238R cells were seeded into 6-well plates and were allowed to attach overnight. The next day the cells were treated with 10 μ M CCG-222740 or 100 nM dasatinib for 24 h. After 24 h total mRNA was extracted, and cDNA was transcribed as described in materials and methods. qPCR was performed for the indicated genes as described in materials and methods.

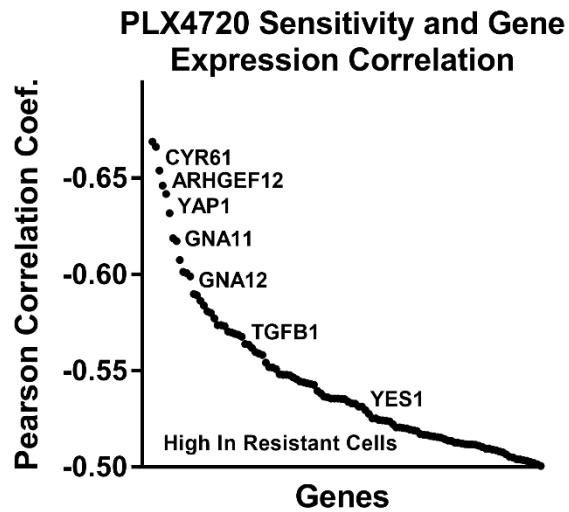


Figure A-2.14: Genes associated with MRTF/YAP1-mediated gene transcription are associated with PLX4720 response Select genes which have high expression in PLX4720-resistant cells and are associated with MRTF/YAP-mediated gene transcription are highlighted. Only the genes with the highest inverse correlation between expression and PLX4720 response (Pearson correlation coefficient < -0.5) are displayed on this plot.

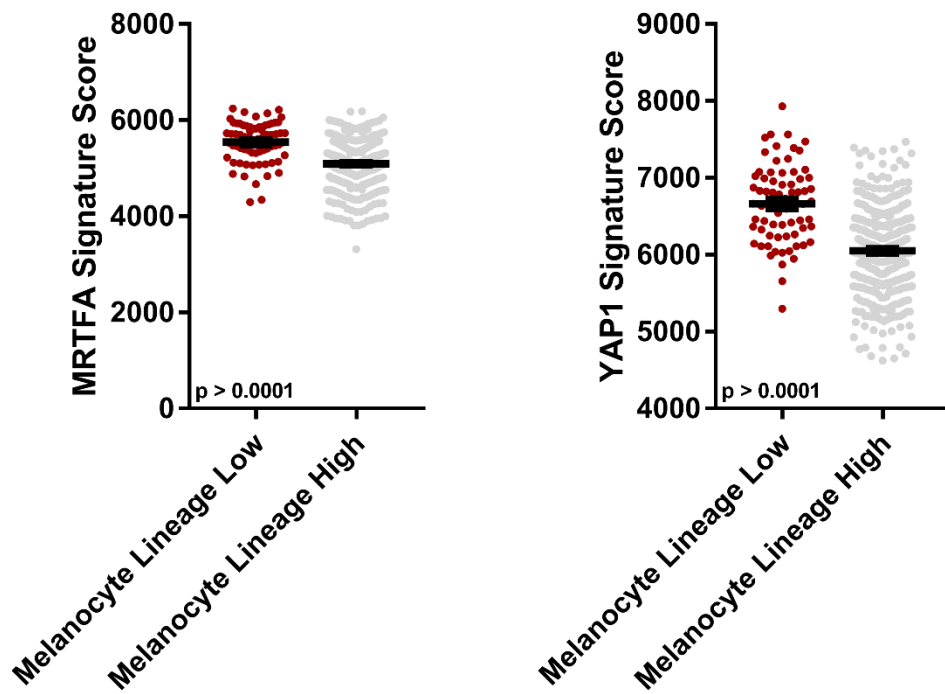


Figure A-2.15: Increased MRTF/YAP1 signature scores in poorly differentiated human melanoma tumors The TCGA SKCM dataset was downloaded and processed as described in Materials and Methods. Melanocyte Differentiation, MRTF, and YAP1 signature scores were calculated using ssGSEA. Tumors were stratified into Melanocyte Lineage High/Low as described in materials and methods.

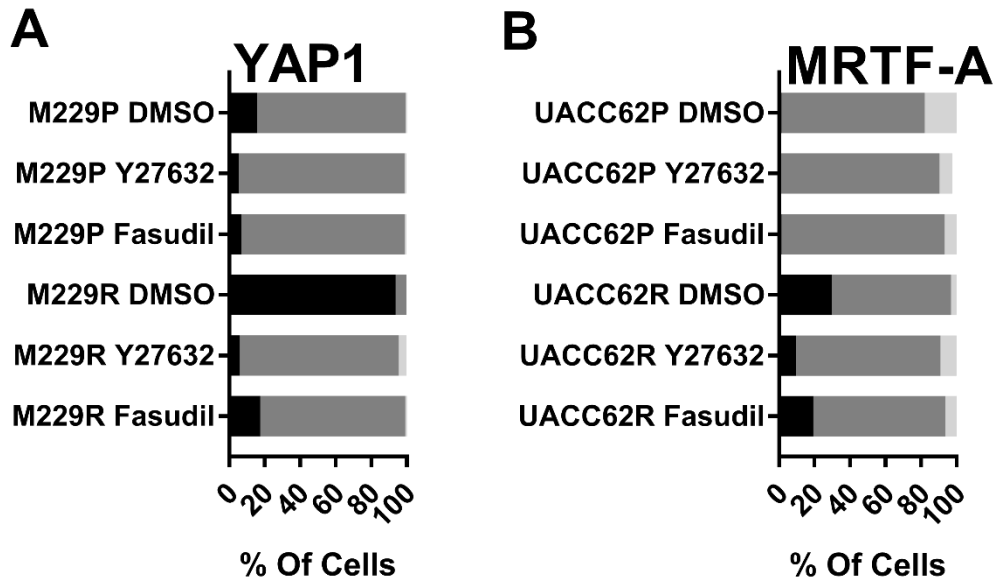


Figure A-2.16: ROCK inhibitors reduce the nuclear accumulation of YAP1 and MRTF-A **A.** M229P/R cells were seeded into 8-well chamber slides and were allowed to attach overnight. The next day the cells were treated with 10 μ M Y27632 or Fasudil. After 24 h the cells were fixed and stained with an anti-YAP1 antibody as described in materials and methods. **B.** UACC62P/R cells were seeded into 8-well chamber slides and were allowed to attach overnight. The next day the cells were treated with 10 μ M Y27632 or Fasudil. After 24 h the cells were fixed and stained with an anti-MRTF-A antibody as described in materials and methods.

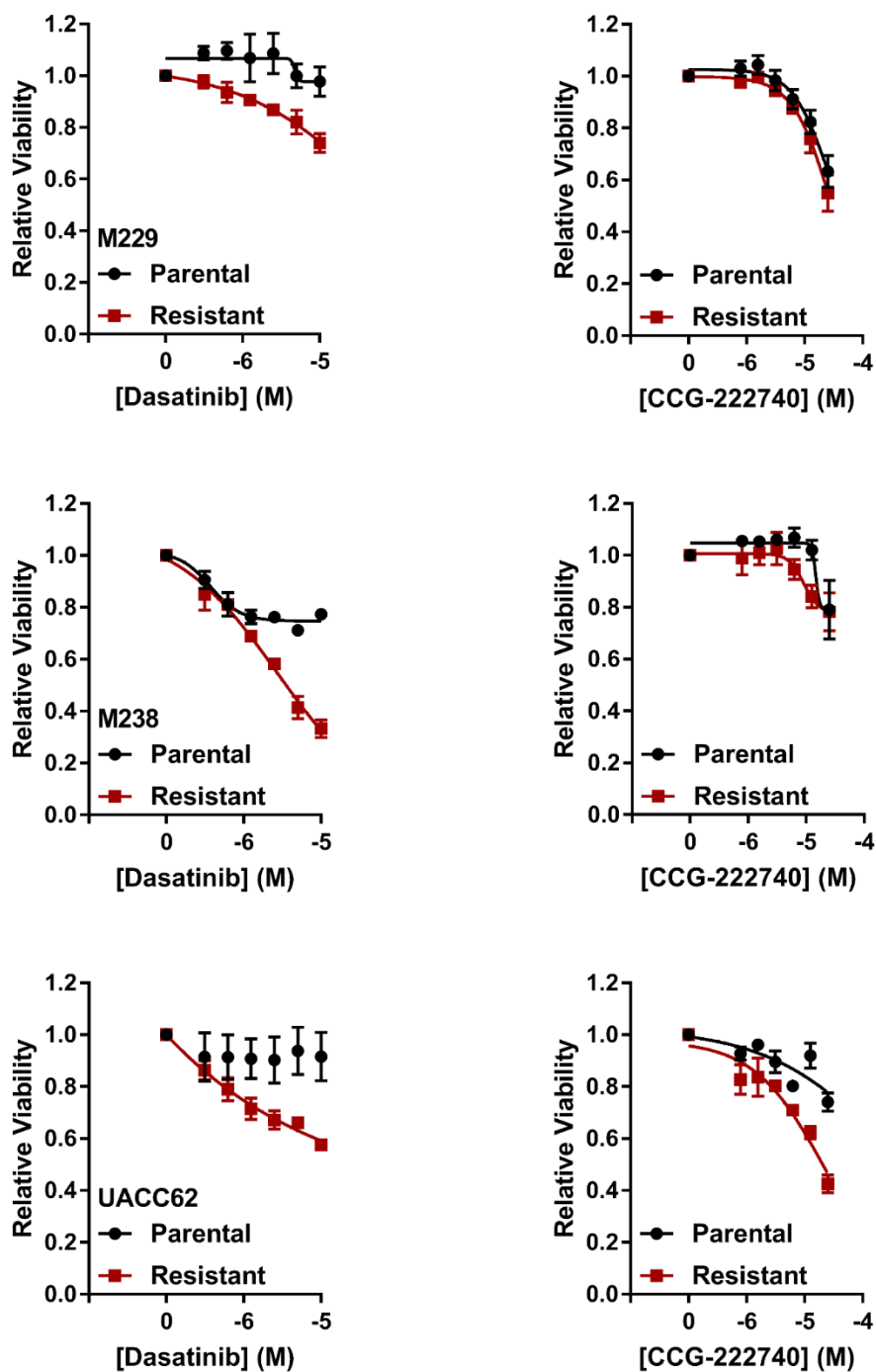


Figure A-2.17: Single agent response curves for dasatinib and CCG-222740 Four matched parental and resistant cell lines were treated with 7 concentrations of dasatinib or CCG-222740 for 72 h and viability was measured with Cell Titer Glo as described in Materials and Methods. Data was plotted and analyzed as described in Materials and Methods.

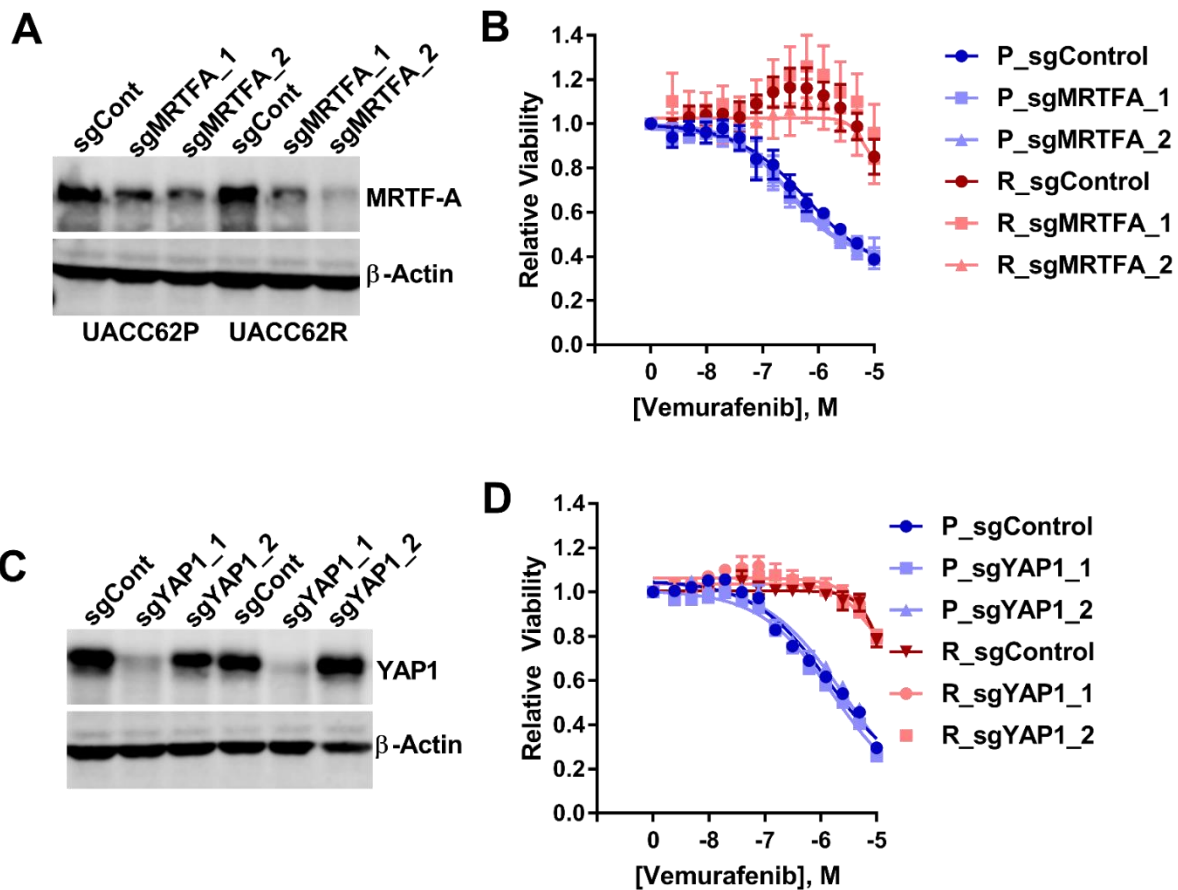


Figure A-2.18: MRTF-A or YAP1 deletion does not alter vemurafenib sensitivity **A.** Immunoblot measuring MRTF-A knockout efficiency in UACC62P and UACC62R cells. **B.** UACC62P/R cells were seeded into 384-well plates and were treated with 14 concentrations of vemurafenib with a top dose of 10 μM in a $\frac{1}{2}$ dilution series. After 72 h the samples were processed as described in materials and methods. **C.** Immunoblot measuring YAP1 knockout efficiency in M229P and M229R cells. **D.** M229P/R cells were seeded into 384-well plates and were treated with 14 concentrations of vemurafenib with a top dose of 10 μM in a $\frac{1}{2}$ dilution series. After 72 h the samples were processed as described in materials and methods.

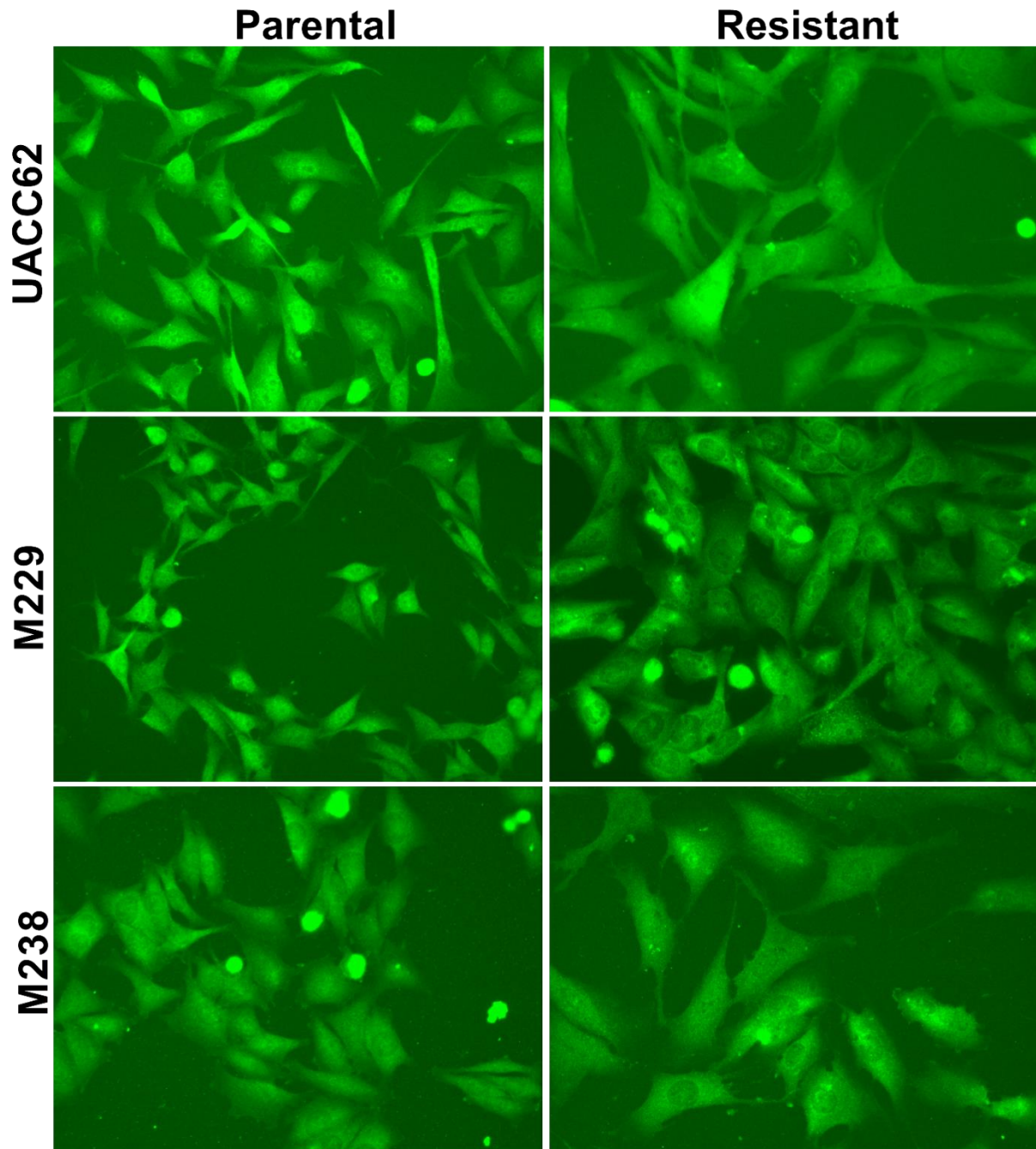


Figure A-2.19: MRTF-B localization is not altered in BRAFi-resistant cells The indicated cell lines were seeded into 8-well chamber slides and were allowed to attach overnight. The next day the cells were fixed and stained with an anti-MRTF-B antibody as described in Materials and Methods.

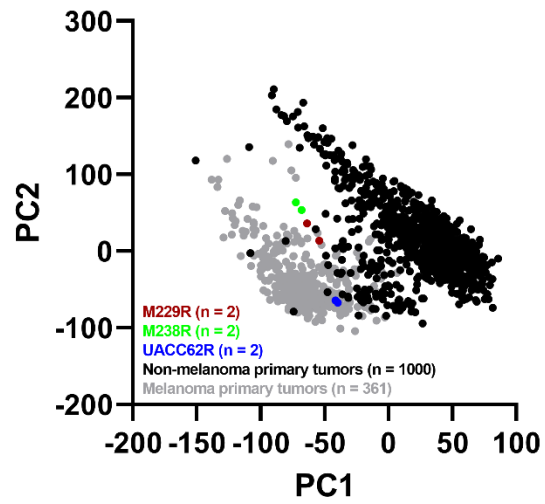


Figure A-3.1: Principal Component Analysis of resistant cell line samples and tumor tissue samples
Principal Component Analysis was performed on 361 primary melanoma tumors, 1,000 non-melanoma primary tumors, and BRAFi-resistant melanoma cell lines (n = 2 for 3 different cell lines).

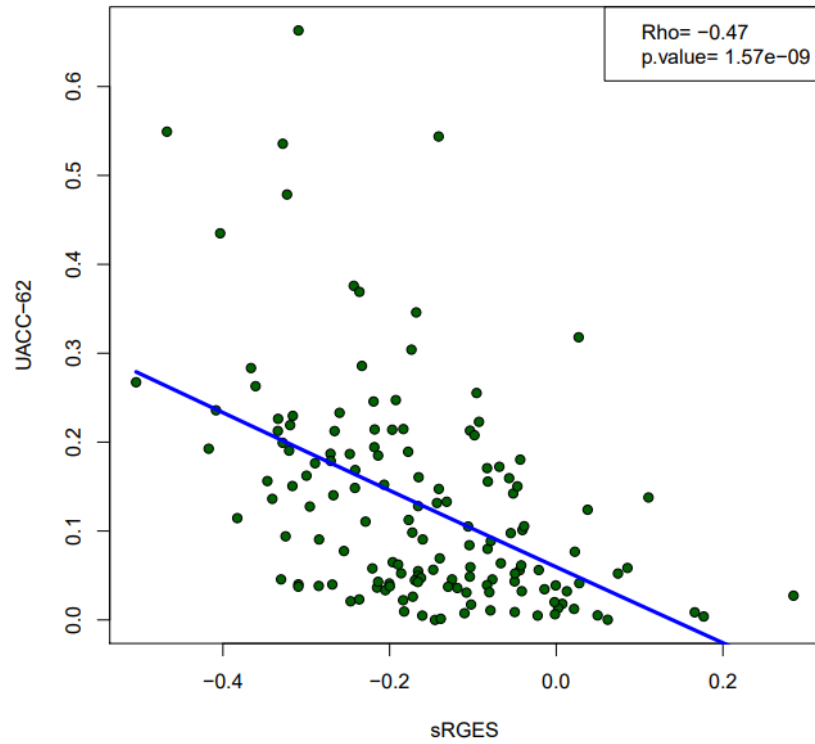


Figure A-3.2: Drug sensitivity correlates with sRGES drug response predictions Predicted drug sensitivity was calculated for UACC62P cells and was correlated with drug response data from the CTRPv2 dataset.

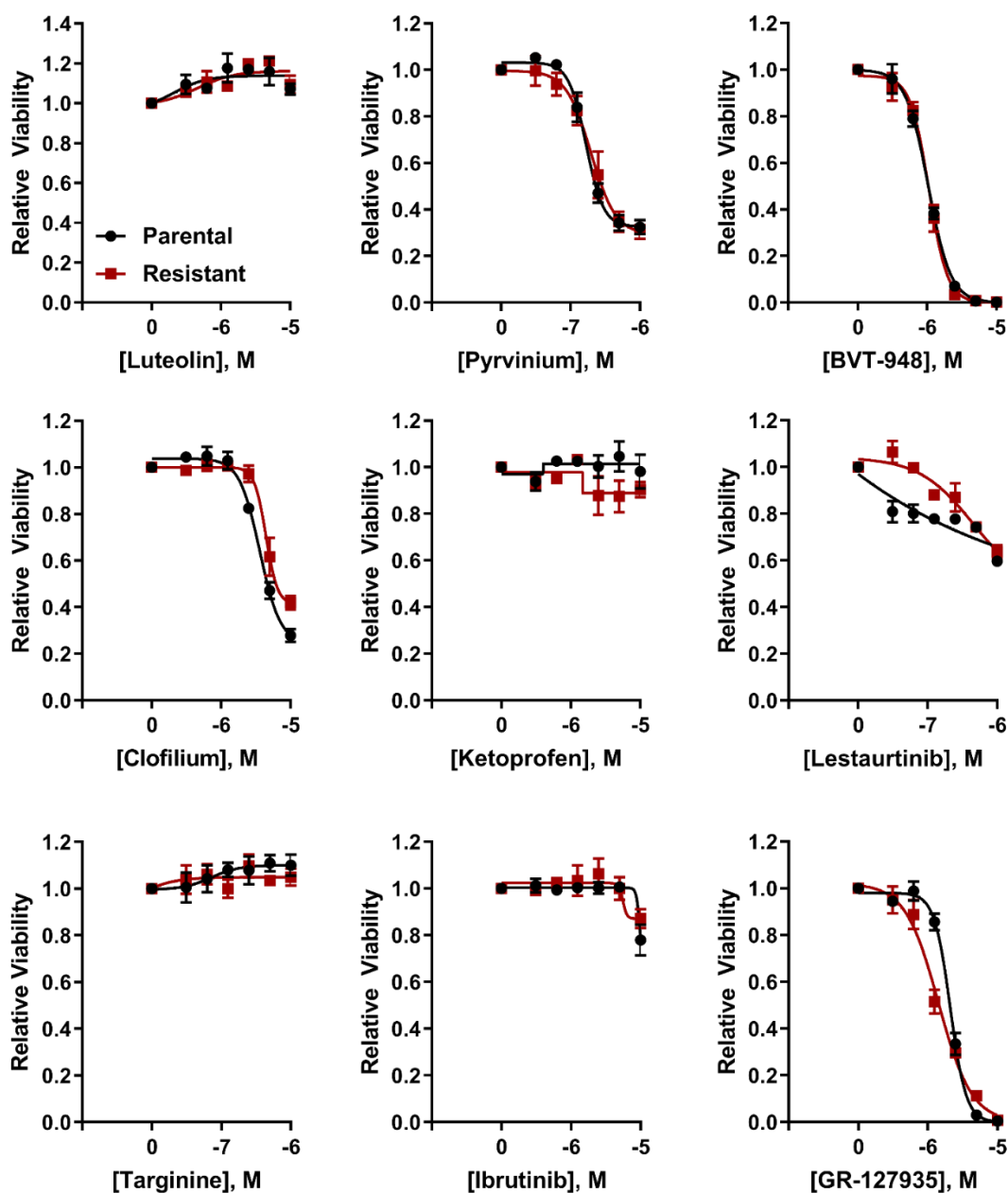


Figure A-3.3: Single-agent activity of compounds identified in the computational screen M229P (black lines) and M229R (red lines) cells were seeded into 384-well plates at a density of 1,000 cells/well. The next day the cells were treated with the indicated compounds. After 72 h viability was measured as described in materials and methods. The single agent response curves were derived from the experiment in Fig S2 but are re-plotted here as a separate figure to improve clarity and ease interpretation of the data.

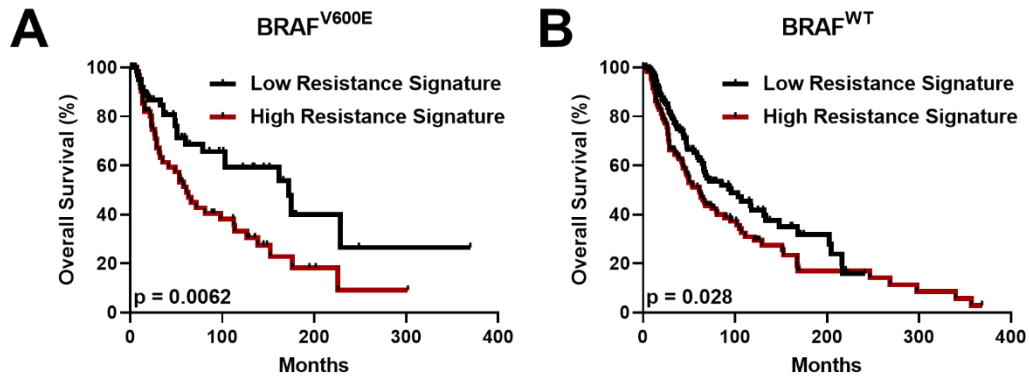


Figure A-3.4: A BRAFi resistance signature is inversely correlated with melanoma overall survival
 The BRAFi-resistance gene expression signature was generated as described in the Materials and Methods section and expression of this signature was calculated for either **A.** BRAF^{V600E} or **B.** BRAF^{WT} melanoma tumors.

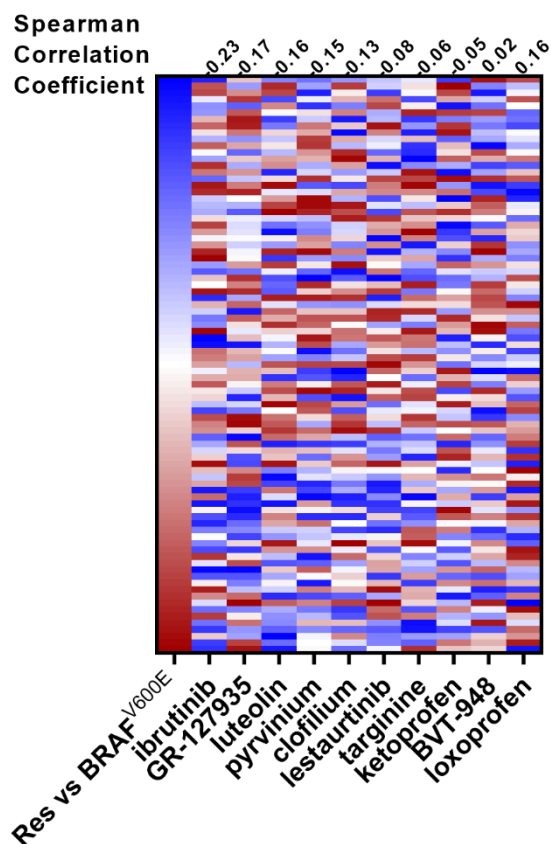


Figure A-3.5: Identification of compounds that reverse a BRAFi resistance gene expression signature

The resistance signature was computed by comparing resistance cell line samples and BRAF^{V600E}-mutant melanoma patient samples. Red boxes indicate that the gene is upregulated, and blue boxes indicate downregulated genes. Loxoprofen was included as a control since this compound was not predicted to reverse the BRAFi resistance signature. For compounds with multiple gene expression profiles, the profile with a median RGEs was chosen for visualization. The correlation coefficients for the BRAFi-resistance signature and the compound-treated signatures are listed above the heatmap.

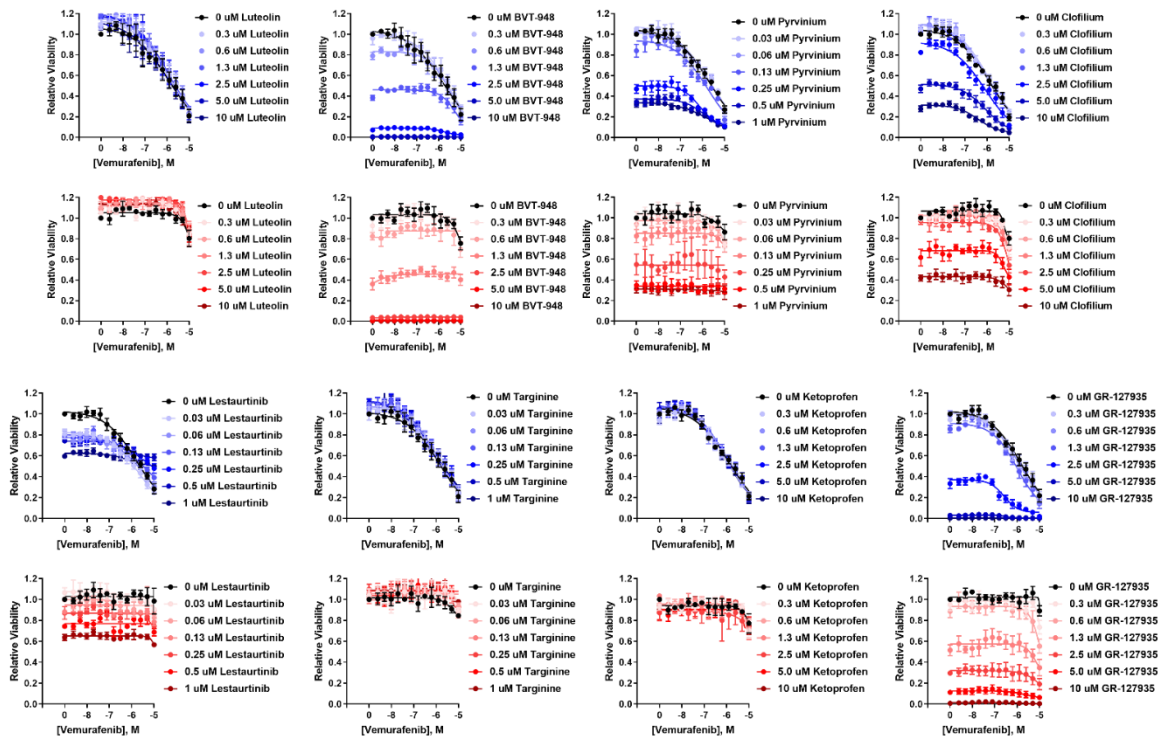


Figure A-3.6: Identification of compounds which re-sensitize BRAFi-resistant cells to vemurafenib M229P (blue lines) and M229R (red lines) cells were seeded into 384-well plates at a density of 1,000 cells/well. The next day the cells were treated with the indicated compounds. After 72 h viability was measured as described in materials and methods.

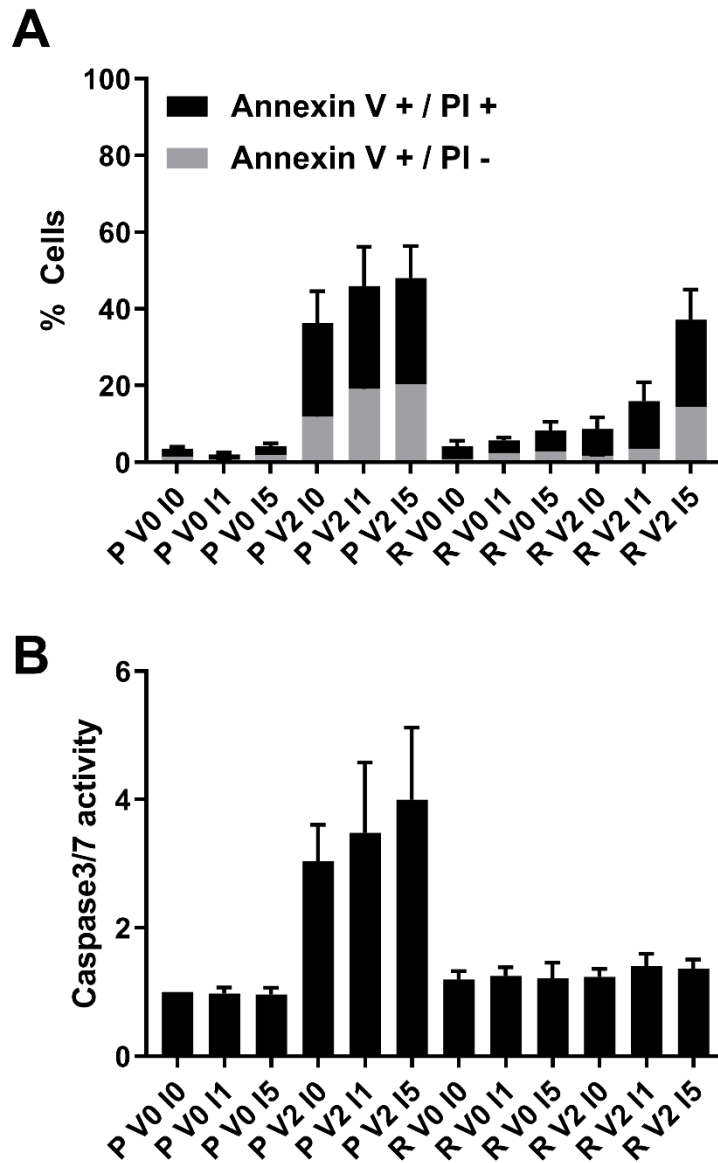


Figure A-3.7: The combination of vemurafenib and ibrutinib increases the number of Annexin V-positive cells but does not alter caspase3/7 activity **A.** The proportion of Annexin V and Propidium Iodide positive M229P/R cells was analyzed with flow cytometry as described in the Materials and Methods section. **B.** DEVD-AFC assays were used to evaluate caspase3/7 activity in M229P/R cellular lysates as described in the Materials and Methods section.

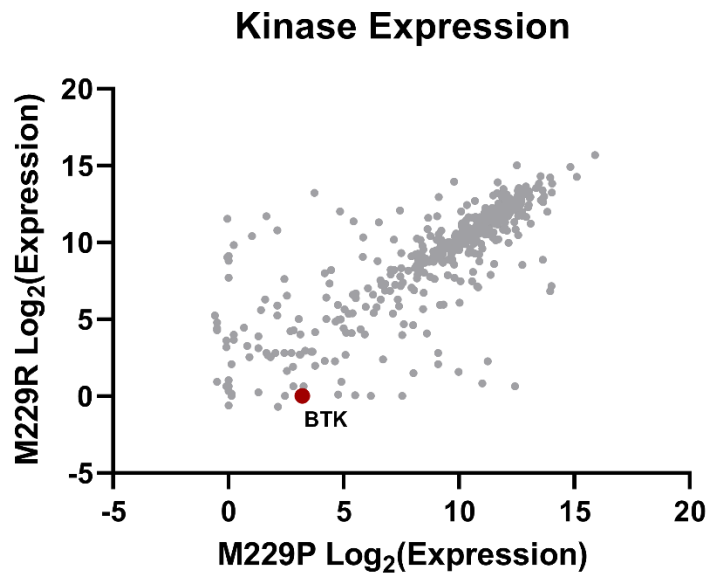


Figure A-3.8: BTK is weakly expressed in M229P/R cells RNA-Seq data for M229P/R cells was processed as described in Materials and Methods and expression of all protein kinases was compared. Relative to other kinases, the number of detected reads for BTK was low.

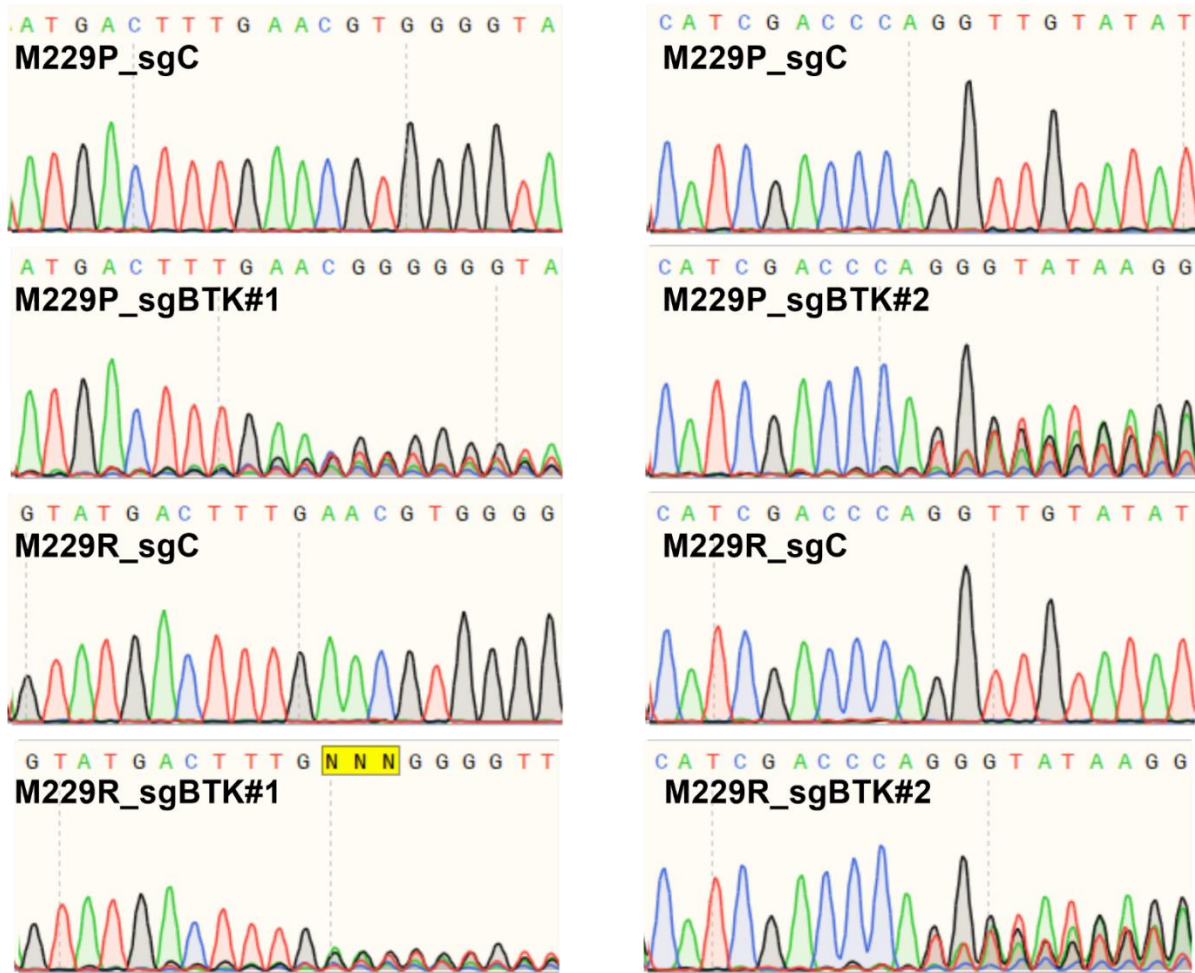


Figure A-3.9: Quantification of BTK knockout efficiency Representative Sanger sequencing traces that were used to measure CRISPR knockout efficiency with the TIDE algorithm as described in the Materials and Methods section.

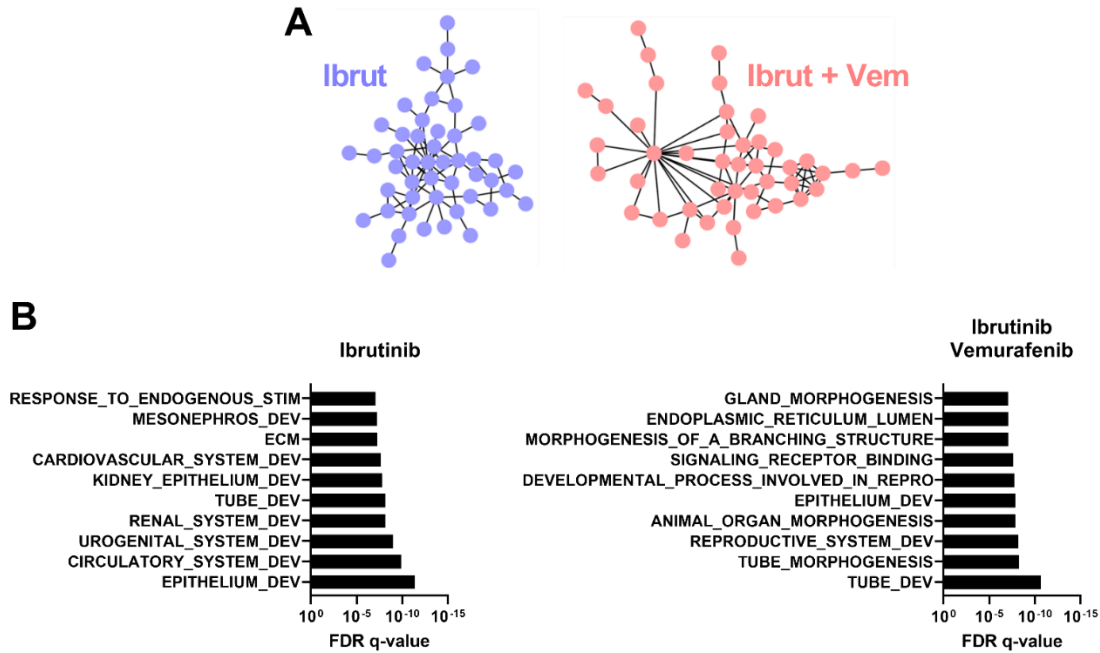


Figure A-3.10: Differential gene expression networks are associated with developmental gene signatures **A.** All differentially expressed genes in the ibrutinib-treated group (n = 101) were analyzed by string network analysis (left, blue). A similar analysis was performed for the top 101 differentially expressed genes in the ibrutinib + vemurafenib combination treatment group (right, red). **B.** Gene ontology analysis of genes within the interaction networks from Figure 3.3B.

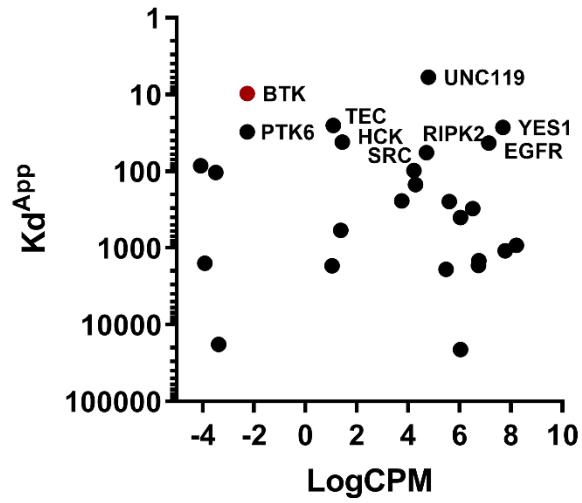


Figure A-3.11: Expression of ibrutinib targets in M229P/R cells Ibrutinib K_d against various kinases ²³⁵ compared with kinase gene expression in M229P/R cells. RNA-seq data processing was performed as described in Materials and Methods.

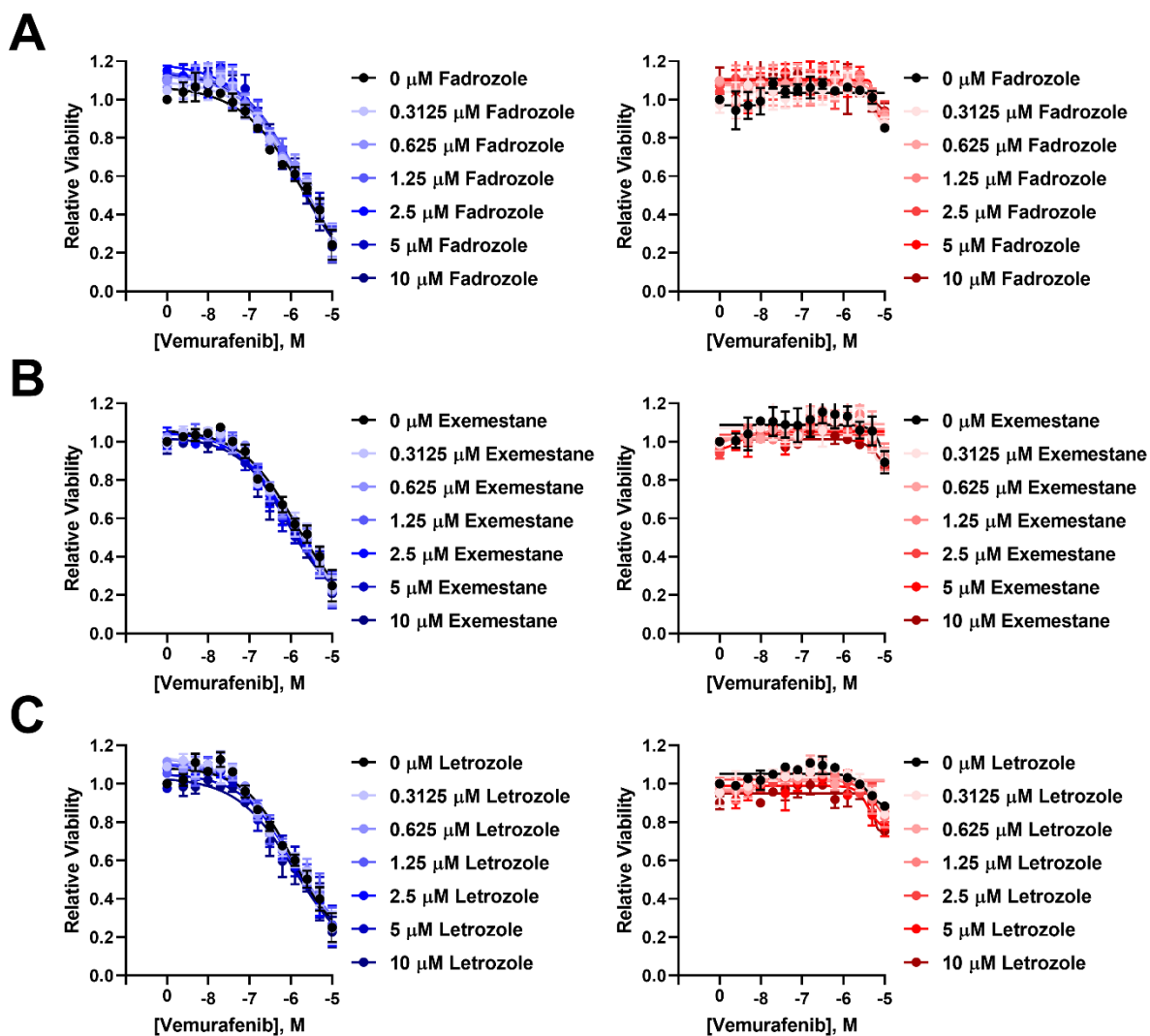


Figure A-3.12: Aromatase inhibitors do not alter BRAFi sensitivity M229P (blue) and M229R (red) cells were seeded into 384-well plates at a density of 1,000 cells/well. The next day the cells were treated with either **A.** Fadrozole, **B.** Exemestane, or **C.** Letrozole and vemurafenib as indicated. After 72 h viability was measured as described in Materials and Methods.

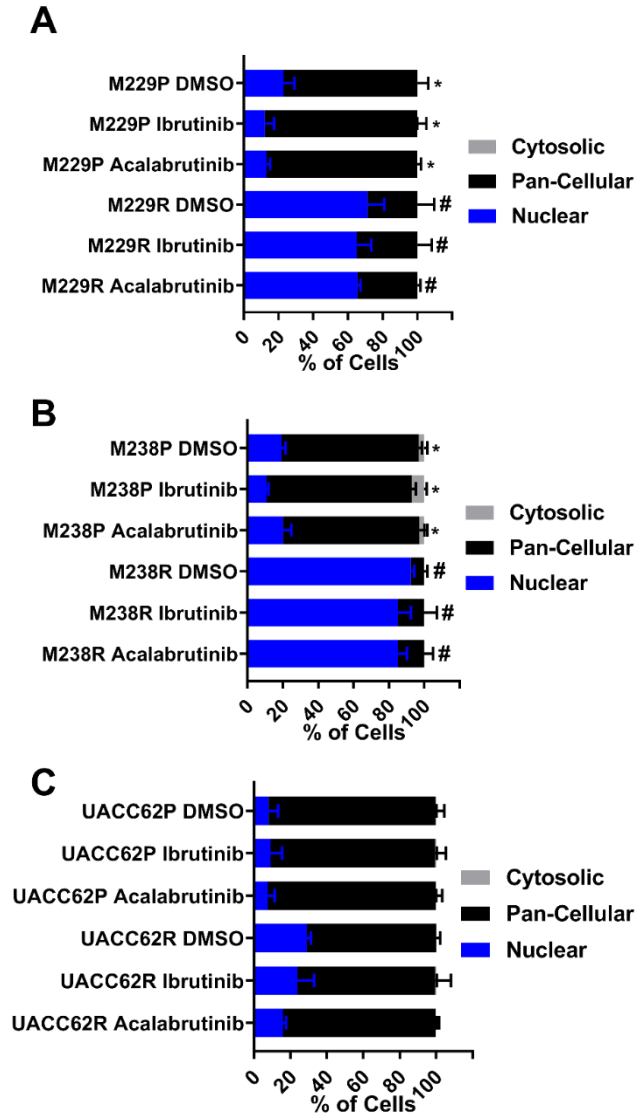


Figure A-3.13: Ibrutinib does not alter TAZ localization in BRAFi-resistant cells **A.** M229P/R, **B.** M238P/R, and **C.** UACC62P/R cells were seeded into 8-well chamber slides as described in Materials and Methods. The cells were treated with either DMSO, 5 μ M ibrutinib, or 5 μ M acalabrutinib. After 24 h the cells were fixed and stained as described in Materials and Methods. The proportion of cells with nuclear, pan-cellular, or cytosolic TAZ localization was quantified as described in Materials and Methods. Statistical analysis was performed on % of cells with nuclear localization where $p < 0.01$ was considered statistically significant. Bars marked with # indicate a statistically significant difference when compared with DMSO-treated parental cells and bars marked with * indicate a statistically significant difference when compared with DMSO-treated resistant cells.

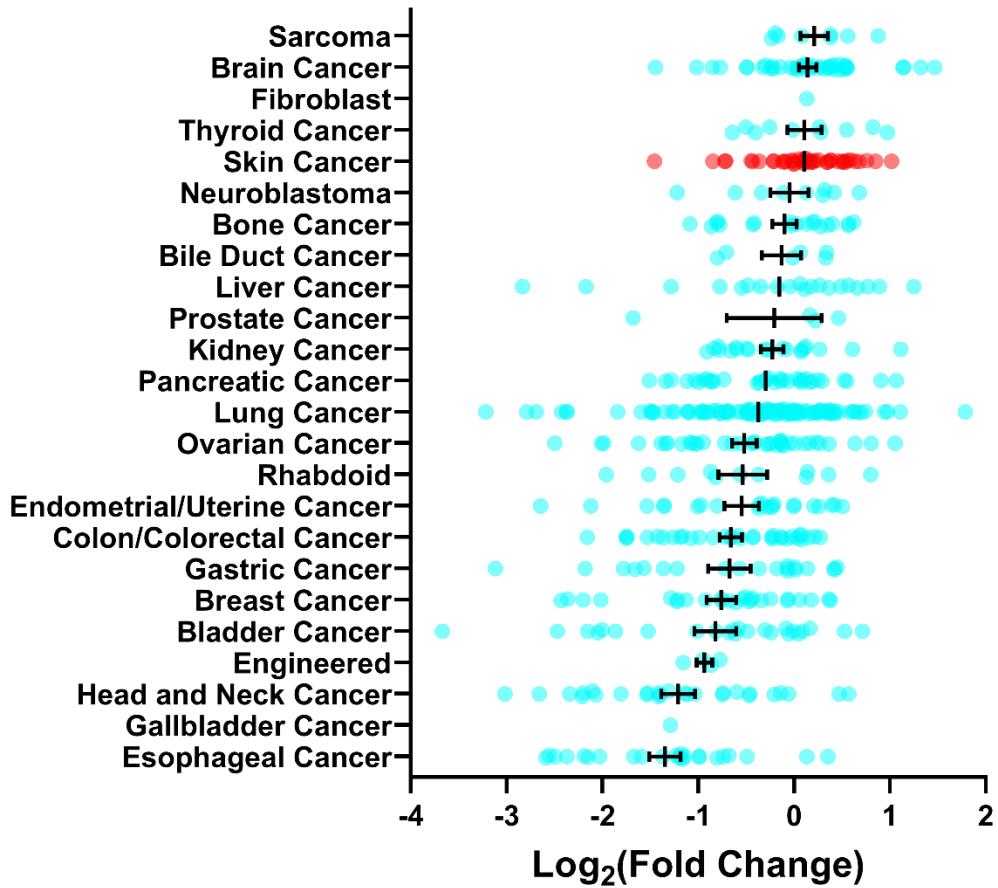


Figure A-3.14: Skin cancer cell lines are not sensitive to single agent ibrutinib treatment The cell lines in the PRISM dataset were stratified based on cancer type and ibrutinib sensitivity was compared. Smaller Log₂(Fold Change) values indicate higher sensitivity to ibrutinib.

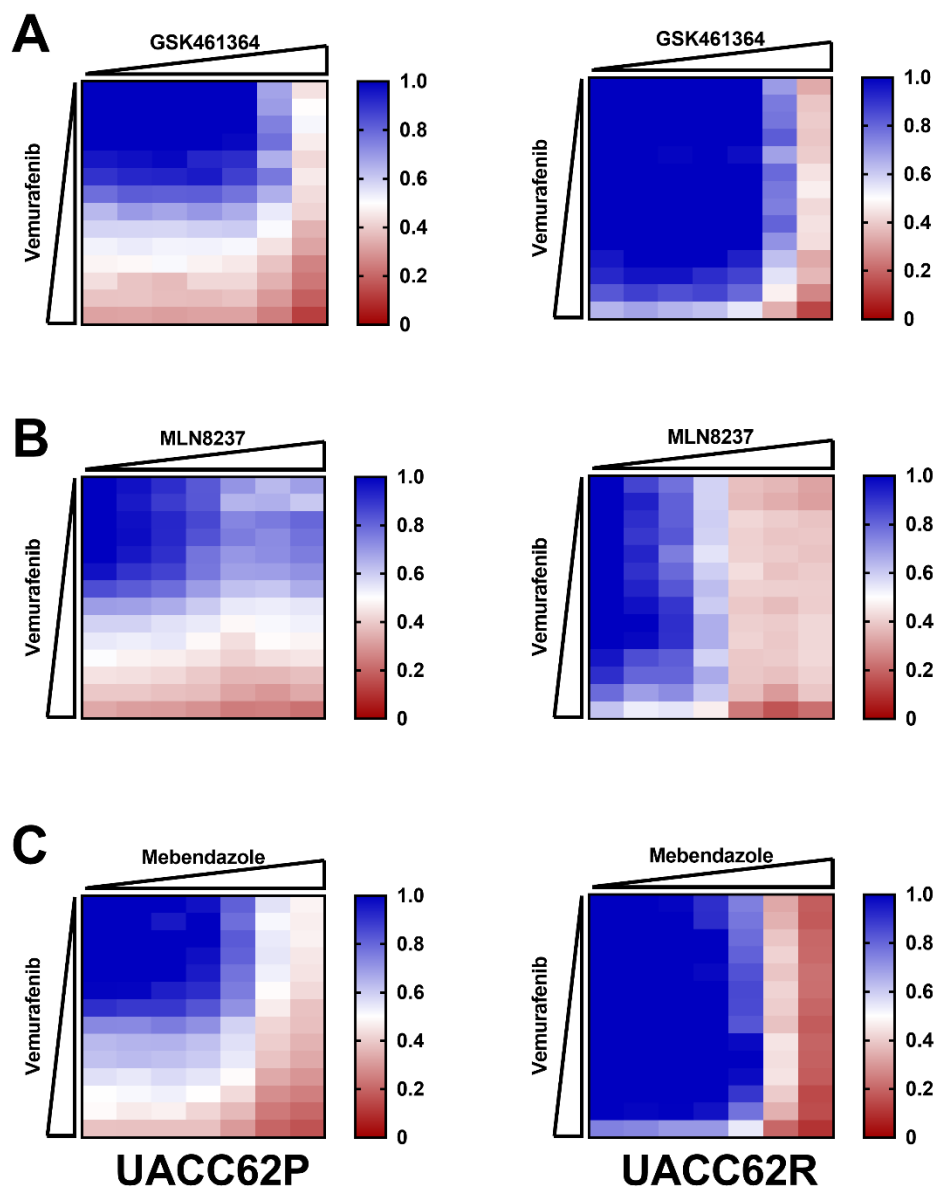


Figure A-4.1: AURK, PLK, and Tubulin inhibitors do not synergize with vemurafenib in UACC62P/R cells UACC62P/R cells were seeded into 384-well plates at a density of 1,000 cells/well. The next day the cells were treated in a concentration response matrix with a top concentration of 10 μ M for all compounds and a $\frac{1}{2}$ dilution series. Viability was analyzed as described in the Materials and Methods section. Data is expressed as relative viability wherein a value of 1 (blue) indicates 100% viability and a value of 0 (red) indicates 0% viability. **A.** UACC62P/R cells were treated with a GSK461364 x Vemurafenib concentration response matrix. **B.** UACC62P/R cells were treated with a MLN8237 x Vemurafenib concentration response matrix. **C.** UACC62P/R cells were treated with a Mebendazole x Vemurafenib concentration response matrix. This experiment was repeated with $n = 3$ biological replicates.

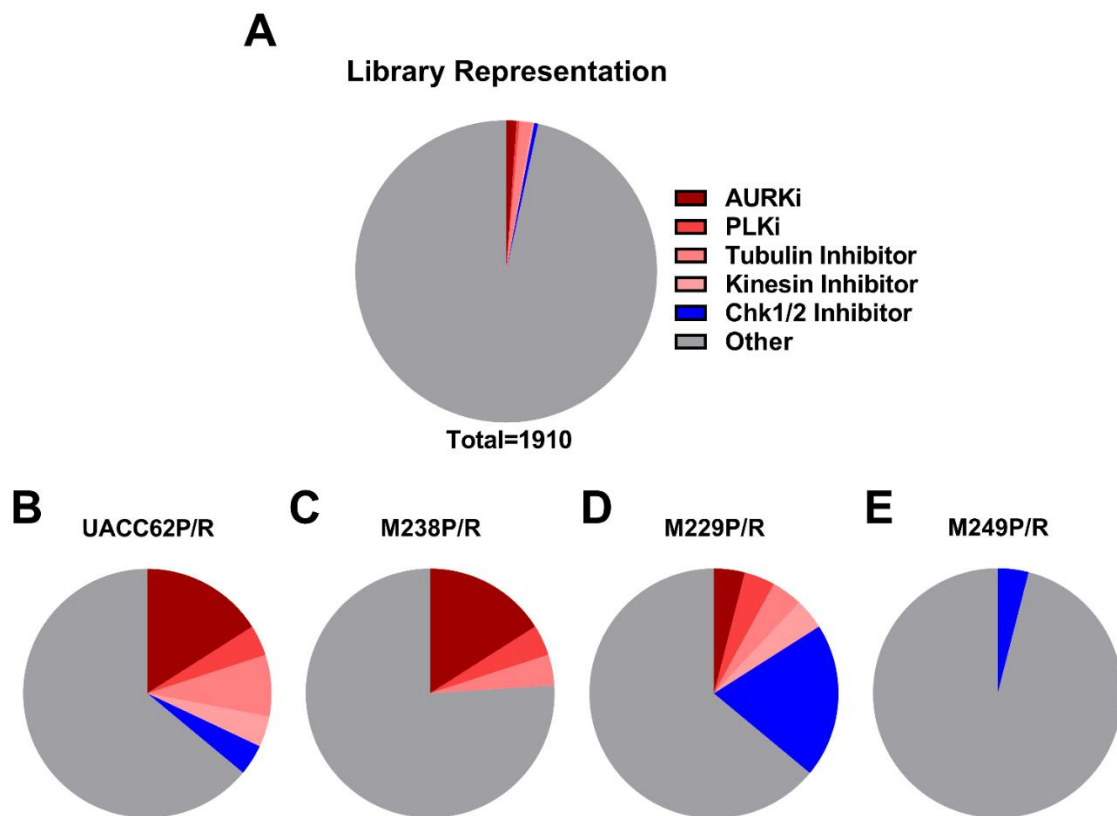


Figure A-4.2: Identification of compound classes which are selective for BRAFi-resistant cells **A.** Overall compound representation in the MIPE library. AURKi, PLKi, Tubulin inhibitors, Kinesin inhibitors, and Chk1/2 inhibitors are highlighted. Compound class enrichment for the top 25 most selective compounds in **B.** UACC62P/R cells, **C.** M238P/R cells, **D.** M229P/R cells, and **E.** M249P/R cells.

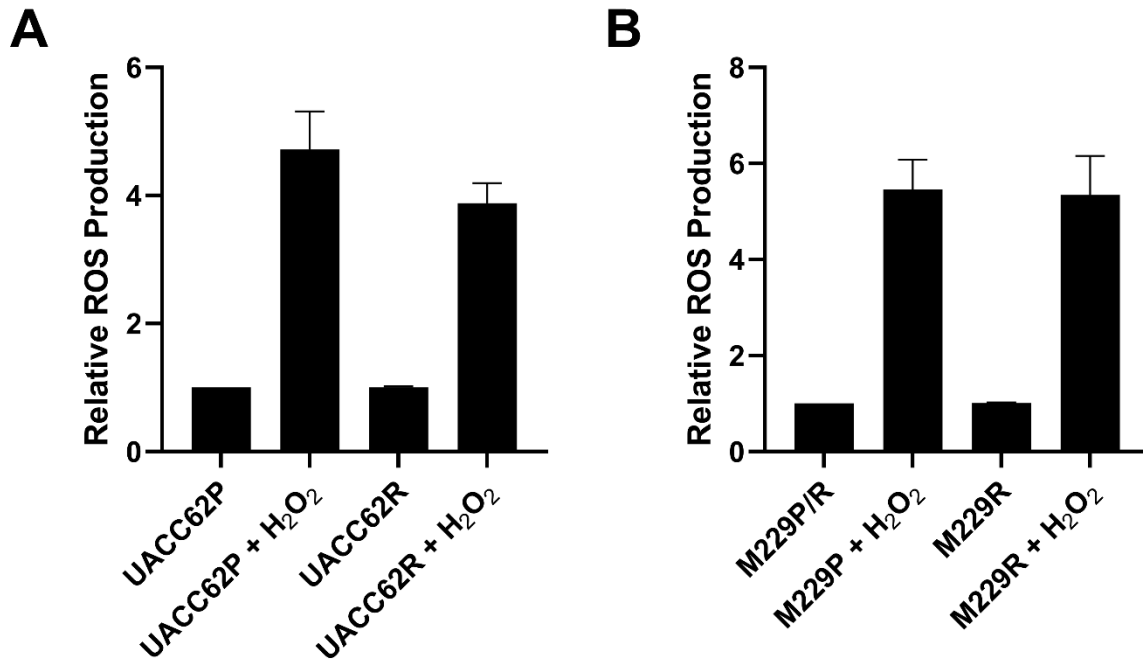


Figure A-4.3: ROS production is not altered in BRAFi-resistant cells A. UACC62P/R and B. M229P/R cells were seeded into 96-well plates. The next day the cells were treated with H₂O₂ and the ROS assay was performed as described in the Materials and Methods section. This experiment was repeated with n = 3 technical replicates and n = 3 biological replicates.

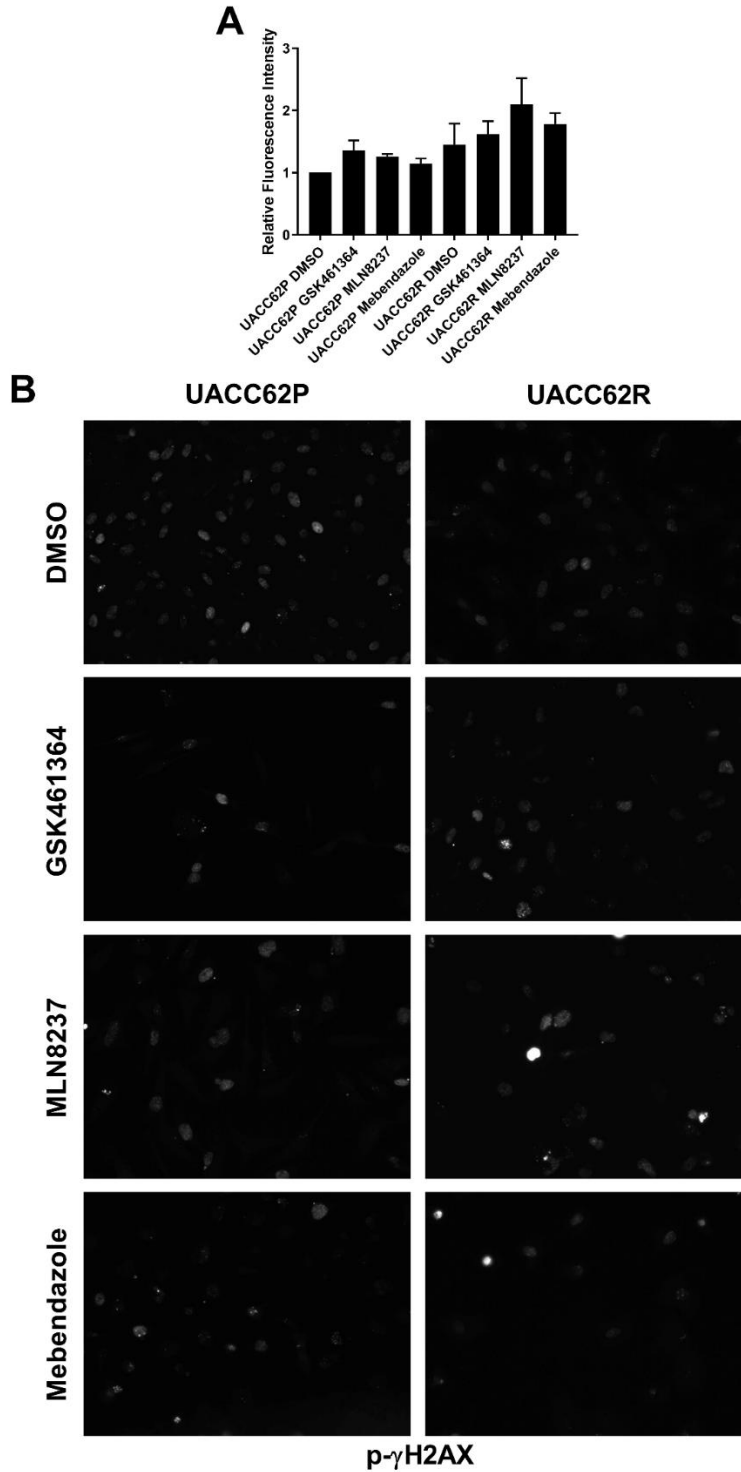


Figure A-4.4: p- γ H2AX staining is not altered in compound-treated UACC62P/R cells **A.** UACC62P/R cells were treated with 1 μ M GSK461364, MLN8237, or Mebendazole for 24 h. The cells were fixed and stained with a p- γ H2AX antibody and quantified as described in materials and methods. **B.** Representative immunofluorescence images. This experiment was repeated with n = 3 biological replicates.

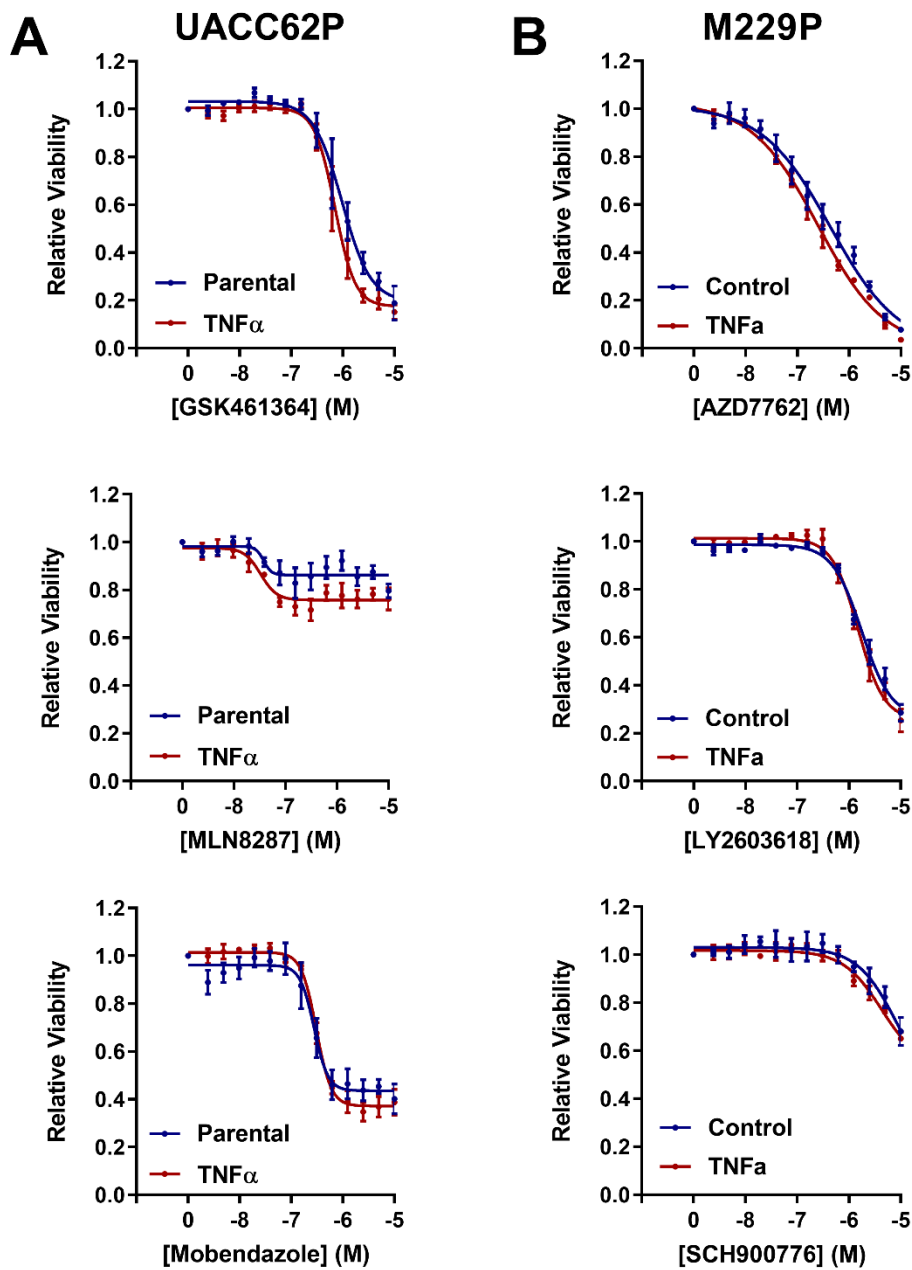


Figure A-4.5: TNF α does not alter AURK, PLK, Tubulin, or Chk1/2 inhibitor sensitivity **A.** UACC62P or **B.** M229P cells were seeded into 384-well plates at a density of 1,000 cells/well. The next day the cells were treated \pm 10 ng/mL TNF α and a concentration gradient of the indicated compound. Viability was measured and quantified as described in the Materials and Methods section. This experiment was repeated with $n = 3$ technical replicates and $n = 3$ biological replicates.

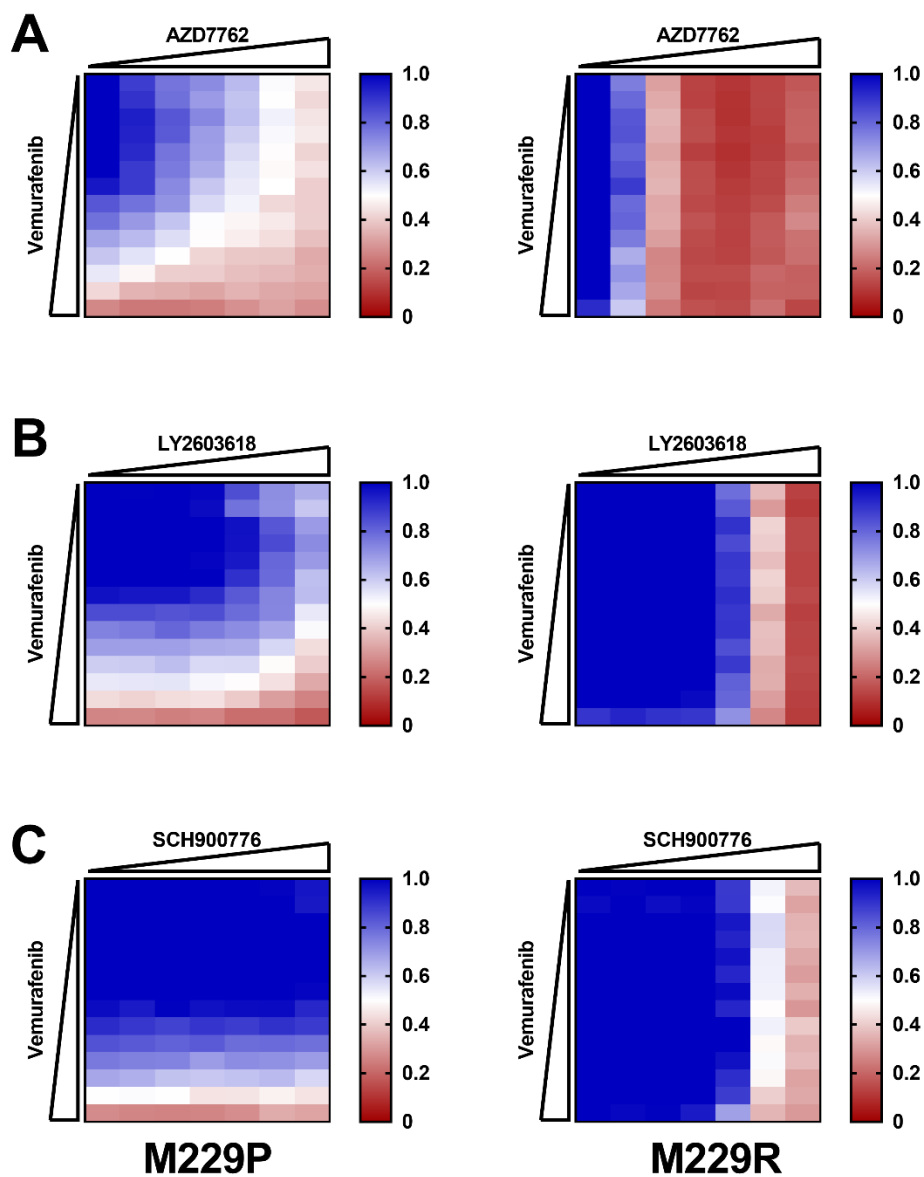


Figure A-4.6: Chk1/2 inhibitors do not synergize with vemurafenib in M229P/R cells M229P/R cells were seeded into 384-well plates at a density of 1,000 cells/well. The next day the cells were treated in a concentration response matrix with a top concentration of 10 μ M for all compounds and a $\frac{1}{2}$ dilution series. Viability was analyzed as described in the Materials and Methods section. Data is expressed as relative viability wherein a value of 1 (blue) indicates 100% viability and a value of 0 (red) indicates 0% viability. **A.** M229P/R cells were treated with AZD7762 x Vemurafenib concentration response matrix. **B.** M229P/R cells were treated with a LY2603618 x Vemurafenib concentration response matrix. **C.** M229P/R cells were treated with a SCH900776 x Vemurafenib concentration response matrix. This experiment was repeated with $n = 3$ biological replicates.

REFERENCES

REFERENCES

- 1 Cancer Genome Atlas, N. Genomic Classification of Cutaneous Melanoma. *Cell* **161**, 1681-1696, doi:10.1016/j.cell.2015.05.044 (2015).
- 2 Hodis, E. *et al.* A landscape of driver mutations in melanoma. *Cell* **150**, 251-263, doi:10.1016/j.cell.2012.06.024 (2012).
- 3 Krauthammer, M. *et al.* Exome sequencing identifies recurrent somatic RAC1 mutations in melanoma. *Nat Genet* **44**, 1006-1014, doi:10.1038/ng.2359 (2012).
- 4 Bevona, C., Goggins, W., Quinn, T., Fullerton, J. & Tsao, H. Cutaneous melanomas associated with nevi. *Arch Dermatol* **139**, 1620-1624; discussion 1624, doi:10.1001/archderm.139.12.1620 (2003).
- 5 Shain, A. H. *et al.* The Genetic Evolution of Melanoma from Precursor Lesions. *N Engl J Med* **373**, 1926-1936, doi:10.1056/NEJMoa1502583 (2015).
- 6 Birkeland, E. *et al.* Patterns of genomic evolution in advanced melanoma. *Nat Commun* **9**, 2665, doi:10.1038/s41467-018-05063-1 (2018).
- 7 Charles M. Balch, A. N. H., Arthur J. Sober, Seng-jaw Soong. *Cutaneous Melanoma, 4th Edition.* (2006).
- 8 Breslow, A. Thickness, cross-sectional areas and depth of invasion in the prognosis of cutaneous melanoma. *Ann Surg* **172**, 902-908, doi:10.1097/00000658-197011000-00017 (1970).
- 9 Cherobin, A., Wainstein, A. J. A., Colosimo, E. A., Goulart, E. M. A. & Bittencourt, F. V. Prognostic factors for metastasis in cutaneous melanoma. *An Bras Dermatol* **93**, 19-26, doi:10.1590/abd1806-4841.20184779 (2018).
- 10 Balch, C. M. *et al.* A multifactorial analysis of melanoma: prognostic histopathological features comparing Clark's and Breslow's staging methods. *Ann Surg* **188**, 732-742, doi:10.1097/00000658-197812000-00004 (1978).
- 11 Clark, W. H., Jr. *et al.* The developmental biology of primary human malignant melanomas. *Semin Oncol* **2**, 83-103 (1975).

- 12 Rabbie, R., Ferguson, P., Molina-Aguilar, C., Adams, D. J. & Robles-Espinoza, C. D. Melanoma subtypes: genomic profiles, prognostic molecular markers and therapeutic possibilities. *J Pathol* **247**, 539-551, doi:10.1002/path.5213 (2019).
- 13 Royer-Bertrand, B. *et al.* Comprehensive Genetic Landscape of Uveal Melanoma by Whole-Genome Sequencing. *Am J Hum Genet* **99**, 1190-1198, doi:10.1016/j.ajhg.2016.09.008 (2016).
- 14 Robertson, A. G. *et al.* Integrative Analysis Identifies Four Molecular and Clinical Subsets in Uveal Melanoma. *Cancer Cell* **32**, 204-220 e215, doi:10.1016/j.ccell.2017.07.003 (2017).
- 15 Yu, F. X. *et al.* Mutant Gq/11 promote uveal melanoma tumorigenesis by activating YAP. *Cancer Cell* **25**, 822-830, doi:10.1016/j.ccr.2014.04.017 (2014).
- 16 Feng, X. *et al.* Hippo-independent activation of YAP by the GNAQ uveal melanoma oncogene through a trio-regulated rho GTPase signaling circuitry. *Cancer Cell* **25**, 831-845, doi:10.1016/j.ccr.2014.04.016 (2014).
- 17 Hayward, N. K. *et al.* Whole-genome landscapes of major melanoma subtypes. *Nature* **545**, 175-180, doi:10.1038/nature22071 (2017).
- 18 Vazquez Vde, L. *et al.* Molecular profiling, including TERT promoter mutations, of acral lentiginous melanomas. *Melanoma Res* **26**, 93-99, doi:10.1097/CMR.0000000000000222 (2016).
- 19 Thomas, N. E. *et al.* Comparison of clinicopathologic features and survival of histopathologically amelanotic and pigmented melanomas: a population-based study. *JAMA Dermatol* **150**, 1306-1314, doi:10.1001/jamadermatol.2014.1348 (2014).
- 20 D'Mello, S. A., Finlay, G. J., Baguley, B. C. & Askarian-Amiri, M. E. Signaling Pathways in Melanogenesis. *Int J Mol Sci* **17**, doi:10.3390/ijms17071144 (2016).
- 21 Law, M. H. *et al.* Genome-wide meta-analysis identifies five new susceptibility loci for cutaneous malignant melanoma. *Nat Genet* **47**, 987-995, doi:10.1038/ng.3373 (2015).
- 22 Cancer Genome Atlas Research Network. Electronic address, a. a. d. h. e. & Cancer Genome Atlas Research, N. Integrated Genomic Characterization of Pancreatic Ductal Adenocarcinoma. *Cancer Cell* **32**, 185-203 e113, doi:10.1016/j.ccell.2017.07.007 (2017).

- 23 Cancer Genome Atlas, N. Comprehensive molecular characterization of human colon and rectal cancer. *Nature* **487**, 330-337, doi:10.1038/nature11252 (2012).
- 24 Cancer Genome Atlas Research, N. Integrated genomic characterization of papillary thyroid carcinoma. *Cell* **159**, 676-690, doi:10.1016/j.cell.2014.09.050 (2014).
- 25 Durham, B. H. *et al.* Genomic analysis of hairy cell leukemia identifies novel recurrent genetic alterations. *Blood* **130**, 1644-1648, doi:10.1182/blood-2017-01-765107 (2017).
- 26 Wellbrock, C. & Arozarena, I. The Complexity of the ERK/MAP-Kinase Pathway and the Treatment of Melanoma Skin Cancer. *Front Cell Dev Biol* **4**, 33, doi:10.3389/fcell.2016.00033 (2016).
- 27 Xu, G. F. *et al.* The catalytic domain of the neurofibromatosis type 1 gene product stimulates ras GTPase and complements ira mutants of *S. cerevisiae*. *Cell* **63**, 835-841, doi:10.1016/0092-8674(90)90149-9 (1990).
- 28 Wan, P. T. *et al.* Mechanism of activation of the RAF-ERK signaling pathway by oncogenic mutations of B-RAF. *Cell* **116**, 855-867, doi:10.1016/s0092-8674(04)00215-6 (2004).
- 29 Tsai, J. *et al.* Discovery of a selective inhibitor of oncogenic B-Raf kinase with potent antimelanoma activity. *Proc Natl Acad Sci U S A* **105**, 3041-3046, doi:10.1073/pnas.0711741105 (2008).
- 30 Bollag, G. *et al.* Clinical efficacy of a RAF inhibitor needs broad target blockade in BRAF-mutant melanoma. *Nature* **467**, 596-599, doi:10.1038/nature09454 (2010).
- 31 Treiber, D. K. & Shah, N. P. Ins and outs of kinase DFG motifs. *Chem Biol* **20**, 745-746, doi:10.1016/j.chembiol.2013.06.001 (2013).
- 32 Devitt, B. *et al.* Clinical outcome and pathological features associated with NRAS mutation in cutaneous melanoma. *Pigment Cell Melanoma Res* **24**, 666-672, doi:10.1111/j.1755-148X.2011.00873.x (2011).
- 33 Smith, M. J., Neel, B. G. & Ikura, M. NMR-based functional profiling of RASopathies and oncogenic RAS mutations. *Proc Natl Acad Sci U S A* **110**, 4574-4579, doi:10.1073/pnas.1218173110 (2013).

- 34 Ershov, F. I., Kadyrova, A. A., Tazulakhova, E. B., Bukata, L. A. & Zhdanov, V. M. [Increase in the antiviral resistance of cells after treating them with messenger RNA for antiviral protein]. *Biull Eksp Biol Med* **86**, 337-339 (1978).
- 35 Arafeh, R. *et al.* Recurrent inactivating RASA2 mutations in melanoma. *Nat Genet* **47**, 1408-1410, doi:10.1038/ng.3427 (2015).
- 36 Rajkumar, S. & Watson, I. R. Molecular characterisation of cutaneous melanoma: creating a framework for targeted and immune therapies. *Br J Cancer* **115**, 145-155, doi:10.1038/bjc.2016.195 (2016).
- 37 Curtin, J. A. *et al.* Distinct sets of genetic alterations in melanoma. *N Engl J Med* **353**, 2135-2147, doi:10.1056/NEJMoa050092 (2005).
- 38 Nazarian, R. *et al.* Melanomas acquire resistance to B-RAF(V600E) inhibition by RTK or N-RAS upregulation. *Nature* **468**, 973-977, doi:10.1038/nature09626 (2010).
- 39 Villanueva, J. *et al.* Acquired resistance to BRAF inhibitors mediated by a RAF kinase switch in melanoma can be overcome by cotargeting MEK and IGF-1R/PI3K. *Cancer Cell* **18**, 683-695, doi:10.1016/j.ccr.2010.11.023 (2010).
- 40 Straussman, R. *et al.* Tumour micro-environment elicits innate resistance to RAF inhibitors through HGF secretion. *Nature* **487**, 500-504, doi:10.1038/nature11183 (2012).
- 41 Watson, I. R. *et al.* The RAC1 P29S hotspot mutation in melanoma confers resistance to pharmacological inhibition of RAF. *Cancer Res* **74**, 4845-4852, doi:10.1158/0008-5472.CAN-14-1232-T (2014).
- 42 Marusiak, A. A. *et al.* Mixed lineage kinases activate MEK independently of RAF to mediate resistance to RAF inhibitors. *Nat Commun* **5**, 3901, doi:10.1038/ncomms4901 (2014).
- 43 Johannessen, C. M. *et al.* COT drives resistance to RAF inhibition through MAP kinase pathway reactivation. *Nature* **468**, 968-972, doi:10.1038/nature09627 (2010).
- 44 Kidger, A. M. & Keyse, S. M. The regulation of oncogenic Ras/ERK signalling by dual-specificity mitogen activated protein kinase phosphatases (MKPs). *Semin Cell Dev Biol* **50**, 125-132, doi:10.1016/j.semcdb.2016.01.009 (2016).

- 45 Zhao, X. *et al.* The Prognostic Significance of Low-Frequency Somatic Mutations in Metastatic Cutaneous Melanoma. *Front Oncol* **8**, 584, doi:10.3389/fonc.2018.00584 (2018).
- 46 Weeraratna, A. T. *et al.* Wnt5a signaling directly affects cell motility and invasion of metastatic melanoma. *Cancer Cell* **1**, 279-288, doi:10.1016/s1535-6108(02)00045-4 (2002).
- 47 Singleton, K. R. *et al.* Melanoma Therapeutic Strategies that Select against Resistance by Exploiting MYC-Driven Evolutionary Convergence. *Cell Rep* **21**, 2796-2812, doi:10.1016/j.celrep.2017.11.022 (2017).
- 48 Golan, T. *et al.* Adipocytes sensitize melanoma cells to environmental TGF-beta cues by repressing the expression of miR-211. *Sci Signal* **12**, doi:10.1126/scisignal.aav6847 (2019).
- 49 Khamari, R. *et al.* Glucose metabolism and NRF2 coordinate the antioxidant response in melanoma resistant to MAPK inhibitors. *Cell Death Dis* **9**, 325, doi:10.1038/s41419-018-0340-4 (2018).
- 50 Irvine, M. *et al.* Oncogenic PI3K/AKT promotes the step-wise evolution of combination BRAF/MEK inhibitor resistance in melanoma. *Oncogenesis* **7**, 72, doi:10.1038/s41389-018-0081-3 (2018).
- 51 Krepler, C. *et al.* Targeting Notch enhances the efficacy of ERK inhibitors in BRAF-V600E melanoma. *Oncotarget* **7**, 71211-71222, doi:10.18632/oncotarget.12078 (2016).
- 52 Sanchez-Vega, F. *et al.* Oncogenic Signaling Pathways in The Cancer Genome Atlas. *Cell* **173**, 321-337 e310, doi:10.1016/j.cell.2018.03.035 (2018).
- 53 Wennerberg, K. & Der, C. J. Rho-family GTPases: it's not only Rac and Rho (and I like it). *J Cell Sci* **117**, 1301-1312, doi:10.1242/jcs.01118 (2004).
- 54 Buhl, A. M., Johnson, N. L., Dhanasekaran, N. & Johnson, G. L. G alpha 12 and G alpha 13 stimulate Rho-dependent stress fiber formation and focal adhesion assembly. *J Biol Chem* **270**, 24631-24634, doi:10.1074/jbc.270.42.24631 (1995).
- 55 Bos, J. L., Rehmann, H. & Wittinghofer, A. GEFs and GAPs: critical elements in the control of small G proteins. *Cell* **129**, 865-877, doi:10.1016/j.cell.2007.05.018 (2007).

- 56 Sanz-Moreno, V. & Marshall, C. J. Rho-GTPase signaling drives melanoma cell plasticity. *Cell Cycle* **8**, 1484-1487, doi:10.4161/cc.8.10.8490 (2009).
- 57 Routhier, A. *et al.* Pharmacological inhibition of Rho-kinase signaling with Y-27632 blocks melanoma tumor growth. *Oncol Rep* **23**, 861-867 (2010).
- 58 Katiyar, P. & Aplin, A. E. FOXD3 regulates migration properties and Rnd3 expression in melanoma cells. *Mol Cancer Res* **9**, 545-552, doi:10.1158/1541-7786.MCR-10-0454 (2011).
- 59 Klein, R. M. & Higgins, P. J. A switch in RND3-RHOA signaling is critical for melanoma cell invasion following mutant-BRAF inhibition. *Mol Cancer* **10**, 114, doi:10.1186/1476-4598-10-114 (2011).
- 60 Feng, C. *et al.* Expression of kindlin-3 in melanoma cells impedes cell migration and metastasis. *Cell Adh Migr* **11**, 419-433, doi:10.1080/19336918.2016.1243645 (2017).
- 61 Diaz-Nunez, M. *et al.* Histone deacetylase inhibitors induce invasion of human melanoma cells in vitro via differential regulation of N-cadherin expression and RhoA activity. *BMC Cancer* **16**, 667, doi:10.1186/s12885-016-2693-3 (2016).
- 62 Liu, H. *et al.* CREPT Promotes Melanoma Progression Through Accelerated Proliferation and Enhanced Migration by RhoA-Mediated Actin Filaments and Focal Adhesion Formation. *Cancers (Basel)* **12**, doi:10.3390/cancers12010033 (2019).
- 63 Medjkane, S., Perez-Sanchez, C., Gaggioli, C., Sahai, E. & Treisman, R. Myocardin-related transcription factors and SRF are required for cytoskeletal dynamics and experimental metastasis. *Nat Cell Biol* **11**, 257-268, doi:10.1038/ncb1833 (2009).
- 64 Kaczorowski, M. *et al.* Low RhoA expression is associated with adverse outcome in melanoma patients: a clinicopathological analysis. *Am J Transl Res* **11**, 4524-4532 (2019).
- 65 Haak, A. J. *et al.* Pharmacological Inhibition of Myocardin-related Transcription Factor Pathway Blocks Lung Metastases of RhoC-Overexpressing Melanoma. *Mol Cancer Ther* **16**, 193-204, doi:10.1158/1535-7163.MCT-16-0482 (2017).
- 66 Tojkander, S., Gateva, G. & Lappalainen, P. Actin stress fibers--assembly, dynamics and biological roles. *J Cell Sci* **125**, 1855-1864, doi:10.1242/jcs.098087 (2012).

- 67 Mouilleron, S., Guettler, S., Langer, C. A., Treisman, R. & McDonald, N. Q. Molecular basis for G-actin binding to RPEL motifs from the serum response factor coactivator MAL. *EMBO J* **27**, 3198-3208, doi:10.1038/emboj.2008.235 (2008).
- 68 Mouilleron, S., Langer, C. A., Guettler, S., McDonald, N. Q. & Treisman, R. Structure of a pentavalent G-actin*MRTF-A complex reveals how G-actin controls nucleocytoplasmic shuttling of a transcriptional coactivator. *Sci Signal* **4**, ra40, doi:10.1126/scisignal.2001750 (2011).
- 69 Esnault, C. *et al.* Rho-actin signaling to the MRTL coactivators dominates the immediate transcriptional response to serum in fibroblasts. *Genes Dev* **28**, 943-958, doi:10.1101/gad.239327.114 (2014).
- 70 Hao, Y., Chun, A., Cheung, K., Rashidi, B. & Yang, X. Tumor suppressor LATS1 is a negative regulator of oncogene YAP. *J Biol Chem* **283**, 5496-5509, doi:10.1074/jbc.M709037200 (2008).
- 71 Morita, T. & Hayashi, K. Tumor Progression Is Mediated by Thymosin-beta4 through a TGFbeta/MRTL Signaling Axis. *Mol Cancer Res* **16**, 880-893, doi:10.1158/1541-7786.MCR-17-0715 (2018).
- 72 Peippo, M. *et al.* FHOD1 formin is upregulated in melanomas and modifies proliferation and tumor growth. *Exp Cell Res* **350**, 267-278, doi:10.1016/j.yexcr.2016.12.004 (2017).
- 73 Kishi, T., Mayanagi, T., Iwabuchi, S., Akasaka, T. & Sobue, K. Myocardin-related transcription factor A (MRTL-A) activity-dependent cell adhesion is correlated to focal adhesion kinase (FAK) activity. *Oncotarget* **7**, 72113-72130, doi:10.18632/oncotarget.12350 (2016).
- 74 Lamar, J. M. *et al.* SRC tyrosine kinase activates the YAP/TAZ axis and thereby drives tumor growth and metastasis. *J Biol Chem* **294**, 2302-2317, doi:10.1074/jbc.RA118.004364 (2019).
- 75 Nallet-Staub, F. *et al.* Pro-invasive activity of the Hippo pathway effectors YAP and TAZ in cutaneous melanoma. *J Invest Dermatol* **134**, 123-132, doi:10.1038/jid.2013.319 (2014).
- 76 Horn, S. *et al.* TERT promoter mutations in familial and sporadic melanoma. *Science* **339**, 959-961, doi:10.1126/science.1230062 (2013).

- 77 Huang, F. W. *et al.* Highly recurrent TERT promoter mutations in human melanoma. *Science* **339**, 957-959, doi:10.1126/science.1229259 (2013).
- 78 Chiba, K. *et al.* Mutations in the promoter of the telomerase gene TERT contribute to tumorigenesis by a two-step mechanism. *Science* **357**, 1416-1420, doi:10.1126/science.aao0535 (2017).
- 79 Nagore, E. *et al.* TERT promoter mutations in melanoma survival. *Int J Cancer* **139**, 75-84, doi:10.1002/ijc.30042 (2016).
- 80 Halaban, R. *et al.* PLX4032, a selective BRAF(V600E) kinase inhibitor, activates the ERK pathway and enhances cell migration and proliferation of BRAF melanoma cells. *Pigment Cell Melanoma Res* **23**, 190-200, doi:10.1111/j.1755-148X.2010.00685.x (2010).
- 81 Sondergaard, J. N. *et al.* Differential sensitivity of melanoma cell lines with BRAFV600E mutation to the specific Raf inhibitor PLX4032. *J Transl Med* **8**, 39, doi:10.1186/1479-5876-8-39 (2010).
- 82 Yang, H. *et al.* RG7204 (PLX4032), a selective BRAFV600E inhibitor, displays potent antitumor activity in preclinical melanoma models. *Cancer Res* **70**, 5518-5527, doi:10.1158/0008-5472.CAN-10-0646 (2010).
- 83 Joseph, E. W. *et al.* The RAF inhibitor PLX4032 inhibits ERK signaling and tumor cell proliferation in a V600E BRAF-selective manner. *Proc Natl Acad Sci U S A* **107**, 14903-14908, doi:10.1073/pnas.1008990107 (2010).
- 84 Chapman, P. B. *et al.* Improved survival with vemurafenib in melanoma with BRAF V600E mutation. *N Engl J Med* **364**, 2507-2516, doi:10.1056/NEJMoa1103782 (2011).
- 85 Hauschild, A. *et al.* Dabrafenib in BRAF-mutated metastatic melanoma: a multicentre, open-label, phase 3 randomised controlled trial. *Lancet* **380**, 358-365, doi:10.1016/S0140-6736(12)60868-X (2012).
- 86 Robert, C. *et al.* Five-Year Outcomes with Dabrafenib plus Trametinib in Metastatic Melanoma. *N Engl J Med* **381**, 626-636, doi:10.1056/NEJMoa1904059 (2019).
- 87 Larkin, J. *et al.* Combined vemurafenib and cobimetinib in BRAF-mutated melanoma. *N Engl J Med* **371**, 1867-1876, doi:10.1056/NEJMoa1408868 (2014).

- 88 Dummer, R. *et al.* Encorafenib plus binimetinib versus vemurafenib or encorafenib in patients with BRAF-mutant melanoma (COLUMBUS): a multicentre, open-label, randomised phase 3 trial. *Lancet Oncol* **19**, 603-615, doi:10.1016/S1470-2045(18)30142-6 (2018).
- 89 Ackerman, A. *et al.* Outcomes of patients with metastatic melanoma treated with immunotherapy prior to or after BRAF inhibitors. *Cancer* **120**, 1695-1701, doi:10.1002/cncr.28620 (2014).
- 90 Petrella, T. *et al.* Single-agent interleukin-2 in the treatment of metastatic melanoma. *Curr Oncol* **14**, 21-26, doi:10.3747/co.2007.97 (2007).
- 91 Kirkwood, J. M. *et al.* Interferon alfa-2b adjuvant therapy of high-risk resected cutaneous melanoma: the Eastern Cooperative Oncology Group Trial EST 1684. *J Clin Oncol* **14**, 7-17, doi:10.1200/JCO.1996.14.1.7 (1996).
- 92 Eggermont, A. M. *et al.* Long-term results of the randomized phase III trial EORTC 18991 of adjuvant therapy with pegylated interferon alfa-2b versus observation in resected stage III melanoma. *J Clin Oncol* **30**, 3810-3818, doi:10.1200/JCO.2011.41.3799 (2012).
- 93 Schadendorf, D. *et al.* Pooled Analysis of Long-Term Survival Data From Phase II and Phase III Trials of Ipilimumab in Unresectable or Metastatic Melanoma. *J Clin Oncol* **33**, 1889-1894, doi:10.1200/JCO.2014.56.2736 (2015).
- 94 Chen, L. *et al.* Costimulation of antitumor immunity by the B7 counterreceptor for the T lymphocyte molecules CD28 and CTLA-4. *Cell* **71**, 1093-1102, doi:10.1016/s0092-8674(05)80059-5 (1992).
- 95 Larkin, J. *et al.* Combined Nivolumab and Ipilimumab or Monotherapy in Untreated Melanoma. *N Engl J Med* **373**, 23-34, doi:10.1056/NEJMoa1504030 (2015).
- 96 Schachter, J. *et al.* Pembrolizumab versus ipilimumab for advanced melanoma: final overall survival results of a multicentre, randomised, open-label phase 3 study (KEYNOTE-006). *Lancet* **390**, 1853-1862, doi:10.1016/S0140-6736(17)31601-X (2017).
- 97 Larkin, J. *et al.* Five-Year Survival with Combined Nivolumab and Ipilimumab in Advanced Melanoma. *N Engl J Med* **381**, 1535-1546, doi:10.1056/NEJMoa1910836 (2019).

- 98 Schadendorf, D. *et al.* Efficacy and Safety Outcomes in Patients With Advanced Melanoma Who Discontinued Treatment With Nivolumab and Ipilimumab Because of Adverse Events: A Pooled Analysis of Randomized Phase II and III Trials. *J Clin Oncol* **35**, 3807-3814, doi:10.1200/JCO.2017.73.2289 (2017).
- 99 Shoushtari, A. N. *et al.* Measuring Toxic Effects and Time to Treatment Failure for Nivolumab Plus Ipilimumab in Melanoma. *JAMA Oncol* **4**, 98-101, doi:10.1001/jamaoncol.2017.2391 (2018).
- 100 Keenan, T. E., Burke, K. P. & Van Allen, E. M. Genomic correlates of response to immune checkpoint blockade. *Nat Med* **25**, 389-402, doi:10.1038/s41591-019-0382-x (2019).
- 101 Sucker, A. *et al.* Acquired IFN γ resistance impairs anti-tumor immunity and gives rise to T-cell-resistant melanoma lesions. *Nat Commun* **8**, 15440, doi:10.1038/ncomms15440 (2017).
- 102 Green, M. R. *et al.* Integrative analysis reveals selective 9p24.1 amplification, increased PD-1 ligand expression, and further induction via JAK2 in nodular sclerosing Hodgkin lymphoma and primary mediastinal large B-cell lymphoma. *Blood* **116**, 3268-3277, doi:10.1182/blood-2010-05-282780 (2010).
- 103 Zhang, J. *et al.* Cyclin D-CDK4 kinase destabilizes PD-L1 via cullin 3-SPOP to control cancer immune surveillance. *Nature* **553**, 91-95, doi:10.1038/nature25015 (2018).
- 104 Teo, M. Y. *et al.* Alterations in DNA Damage Response and Repair Genes as Potential Marker of Clinical Benefit From PD-1/PD-L1 Blockade in Advanced Urothelial Cancers. *J Clin Oncol* **36**, 1685-1694, doi:10.1200/JCO.2017.75.7740 (2018).
- 105 Forget, M.-A. *et al.* The impact of checkpoint blockade prior to adoptive cell therapy using tumor-infiltrating lymphocytes for metastatic melanoma: An update from MD Anderson Cancer Center. *Journal of Clinical Oncology* **35**, 138-138, doi:10.1200/JCO.2017.35.7_suppl.138 (2017).
- 106 Homet Moreno, B., Mok, S., Comin-Anduix, B., Hu-Lieskovan, S. & Ribas, A. Combined treatment with dabrafenib and trametinib with immune-stimulating antibodies for BRAF mutant melanoma. *Oncoimmunology* **5**, e1052212, doi:10.1080/2162402X.2015.1052212 (2016).

- 107 Deken, M. A. *et al.* Targeting the MAPK and PI3K pathways in combination with PD1 blockade in melanoma. *Oncoimmunology* **5**, e1238557, doi:10.1080/2162402X.2016.1238557 (2016).
- 108 Hu-Lieskovan, S. *et al.* Improved antitumor activity of immunotherapy with BRAF and MEK inhibitors in BRAF(V600E) melanoma. *Sci Transl Med* **7**, 279ra241, doi:10.1126/scitranslmed.aaa4691 (2015).
- 109 Ribas, A. *et al.* Combined BRAF and MEK inhibition with PD-1 blockade immunotherapy in BRAF-mutant melanoma. *Nat Med* **25**, 936-940, doi:10.1038/s41591-019-0476-5 (2019).
- 110 Yang, W. *et al.* Genomics of Drug Sensitivity in Cancer (GDSC): a resource for therapeutic biomarker discovery in cancer cells. *Nucleic Acids Res* **41**, D955-961, doi:10.1093/nar/gks1111 (2013).
- 111 Basu, A. *et al.* An interactive resource to identify cancer genetic and lineage dependencies targeted by small molecules. *Cell* **154**, 1151-1161, doi:10.1016/j.cell.2013.08.003 (2013).
- 112 Corsello, S. M. *et al.* Discovering the anticancer potential of non-oncology drugs by systematic viability profiling. *Nature Cancer* **1**, 235-248, doi:10.1038/s43018-019-0018-6 (2020).
- 113 Yu, C. *et al.* High-throughput identification of genotype-specific cancer vulnerabilities in mixtures of barcoded tumor cell lines. *Nat Biotechnol* **34**, 419-423, doi:10.1038/nbt.3460 (2016).
- 114 Konieczkowski, D. J. *et al.* A melanoma cell state distinction influences sensitivity to MAPK pathway inhibitors. *Cancer Discov* **4**, 816-827, doi:10.1158/2159-8290.CD-13-0424 (2014).
- 115 Luebker, S. A. & Koepsell, S. A. Diverse Mechanisms of BRAF Inhibitor Resistance in Melanoma Identified in Clinical and Preclinical Studies. *Front Oncol* **9**, 268, doi:10.3389/fonc.2019.00268 (2019).
- 116 Ben-David, U. *et al.* Genetic and transcriptional evolution alters cancer cell line drug response. *Nature* **560**, 325-330, doi:10.1038/s41586-018-0409-3 (2018).

- 117 Shalem, O. *et al.* Genome-scale CRISPR-Cas9 knockout screening in human cells. *Science* **343**, 84-87, doi:10.1126/science.1247005 (2014).
- 118 Li, Z. *et al.* CRISPR Screens Identify Essential Cell Growth Mediators in BRAF-inhibitor Resistant Melanoma. *bioRxiv*, 2019.2012.2016.876631, doi:10.1101/2019.12.16.876631 (2019).
- 119 Sanjana, N. E. *et al.* High-resolution interrogation of functional elements in the noncoding genome. *Science* **353**, 1545-1549, doi:10.1126/science.aaf7613 (2016).
- 120 Brenan, L. *et al.* Phenotypic Characterization of a Comprehensive Set of MAPK1/ERK2 Missense Mutants. *Cell Rep* **17**, 1171-1183, doi:10.1016/j.celrep.2016.09.061 (2016).
- 121 Giacomelli, A. O. *et al.* Mutational processes shape the landscape of TP53 mutations in human cancer. *Nat Genet* **50**, 1381-1387, doi:10.1038/s41588-018-0204-y (2018).
- 122 Wagle, N. *et al.* Dissecting therapeutic resistance to RAF inhibition in melanoma by tumor genomic profiling. *J Clin Oncol* **29**, 3085-3096, doi:10.1200/JCO.2010.33.2312 (2011).
- 123 Brighton, H. E. *et al.* New Mechanisms of Resistance to MEK Inhibitors in Melanoma Revealed by Intravital Imaging. *Cancer Res* **78**, 542-557, doi:10.1158/0008-5472.CAN-17-1653 (2018).
- 124 Long, J. E. *et al.* Therapeutic resistance and susceptibility is shaped by cooperative multi-compartment tumor adaptation. *Cell Death Differ* **26**, 2416-2429, doi:10.1038/s41418-019-0310-0 (2019).
- 125 Kwong, L. N. *et al.* Co-clinical assessment identifies patterns of BRAF inhibitor resistance in melanoma. *J Clin Invest* **125**, 1459-1470, doi:10.1172/JCI78954 (2015).
- 126 Krepler, C. *et al.* A Comprehensive Patient-Derived Xenograft Collection Representing the Heterogeneity of Melanoma. *Cell Rep* **21**, 1953-1967, doi:10.1016/j.celrep.2017.10.021 (2017).
- 127 Rambow, F. *et al.* Toward Minimal Residual Disease-Directed Therapy in Melanoma. *Cell* **174**, 843-855 e819, doi:10.1016/j.cell.2018.06.025 (2018).

- 128 Van Allen, E. M. *et al.* The genetic landscape of clinical resistance to RAF inhibition in metastatic melanoma. *Cancer Discov* **4**, 94-109, doi:10.1158/2159-8290.CD-13-0617 (2014).
- 129 Wagle, N. *et al.* MAP kinase pathway alterations in BRAF-mutant melanoma patients with acquired resistance to combined RAF/MEK inhibition. *Cancer Discov* **4**, 61-68, doi:10.1158/2159-8290.CD-13-0631 (2014).
- 130 Shi, H. *et al.* Melanoma whole-exome sequencing identifies (V600E)B-RAF amplification-mediated acquired B-RAF inhibitor resistance. *Nat Commun* **3**, 724, doi:10.1038/ncomms1727 (2012).
- 131 Hugo, W. *et al.* Non-genomic and Immune Evolution of Melanoma Acquiring MAPKi Resistance. *Cell* **162**, 1271-1285, doi:10.1016/j.cell.2015.07.061 (2015).
- 132 Tirosh, I. *et al.* Dissecting the multicellular ecosystem of metastatic melanoma by single-cell RNA-seq. *Science* **352**, 189-196, doi:10.1126/science.aad0501 (2016).
- 133 Fattore, L., Ruggiero, C. F., Liguoro, D., Mancini, R. & Ciliberto, G. Single cell analysis to dissect molecular heterogeneity and disease evolution in metastatic melanoma. *Cell Death Dis* **10**, 827, doi:10.1038/s41419-019-2048-5 (2019).
- 134 Ho, Y. J. *et al.* Single-cell RNA-seq analysis identifies markers of resistance to targeted BRAF inhibitors in melanoma cell populations. *Genome Res* **28**, 1353-1363, doi:10.1101/gr.234062.117 (2018).
- 135 Johnson, D. B. *et al.* Acquired BRAF inhibitor resistance: A multicenter meta-analysis of the spectrum and frequencies, clinical behaviour, and phenotypic associations of resistance mechanisms. *Eur J Cancer* **51**, 2792-2799, doi:10.1016/j.ejca.2015.08.022 (2015).
- 136 Wilson, T. R. *et al.* Widespread potential for growth-factor-driven resistance to anticancer kinase inhibitors. *Nature* **487**, 505-509, doi:10.1038/nature11249 (2012).
- 137 Yadav, V. *et al.* Reactivation of mitogen-activated protein kinase (MAPK) pathway by FGF receptor 3 (FGFR3)/Ras mediates resistance to vemurafenib in human B-RAF V600E mutant melanoma. *J Biol Chem* **287**, 28087-28098, doi:10.1074/jbc.M112.377218 (2012).
- 138 Atzori, M. G. *et al.* Role of VEGFR-1 in melanoma acquired resistance to the BRAF inhibitor vemurafenib. *J Cell Mol Med* **24**, 465-475, doi:10.1111/jcmm.14755 (2020).

- 139 Ji, Z. *et al.* MITF Modulates Therapeutic Resistance through EGFR Signaling. *J Invest Dermatol* **135**, 1863-1872, doi:10.1038/jid.2015.105 (2015).
- 140 Wang, J. *et al.* Epigenetic changes of EGFR have an important role in BRAF inhibitor-resistant cutaneous melanomas. *J Invest Dermatol* **135**, 532-541, doi:10.1038/jid.2014.418 (2015).
- 141 Shaffer, S. M. *et al.* Rare cell variability and drug-induced reprogramming as a mode of cancer drug resistance. *Nature* **546**, 431-435, doi:10.1038/nature22794 (2017).
- 142 Sun, C. *et al.* Reversible and adaptive resistance to BRAF(V600E) inhibition in melanoma. *Nature* **508**, 118-122, doi:10.1038/nature13121 (2014).
- 143 Pao, W. *et al.* Acquired resistance of lung adenocarcinomas to gefitinib or erlotinib is associated with a second mutation in the EGFR kinase domain. *PLoS Med* **2**, e73, doi:10.1371/journal.pmed.0020073 (2005).
- 144 Kwak, E. L. *et al.* Irreversible inhibitors of the EGF receptor may circumvent acquired resistance to gefitinib. *Proc Natl Acad Sci U S A* **102**, 7665-7670, doi:10.1073/pnas.0502860102 (2005).
- 145 Thress, K. S. *et al.* Acquired EGFR C797S mutation mediates resistance to AZD9291 in non-small cell lung cancer harboring EGFR T790M. *Nat Med* **21**, 560-562, doi:10.1038/nm.3854 (2015).
- 146 Haarberg, H. E. & Smalley, K. S. Resistance to Raf inhibition in cancer. *Drug Discov Today Technol* **11**, 27-32, doi:10.1016/j.ddtec.2013.12.004 (2014).
- 147 Trunzer, K. *et al.* Pharmacodynamic effects and mechanisms of resistance to vemurafenib in patients with metastatic melanoma. *J Clin Oncol* **31**, 1767-1774, doi:10.1200/JCO.2012.44.7888 (2013).
- 148 Heidorn, S. J. *et al.* Kinase-dead BRAF and oncogenic RAS cooperate to drive tumor progression through CRAF. *Cell* **140**, 209-221, doi:10.1016/j.cell.2009.12.040 (2010).
- 149 Kaplan, F. M. *et al.* SHOC2 and CRAF mediate ERK1/2 reactivation in mutant NRAS-mediated resistance to RAF inhibitor. *J Biol Chem* **287**, 41797-41807, doi:10.1074/jbc.M112.390906 (2012).

- 150 Poulidakos, P. I. *et al.* RAF inhibitor resistance is mediated by dimerization of aberrantly spliced BRAF(V600E). *Nature* **480**, 387-390, doi:10.1038/nature10662 (2011).
- 151 Lionarons, D. A. *et al.* RAC1(P29S) Induces a Mesenchymal Phenotypic Switch via Serum Response Factor to Promote Melanoma Development and Therapy Resistance. *Cancer Cell* **36**, 68-83 e69, doi:10.1016/j.ccell.2019.05.015 (2019).
- 152 Muller, J. *et al.* Low MITF/AXL ratio predicts early resistance to multiple targeted drugs in melanoma. *Nat Commun* **5**, 5712, doi:10.1038/ncomms6712 (2014).
- 153 Fallahi-Sichani, M. *et al.* Adaptive resistance of melanoma cells to RAF inhibition via reversible induction of a slowly dividing de-differentiated state. *Mol Syst Biol* **13**, 905, doi:10.15252/msb.20166796 (2017).
- 154 Somasundaram, R. *et al.* Tumor-associated B-cells induce tumor heterogeneity and therapy resistance. *Nat Commun* **8**, 607, doi:10.1038/s41467-017-00452-4 (2017).
- 155 Wang, T. *et al.* BRAF Inhibition Stimulates Melanoma-Associated Macrophages to Drive Tumor Growth. *Clin Cancer Res* **21**, 1652-1664, doi:10.1158/1078-0432.CCR-14-1554 (2015).
- 156 Steinberg, S. M. *et al.* Myeloid Cells That Impair Immunotherapy Are Restored in Melanomas with Acquired Resistance to BRAF Inhibitors. *Cancer Res* **77**, 1599-1610, doi:10.1158/0008-5472.CAN-16-1755 (2017).
- 157 Erkes, D. A. *et al.* Mutant BRAF and MEK Inhibitors Regulate the Tumor Immune Microenvironment via Pyroptosis. *Cancer Discov* **10**, 254-269, doi:10.1158/2159-8290.CD-19-0672 (2020).
- 158 Hirata, E. *et al.* Intravital imaging reveals how BRAF inhibition generates drug-tolerant microenvironments with high integrin beta1/FAK signaling. *Cancer Cell* **27**, 574-588, doi:10.1016/j.ccell.2015.03.008 (2015).
- 159 Delmas, A. *et al.* The c-Jun/RHOB/AKT pathway confers resistance of BRAF-mutant melanoma cells to MAPK inhibitors. *Oncotarget* **6**, 15250-15264, doi:10.18632/oncotarget.3888 (2015).
- 160 Smit, M. A. *et al.* ROCK1 is a potential combinatorial drug target for BRAF mutant melanoma. *Mol Syst Biol* **10**, 772, doi:10.15252/msb.20145450 (2014).

- 161 Vogel, C. J. *et al.* Cooperative induction of apoptosis in NRAS mutant melanoma by inhibition of MEK and ROCK. *Pigment Cell Melanoma Res* **28**, 307-317, doi:10.1111/pcmr.12364 (2015).
- 162 Orgaz, J. L. *et al.* Myosin II Reactivation and Cytoskeletal Remodeling as a Hallmark and a Vulnerability in Melanoma Therapy Resistance. *Cancer Cell* **37**, 85-103 e109, doi:10.1016/j.ccell.2019.12.003 (2020).
- 163 Kim, M. H. *et al.* Actin remodeling confers BRAF inhibitor resistance to melanoma cells through YAP/TAZ activation. *EMBO J* **35**, 462-478, doi:10.15252/embj.201592081 (2016).
- 164 Fisher, M. L., Grun, D., Adhikary, G., Xu, W. & Eckert, R. L. Inhibition of YAP function overcomes BRAF inhibitor resistance in melanoma cancer stem cells. *Oncotarget* **8**, 110257-110272, doi:10.18632/oncotarget.22628 (2017).
- 165 Lin, L. *et al.* The Hippo effector YAP promotes resistance to RAF- and MEK-targeted cancer therapies. *Nat Genet* **47**, 250-256, doi:10.1038/ng.3218 (2015).
- 166 Girard, C. A. *et al.* A feed-forward mechanosignaling loop confers resistance to therapies targeting the MAPK pathway in BRAF-mutant melanoma. *Cancer Res*, doi:10.1158/0008-5472.CAN-19-2914 (2020).
- 167 Shi, H. *et al.* Acquired resistance and clonal evolution in melanoma during BRAF inhibitor therapy. *Cancer Discov* **4**, 80-93, doi:10.1158/2159-8290.CD-13-0642 (2014).
- 168 Emery, C. M. *et al.* MEK1 mutations confer resistance to MEK and B-RAF inhibition. *Proc Natl Acad Sci U S A* **106**, 20411-20416, doi:10.1073/pnas.0905833106 (2009).
- 169 Whittaker, S. R. *et al.* A genome-scale RNA interference screen implicates NF1 loss in resistance to RAF inhibition. *Cancer Discov* **3**, 350-362, doi:10.1158/2159-8290.CD-12-0470 (2013).
- 170 Saei, A. *et al.* Loss of USP28-mediated BRAF degradation drives resistance to RAF cancer therapies. *J Exp Med* **215**, 1913-1928, doi:10.1084/jem.20171960 (2018).
- 171 Shen, C. H. *et al.* Loss of cohesin complex components STAG2 or STAG3 confers resistance to BRAF inhibition in melanoma. *Nat Med* **22**, 1056-1061, doi:10.1038/nm.4155 (2016).

- 172 Abel, E. V. *et al.* Melanoma adapts to RAF/MEK inhibitors through FOXD3-mediated upregulation of ERBB3. *J Clin Invest* **123**, 2155-2168, doi:10.1172/JCI65780 (2013).
- 173 Robert, C. *et al.* Improved overall survival in melanoma with combined dabrafenib and trametinib. *N Engl J Med* **372**, 30-39, doi:10.1056/NEJMoa1412690 (2015).
- 174 Song, C. *et al.* Recurrent Tumor Cell-Intrinsic and -Extrinsic Alterations during MAPKi-Induced Melanoma Regression and Early Adaptation. *Cancer Discov* **7**, 1248-1265, doi:10.1158/2159-8290.CD-17-0401 (2017).
- 175 Das Thakur, M. *et al.* Modelling vemurafenib resistance in melanoma reveals a strategy to forestall drug resistance. *Nature* **494**, 251-255, doi:10.1038/nature11814 (2013).
- 176 Hong, A. *et al.* Exploiting Drug Addiction Mechanisms to Select against MAPKi-Resistant Melanoma. *Cancer Discov* **8**, 74-93, doi:10.1158/2159-8290.CD-17-0682 (2018).
- 177 Moriceau, G. *et al.* Tunable-combinatorial mechanisms of acquired resistance limit the efficacy of BRAF/MEK cotargeting but result in melanoma drug addiction. *Cancer Cell* **27**, 240-256, doi:10.1016/j.ccell.2014.11.018 (2015).
- 178 Vega, F. M., Fruhwirth, G., Ng, T. & Ridley, A. J. RhoA and RhoC have distinct roles in migration and invasion by acting through different targets. *J Cell Biol* **193**, 655-665, doi:10.1083/jcb.201011038 (2011).
- 179 Clark, E. A., Golub, T. R., Lander, E. S. & Hynes, R. O. Genomic analysis of metastasis reveals an essential role for RhoC. *Nature* **406**, 532-535, doi:10.1038/35020106 (2000).
- 180 Ruth, M. C. *et al.* RhoC promotes human melanoma invasion in a PI3K/Akt-dependent pathway. *J Invest Dermatol* **126**, 862-868, doi:10.1038/sj.jid.5700211 (2006).
- 181 Sit, S. T. & Manser, E. Rho GTPases and their role in organizing the actin cytoskeleton. *J Cell Sci* **124**, 679-683, doi:10.1242/jcs.064964 (2011).
- 182 Spiering, D. & Hodgson, L. Dynamics of the Rho-family small GTPases in actin regulation and motility. *Cell Adh Migr* **5**, 170-180 (2011).
- 183 Hodge, R. G. & Ridley, A. J. Regulating Rho GTPases and their regulators. *Nat Rev Mol Cell Biol* **17**, 496-510, doi:10.1038/nrm.2016.67 (2016).

- 184 Bell, J. L. *et al.* Optimization of novel nipecotic bis(amide) inhibitors of the Rho/MKL1/SRF transcriptional pathway as potential anti-metastasis agents. *Bioorg Med Chem Lett* **23**, 3826-3832, doi:10.1016/j.bmcl.2013.04.080 (2013).
- 185 Haak, A. J. *et al.* Pharmacological inhibition of Myocardin-related transcription factor pathway blocks lung metastases of RhoC overexpressing melanoma. *Mol Cancer Ther*, doi:10.1158/1535-7163.MCT-16-0482 (2016).
- 186 Hutchings, K. M. *et al.* Pharmacokinetic optimization of CCG-203971: Novel inhibitors of the Rho/MRTF/SRF transcriptional pathway as potential antifibrotic therapeutics for systemic scleroderma. *Bioorg Med Chem Lett* **27**, 1744-1749, doi:10.1016/j.bmcl.2017.02.070 (2017).
- 187 Tsoi, J. *et al.* Multi-stage Differentiation Defines Melanoma Subtypes with Differential Vulnerability to Drug-Induced Iron-Dependent Oxidative Stress. *Cancer Cell* **33**, 890-904 e895, doi:10.1016/j.ccell.2018.03.017 (2018).
- 188 Pan, M. *et al.* Regional glutamine deficiency in tumours promotes dedifferentiation through inhibition of histone demethylation. *Nat Cell Biol* **18**, 1090-1101, doi:10.1038/ncb3410 (2016).
- 189 van Dijk, D. *et al.* Recovering Gene Interactions from Single-Cell Data Using Data Diffusion. *Cell* **174**, 716-729 e727, doi:10.1016/j.cell.2018.05.061 (2018).
- 190 Barretina, J. *et al.* The Cancer Cell Line Encyclopedia enables predictive modelling of anticancer drug sensitivity. *Nature* **483**, 603-607, doi:10.1038/nature11003 (2012).
- 191 Shakhova, O. *et al.* Antagonistic cross-regulation between Sox9 and Sox10 controls an anti-tumorigenic program in melanoma. *PLoS Genet* **11**, e1004877, doi:10.1371/journal.pgen.1004877 (2015).
- 192 Fujisawa, K., Fujita, A., Ishizaki, T., Saito, Y. & Narumiya, S. Identification of the Rho-binding domain of p160ROCK, a Rho-associated coiled-coil containing protein kinase. *J Biol Chem* **271**, 23022-23028 (1996).
- 193 Nakagawa, O. *et al.* ROCK-I and ROCK-II, two isoforms of Rho-associated coiled-coil forming protein serine/threonine kinase in mice. *FEBS Lett* **392**, 189-193 (1996).

- 194 Nobes, C. D. & Hall, A. Rho GTPases control polarity, protrusion, and adhesion during cell movement. *J Cell Biol* **144**, 1235-1244 (1999).
- 195 Yin, L. *et al.* Fasudil inhibits vascular endothelial growth factor-induced angiogenesis in vitro and in vivo. *Mol Cancer Ther* **6**, 1517-1525, doi:10.1158/1535-7163.MCT-06-0689 (2007).
- 196 Yu, O. M. *et al.* YAP and MRTF-A, transcriptional co-activators of RhoA-mediated gene expression, are critical for glioblastoma tumorigenicity. *Oncogene*, doi:10.1038/s41388-018-0301-5 (2018).
- 197 Foster, C. T., Gualdrini, F. & Treisman, R. Mutual dependence of the MRTF-SRF and YAP-TEAD pathways in cancer-associated fibroblasts is indirect and mediated by cytoskeletal dynamics. *Genes Dev* **31**, 2361-2375, doi:10.1101/gad.304501.117 (2017).
- 198 Rosenbluh, J. *et al.* beta-Catenin-driven cancers require a YAP1 transcriptional complex for survival and tumorigenesis. *Cell* **151**, 1457-1473, doi:10.1016/j.cell.2012.11.026 (2012).
- 199 Lamar, J. M. *et al.* SRC tyrosine kinase activates the YAP/TAZ axis and thereby drives tumor growth and metastasis. *J Biol Chem*, doi:10.1074/jbc.RA118.004364 (2018).
- 200 Lisabeth, E. M. *et al.* Identification of Pirin as a Molecular Target of the CCG-1423/CCG-203971 Series of Anti-Fibrotic and Anti-Metastatic Compounds. *bioRxiv*, 458554, doi:10.1101/458554 (2018).
- 201 Seo, J. & Kim, J. Regulation of Hippo signaling by actin remodeling. *BMB Rep* **51**, 151-156 (2018).
- 202 Si, Y. *et al.* Src inhibits the Hippo tumor suppressor pathway through tyrosine phosphorylation of Lats1. *Cancer Res*, doi:10.1158/0008-5472.CAN-17-0391 (2017).
- 203 Posern, G. & Treisman, R. Actin' together: serum response factor, its cofactors and the link to signal transduction. *Trends Cell Biol* **16**, 588-596, doi:10.1016/j.tcb.2006.09.008 (2006).
- 204 Licciulli, S. *et al.* Pirin delocalization in melanoma progression identified by high content immuno-detection based approaches. *BMC Cell Biol* **11**, 5, doi:10.1186/1471-2121-11-5 (2010).

- 205 Miyazaki, I., Simizu, S., Okumura, H., Takagi, S. & Osada, H. A small-molecule inhibitor shows that pirin regulates migration of melanoma cells. *Nat Chem Biol* **6**, 667-673, doi:10.1038/nchembio.423 (2010).
- 206 Licciulli, S. *et al.* Pirin inhibits cellular senescence in melanocytic cells. *Am J Pathol* **178**, 2397-2406, doi:10.1016/j.ajpath.2011.01.019 (2011).
- 207 Zuckerbraun, B. S., Shapiro, R. A., Billiar, T. R. & Tzeng, E. RhoA influences the nuclear localization of extracellular signal-regulated kinases to modulate p21Waf/Cip1 expression. *Circulation* **108**, 876-881, doi:10.1161/01.CIR.0000081947.00070.07 (2003).
- 208 Pich, C. *et al.* Melanoma Expressed-CD70 Is Regulated by RhoA and MAPK Pathways without Affecting Vemurafenib Treatment Activity. *PLoS One* **11**, e0148095, doi:10.1371/journal.pone.0148095 (2016).
- 209 Taglietti, V. *et al.* RhoA and ERK signalling regulate the expression of the transcription factor Nfix in myogenic cells. *Development* **145**, doi:10.1242/dev.163956 (2018).
- 210 Marinissen, M. J. *et al.* The small GTP-binding protein RhoA regulates c-jun by a ROCK-JNK signaling axis. *Mol Cell* **14**, 29-41 (2004).
- 211 Perona, R. *et al.* Activation of the nuclear factor-kappaB by Rho, CDC42, and Rac-1 proteins. *Genes Dev* **11**, 463-475, doi:10.1101/gad.11.4.463 (1997).
- 212 Ramsdale, R. *et al.* The transcription cofactor c-JUN mediates phenotype switching and BRAF inhibitor resistance in melanoma. *Sci Signal* **8**, ra82, doi:10.1126/scisignal.aab1111 (2015).
- 213 Su, Y. *et al.* Single-cell analysis resolves the cell state transition and signaling dynamics associated with melanoma drug-induced resistance. *Proc Natl Acad Sci U S A* **114**, 13679-13684, doi:10.1073/pnas.1712064115 (2017).
- 214 Liu, X. *et al.* Tead and AP1 Coordinate Transcription and Motility. *Cell Rep* **14**, 1169-1180, doi:10.1016/j.celrep.2015.12.104 (2016).
- 215 Zanconato, F. *et al.* Genome-wide association between YAP/TAZ/TEAD and AP-1 at enhancers drives oncogenic growth. *Nat Cell Biol* **17**, 1218-1227, doi:10.1038/ncb3216 (2015).

- 216 Ye, S. *et al.* YAP1-Mediated Suppression of USP31 Enhances NFkappaB Activity to Promote Sarcomagenesis. *Cancer Res* **78**, 2705-2720, doi:10.1158/0008-5472.CAN-17-4052 (2018).
- 217 Nishimura, E. K. *et al.* Key roles for transforming growth factor beta in melanocyte stem cell maintenance. *Cell Stem Cell* **6**, 130-140, doi:10.1016/j.stem.2009.12.010 (2010).
- 218 Yang, G. *et al.* Inhibition of PAX3 by TGF-beta modulates melanocyte viability. *Mol Cell* **32**, 554-563, doi:10.1016/j.molcel.2008.11.002 (2008).
- 219 Lamb, J. *et al.* The Connectivity Map: using gene-expression signatures to connect small molecules, genes, and disease. *Science* **313**, 1929-1935, doi:10.1126/science.1132939 (2006).
- 220 Subramanian, A. *et al.* A Next Generation Connectivity Map: L1000 Platform and the First 1,000,000 Profiles. *Cell* **171**, 1437-1452 e1417, doi:10.1016/j.cell.2017.10.049 (2017).
- 221 Chen, B. *et al.* Reversal of cancer gene expression correlates with drug efficacy and reveals therapeutic targets. *Nat Commun* **8**, 16022, doi:10.1038/ncomms16022 (2017).
- 222 Chen, B. *et al.* Computational Discovery of Niclosamide Ethanolamine, a Repurposed Drug Candidate That Reduces Growth of Hepatocellular Carcinoma Cells In Vitro and in Mice by Inhibiting Cell Division Cycle 37 Signaling. *Gastroenterology* **152**, 2022-2036, doi:10.1053/j.gastro.2017.02.039 (2017).
- 223 Jahchan, N. S. *et al.* A drug repositioning approach identifies tricyclic antidepressants as inhibitors of small cell lung cancer and other neuroendocrine tumors. *Cancer Discov* **3**, 1364-1377, doi:10.1158/2159-8290.CD-13-0183 (2013).
- 224 Antolin, A. A., Workman, P., Mestres, J. & Al-Lazikani, B. Polypharmacology in Precision Oncology: Current Applications and Future Prospects. *Curr Pharm Des* **22**, 6935-6945, doi:10.2174/1381612822666160923115828 (2016).
- 225 Buchdunger, E. *et al.* Inhibition of the Abl protein-tyrosine kinase in vitro and in vivo by a 2-phenylaminopyrimidine derivative. *Cancer Res* **56**, 100-104 (1996).
- 226 Deininger, M. W., Goldman, J. M., Lydon, N. & Melo, J. V. The tyrosine kinase inhibitor CGP57148B selectively inhibits the growth of BCR-ABL-positive cells. *Blood* **90**, 3691-3698 (1997).

- 227 Druker, B. J. *et al.* Effects of a selective inhibitor of the Abl tyrosine kinase on the growth of Bcr-Abl positive cells. *Nat Med* **2**, 561-566, doi:10.1038/nm0596-561 (1996).
- 228 Rubin, B. P. *et al.* Molecular targeting of platelet-derived growth factor B by imatinib mesylate in a patient with metastatic dermatofibrosarcoma protuberans. *J Clin Oncol* **20**, 3586-3591, doi:10.1200/JCO.2002.01.027 (2002).
- 229 Sjoblom, T. *et al.* Growth inhibition of dermatofibrosarcoma protuberans tumors by the platelet-derived growth factor receptor antagonist STI571 through induction of apoptosis. *Cancer Res* **61**, 5778-5783 (2001).
- 230 Shimizu, A. *et al.* The dermatofibrosarcoma protuberans-associated collagen type Ialpha1/platelet-derived growth factor (PDGF) B-chain fusion gene generates a transforming protein that is processed to functional PDGF-BB. *Cancer Res* **59**, 3719-3723 (1999).
- 231 Greco, A. *et al.* Growth-inhibitory effect of STI571 on cells transformed by the COL1A1/PDGFB rearrangement. *Int J Cancer* **92**, 354-360, doi:10.1002/ijc.1190 (2001).
- 232 Joensuu, H. *et al.* Effect of the tyrosine kinase inhibitor STI571 in a patient with a metastatic gastrointestinal stromal tumor. *N Engl J Med* **344**, 1052-1056, doi:10.1056/NEJM200104053441404 (2001).
- 233 Tuveson, D. A. *et al.* STI571 inactivation of the gastrointestinal stromal tumor c-KIT oncoprotein: biological and clinical implications. *Oncogene* **20**, 5054-5058, doi:10.1038/sj.onc.1204704 (2001).
- 234 Lin, A. *et al.* Off-target toxicity is a common mechanism of action of cancer drugs undergoing clinical trials. *Sci Transl Med* **11**, doi:10.1126/scitranslmed.aaw8412 (2019).
- 235 Klaeger, S. *et al.* The target landscape of clinical kinase drugs. *Science* **358**, doi:10.1126/science.aan4368 (2017).
- 236 Zhao, B. *et al.* Inactivation of YAP oncoprotein by the Hippo pathway is involved in cell contact inhibition and tissue growth control. *Genes Dev* **21**, 2747-2761, doi:10.1101/gad.1602907 (2007).

- 237 Oka, T., Mazack, V. & Sudol, M. Mst2 and Lats kinases regulate apoptotic function of Yes kinase-associated protein (YAP). *J Biol Chem* **283**, 27534-27546, doi:10.1074/jbc.M804380200 (2008).
- 238 Zhao, B. *et al.* Cell detachment activates the Hippo pathway via cytoskeleton reorganization to induce anoikis. *Genes Dev* **26**, 54-68, doi:10.1101/gad.173435.111 (2012).
- 239 Wada, K., Itoga, K., Okano, T., Yonemura, S. & Sasaki, H. Hippo pathway regulation by cell morphology and stress fibers. *Development* **138**, 3907-3914, doi:10.1242/dev.070987 (2011).
- 240 Zhao, B., Li, L., Tumaneng, K., Wang, C. Y. & Guan, K. L. A coordinated phosphorylation by Lats and CK1 regulates YAP stability through SCF(beta-TRCP). *Genes Dev* **24**, 72-85, doi:10.1101/gad.1843810 (2010).
- 241 Misek, S. A. *et al.* Rho-mediated signaling promotes BRAF inhibitor resistance in de-differentiated melanoma cells. *Oncogene* **39**, 1466-1483, doi:10.1038/s41388-019-1074-1 (2020).
- 242 Chen, D. *et al.* LIFR is a breast cancer metastasis suppressor upstream of the Hippo-YAP pathway and a prognostic marker. *Nat Med* **18**, 1511-1517, doi:10.1038/nm.2940 (2012).
- 243 Orr, B. A. *et al.* Yes-associated protein 1 is widely expressed in human brain tumors and promotes glioblastoma growth. *J Neuropathol Exp Neurol* **70**, 568-577, doi:10.1097/NEN.0b013e31821ff8d8 (2011).
- 244 Zhang, W. *et al.* Downstream of mutant KRAS, the transcription regulator YAP is essential for neoplastic progression to pancreatic ductal adenocarcinoma. *Sci Signal* **7**, ra42, doi:10.1126/scisignal.2005049 (2014).
- 245 Tschaharganeh, D. F. *et al.* Yes-associated protein up-regulates Jagged-1 and activates the Notch pathway in human hepatocellular carcinoma. *Gastroenterology* **144**, 1530-1542 e1512, doi:10.1053/j.gastro.2013.02.009 (2013).
- 246 Chaib, I. *et al.* Co-activation of STAT3 and YES-Associated Protein 1 (YAP1) Pathway in EGFR-Mutant NSCLC. *J Natl Cancer Inst* **109**, doi:10.1093/jnci/djx014 (2017).

- 247 Lui, J. W. *et al.* The Efficiency of Verteporfin as a Therapeutic Option in Pre-Clinical Models of Melanoma. *J Cancer* **10**, 1-10, doi:10.7150/jca.27472 (2019).
- 248 Brinkman, E. K., Chen, T., Amendola, M. & van Steensel, B. Easy quantitative assessment of genome editing by sequence trace decomposition. *Nucleic Acids Res* **42**, e168, doi:10.1093/nar/gku936 (2014).
- 249 Arango, D. *et al.* Apigenin induces DNA damage through the PKCdelta-dependent activation of ATM and H2AX causing down-regulation of genes involved in cell cycle control and DNA repair. *Biochem Pharmacol* **84**, 1571-1580, doi:10.1016/j.bcp.2012.09.005 (2012).
- 250 Qin, Q. *et al.* Lisa: inferring transcriptional regulators through integrative modeling of public chromatin accessibility and ChIP-seq data. *Genome Biol* **21**, 32, doi:10.1186/s13059-020-1934-6 (2020).
- 251 Zeng, B. *et al.* OCTAD: an open workplace for virtually screening therapeutics targeting precise cancer patient groups using gene expression features. *bioRxiv*, 821546, doi:10.1101/821546 (2019).
- 252 Risso, D., Ngai, J., Speed, T. P. & Dudoit, S. Normalization of RNA-seq data using factor analysis of control genes or samples. *Nat Biotechnol* **32**, 896-902, doi:10.1038/nbt.2931 (2014).
- 253 Robinson, M. D., McCarthy, D. J. & Smyth, G. K. edgeR: a Bioconductor package for differential expression analysis of digital gene expression data. *Bioinformatics* **26**, 139-140, doi:10.1093/bioinformatics/btp616 (2010).
- 254 Hanzelmann, S., Castelo, R. & Guinney, J. GSVA: gene set variation analysis for microarray and RNA-seq data. *BMC Bioinformatics* **14**, 7, doi:10.1186/1471-2105-14-7 (2013).
- 255 Gao, J. *et al.* Integrative analysis of complex cancer genomics and clinical profiles using the cBioPortal. *Sci Signal* **6**, p11, doi:10.1126/scisignal.2004088 (2013).
- 256 Kuleshov, M. V. *et al.* Enrichr: a comprehensive gene set enrichment analysis web server 2016 update. *Nucleic Acids Res* **44**, W90-97, doi:10.1093/nar/gkw377 (2016).

- 257 Chen, B. *et al.* Relating Chemical Structure to Cellular Response: An Integrative Analysis of Gene Expression, Bioactivity, and Structural Data Across 11,000 Compounds. *CPT Pharmacometrics Syst Pharmacol* **4**, 576-584, doi:10.1002/psp4.12009 (2015).
- 258 Corsello, S. M. *et al.* The Drug Repurposing Hub: a next-generation drug library and information resource. *Nat Med* **23**, 405-408, doi:10.1038/nm.4306 (2017).
- 259 Sirota, M. *et al.* Discovery and preclinical validation of drug indications using compendia of public gene expression data. *Sci Transl Med* **3**, 96ra77, doi:10.1126/scitranslmed.3001318 (2011).
- 260 Patel, V. *et al.* Comparison of Acalabrutinib, A Selective Bruton Tyrosine Kinase Inhibitor, with Ibrutinib in Chronic Lymphocytic Leukemia Cells. *Clin Cancer Res* **23**, 3734-3743, doi:10.1158/1078-0432.CCR-16-1446 (2017).
- 261 Herman, S. E. M. *et al.* The Bruton Tyrosine Kinase (BTK) Inhibitor Acalabrutinib Demonstrates Potent On-Target Effects and Efficacy in Two Mouse Models of Chronic Lymphocytic Leukemia. *Clin Cancer Res* **23**, 2831-2841, doi:10.1158/1078-0432.CCR-16-0463 (2017).
- 262 Kim, M., Kim, T., Johnson, R. L. & Lim, D. S. Transcriptional co-repressor function of the hippo pathway transducers YAP and TAZ. *Cell Rep* **11**, 270-282, doi:10.1016/j.celrep.2015.03.015 (2015).
- 263 Feddersen, C. R. *et al.* Src-Dependent DBL Family Members Drive Resistance to Vemurafenib in Human Melanoma. *Cancer Res* **79**, 5074-5087, doi:10.1158/0008-5472.CAN-19-0244 (2019).
- 264 Girotti, M. R. *et al.* Inhibiting EGF receptor or SRC family kinase signaling overcomes BRAF inhibitor resistance in melanoma. *Cancer Discov* **3**, 158-167, doi:10.1158/2159-8290.CD-12-0386 (2013).
- 265 Girotti, M. R. *et al.* Paradox-breaking RAF inhibitors that also target SRC are effective in drug-resistant BRAF mutant melanoma. *Cancer Cell* **27**, 85-96, doi:10.1016/j.ccell.2014.11.006 (2015).
- 266 Basu, S., Totty, N. F., Irwin, M. S., Sudol, M. & Downward, J. Akt phosphorylates the Yes-associated protein, YAP, to induce interaction with 14-3-3 and attenuation of p73-mediated apoptosis. *Mol Cell* **11**, 11-23 (2003).

- 267 Sugihara, T. *et al.* YAP Tyrosine Phosphorylation and Nuclear Localization in Cholangiocarcinoma Cells Are Regulated by LCK and Independent of LATS Activity. *Mol Cancer Res* **16**, 1556-1567, doi:10.1158/1541-7786.MCR-18-0158 (2018).
- 268 Byrd, J. C. *et al.* Targeting BTK with ibrutinib in relapsed chronic lymphocytic leukemia. *N Engl J Med* **369**, 32-42, doi:10.1056/NEJMoa1215637 (2013).
- 269 Wang, M. L. *et al.* Targeting BTK with ibrutinib in relapsed or refractory mantle-cell lymphoma. *N Engl J Med* **369**, 507-516, doi:10.1056/NEJMoa1306220 (2013).
- 270 Roller, D. G. *et al.* Combinatorial drug screening and molecular profiling reveal diverse mechanisms of intrinsic and adaptive resistance to BRAF inhibition in V600E BRAF mutant melanomas. *Oncotarget* **7**, 2734-2753, doi:10.18632/oncotarget.6548 (2016).
- 271 Sima, N. *et al.* Small Molecules Identified from a Quantitative Drug Combinational Screen Resensitize Cisplatin's Response in Drug-Resistant Ovarian Cancer Cells. *Transl Oncol* **11**, 1053-1064, doi:10.1016/j.tranon.2018.06.002 (2018).
- 272 Seervi, M. *et al.* A high-throughput image-based screen for the identification of Bax/Bak-independent caspase activators against drug-resistant cancer cells. *Apoptosis* **19**, 269-284, doi:10.1007/s10495-013-0921-8 (2014).
- 273 Echizenya, S. *et al.* Discovery of a new pyrimidine synthesis inhibitor eradicating glioblastoma-initiating cells. *Neuro Oncol* **22**, 229-239, doi:10.1093/neuonc/noz170 (2020).
- 274 Brito, D. A. & Rieder, C. L. Mitotic checkpoint slippage in humans occurs via cyclin B destruction in the presence of an active checkpoint. *Curr Biol* **16**, 1194-1200, doi:10.1016/j.cub.2006.04.043 (2006).
- 275 Meek, D. W. The role of p53 in the response to mitotic spindle damage. *Pathol Biol (Paris)* **48**, 246-254 (2000).
- 276 Mathews Griner, L. A. *et al.* High-throughput combinatorial screening identifies drugs that cooperate with ibrutinib to kill activated B-cell-like diffuse large B-cell lymphoma cells. *Proc Natl Acad Sci U S A* **111**, 2349-2354, doi:10.1073/pnas.1311846111 (2014).
- 277 Landsberg, J. *et al.* Melanomas resist T-cell therapy through inflammation-induced reversible dedifferentiation. *Nature* **490**, 412-416, doi:10.1038/nature11538 (2012).

- 278 Mehta, A. *et al.* Immunotherapy Resistance by Inflammation-Induced Dedifferentiation. *Cancer Discov* **8**, 935-943, doi:10.1158/2159-8290.CD-17-1178 (2018).
- 279 Thomas, N. *et al.* Characterization and gene expression profiling of a stable cell line expressing a cell cycle GFP sensor. *Cell Cycle* **4**, 191-195, doi:10.4161/cc.4.1.1405 (2005).
- 280 Bartek, J. & Lukas, J. Chk1 and Chk2 kinases in checkpoint control and cancer. *Cancer Cell* **3**, 421-429, doi:10.1016/s1535-6108(03)00110-7 (2003).
- 281 Raab, M. *et al.* Mitotic arrest and slippage induced by pharmacological inhibition of Polo-like kinase 1. *Mol Oncol* **9**, 140-154, doi:10.1016/j.molonc.2014.07.020 (2015).
- 282 Tsuda, Y. *et al.* Mitotic slippage and the subsequent cell fates after inhibition of Aurora B during tubulin-binding agent-induced mitotic arrest. *Sci Rep* **7**, 16762, doi:10.1038/s41598-017-17002-z (2017).
- 283 Cheng, B. & Crasta, K. Consequences of mitotic slippage for antimicrotubule drug therapy. *Endocr Relat Cancer* **24**, T97-T106, doi:10.1530/ERC-17-0147 (2017).
- 284 Lukas, C. *et al.* Accumulation of cyclin B1 requires E2F and cyclin-A-dependent rearrangement of the anaphase-promoting complex. *Nature* **401**, 815-818, doi:10.1038/44611 (1999).
- 285 Wylie, A. A. *et al.* The allosteric inhibitor ABL001 enables dual targeting of BCR-ABL1. *Nature* **543**, 733-737, doi:10.1038/nature21702 (2017).
- 286 Feldman, D. *et al.* Optical Pooled Screens in Human Cells. *Cell* **179**, 787-799 e717, doi:10.1016/j.cell.2019.09.016 (2019).
- 287 Zeng, X. *et al.* Pharmacologic inhibition of the anaphase-promoting complex induces a spindle checkpoint-dependent mitotic arrest in the absence of spindle damage. *Cancer Cell* **18**, 382-395, doi:10.1016/j.ccr.2010.08.010 (2010).
- 288 Gembarska, A. *et al.* MDM4 is a key therapeutic target in cutaneous melanoma. *Nat Med* **18**, 1239-1247, doi:10.1038/nm.2863 (2012).

289 Origanti, S., Cai, S. R., Munir, A. Z., White, L. S. & Piwnica-Worms, H. Synthetic lethality of Chk1 inhibition combined with p53 and/or p21 loss during a DNA damage response in normal and tumor cells. *Oncogene* **32**, 577-588, doi:10.1038/onc.2012.84 (2013).